Advancement of Using Portable Free Fall Penetrometers for Geotechnical Site Characterization of Energetic Sandy Nearshore Areas

Ali Hefdhallah Ali Albatal

Dissertation submitted to the faculty of the Virginia Polytechnic Institute and State University in partial fulfillment of the requirements for the degree of

Doctor of Philosophy
In
Civil Engineering

Nina Stark, Chair
Bernardo A. Castellanos
Heidi M. Wadman
Christopher W. Zobel
Jennifer L. Irish

March 19, 2018

Blacksburg, Virginia

Keywords: Free-fall penetrometer, nearshore site investigation, sediment classification, sand friction angle

Advancement of Using Portable Free Fall Penetrometers for Geotechnical Site Characterization of Energetic Sandy Nearshore Areas

Ali H. Albatal

Academic Abstract

Portable Free Fall Penetrometers (PFFPs) are lightweight tools used for rapid and economic characterization of surficial subaqueous sediments. PFFPs vary in weight, shape and size with options for using add-on units. The different configurations enable deployments in various environments and water depths, including the nearshore zone where conventional methods are challenged by energetic hydrodynamics and limited navigable depth. Moreover, PFFPs offer an opportunity to reduce the high site investigation costs associated with conventional offshore geotechnical site investigation methods. These costs are often a major obstacle for small projects serving remote communities or testing novel renewable energy harvesting machines. However, PFFPs still face issues regarding data analysis and interpretation, particularly in energetic sandy nearshore areas. This includes a lack of data and accepted analysis methods for such environments. Therefore, the goal of this research was to advance data interpretation and sediments characterization methods using PFFPs with emphasis on deployments in energetic nearshore environments.

PFFP tests were conducted in the nearshore areas of: Yakutat Bay, AK; Cannon Beach, AK; and the U.S. Army Corps of Engineers' Field Research Facility's beach, Duck, NC. From the measurements, the research goal was addressed by: (1) introducing a methodology to create a regional sediment classification scheme utilizing the PFFP deceleration and pore pressure measurements, sediment traces on the probe upon retrieval, and previous literature; (2) investigating the effect of wave forcing on the sediments' behavior through correlating variations in sediment strength to wave climate, sandbar migration, and depth of closure, as well as identifying areas of significant sediment mobilization processes; and (3) estimating the relative density and friction angle of sand in energetic nearshore areas from PFFP measurements. For the latter, the field data was supported by vacuum triaxial tests and PFFP deployments under controlled laboratory conditions on sand samples prepared at different relative densities.

The research outcomes address gaps in knowledge with regard to the limited studies available that investigate the sand geotechnical properties in energetic nearshore areas. More specifically, the research contributes to the understanding of surficial sediment geotechnical properties in energetic nearshore areas and the enhancement of sediment characterization and interpretation methods.

Advancement of Using Portable Free Fall Penetrometers for Geotechnical Site Characterization of Energetic Sandy Nearshore Areas

Ali H. Albatal

General Audience Abstract

The increasing demand for energy, fluctuations of oil prices, and the expected reduction in the world's oil production in addition to concerns associated to the global climate change drive the search for renewable energy sources. Out of the different sources of renewable energy, the reliable availability of waves is an advantage over other sources like solar and wind. However, different challenges are still facing the advancement of generating energy from waves. One important challenge is the reliability of the anchoring or foundation system, and the associated site characterization and data collection. The stability of the systems depends on the sediment strength (ability accommodate loads), sediments susceptibility to scour (removal of the sediments around the foundations), and local morphodynamics (changes in the seabed shape). In fact, the stability of the foundations in the seabed represents a major concern for many nearshore and offshore structures. Accordingly, the site characterization stage of any project is essential to mitigate the risks of failures, as well as to achieve cost-effective designs.

Portable Free fall penetrometers (PFFPs) are rapid and economical tools used to characterize uppermost seabed sediments. The variability of such devices in weight, shape and size enables the use in different environments and water depths. However, data of PFFPs in sandy sediments is still limited which contradicts the fact that sand represents the most common soil type on the beaches worldwide. Accordingly, the aim of this research is to investigate the sediment behavior in energetic wave areas, and to advance the methods of interpreting the PFFP data in sandy nearshore zones.

A PFFP was used to characterize the sediments in three main areas: Yakutat Bay, AK, Cannon Beach, AK and the U.S. Army Corps of Engineers' Field Research Facility's beach, Duck, NC. The results were utilized to introduce a sediment classification scheme and complete an existing sediment distribution map for Yakutat Bay, AK; study the effect of storms on the seabed sediment strength; and to determine sand strength parameters using PFFP measurements. The results of this research will contribute to improve the sediment characterization methods and to understand topmost sediment layers' properties.

ACKNOWLEDGMENTS

I am grateful to my supervisor Dr. Nina Stark for the support, encouragement, guidance and motivation. I would like to thank Dr. Bernardo Castellanos, Dr. Heidi Wadman, Dr. Christopher Zobel and Dr. Jennifer Irish for serving on my committee and providing insightful comments and suggestions. I would like also to thank Dr. Heidi Wadman, Dr. Jesse McNinch and the staff of the USACE Field Research Facility for conducting field surveys even in bad weather conditions, and for providing on-site support. I appreciate the assistance of Brandon Quinn, Fred Falcone, Dillon Braud and Cagdas Bilici during the field investigations. I would like also to acknowledge the staff of the City and Borough of Yakutat specifically Rhonda Coston and Bill Lucy for on-site support. I also thank Dr. Thomas Brandon and Dr. Bernardo Castellanos for providing advice and support during the laboratory tests. I also appreciate the help by Muhammad Bilal Mumtaz, Nick Brilli, Julie Paprocki, Christopher McBride and Dennis Kiptoo with the laboratory tests. I would like to thank all the geotechnical department faculty members for their support.

I am thankful for the encouragement of each member in my family throughout my research period.

PREFACE

The chapters of this dissertation consist of a series of paper manuscripts, which are combined to form the dissertation body. Chapters 2 through 6 are each individual paper manuscripts while chapter 1 is an introduction. The dissertation author is the lead author of each manuscript. Three of these are journal manuscripts (Chapters 2, 4 and 6), and two are peer-reviewed conference paper manuscripts (Chapters 3 and 5). The contributors to each manuscript and the publication/ submission information are provided at the beginning of each chapter.

TABLE OF CONTENTS

LIST OF FIGURES

LIST OF TABLES

Chapter 1: Introduction

1.1 Motivation

Nearshore areas are characterized by the presence of waves most of the time. Waves can travel for very long distances due to the small dissipation in wave energy in deep waters. The energy imparted to the waves along these distances is then dissipated through different processes in nearshore areas (Dean and Dalrymple 2004). The interactions between the wave processes and the seabed in nearshore zone result in a dynamic seabed profile that varies depending on the wave climate. The seabed profile, in turn, affects the nearshore hydrodynamics, especially wave shoaling and breaking (e.g., Holman 1995; McNinch 2004). The sediment remobilization and redeposition activities associated with the profile dynamics influence the stability of the coastlines and nearshore structures in energetic areas. Accordingly, studying the relationship between morphodynamics and geotechnical seabed characteristics in such areas is essential for planning any construction project or coastline preservation measures (Stark 2010).

Among the different methods for characterizing seabed sediments, portable free fall penetrometers (PFFPs) have the advantage of being lightweight tools, enabling deployment in different wave conditions and water depths. This makes PFFPs specifically interesting for nearshore site investigation where the use of conventional methods can be challenging due to the energetic hydrodynamics, limited navigable depths, and large costs. As a geotechnical investigation tool, PFFPs are specifically useful for sediment characterization during the early site assessment stage during which a project's budget is usually limited, large survey areas are still being considered, initial sediment information is limited, and the feasibility of the project is being determined (Randolph et al. 2005, Stark et al. 2014).

Information about the surficial sediment type and shear strength can be estimated using PFFP measurements. However, a number of challenges still exist, particularly regarding data processing methods and interpretation. For example, limited sediment classification schemes based on PFFP measurement are available in the literature (e.g., Stoll et al. 2007; Mulukutla et al. 2011). These schemes were developed for specific penetrometers and/or specific sites. Therefore, they are often not suitable to be used for a different penetrometer or in other locations. Moreover, pore pressure measurements have rarely been considered, even though they represent an important parameter in

standard Cone Penetration Testing (CPT) (Sandven 2010; Lunne 2012). Another factor that has rarely been considered during data interpretation is the role of active wave forcing and its impact on surficial seabed sediments (e.g. Stark and Kopf 2011). Regarding existing studies and literature, lightweight hand-deployed penetrometers have mainly been used in clayey sediments to estimate the undrained shear strength. However, to-date no method has been validated to determine the in-situ friction angle, relative density, or shear strength of sands based on the deceleration measurements by PFFPs. This is an issue for nearshore site investigation as most energetic nearshore zones contain predominantly sandy sediments. Thus, advances aiming to address the issues listed above are needed to assess how valuable PFFP surveying may be for early site assessment of nearshore engineering projects and to establish the use of PFFP for more cost-effective nearshore geotechnical site investigations.

1.2 Background

1.2.1 Nearshore Site Characterization

The complexity of combinations of the geologic, environmental, physical and chemical processes during soil[1] formation results in an inherent soil variability in the vertical and horizontal directions (Phoon and Kulhawy 1999). The uncertainty in soil conditions represents a major risk for onshore and offshore projects, and failing to characterize such uncertainties can impact the project cost, design, time, construction methods, personnel health and safety, and the environment (Peuchen 2012; Cook et al. 2014). Cook et al. (2014) listed the problems associated with offshore renewable energy projects that are related to soil conditions as follows:

1. Presence of soft soils that can affect the foundation's stability.
2. Presence of mobile sediment layers that may affect the foundation's behavior and cable protection.
3. Presence of hard soils that need special equipment to handle.
4. Rapid change in soil conditions which may require the use of more than one foundation type for the same project.
5. Presence of surface or buried obstructions like unexploded ordnances (UXO).

[1] 'soils' and 'sediments' are synonymous, and used interchangeably in this dissertation.

6. Presence of shallow gas that represents a risk for drilling.
7. Risk of seismic activities and associated soil liquefaction.

Accordingly, detailed site characterization is necessary to make sure that there are no undesirable conditions at the project site at any time and to plan how to account for such conditions if present (Clayton et al. 1995).

The site characterization stages of any project can be divided into reconnaissance, preliminary and detailed investigations (Jaksa 2000; Baecher and Christian 2003; Stark et al. 2014b). During the preliminary site investigation stage (also known as early site assessment), it is required to find the proper location and to estimate the initial soil properties for design (Baecher and Christian 2003). Additionally, Stark et al. (2014) emphasized the importance of bathymetry, morphodynamics, and sediment dynamics in environments characterized by strong hydrodynamic conditions (Figure 1.1). The results of the preliminary investigation stage are expected to identify a favorable location and lead to a plan for a detailed geotechnical site investigation program (Holubec 2010). During the preliminary site investigation stage, the project's budget can be limited, and the final decision regarding proceeding of the project may not have been made yet (Randolph et al. 2005; Stark et al. 2014b).

Geotechnical site investigations commonly include the collection of soil samples and controlled laboratory tests on these samples and in-situ geotechnical tests (Lunne and Long 2006; Randolph and Gourvenec 2011). In the offshore site investigation practice, the site investigation generally includes recovering samples of fine-grained soils and performing in-situ testing such as penetration and vane shear testing (e.g., Lunne and Long 2006; Peuchen 2012). Due to challenges with the collection of undisturbed sand samples, in-situ testing is a crucial component in the case of sandy sediments (Randolph and Gourvenec 2011). For example, gravity and vibro-core samplers are frequently used for offshore sampling; however, such techniques yield disturbed samples due to altering the in-situ stresses as well as the mechanical disturbance by the samplers (Lunne et al. 1998).

The Cone Penetration Test (CPT) is the most common and accepted in-situ testing method in the offshore geotechnical site investigation practice (Randolph et al. 2005; Lunne 2012; Stephan 2015). A continuous profile can be obtained that allows detecting even thin layers using CPT tests. Furthermore, the process of using CPT testing is fully established, including deployment,

maintenance and procedures in addition to the possibility of conducting customized tests like dissipation and seismicity tests (Hodgson et al. 1995; ISO 2012; Peuchen 2012). Moreover, CPTs can penetrate up to 100 m below the seabed surface in water depths up to 3000 m (Lunne 2012). However, the process of using CPT testing in offshore areas is expensive and time-consuming due to the required mobilization of specialized survey vessels. Typically, the time between planning and data reporting exceeds a year with a cost of several million dollars (Randolph and Gourvenec 2011). The cost of the mobilization of survey vessels becomes a major factor for remote locations (Peuchen 2012). Due to the limited water depths, shoaling and breaking waves, strong currents, and potential traffic movement in some cases, offshore survey vessels might not be practical in nearshore zones (Gillon 2008). An additional disadvantage appears when surface sediment layers are considered. A large CPT reaction frame is usually lowered to the seabed in order to support the CPT's engine, which disturbs the uppermost layers of the seabed and the flow (Stark 2010).

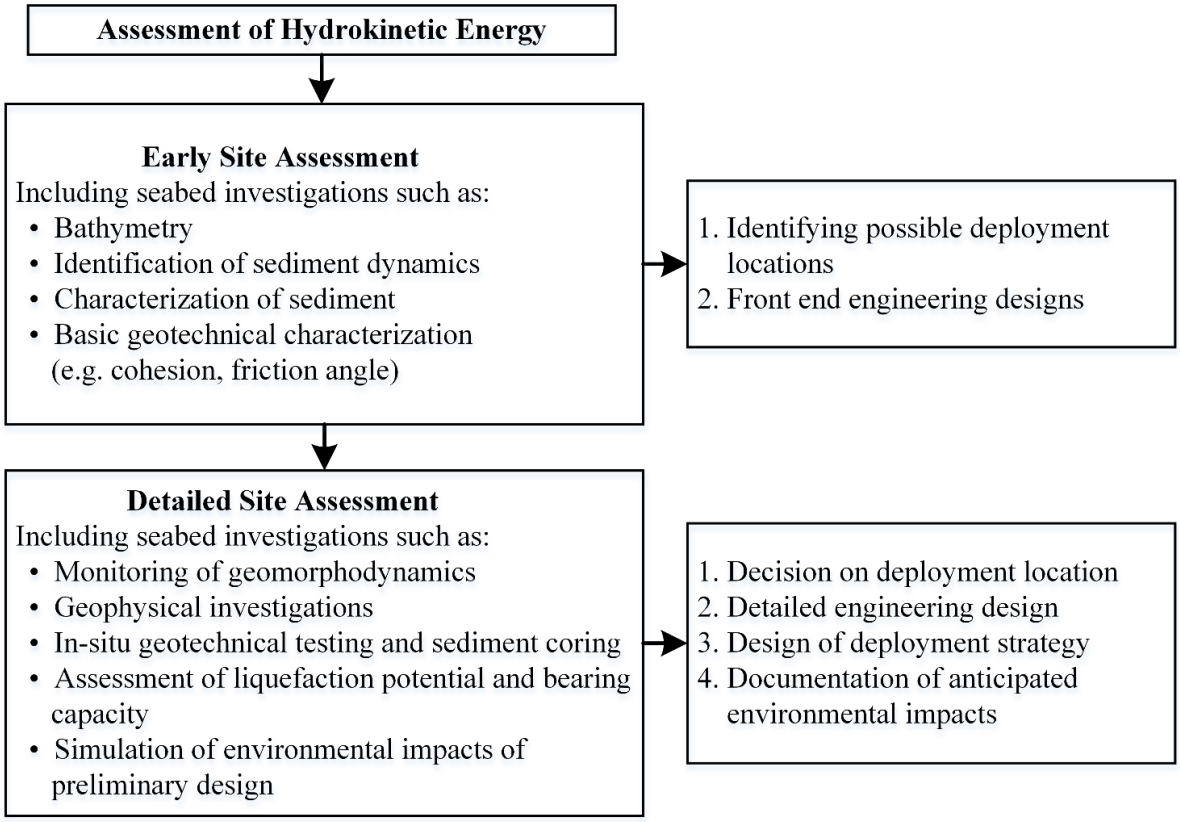

Figure 1.1. Site investigation stages and expected tasks at each stage: preliminary and detailed site investigations. (Source: Stark et al 2014).

The in-situ site investigation in the coastal and nearshore areas can sometimes be conducted using onshore techniques. A CPT truck can be mounted on a locally chartered barge; however, such methods can be used only in sheltered areas where no energetic waves are expected (Hodgson et al. 1995). Another type of platform that is typically used for nearshore site investigation are jack-up platforms. Jack-up platforms provide a stable working platform that overcomes the disadvantage of using a survey vessel in energetic shallow areas. They are manufactured in different sizes and shapes, and the maximum water depth that can be investigated using a jack-up platform keeps increasing. However, there are limitations for using jack-up platforms including the difficulty of moving them from one location to another which might need remobilization each time; daily rates are expensive (typically in a range of the low hundreds of thousands of dollars); and backup support vessels are required at all time (Randolph and Gourvenec 2011). Another disadvantage appears when remote areas are targeted which may require moving a platform over long distances. In this case, the mobilization cost can be in the range of several millions of dollars. Accordingly, novel methods are needed to decrease the site investigation costs and to overcome the difficulties associated with investigating energetic nearshore areas.

1.2.2 Free Fall Penetrometers

Free fall penetrometers offer an economical, fast and robust option to investigate the seabed, especially if deep penetration is not needed (Dayal 1980; Stark et al. 2009). One of the first versions of free fall penetrometers was by Scott (1967) who attached an accelerometer to a gravity corer to measure the sampler deceleration during its penetration after falling freely in the water column (Chari et al. 1981). Afterwards, the concept of using a free fall penetrometer designed to estimate the sediment strength was introduced by Dayal and Allen (1973). In the following decades, different free fall penetrometers were introduced that differ in the device shape, mass, deployment method, and measuring sensors. According to the shape type, free fall penetrometers can be categorized into projectile-like, and lance-like (Stark 2010; Dorvinen 2016) (Figure 1.2). Considering the penetrometer mass, they can be categorized to lightweight (e.g., 7 kg for the eXpendable Bottom Penetrometer *XBP*, Stoll and Akal 1999; 11 kg for *Nimrod*, Stark et al. 2009), intermediate (e.g, 40-170 kg for FF-CPT, Stegmann et al. 2006) and heavy (e.g., 500-200 kg for *LIRmeter*, Fabian et al. 2008; 3200-3400 kg for *CPT Stinger*, Young et al. 2011). Lightweight

systems can be retrievable (e.g. *Nimrod*) or expendable (e.g. *XBP*). Intermediate and heavy devices are all retrievable. Measurements can include acceleration, cone resistance, and sleeve friction with or without pore pressure measurement, and more uncommon measurements such as temperature. However, even if an impact penetrometer measures the cone resistance and/or sleeve friction, the device needs to be equipped with sensor to estimate the penetrated depth. More information about the weight, shape, measuring sensors and deploying techniques can be found in Stephan (2015).

Portable free fall penetrometers PFFPs belong to the lightweight category of the impact penetrometers. The lightweight characteristic makes handling and deploying PFFPs an easy process, which enables application from small vessels of opportunity ranging from a kayak to larger fishery vessels (Stoll et al. 2007; Stark et al. 2009). Accordingly, PFFPs are suitable

Figure 1.2. The projectile-like free fall penetrometer *BlueDrop* (left image), b) the lance-like free fall penetrometer *LIRmeter* (right image) (*from: http://www.geo.uni-bremen.de*). The images also show the size and then required personnel to handle the device.

for a rapid and economic assessment of the uppermost seabed surface sediments in energetic nearshore areas. This makes them specifically interesting for the early site assessment of nearshore projects, particularly if a limited budget. Using PFFPs can be specifically convenient for small projects for which the high site characterization costs can represent a major obstacle.

PFFPs are robust devices due to using accelerometers only instead of load cells located in the tip, which makes them particularly suitable for energetic conditions, and/or environments for which little information is available prior to the survey. Micro-electro-mechanical systems (MEMS) accelerometers measure continuously, including the probe's deceleration during seabed penetration after falling freely in the water column. The deceleration-time records can then be used to derive the penetration depth, sediment strength, and impact and penetration velocities as outlined in Section 1.2.3. Some PFFPs are also equipped with a pressure transducer that is usually located behind the penetrometer's tip (i.e., u_2 position; Figure 1.3). However, the use of pore pressure measurements in the data analysis for PFFPs is still limited and more research is needed in this area (e.g., Stegmann et al. 2006 Seifert et al. 2008 Stark et al. 2015)

1.2.3 Processing of the PFFP measurements

The penetrometer impacts the soil at an initial impact velocity which depends on the probe's terminal free fall velocity in water, rope drag and distance of fall (Stark and Kopf 2011). During the free fall and penetration, PFFPs are being subjected to different forces (Figure 1.3). Jeanjean et al. (2012) formulated the equation of motion for a PFFP during penetration as follows:

$$ma = W' - F_{BE} - F_{AD} - F_{BS} - F_D - F_{D,R} \tag{1.1}$$

where m is the mass of the probe, a is the probe acceleration, W' is the buoyant weight of the probe, F_{BE} is the end bearing force, F_{AD} the side adhesion force on the cone and shaft, F_{BS} is the buoyancy force in soil, and F_D and $F_{D,R}$ are the drag forces on the probe and rope, respectively. Solving Equation 1.1 can be difficult and associated with unknown empirical factors, and becomes even more complicated for partial penetration in the soil, which is the case when penetrating sandy sediments. Accordingly, Equation 1.1 is usually simplified by neglecting the least significant terms. The soil buoyancy can be neglected due to the limited penetration depths, especially in

sandy sediments. Stark (2016) found that neglecting the soil buoyance results in an error of about 1% of the sediment's resistance to penetration depths less than 20 cm. The expected penetration depths for lightweight PFFPs in sandy sediments is usually less than 20 cm (e.g., Lucking et al. 2017; Stark et al. 2009, 2012b, 2014). The impact of drag and adhesion forces can also be neglected due to the limited penetration depth, and because of the penetrometer's shape which reduces the drag force (Aubeny and Shi 2006; Stark et al. 2017). Moreover, the adhesion force can be negligible if a clearance between the probe and soil was created due to the fast penetration and soil failure (True 1976). Therefore, simplifying Equation 1.1 above results in the following equation:

$$ma = W' - F_{BE} \tag{1.2}$$

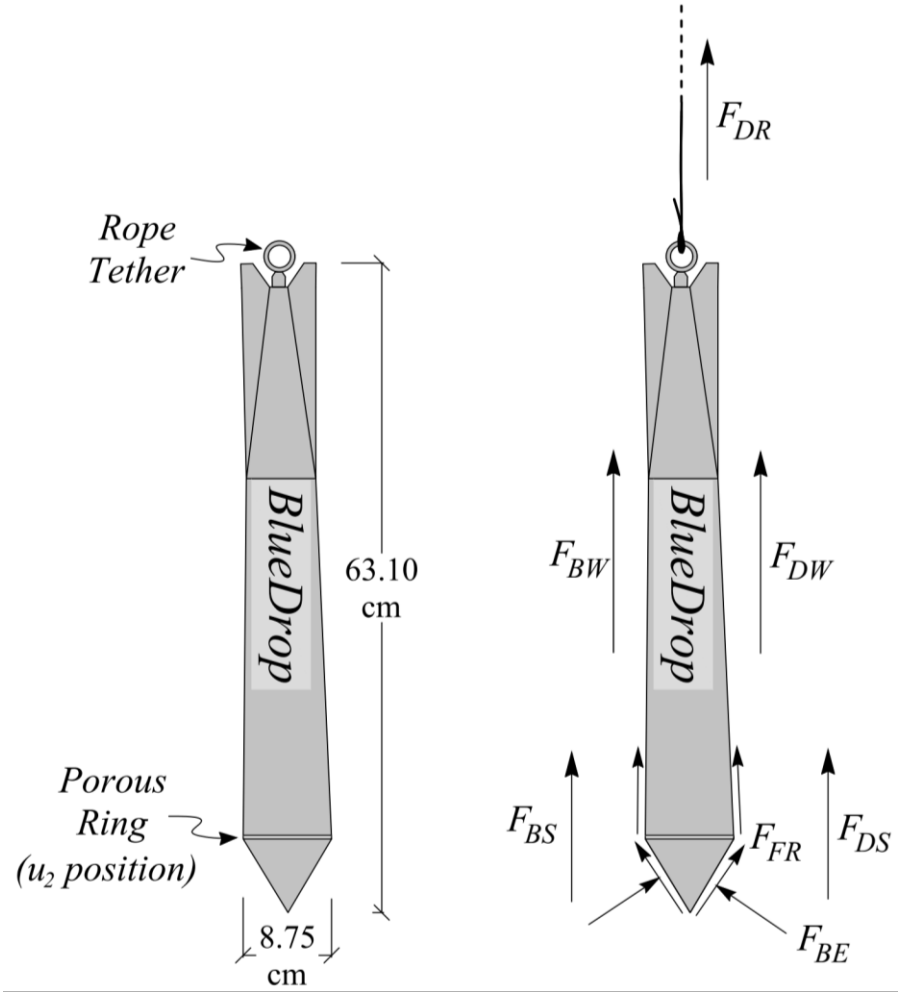

Figure 1.3. The forces exerted on a free fall penetrometer during penetration. The PFFP *BlueDrop* was used as an example.

In Equation 1.2, the only unknown term is the bearing force, which is used to determine the sediment bearing capacity (i.e. the maximum stress the soil can bear without failing (Terzaghi 1943); see section 1.2.2).

The resulting bearing force from solving the equation of motion is used to determine the dynamic bearing capacity of sediment during penetration. Knowing the bearing resistance force, F_{BE}, and the area subjected to load, A, an ultimate dynamic bearing capacity, q_{ud}, the probe is subjected to during penetration can be estimated as follows:

$$q_{ud} = F_{BE}/A \tag{1.3}$$

In general, soils exhibit a higher resistance with increasing the loading. Accordingly, a strain rate factor is used to account for this increase. The application of a strain rate factor is common in geotechnical problems when testing the soil under large strain rates. For example, for triaxial compression tests, each ten folds increase in the strain rate is expected to result in 10 percent increase in the value of the undrained shear strength of clay (Kulhawy and Mayne 1990). Similarly, the ultimate dynamic bearing capacity is usually higher than the soil bearing resistance that would be expected for static (conventional) loads. Dayal and Allen (1973) proposed to correct the dynamic sediment strength for this increase, using a strain rate factor, leading to a quasi-static strength equivalent to measurements conducted at a chosen constant reference velocity. Accordingly, to determine an equivalent of static resistance $q_{c,eq}$ (also known as *qsbc*), a strain rate correction, f_{sr}, is applied (Dayal and Allen 1973; Stark et al. 2011, 2012b; Steiner et al. 2014):

$$q_{c,eq} = qsbc = q_{ud}/f_{sr} \tag{1.4}$$

The most commonly used strain rate factor coefficient for the case of sandy soils is expressed as a logarithmic equation (e.g., Stoll et al. 2007, Stark et al. 2009, 2012, Stephan et al. 2015):

$$f_{sr} = 1 + K\ \log_{10}\left(v_{dyn}/v_{ref}\right) \tag{1.5}$$

where v_{dyn} is the dynamic penetration velocity which can be determined by integrating the measured deceleration over time, v_{ref} is a chosen reference penetration velocity (usually the standard penetration velocity for Cone Penetration Testing; 2 cm/s), and K is a dimensionless empirical coefficient.

Different strain rate factor values have been used in the literature. For sandy sediments, the values of f_{sr} ranged from 1 (K coefficient of zero, for penetration velocity up to 0.8 m/s) (Dayal et al. 1975) to values of 3-5 (K coefficient of 0.8-1.5 at impact velocities > 3 m/s) (Stoll et al. 2007, Stark et al. 2012, Stephan et al. 2015). A similar variation is also available in the literation for the strain rate factor for cohesive sediments. The strain rate factor coefficient K varied between 0.03 to 1.5 (Dayal et al. 1975; Steiner et al. 2014). Additionally, the strain rate factor can vary for the same soil. Seed and Lundgren (1954) found that dense sands have higher sensitivity for changes in the strain rate factor than loose sand. Dayal et al. (1975) found the reverse for clay where they found that the strain rate decreases with the increase of the clay undrained shear strength. However, no relationship is available that correlates the sand density or the clay shear strength to the value of the strain rate factor and one value is usually used for the same soil regardless of the change in the properties. This makes the uncertainty in the strain rate factor the highest source of error during data analysis for FFP tests (Chow and Airey 2014).

Beside the logarithmic equation, other equations have been introduced like the inverse hyperbolic sine and power-law equations (Biscontin and Pestana 2001; Randolph 2004). However, the use of these equations is still limited to fine-grained soils, and no literature was found that utilizes these equations in sandy sediments.

The quality of the analysis method of the PFFP deceleration-depth measurements is commonly assessed by comparing the calculated equivalent cone resistance, $q_{c,eq}$, with the cone resistance obtained from CPT tests, q_c (e.g., Bowman et al. 1995, Steiner et al. 2014, Stephan et al. 2015). Hence, if the equivalent of static resistance $q_{c,eq}$ is assumed to equals the cone resistance achieved by CPT tests, the shear strength of sediment can be determined using the methods proposed for CPT testing.

1.2.4 Bearing capacity of soil

The forces resisting the advancement of penetrating probe in soil are similar to the forces resisting the bearing failure of foundations (True 1976). Thus, the capability of soil to resist a penetrating probe can be compared to the soil bearing capacity. The bearing capacity is the maximum load (or critical load) per unit area that the soil can take without failing (Terzaghi 1943). In other words,

the bearing capacity is the minimum stress that triggers failure for the soil. The bearing capacity of the soil depends on the soil properties and size, shape and depth of the loaded area. The bearing capacity equation that considers soil cohesion, friction and surcharge weight was first introduced by Terzaghi (1943). The ultimate bearing capacity equation for strip foundations is:

$$q_u = cN_c + \frac{1}{2}B\,\gamma_s N_\gamma + qN_q \tag{1.6}$$

where q_u is the ultimate bearing capacity of soil, c is soil cohesion, B is the width of the foundation, γ_s is the effective unit weigh of soil below the foundation base, q is the surcharge weight of the soil above the foundation base, and N_c, N_γ and N_q are bearing capacity factors which their value depend on ϕ. A more detailed bearing capacity equation was propose by Brinch Hansen (1961) which takes to consideration the shape of the load and the embedment depth. The equation for vertical loads is:

$$q_u = cN_c d_c \xi_c + \frac{1}{2}B\,\gamma_s N_\gamma d_\gamma \xi_\gamma + qN_q d_q \xi_q \tag{1.7}$$

$$N_q = e^{\pi\, tan\phi}\; tan^2\,(45 + \phi/2) \tag{1.8}$$

$$N_c = (N_q - 1)\; cot\phi \tag{1.9}$$

$$N_\gamma = 1.8\,(N_q - 1)\; tan\phi \tag{1.10}$$

$$d_c = 1.0 + \frac{0.35}{\frac{B}{D} + [0.6/(1 + 7tan^4\phi)]} \tag{1.11}$$

$$d_\gamma = 1 \tag{1.12}$$

$$d_q = d_c - \frac{d_c - 1}{N_q} \tag{1.13}$$

$$\xi_c = 1 + (0.2 + tan^6\phi)\frac{B}{L} \tag{1.14}$$

$$\xi_\gamma = 1 - \frac{1}{2}(0.2 + tan^6\phi)\frac{B}{L} \tag{1.15}$$

$$\xi_q = \xi_c - \frac{\xi_c - 1}{N_q} \tag{1.16}$$

where d_c,d_γ,d_q are depth factors for cohesion, friction, and surcharge, ξ_c, ξ_γ, ξ_q are empirical shape factors for cohesion, friction, and surcharge, L is the foundation length, and *D* is the embedment depth. Later on, corrections were suggested for some of these factors. These corrections will not be discussed here, because it is not within the scope of this dissertation.

Equations 1.6 and 1.7 were derived for flat base footings. Meyerhof (1961) proposed a method to determine the bearing capacity for wedged and cone shaped foundations. An advantage of Meyerhof's method is that it distinguishes between deep and shallow penetrations as well as the base roughness. However, only perfectly smooth and perfectly rough cases were considered, and Meyerhof suggested using linear interpolation to estimate other roughness degrees. For conical shapes, the bearing capacity equation was:

$$q_r = cN_{cr} + p_o N_{qr} + \frac{1}{2}\gamma B N_{\gamma r} \tag{1.17}$$

where $p_o = K_b \gamma D$, K_b is an earth pressure factor (0.5 for sand and 1.0 for clay), and N_{qr} and $N_{\gamma r}$ are bearing capacity factors. Durgunoglu and Mitchell (1973) showed that there are shortcomings for the Meyerhof (1961) method including that the method distinguishes only between shallow ($D/B \leq 1$) and deep penetrations ($D/B \geq 4$) and between the completely smooth and rough base, while an interpolation is required for intermediate cases. Nevertheless, this method was found to achieve reasonable results to estimate the friction angle of sand from CPT measurements (e.g., Mitchell and Lunne 1978; Lunne and Christoffersen 1983).

Durgunoglu and Mitchell (1973) introduced a rigorous bearing capacity approach to determine the shear strength parameters of soil from CPT tests. This approach distinguishes between a shallow and a deep penetration by specifying a "critical depth". This depth depends on the friction angle, cone roughness and penetrometer tip angle. The cone resistance, q_c, can be represented by:

$$q_c = cN_c\xi_c + \gamma_s B N_{\gamma q}\xi_{\gamma q} \tag{1.18}$$

where γ_s is the submerged unit weight of soil, *B* is the penetrometer diameter, $N_{\gamma q}$ is the bearing capacity factor which includes both friction and surcharge factors (N_γ, N_q), and ξ_c and $\xi_{\gamma q}$ are shape factors. The values of N_c and $N_{\gamma q}$ depend on the effective friction angle ϕ', cone roughness δ/ϕ', the penetration depth normalized to the penetrometer diameter *D/B*, and the penetrometer tip angle α. Later on, cavity expansion theory based methods were proposed to determine the shear strength

parameters from CPT tests (some of these methods are summarized by Yu and Mitchell (1998)); however, these methods are not within the scope of this dissertation and will not be discussed here.

1.2.5 Shear Strength of Sand

The seabed resistance for a PFFP penetration is controlled by the shear strength of sediments. The shear strength of soil is also essential for any type of geotechnical analyses or design. Additionally, the shear strength parameters of sand, specifically, the friction angle and correlated angle of repose, control the critical shear stress required for the initiation of motion and then sediment transport (e.g., Kirchner et al. 1990). Therefore, it is important to investigate the factors that affect the shear strength of sand.

Sand is considered as a drained material under conventional loads. The shear strength of sand is usually represented by Mohr-Coulomb strength envelope equation:

$$s = c' + \sigma' \tan \phi' \tag{1.19}$$

where s is the shear strength, c' is the cohesion intercept, σ' is the effective normal stress on the failure plane, and ϕ' is the effective stress friction angle. Since the sand is a cohesionless material, the shear strength envelope of sandy soils should pass by zero at zero σ'. Consequently, the shear strength of sand can be represented by the second term of the equation only (i.e. $s = \sigma' \tan \phi'$). Different factors affect the value of the friction angle and the shape of the failure envelope including confining pressure, relative density, particles size and distribution, mineralogy, and particles shapes. The soil mineralogy does not usually change in the same location while the other factors can vary within the same location. The effect of these factors on the sand friction angle can be summarized as follows:

1.2.5.1 Effect of the confining pressure

The Mohr-Coulomb envelope slope for sandy soils changes depending on the confining pressure. This change is due to the variation in the tendency for volume change and particle crushing with changes in confining pressures. Lee and Seed (1967) discussed the effect of the confining pressure on the three sources of the friction angle of sand: surface friction, volume change, and crushing.

They suggested that the sliding friction angle is almost constant at any confining pressure because it depends only on the material properties. At low confining pressures, crushing of the particle is not expected, thus the shear stress (and then the friction angle) is due to sliding friction, rearrangement of particles and related dilatancy (particle rolling over neighboring particles) (Figure 1.5). Increasing the confining pressure results in a decrease in the dilatant behavior, but the particles crushing increases. Under high confining pressures, particles crushing requires less energy than the energy required for rearrangement or rolling (Duncan et al. 2014). This results in a curvature in the failure envelope. Therefore, using an average failure envelope may result in underestimating the friction angle at low confining pressures and overestimating for the friction angle at high confining pressures.

Different methods have been suggested to address the curvature in the failure envelope. The least used method is using a cohesion intercept as done by Ponce and Bell (1971) who found using a cohesion intercept appropriate to represent the failure envelope at extremely low confining pressures. The use of the secant friction angle represents a practical method to address the change in the failure envelope with the confining pressure change (Terzaghi et al. 1996; Duncan et al. 2014). In this method, the friction angle is determined by measuring, or by calculating, the angle between the abscissa and the line tangent to Mohr's circle and passes by the origin (Figure 1.5). Following this method, the friction angle is expected to decrease with the increase of the confining pressure for samples prepared at the same initial void ratio. Another method to determine the friction angle is using the ϕ_0 and $\Delta\phi$ method (Duncan et al. 2014), which can be formulated as follows.

$$\phi' = \phi_0 - \Delta\phi \, log_{10} \left(\frac{\sigma_3'}{p_a}\right) \tag{1.20}$$

where ϕ_0 is the value of friction angle at confining pressure of one atmosphere, $\Delta\phi$ is the reduction in friction angle for a 10-fold increase in confining pressure, σ_3' is the confning pressure, and p_a is atmospheric pressure.

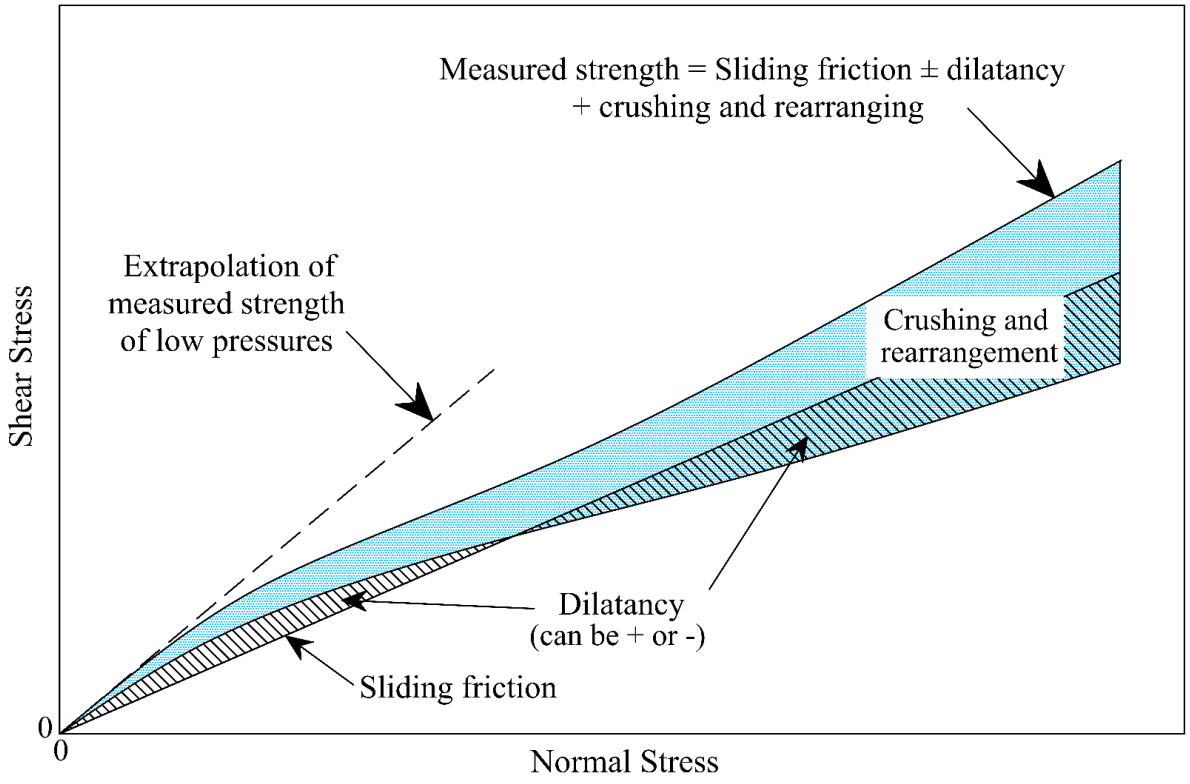

Figure 1.4. Schematic illustration of the contribution of sliding friction, dilatancy and crushing to the measured Mohr envelope for drained tests on sand (replotted after: Lee and Seed 1967).

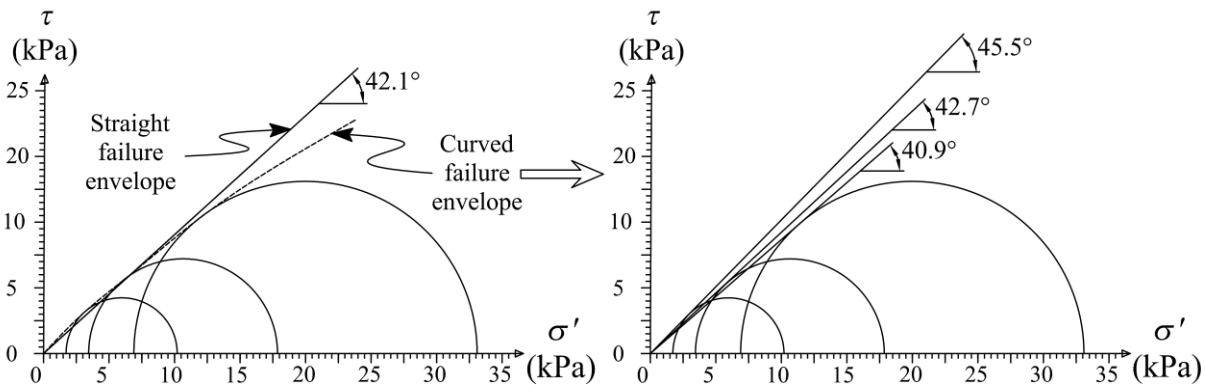

Figure 1.5. Straight failure enveloped versus curved failure envelope. Shown results are for sand samples from Cannon Beach, Yakutat, AK tested in vacuum triaxial test at initial relative density of 40%.

1.2.5.2 Effect of the relative density

The relative density is the most important property of cohesionless sediments (Terzaghi et al. 1996). The ASTM D4253 defines the relative density as "the ratio, expressed as a percentage, of the difference between the maximum index void ratio and any given void ratio of a cohesionless, free-draining soil; to the difference between its maximum and minimum index void ratios". The sand's natural (field) void ratio can be determined directly using in-situ tests (e.g., sand cone method ASTM D1556), or indirectly using correlations. The maximum void ratio is the void ratio associated with the minimum possible dry unit weight of soil while the minimum void ratio is the void ratio associated with the maximum possible dry unit weight of soil. The maximum and minimum void ratios are usually determined in the laboratory following the ASTM D4254 and D4253 procedures, respectively.

The friction angle of sand increases with the relative density increase. This is due to the change in the relatively easy movement for particles in loose packing versus dense packing (Terzaghi et al. 1996). For the same sand, the difference between the friction angle in dense state and loose state depends on the confining pressure. This difference is higher for low confining pressures, and decreases with the increase of the confining pressures (Andersen and Schjetne 2013; Duncan et al. 2014). At low confining pressures, the tendency of dilation is larger which results in a relatively larger freedom for a particle to roll over the neighboring particles.

1.2.5.3 Effect of grain size and gradation

If the sand is well graded, the small particles tend to fill the gaps of the larger particle. This result in forming a denser pack compared to uniform sand which in turn results in higher shear strength (Duncan et al. 2014). On the other hand, it seems that there is no agreement on the effect of the particle size on the friction angle value. Schmertmann (1978) suggested that the friction angle of sand increases with the grain size increase. However, Andersen and Schjetne (2013) found that the Norwegian Geotechnical Institute database does not support this suggestion. Actually, it has been found that the sand penetration resistance decreases with the particle size increase (Stark et al. 2009, 2012a). It should be emphasized here that these observations were found for clean sand (i.e. no fines content) with a small range of particle size (i.e. uniform sand).

1.2.5.4 Effect of particle shape

Cho et al. (2006) pointed out that the particle shape is a significant soil index property that needs to be appropriately characterized especially in clean sands and gravels. They defined three scales for the particle shape sphericity, roundness, and roughness or surface texture. As the roughness of soil increases, the tendency to dilate increases especially for densely packed sands (Santamarina and Cho 2004). As the particle surface becomes rougher, the particle-particle friction is enhanced which increases the shearing resistance of sand. With regard to the sphericity and roundness, Stark et al. (2014a) found that flat, elliptic shaped particles from Advocate Beach exhibit a larger friction angle due to particles re-arrangement and alignment. However, the research on the effect of particle shape on the shear strength of sediments is still limited probably, because the particle shape characteristics are difficult to measure (Das and Sobhan 2013; Zheng and Hryciw 2015).

1.3 Gaps in Knowledge

One of the early steps of any site investigation is to determine the soil type (i.e. classify the sediments). Although the currently available PFFPs do not carry a sampling unit, limited soil classification schemes were suggested based on the PFFP measurements. For example, Stoll and Akal (1999) classified the sediments based on the maximum deceleration of the eXpendable Bottom Penetrometer (*XBP*) into three broad categories: granular, fine-grained, and intermediate sediments. Mulukutla et al. (2011) suggested a more detailed classification scheme based on a so-called Firmness Factor that is a function of the maximum deceleration, impact velocity and the penetration time. Moreover, the deceleration records, and derived quasi-static bearing capacities (*qsbc)* were found to reflect different sediment properties including particle size, mineralogy, and sand relative density (Akal and Stoll 1995; Mulukutla et al. 2011; Stark et al. 2012a, 2012b). However, the sediment response depends not only on the sediment properties, but also varies with the variation of the probe geometry and penetration velocity. This makes it difficult to characterize the sediments based on the measured deceleration or even derived *qsbc* alone. Another potential issue is that the existing classification schemes were developed based on laboratory or field tests in non-energetic environments. In such environments, the effect of the wave impact results in an additional variability in the strength which is not taken to account in these classification schemes. Therefore, using a classification scheme that was developed for a specific site or a certain

penetrometer might not be transferable to other areas and/or other penetrometers. Thus, a strategy to develop a local sediment classification scheme for each investigated region and device would represent a more transferable approach, ensuring the applicability of the classification scheme. Such a strategy should include using more than only the measured deceleration and its derivatives.

The pore water pressure (PWP) response during the CPT penetration was found to complement the cone and sleeve friction measurements and to reveal additional soil characteristics like soil permeability and stress history (e.g., Robertson et al. 1992; Burns and Mayne 1998; Mayne 2001; Sandven 2010). The PWP measurements in CPT tests have become an essential part of the tests especially in offshore site investigation (e.g., Lunne 2012). However, the studies on the pore pressure behavior during and after the fast penetrations by PFFPs are still limited. For example, Stegmann et al. (2006) noticed that the PWP in clay increases during penetration but dissipates shortly afterwards, and concluded that impact penetrometers are capable of detecting different pore pressure responses including the PWP caused by deployment artefacts (i.e. water being pushed away from the probe affected by the rapid penetration) and due to the sediment natural properties. Seifert et al. (2008) found that the PWP during penetration and dissipation differ in different soil types and highlighted the possibility of characterizing the sediments using PWP obtained from an impact penetrometer. Following that, Stark et al. (2015) linked the sedimentation history of clay to the PWP behavior. These findings highlighted the possibility of utilizing the PWP measurements during and after penetration to characterize the seabed sediments, and potentially develop soil behavior charts similar to the commonly used charts to classify the sediments based on the CPT cone resistance and pore pressure measurements.

One of the preliminary site investigation tasks is to determine sediment dynamics and to study the region's morphodynamics (Figure. 1.1) (Danson 2005; Stark et al. 2014b). Sediment dynamics result in variations in beach profile, and affect the sediment strength and scour processes, which in turn influence the stability of any structure on the seabed. More specifically, the bar migration represents the main component that controllers the beach profile variability, and influences the short and long-term beach stability (Lippmann and Holman 1990; Plant et al. 1999). This is mainly due to the daily changes in magnitude and direction of waves and associated currents which results in a complex and dynamic profile in the nearshore zone (Johnson 1956; Lippmann and Holman 1990; Schwartz and Birkemeier 2004). In general, long periods of low wave energy result in a steep profile with discontinuous or no bars, while the slope becomes less steep and offshore bars

become more noticeable during storms (Lippmann and Holman 1990; Dean and Dalrymple 2004). During low wave energy periods, the onshore sediment transport is caused by near-bottom wave orbital motions (Fernández-Mora et al. 2015). The offshore-directed flow (undertow) becomes strong during storms which results in a net offshore sediment transport (Dean and Dalrymple 2004; Davidson-Arnott 2013).

Generally, the effect of the remobilization and redeposition processes on the geotechnical properties of the topmost sediment layers has rarely been investigated. Such processes are controlled by the hydrodynamics in addition to the different variables that affect the sediment behavior and strength such as particle size, shape, gradation, fabric, density, and composition (e.g., Dean and Dalrymple 2004; Davidson-Arnott 2013). Accordingly, a detailed site-specific characterization is required to map the areas of significant sediment remobilization processes, and to quantify mobile sediment layers with a high resolution (Stark and Kopf 2011). Characteristics of the mobile sediment layers can be investigated using different methods like multi beam echo sounders, acoustic Doppler profilers, bedload samplers, or portable free fall penetrometers (Stark and Kopf 2011; Bilici and Stark 2017). Most of the acoustic methods detect zones of sediment erosion and deposition, and allow the detection of suspended sediments; however, they might fail to distinguish between the loosely deposited top layers and underlying stable bed layers (Stark and Kopf 2011). Direct sampling from the bed is expensive, time-consuming, and the samplers tend to disturb the sediments and flow (Gaeuman and Jacobson 2006). PFFPs have been used successfully to map the areas of significant sediment transport, and to quantify the thickness of mobile sediment layers due to the layer's distinguished signature in the *qsbc*-depth profile (Stark and Kopf 2011). However, similar to the direct sampling, a disadvantage of using PFFP is that discrete points are obtained which needs an interpolation to obtain a complete map for the sedimentation processes. Unlike the seabed samplers, such a disadvantage can be easily mitigated in the case of PFFPs by using a small distance between the investigated points.

Due to the high sampling rate for the Micro-electro-mechanical systems (MEMS) accelerometers (up to 2 kHz), PFFPs can detect thicknesses of the active surface layers with less than 1 cm resolution. Stark and Kopf (2011) used the PFFP *Nimrod* (sampling rate of 1 kHz) in a laboratory wave channel and in different locations in the field, and found that PFFPs can be used to quantify the mobile sediment layer, being represented by loose sediment top layers, with a resolution of about 1 cm. Bilici and Stark (2017) developed a sampler add-on unit that can be used as a

replacement for the PFFP *BlueDrop* tip in order to collect samples from the topmost sediment layers including the mobile layers. However, the sampler is still under development and testing, and has not been proven to work properly in energetic areas, yet. On the other hand, limited studies are available that correlate the nearshore hydrodynamics and morphodynamics to the geotechnical sediment properties, and more studies are still needed to link the different sediment remobilization and redeposition processes to the geotechnical characteristics of the seabed sediments.

PFFPs have mostly been deployed in clayey sediments. Different approaches were proposed to estimate the undrained shear strength of clay based on controlled laboratory tests (e.g., Chow and Airey 2014), numerical modelling (e.g., Aubeny and Shi 2006; Nazem et al. 2012), centrifuge models (e.g., Morton et al. 2015; Chow et al. 2017), or field tests in comparison to other testing method like CPT (e.g., Steiner et al. 2014). Although sand represents the most predominant surficial sediment type on the continental shelves and in nearshore areas (Shore Protection Manual 1974; Richards et al. 1975), the use of PFFP in sandy areas is still limited. This is due to limitations like the small penetration depth, and that sand behaves mostly as an undrained material for the case of large penetration velocity (> 2 m/s) which disagrees with the fact that sand behaves as a drained material under conventional static loads. For these reasons, no method has been proposed, and validated to estimate the sand shear strength, or more specifically, in-situ friction angles from lightweight PFFP deceleration measurements. Currently, the analysis of deployments in sand are usually concluded with determining the dynamic forces exerted by the sediments during penetration, or an equivalent cone resistance for the deceleration measurements (Akal and Stoll 1995; Stoll et al. 2007; Stark et al. 2009, 2012b, 2017, Stephan et al. 2011, 2015; Lucking et al. 2017). This results in the need for a method to estimate the in-situ friction angle of sands from PFFP measurements. Accordingly, this dissertation is mainly focused on advancing the use of PFFPs in sandy sediments.

1.4 Contributions

This research makes the following briefly summarized contributions:

1. A methodology to create a regional sediment classification scheme to develop sediment distribution maps in areas of difficult access and logistics was proposed. The classification scheme was created utilizing the PFFP deceleration and pore pressure measurements from 149 deployments in Yakutat Bay, Alaska in addition to the sediment traces on the probe upon retrieval and previous literature.

2. The effect of the geomorphodynamics, and specifically, sandbar migration, and depth of closure on the sediment strength was investigated in energetic nearshore environments, using data sets from Cannon Beach, Yakutat AK and the United States Army Corps of Engineers' Field Research Facility's beach, Duck, NC. This included the quantification of spatial and temporal changes in sediment strength. The deployments were conducted in different wave climates from calm to stormy. A relationship was found between the sediment strength and wave conditions. A coefficient of wave impact on the sediment strength was then investigated.

3. A method of determining the friction angle of sand from PFFPs was proposed utilizing two bearing capacity based methods that are commonly used to determine the friction angle for sand from Cone Penetration Tests. The resulting friction angles were compared to estimates of relative density supported by laboratory vacuum triaxial tests conducted at low confining pressures that simulate the limited penetration depths achieved by PFFP. The relative densities were estimated based on laboratory tests in which a PFFP was deployed to sand samples prepared at different relative densities. The resulting in-situ friction angles agree well with many previous studies to determine the sand friction angles from Cone Penetration Tests.

1.5 Dissertation Structure and Content

The chapters of this dissertation consist of a series of paper manuscripts, which are combined to make the contributions outlined in the previous section. The dissertation contains an introductory chapter, five manuscript chapters, and four appendices.

Chapter 2 is introducing a simple sediment classification scheme that was developed based on a) available sediment classification schemes in the literature, b) limited existing sediment information from literature, and c) PFFP deceleration and pore pressure measurements. One hundred and forty-nine deployments were conducted in Yakutat Bay, Alaska that is characterized by spatial variability in hydrodynamic conditions, geomorphology, sedimentation processes, and sediment types were utilized to create the sediment classification scheme. The sediment classification scheme was then used to fill the gaps in existing sediment distributions maps. In this chapter, a novel method to investigate fine sediment sedimentation history using PFFP pore pressure measurements was introduced.

Chapter 3 is an early site assessment for the proposed WEC site near Cannon Beach, Yakutat, Alaska using a PFFP. Here, 151 deployments were utilized to investigate the spatial variation in the sediment bearing capacity. This location was characterized by negligible variations in sediment particle size. It was found that deeper water depths were associated with (i) a decrease in the penetration depth, an increase in the sediment bearing capacity, and a decrease in the loose top layer thickness.

Chapter 4 purpose is to estimate the sand friction angle from the PFFP deceleration measurements in order to derive a relevant engineering design parameter from the PFFP measurements. Four steps were followed to determine the sand friction angle. Step 1: estimate the field friction angle utilizing the equivalent cone resistance, derived from the deceleration-time records, using Durgunoglu and Mitchell (1973) and Meyerhof (1961) bearing capacity methods. Step 2: determine the sand friction angle in the laboratory using vacuum triaxial test at low confining pressures. Step 3: determine the field friction angle utilizing laboratory test of deploying a PFFP into sand at different relative densities in association with Duncan et al. (2014)'s correlation that estimates the friction angle based on the relative density, confining pressure and grain size distribution. Step 4: Compare the results of step 1 to the results of step 3 in order to validate the friction angles estimated using Durgunoglu and Mitchell (1973) and Meyerhof (1961).

Chapter 5 assesses the effect of the geomorphodynamics, and specifically, sandbar migration, and depth of closure on the sediment strength in energetic nearshore environments. Eighty deployments in four cross-shore transects were conducted in the energetic nearshore zone of the U.S. Army Corps of Engineers Field Research Facility at Duck, NC. A strong relationship was found between geotechnical characteristics and active morphodynamics of the nearshore seabed. The depth of closure was also reflected in the PFFP results.

Chapter 6 investigates the spatial and short-term temporal nearshore sandy sediment characteristics using a portable free fall penetrometer. A PFFP was deployed 335 times over six non-consecutive days Field Research Facility's 560 m long pier. During the surveying period, the significant wave heights varied between 0.8-2.4 m. A relationship between the wave heights and sediment strength was found, which can be correlated to the sediment transport and bar migration direction. In this manuscript, the coefficient of wave impact on sediment surface strength (*CWS*) proposed by Bilici et al. (2018) to characterize the sediments in energetic nearshore areas considering both the sediment geotechnical properties measured by PFFP and the effect of the waves was investigated. The *CWS* was found to reflect both the wave breaking and depth of closure.

Appendix A contains the data repository information and link in addition to the readme file that describes the repository files organization and contents.

Appendix B contains a summary of the laboratory tests conducted on Cannon Beach's sand. The laboratory tests included sieve analysis, vacuum triaxial tests and direct shear tests.

Appendix C is a comparison between the results of the PFFP deployments in nearshore zones of Cannon Beach, AK and the USACE's Field Research Facility Beach, NC (i.e. Chapters 3 and 5). The purpose here is to illustrate the effect of the variations in the particle size and wave climate in the PFFP measurements.

Appendix D is the abstract of a conference manuscript that is related to the research, but the dissertation author is not the lead author of this manuscript. The manuscript is titled "Quantifying the effect of wave action on seabed surface sediment strength using a portable free fall penetrometer". This manuscript introduces the coefficient of wave impact on sediment surface strength (*CWS*).

Appendix E is also an abstract of a manuscript that is related to the research but the dissertation author is not the lead author of this manuscript. The manuscript is titled "Friction angles at sandy beaches from remote imagery". Here, a novel method to estimate the lower bound friction angle using satellite and camera's images was introduced.

1.6 References

Akal, T., and Stoll, R. D. (1995). "An expendable penetrometer for rapid assessment of seafloor parameters." OCEANS 1995. *MTS/IEEE, Challenges of Our Changing Global Environment.*, IEEE, San Diego, CA, 1822–1826.

Andersen, K. H., and Schjetne, K. (2013). "Database of Friction Angles of Sand and Consolidation Characteristics of Sand, Silt, and Clay." *Journal of Geotechnical and Geoenvironmental Engineering*, ASCE, 139(7), 1140–1155.

Aubeny, C. P., and Shi, H. (2006). "Interpretation of Impact Penetration Measurements in Soft Clays." *Journal of Geotechnical and Geoenvironmental Engineering*, 132(6), 770–777.

Baecher, G. B., and Christian, J. T. (2003). *Reliability and Statistics in Geotechnical Engineering*. Wiley.

Bilici, C., and Stark, N. (2017). "Design and Preliminary Tests of Mobile Seafloor Layer Sampler Prototypes as an Add-On Unit for Portable Free-Fall Penetrometers." *Geotechnical Frontiers 2017*, Proceedings, ASCE, 379–388.

Bilici, C., Stark, N., Albatal, A., Wadman, H., and McNinch, J. E. (2018). "Quantifying the effect of wave action on the seabed surface sediment strength using a portable free fall penetrometer." *4th International Symposium on Cone Penetration Testing, CPT'18*, ISSMGE, Delft, Netherlands.

Biscontin, G., and Pestana, J. M. (2001). "Influence of peripheral velocity on vane shear strength of an artificial clay." *Geotechnical Testing Journal*, ASTM International, 24(4), 423–429.

Brinch Hansen, J. (1961). "A General Formula for Bearing Capacity." *Bulletin No, 11, 1961, Danish Geotechnical Institute*, 38–46.

Burns, S. E., and Mayne, P. W. (1998). "Penetrometers for soil permeability and chemical detection." *Report No GIT-GEEGEO-98-1 prepared for NSF and ARO*, Georgia Institute of Technology. Atlanta, GA.

Casagrande, A., and Shannon, W. L. (1949). "Strength of soils under dynamic loads." *Transactions of the American Society of Civil Engineers*, ASCE, 114(1), 755–772.

U.S. Army Corps of Engineers (1974). *Shore protection manual*. Coastal Engineering Research Center, U.S. Army Coastal Engineering Research Center.

Chari, T. R., Smith, W. G., and Chaudhuri, S. N. (1981). "Development of the Free-Fall Penetrometer." *OCEANS 81*, IEEE, Boston, MA, 678–682.

Cho, G.-C., Dodds, J., and Santamarina, J. C. (2006). "Particle Shape Effects on Packing Density, Stiffness, and Strength: Natural and Crushed Sands." *Journal of Geotechnical and Geoenvironmental Engineering*, ASCE, 132(5), 591–602.

Chow, S. H., and Airey, D. W. (2014). "Free-Falling Penetrometers: A Laboratory Investigation in Clay." *Journal of Geotechnical & Geoenvironmental Engineering*, 140(1), 201–214.

Chow, S. H., O'Loughlin, C. D., White, D. J., and Randolph, M. F. (2017). "An extended interpretation of the free-fall piezocone test in clay." *Géotechnique*, 67(12), 1–14.

Cook, M., Barwise, A., Cleverly, W., Hobbs, R., Hodgson, T., James, L., Jenner, C., Morgan, N., Wood, A. M., Orren, R., Osborne, J., Rowland, R., and Wark, C. (2014). *Guidance Notes for the Planning and Execution of Geophysical and Geotechnical Ground Investigations for Off shore Renewable Energy Developments*. The Society for Underwater Technology, London, UK.

Danson, E. (2005). *Geotechnical and geophysical investigations for offshore and nearshore developments*. Technical Committee 1, International Society for Soil Mechanics and Geotechnical Engineering ISSMGE.

Das, B. M., and Sobhan, K. (2013). *Principles of geotechnical engineering*. Cengage Learning.

Davidson-Arnott, R. G. D. (2013). "Nearshore Bars." *Treatise on Geomorphology*, Academic Press, San Diego, 130–148.

Dayal, U. (1980). "Free fall penetrometer: a performance evaluation." *Applied Ocean Research*, 2(1), 39–43.

Dayal, U., and Allen, J. H. (1973). "Instrumented Impact Cone Penetrometer." *Canadian Geotechnical Journal*, 10(3), 397–409.

Dayal, U., Allen, J. H., and Jones, J. M. (1975). "Use of an Impact Penetrometer for the Evaluation of the In-Situ Strength of Marine Sediments." *Marine Geotechnology*, 1(2), 73–89.

Dean, R. G., and Dalrymple, R. A. (2004). *Coastal processes with engineering applications*. Cambridge University Press.

Dorvinen, J. I. (2016). “A Method for Interpreting the In-Situ Consolidation State of Surficial Seabed Sediments using a Free-Fall Penetrometer.” M.S. Thesis, Virginia Polytechnic Institute and State University. Blacksburg, Virginia

Duncan, J. M., Wright, S. G., and Brandon, T. L. (2014). *Soil strength and slope stability*. John Wiley & Sons, Hoboken, NJ.

Durgunoglu, H. T., and Mitchell, J. K. (1973). *Static penetration resistance of soils*. Research report number NASA-CR-133460, prepared for NASA Headquarters, Washington, D.C.

Fabian, M., Kaul, N., and Gmeinder, T. (2008). “The Bremen lance insertion retardation (LIR) meter to assess sea floor stability.” *Sea Technol*ogy, 49(10), 10–13.

Fernández-Mora, A., Calvete, D., Falqués, A., and de Swart, H. E. (2015). “Onshore sandbar migration in the surf zone: New insights into the wave-induced sediment transport mechanisms.” *Geophysical Research Letters*, 42(8), 2869–2877.

Gaeuman, D., and Jacobson, R. B. (2006). “Acoustic bed velocity and bed load dynamics in a large sand bed river.” *Journal of Geophysical Research: Earth Surface*, 111(F2), 1–14.

Gillon, R. (2008). “The ROV in Nearshore Site Investigation.” Hydro International, <https://www.hydro-international.com/content/article/the-rov-in-nearshore-site-investigation>.

Hodgson, A. J., Adam, C. H., and Sneddon, M. (1995). “Recent developments in planning and execution of nearshore site investigation.” *Advances in site investigation practice*, 13–24.

Holman, R. (1995). “Nearshore processes.” *Reviews of Geophysics*, 33(S2), 1237–1247.

Holubec, I. (2010). *Geotechnical site investigation guidelines for building foundations in permafrost*. Department of Public Works and Services, Government of the Northwest Territories.

ISO. (2012). “Geotechnical investigation and testing -- Field testing -- Part 1: Electrical cone and piezocone penetration test.” *ISO International*.

Jaksa, M. B. (2000). “Geotechnical Risk and Inadequate Site Investigations: A Case Study.” *Australian Geomechanics*, 35(2), 39–46.

Jeanjean, P., Spikula, D., and Young, A. (2012). “Technical Vetting of Free-Fall Cone Penetrometer.” *SUT Offshore Site Investigation and Geotechnics*, 15–18.

Johnson, J. W. (1956). “Dynamics of nearshore sediment movement.” *AAPG Bulletin, American Association of Petroleum Geologists*, 40(9), 2211–2232.

Kirchner, J. W., Dietrich, W. E., Iseya, F., and Ikeda, H. (1990). "The variability of critical shear stress, friction angle, and grain protrusion in water-worked sediments." *Sedimentology*, Blackwell Publishing Ltd, 37(4), 647–672.

Kulhawy, F. H., and Mayne, P. W. (1990). *Manual on estimating soil properties for foundation design*. Electric Power Research Inst., Palo Alto, CA (USA); Cornell Univ., Ithaca, NY (USA). Geotechnical Engineering Group.

Lee, K. L., and Seed, H. B. (1967). "Drained strength characteristics of sands." *Journal of Soil Mechanics and Foundations Division*, SM6, 117–141.

Lippmann, T. C., and Holman, R. a. (1990). "The spatial and temporal variability of sand bar morphology." *Journal of Geophysical Research*, 95(C7), 11575.

Lucking, G., Stark, N., Lippmann, T., and Smyth, S. (2017). "Variability of in situ sediment strength and pore pressure behavior of tidal estuary surface sediments." *Geo-Marine Letters*, 37(5), 441-456.

Lunne, T. (2012). "The Fourth James K. Mitchell Lecture: The CPT in offshore soil investigations-a historic perspective." *Geomechanics and Geoengineering*, Taylor & Francis, 7(2), 75–101.

Lunne, T., Berre, T., and Strandvik, S. (1998). "Sample disturbance effects in deep water soil investigations." *Offshore Site Investigation and Foundation Behaviour 'New Frontiers: Proceedings of an International Conference, Society of Underwater Technology*, London, UK, 199–220,

Lunne, T., and Christoffersen, H. P. (1983). "Interpretation of Cone Penetrometer Data for Offshore Sands." *Offshore Technology Conference*, Houston, TX, 181–188.

Lunne, T., and Long, M. (2006). "Review of long seabed samplers and criteria for new sampler design." *Marine Geology*, 226(1), 145–165.

Mayne, P. W. (2001). "Stress-strain-strength-flow parameters from enhanced in-situ tests." *International Conference on In-Situ Measurement of Soil Properties & Case Histories* (In-Situ 2001), Bali, Indonesia, 27–48.

McNinch, J. E. (2004). "Geologic control in the nearshore: shore-oblique sandbars and shoreline erosional hotspots, Mid-Atlantic Bight, USA." *Marine Geology*, 211(1), 121–141.

Meyerhof, G. G. (1961). "The ultimate bearing capacity of wedge-shaped foundations." *Proceedings, 5th International Conference on Soil Mechanics and Foundation Engineering ICSMFE*, Paris, 105–109.

Mitchell, J. K., and Lunne, T. A. (1978). "Cone resistance as measure of sand strength." *Journal of the Geotechnical Engineering Division*, 104(7), 995–1012.

Morton, J. P., O'Loughlin, C., and White, D. (2015). "Centrifuge modelling of an instrumented free-fall sphere for measurement of undrained strength in fine-grained soils." *Canadian Geotechnical Journal*, 53(6), 918–929.

Mulukutla, G. K., Huff, L. C., Melton, J. S., Baldwin, K. C., and Mayer, L. A. (2011). "Sediment identification using free fall penetrometer acceleration-time histories." *Marine Geophysical Research*, 32(3), 397–411.

Nazem, M., Carter, J., Airey, D., and Chow, S. (2012). "Dynamic analysis of a smooth penetrometer free-falling into uniform clay." *Géotechnique*, 62(10), 893–905.

Peuchen, J. (2012). "Site characterization in nearshore and offshore geotechnical projects." *4th Geotechnical and geophysical site characterization Conference*, Porto de Galinhas, Pernambuco, Brazil, 83–112.

Plant, N. G., Holman, R. A., Freilich, M. H., and Birkemeier, W. A. (1999). "A simple model for interannual sandbar behavior." *Journal of Geophysical Research: Oceans*, 104(C7), 15755–15776.

Ponce, V. M., and Bell, J. M. (1971). "Shear strength of sand at extremely low pressures." *Journal of Soil Mechanics & Foundations Division*, SM4, 625–638.

Randolph, M., Cassidy, M., Gourvenec, S., and Erbrich, C. (2005). "Challenges of offshore geotechnical engineering." *Proceedings of the 16th International Conference on Soil Mechanics and Geotechnical Engineering*, Balkema Publishers, 123–176.

Randolph, M. F. (2004). "Characterisation of soft sediments for offshore applications." *Proceedings of the 2nd International Conference on Site Characterisation*, Porto, Portugal, 209–231.

Randolph, M. F., and Gourvenec, S. M. (2011). *Offshore Geotechnical Engineering*. Spon Press.

Richards, A. F., Palmer, H. D., and Perlow, M. (1975). "Review of continental shelf marine geotechnics: Distribution of soils, measurement of properties, and environmental hazards." *Marine Geotechnology*, Taylor & Francis, 1(1), 33–67.

Robertson, P. K., Sully, J. P., Woeller, D. J., Lunne, T., Powell, J. J. M., and Gillespie, D. G. (1992). "Estimating coefficient of consolidation from piezocone tests." *Canadian Geotechnical Journal*, 29(4), 539–550.

Sandven, R. (2010). “Influence of test equipment and procedures on obtained accuracy in CPTU.” *2nd International Symposium on Cone Penetration Testing*, Huntington Beach, CA, 26.

Santamarina, J. C., and Cho, G. C. (2004). “Soil behaviour: The role of particle shape.” *Advances in geotechnical engineering: The Skempton conference*, 604–617.

Schmertmann, J. H. (1978). *Guidelines for Cone Penetration Test: Performance and Design*. Federal Highway Administration Report Number FHWA-TS-78-209, Washington, DC.

Schwartz, R. K., and Birkemeier, W. A. (2004). “Sedimentology and morphodynamics of a barrier island shoreface related to engineering concerns, Outer Banks, NC, USA.” *Marine Geology*, 211(3), 215–255.

Scott, R. F. (1967). “In-place soil mechanics measurements.” *Marine geotechnique*, 263–271.

Seed, H. B., and Lundgren, R. (1954). “Investigation of the effect of transient loading on the strength and deformation characteristics of saturated sands.” *ASTM International*, ASTM, 1288–1306.

Seifert, A., Stegmann, S., Mörz, T., Lange, M., Wever, T., and Kopf, A. (2008). “In situ pore-pressure evolution during dynamic CPT measurements in soft sediments of the western Baltic Sea.” *Geo-Marine Letters*, 28(4), 213–227.

Stark, N. (2010). “Geotechnical investigation of sediment remobilization processes using dynamic penetrometers.” Ph.D. Dissertation, University of Bremen, Bremen, Germany.

Stark, N. (2016). “Geotechnical Site Investigation in Energetic Nearshore Zones: Opportunities & Challenges.” *Australian Geomechanics Journal*, 51(4), 95–107.

Stark, N., Coco, G., Bryan, K. R., and Kopf, A. (2012a). “In-Situ Geotechnical Characterization of Mixed-Grain-Size Bedforms Using A Dynamic Penetrometer.” *Journal of Sedimentary Research*, 82(7), 540–544.

Stark, N., Hanff, H., Svenson, C., Ernstsen, V. B., Lefebvre, A., Winter, C., and Kopf, A. (2011). “Coupled penetrometer, MBES and ADCP assessments of tidal variations in surface sediment layer characteristics along active subaqueous dunes, Danish Wadden Sea.” *Geo-Marine Letters*, 31(4), 249–258.

Stark, N., Hay, A. E., Cheel, R., and Lake, C. B. (2014a). “The impact of particle shape on the angle of internal friction and the implications for sediment dynamics at a steep, mixed sand–gravel beach.” *Earth Surface Dynamics*, 2(2), 469–480.

Stark, N., Hay, A. E., and Trowse, G. (2014b). "Cost-effective Geotechnical and Sedimentological Early Site Assessment for Ocean Renewable Energies." *IEEE Oceans 2014* - St. John's, Newfoundland, Canada 1–8.

Stark, N., and Kopf, A. (2011). "Detection and quantification of sediment remobilization processes using a dynamic penetrometer." *IEEE/MTS Oceans 2011*, Waikoloa, HI., 1–9.

Stark, N., Kopf, A., Hanff, H., Stegmann, S., and Wilkens, R. (2009). "Geotechnical investigations of sandy seafloors using dynamic penetrometers." *IEEE/MTS Oceans 2009*, Biloxi, MS, 1–10.

Stark, N., Quinn, B., Ziotopoulou, K., and Lantuit, H. (2015). "Geotechnical Investigation of Pore Pressure Behavior of Muddy Seafloor Sediments in an Arctic Permafrost Environment." *ASME 2015, 34th International Conference on Ocean, Offshore and Arctic Engineering (OMAE2015)*, ASME, Newfoundland, Canada, 1–10.

Stark, N., Radosavljević, B., Quinn, B. M., and Lantuit, H. (2017). "Application of a portable free-fall penetrometer for the geotechnical investigation of the Arctic nearshore zone." *Canadian Geotechnical Journal*, 54(1), 31–46.

Stark, N., Wilkens, R., Ernstsen, V. B., Lambers-Huesmann, M., Stegmann, S., and Kopf, A. (2012b). "Geotechnical Properties of Sandy Seafloors and the Consequences for Dynamic Penetrometer Interpretations: Quartz Sand Versus Carbonate Sand." *Geotechnical and Geological Engineering*, 30(1), 1–14.

Stegmann, S., Villinger, H., and Kopf, A. (2006). "Design of a Modular, Marine Free-Fall Cone Penetrometer." *Sea Technology*, (2), 27–33.

Steiner, A., Kopf, A. J., L'Heureux, J.-S., Kreiter, S., Stegmann, S., Haflidason, H., and Moerz, T. (2014). "In situ dynamic piezocone penetrometer tests in natural clayey soils—a reappraisal of strain-rate corrections." *Canadian Geotechnical Journal*, 51(3), 272–288.

Stephan, S. (2015). "A rugged marine impact penetrometer for sea floor assessment." Ph.D. Dissertation, University of Bremen, Bremen, Germany.

Stephan, S., Kaul, N., Stark, N., Villinger, H., and Wever, T. (2011). "LIRmeter: A new tool for rapid assessment of sea floor parameters. Bridging the gap between free-fall instruments and frame-based CPT." *MTS/IEEE Oceans'11*, Waikoloa, HI, 1–10.

Stephan, S., Kaul, N., and Villinger, H. (2015). "Validation of impact penetrometer data by cone penetration testing and shallow seismic data within the regional geology of the Southern North Sea." *Geo-Marine Letters*, 35(3), 203–219.

Stoll, R. D., and Akal, T. (1999). “XBP - Tool for rapid assessment of seabed sediment properties.” *Sea Technology*, 40(2), 47–51.

Stoll, R. D., Sun, Y. F., and Bitte, I. (2007). “Seafloor properties from penetrometer tests.” IEEE *Journal of Oceanic Engineering*, 32(1), 57–63.

Terzaghi, K. (1943). Theoretical soil mechanics. Wiley, New York.

Terzaghi, K., Peck, R. B., and Mesri, G. (1996). *Soil mechanics in engineering practice*. John Wiley & Sons.

True, D. G. (1976). “Undrained vertical penetration into ocean bottom soils.” Ph.D. Dissertation, Department of Civil Engineering, University of California-Berkeley, Berkeley, CA.

Young, A. G., Bernard, B. B., Remmes, B. D., Babb, L., and Brooks, J. M. (2011). “‘CPT Stinger’ - An Innovative Method to Obtain CPT Data for Integrated Geoscience Studies.” *Offshore Technology Conference*, Houston, TX.

Yu, H. S., and Mitchell, J. K. (1998). “Analysis of Cone Resistance: Review of Methods.” *Journal of Geotechnical and Geoenvironmental Engineering*, 124(2), 140–149.

Zheng, J., and Hryciw, R. D. (2015). “Traditional soil particle sphericity, roundness and surface roughness by computational geometry.” *Géotechnique*, 65(6), 494–506.

Chapter 2: Rapid sediment mapping and in-situ geotechnical characterization in challenging aquatic areas

The contributions of authors to the composition of this manuscript are delineated as follows:

Ali Albatal:

- Participated in one of the three field surveys (August 2015) conducted in Yakutat Bay.
- Initiated the idea of developing a sediment classification scheme.
- Reviewed the literature; performed all analyses; prepared figures and tables; wrote the draft manuscript.
- Addresses the comments and suggestions of the coauthor in developing the draft manuscript.
- Addressed the reviewers' comments and prepared the final version of the manuscript.

Nina Stark:

- Planned, supervised and participated in the three field surveys conducted in Yakutat Bay.
- Supervised the study.
- Helped finalizing the idea.
- Reviewed and edited the draft manuscript.
- Reviewed and edited the response to reviewers' comments and final version of the manuscript.

Rapid sediment mapping and in-situ geotechnical characterization in challenging aquatic areas

Ali Albatal and Nina Stark

Submitted to the Limnology and Oceanography: Methods Journal 11/11/2016

Accepted for Publication 05/16/2017

Published online 06/07/2019

Reference:

Albatal, A., and Stark, N. (2017). "Rapid sediment mapping and in situ geotechnical characterization in challenging aquatic areas." Limnology and Oceanography: Methods, 15(8), 690–705. DOI:10.1002/lom3.10192.

2.1 Abstract

Yakutat Bay, Southeast Alaska, is characterized by significant spatial variations in sediment type and dynamics. The northwestern side is supplied by sediments from the nearby glaciers, and is affected by longshore sediment transport processes, while the southeastern side has no direct sediment input, and is affected by human activities. In-situ seabed investigations can be difficult, and expensive, due to logistical challenges in such remote locations. A portable free fall penetrometer (PFFP) was deployed 149 times along 16 transects in water depths of 2-48 m. The deceleration and pore pressure records during the probe's penetration into the seabed were used to characterize the surficial sediments. Equivalents of quasi-static bearing capacity were determined using the deceleration-depth signatures, and yielded strong variabilities ranging from 5-107 kPa at sediment depths of 10.3-41.9 cm. Correlating the PFFP results to visual field observations and literature, a regional classification scheme, and an updated sediment distribution map were derived. The pore pressure response was correlated to the different sediment types, and was used to assess the sediment's consolidation state. At the northwestern side, an increasing pore pressure trend indicated underconsolidated cohesive sediments. At the southeastern side, clayey sediments appeared to be more consolidated except of sediments of high organic content near the populated areas. The use of the pore pressure measurements represents a novel way for rapid sediment characterization. The presented approach to create rapidly a regional sediment classification scheme offers a time- and cost-effective method to derive seabed sediment maps in areas of difficult access and logistics.

2.2 Introduction

The sediment distribution in Yakutat Bay, Southeast Alaska, is affected by glacial, climatic, and marine factors, forming a complex morphology and sediment distribution (Wright 1972). Yakutat Bay was covered by Hubbard Glacier last around 600 years ago, and currently, no ice is formed in the bay anymore (Carlson et al. 1978; Wright 1972). The historic glacial activity is expected to be reflected in a high sediment bulk density (i.e. overconsolidated) due to sediment consolidation under the expanding glaciers (Boulton and Dobbie 1993). However, the continuous deposition of sediments after the glacier's retreat results in surficial sediment layers of lower densities, being likely in a state of underconsolidation. Underconsolidated sediments are commonly found where

the sedimentation rate is more rapid than the consolidation rate, and where excess pore water pressures have not dissipated yet (Dean 2010). High sediment deposition rates have been observed in many embayments and fjords in the Gulf of Alaska (Sangrey et al. 1979). Within Yakutat Bay, the sedimentation rates and sources differ from one location to another (Tarr and Butler 1909; Molnia 1979; Cowan et al. 1996; Willems et al. 2011). With variations in sedimentation rate and source, differences in the physical and geotechnical characteristics of the uppermost seabed sediment layers are expected. However, seabed surveying can be restricted by logistical challenges in remote locations such as Yakutat. This emphasizes the need for easy deployable, time- and cost-effective tools for the mapping and characterization of seabed sediments.

Portable free fall penetrometers (PFFPs) have emerged with regard to the in-situ geotechnical investigation of the uppermost seabed layers. Different soil classification schemes have been proposed based on the PFFP deceleration-time signatures. Stoll and Akal (1999) classified the soil based on the maximum deceleration of the expendable bottom penetrometer (*XBP*) into three categories: granular, fine-grained and intermediate sediments. Stark and Wever (2009) were able to correlate sediment type, and embedded features, such as shells and plant fibers, directly to the deceleration profiles of the same penetrometer. Mulukutla et al. (2011) introduced the Firmness Factor (FF) which expresses the relationship between the maximum deceleration, the impact velocity and the penetration time. Stark et al. (2012) suggested to derive an equivalent of quasi-static bearing capacity from the penetrometer records. These authors demonstrated that the deceleration-penetration depth profiles can be utilized to derive information on sediment type, overall geotechnical characteristics, and most recent sediment remobilization processes. Aubeny and Shi (2006), Stegmann et al. (2006), Stoll et al. (2007), and Steiner et al. (2013) also estimated undrained shear strength for cohesive sediments from PFFP measurements.

The pore water pressure (PWP) response to the insertion of penetrometers can reveal additional soil characteristics, i.e., soil permeability, soil stress history (Robertson et al. 1992; Burns and Mayne 1998; Mayne 2001; Sandven 2010). However, most studies investigated pushed Cone Penetration Tests (CPT), being characterized by a constant penetration velocity of typically 2 cm/s, and requiring heavier equipment and larger ship support than a PFFP. Stegmann et al. (2006) presented PWP profiles of a free-fall CPT with velocities of up to 6 m/s, and demonstrated the potential of these measurements, but also highlighted the deviations to measurements carried out with a constant and slow penetration velocity. However, the number of available PWP data sets

from PFFPs is still limited, and more research is required to understand the behavior of pore pressure during and after high velocity impacts (> 1 m/s; being more than 50 times faster than a standard pushed CPT).

In this paper, the results of three field surveys carried out in May and July 2014, and August 2015, using the PFFP *BlueDrop* in Yakutat Bay, Alaska, are presented. Significant spatial and temporal variations in sedimentation, and sediment transport processes were expected in the survey area. Sediment maps were incomplete or challenged by local knowledge. The goal of the study is to test the applicability of using PFFP deceleration and pore pressure measurements to characterize the topmost sediment layers in logistically challenging aquatic environments in order to map the different sediment types, and to derive additional information about the geotechnical characteristics. Measurements were carried out in short time periods, and from a local, small vessel of opportunity. A regional soil classification scheme was developed based on the site-specific maximum deceleration of the penetrometer. Pore pressure measurements were related to the different soil types, and pore pressure response to CPT from the literature. The following research questions were addressed with regard to the use of PFFPs for the in-situ sediment characterization in areas of active sediment transport processes and challenging logistics: (1) Can a regional soil classification scheme be developed rapidly (possibly, even on site), and be used for creating a sediment distribution map, based on the penetrometer results? (2) Can pore pressures measured at high velocity penetrations contribute to sediment classification and characterization? (3) What information can be derived regarding the local sedimentation and sediment transport processes?

2.3 Regional context

Yakutat Bay is about 30 km wide at the entrance, and is enclosed by the lowlands of Yakutat Foreland in the Southeast, the St. Elias Mountains in the North, and Malaspina Glacier in the Northwest (Figure 2.1). The local sedimentation processes in the bay vary significantly. The forelands at the northwestern side of Yakutat Bay are still prograding seaward with a continuous sediment supply by Malaspina Glacier, while no significant changes in morphology have been observed at the southeastern side (Tarr and Butler 1909). Within Yakutat Bay, Disenchantment Bay is located in the Northeast, and receives sediments from Turner, Haenke and Hubbard Glaciers (Figure 2.1) (Cowan et al. 1996). During the summer, discharging meltwater carries fine

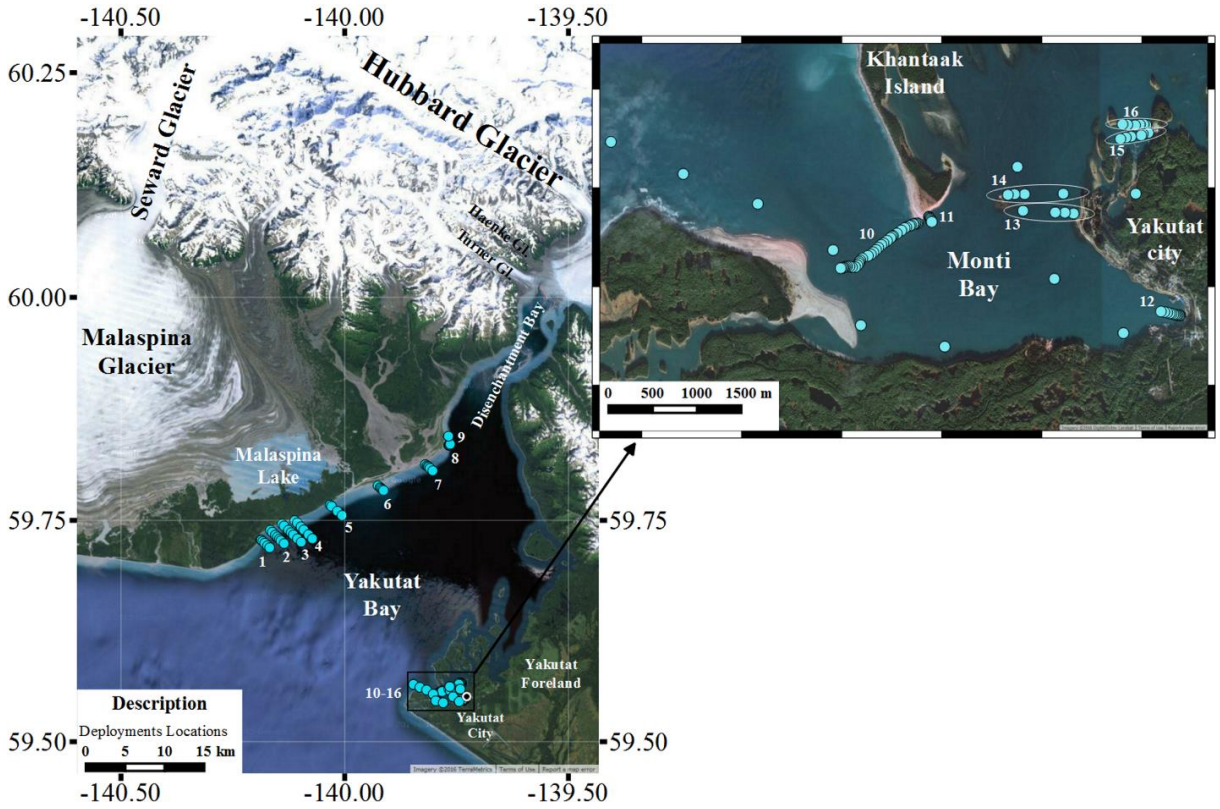

Figure 2.1. Google™ Earth (2016) images for Yakutat Bay showing the penetrometer deployment locations (mint dots), and the respective transect numbers. Yakutat City coordinates are 59.5469° N, 139.7272° W.

sediments, while the iceberg rafts bring coarse sediments further into the bay during winter (Cowan et al. 1997; Ullrich et al. 2009). The sediment deposition rate decreases from 48 to 14 cm/yr over a distance of approximately 15 km from Hubbard Glacier (Cowan et al. 1997). At the southeastern side of Yakutat Bay, Jordan (1962) reported an average change in water depth of 10 m between 1892 and 1941, and of 5.9 m between 1941 and 1958 in Monti Bay, affected by sediment slumps during earthquakes (Jordan 1962; Molnia 1979).

Wright (1972) found a large variety of sediment fractions from gravel to clay in samples collected from Yakutat Bay, with mud representing the most common sediment class. In general, there is a decrease in the sediment grain size with the increase of the water depth, and distance from the shore (Armentrout 1980). The collected samples by Wright (1972), and later by Armentrout (1980) showed that the mud was composed of different fractions of silt and clay. The clay content ranged between 7-48 % with an average of 35 % in the silt samples, while the silt content represented 14-

44 % with an average of 34 % in the clay samples (Wright 1972). Molnia and Hein (1982) examined the mineralogy of marine clays in the Northeastern Gulf of Alaska continental shelf region, and found that they mainly included different percentages of kaolinite, chlorite and illite. Samples from the mouth of Yakutat Bay were composed of 55% kaolinite and chlorite, and 45% illite.

Yakutat is located in a seismically active zone, and earthquakes are causing changes to the area's shorelines (Twenhofel 1952; Bauer et al. 2014). The most severe earthquake known to-date was in 1899 which caused an uplift of the shores at the head of Yakutat Bay of up to about 14 m while other shores were submerged (Tarr and Martin 1912; Jordan 1962; Hayes et al. 1976).

Typical wave heights vary for the investigated locations. The annual average significant wave height of the northwestern side of Yakutat Bay ranged from about 1.5 m near the bay inlet to less than 1.0 m at the mouth of Disenchantment Bay in 2008 (Previsic and Bedard 2009). The investigated areas at the southeastern side of Yakutat Bay are less energetic with an annual average significant wave height of about 1.0 m at the bay entrance, and less than 0.5 m inside Monti Bay (Previsic and Bedard 2009). The tidal current speed in the Yakutat area reaches about 0.77-1.03 m/s with a mean tidal range of about 3.3 m (Wright 1972).

2.4 Methods

2.4.1 Free Fall Penetrometer

The portable free fall penetrometer *BlueDrop* (Figure 2.2; 7.7 kg using conical tip; 63.1 cm in length) records continuously acceleration/deceleration, and pressure at a sampling rate of 2 kHz. It is equipped with five vertical accelerometers with capacities of ± 2 *g*, ± 18 *g*, ± 50 *g*, ± 200 *g* and ± 250 *g* (with *g* being the gravitational acceleration) in addition to a dual-axis accelerometer with a capacity of ± 55 *g* to detect tilt. The pressure transducer measures hydrostatic and pore pressures up to 2 MPa. The pressure gauge was calibrated before the first survey in May 2014. In order to saturate the porous filter, it was submerged in water overnight before every survey.

Figure 2.2. Deployment of the *BlueDrop* in Yakutat Bay, Alaska.

2.4.2 Analysis of deceleration measurements

The penetrometer impacts the soil at an initial impact velocity which depends on the probe's terminal free fall velocity in water and rope drag (Stark and Kopf 2011). Upon impact and during advancement through the soil, its deceleration is governed by the soil resistance against the probe. When its kinetic energy is depleted, it comes to a halt. The derived deceleration-depth profile reflects the sediment type and strength (Dayal and Allen 1973; Stoll and Akal 1999; Stark et al. 2011). Attempts have been made to relate the recorded decelerations to geotechnical soil properties such as undrained shear strength or bearing capacity (Dayal and Allen 1973; Aubeny and Shi 2006; Stoll et al. 2007; Stark et al. 2012b). In this study, the approach by Stark et al. (2011, 2012) was used to estimate an equivalent of quasi-static bearing capacity, and is outlined in the following.

The force decelerating the probe during impact and penetration into the soil, F_d, can be derived from the submerged penetrometer mass m, and measured deceleration during penetration dec using Newton's second law:

$$F_d = m\ dec \tag{2.1}$$

Neglecting the inertial force (Aubeny and Shi 2006; Stark et al. 2011), the measured resistance force is balanced by the soil resistance force F_s and the soil buoyancy of the penetrometer F_b:

$$F_d = Fs + F_b \quad (2.2)$$

Buoyancy in sea water is considered for this calculation, while soil buoyancy was neglected due to the limited penetration depth (Stark et al. 2016). Side adhesion and friction were neglected here, considering the short section of maximum diameter of the probe and the limited penetration depth.

The bearing load is the maximum load before soil failure, and the ultimate bearing capacity is this load per unit area (Terzaghi 1943). Accordingly, the ultimate dynamic bearing capacity q_{ud} can be estimated using:

$$q_{ud} = F_s/A \quad (2.3)$$

where A is the area subjected to load, and F_s is the maximum soil resistance force before failure (i.e. limit equilibrium), or in other words, the maximum loading force before failure for every soil layer over the penetrated sediment depth. At penetration depths smaller than the length of the penetrometer tip, the loaded area A depends on the penetration depth and penetrometer tip shape (60° conical in this study). For deeper penetrations, A remains constant.

Dayal and Allen (1973) proposed to correct the dynamic sediment strength (dynamic refers to changing penetration velocity and strain rate) for the strain rate effect, leading to a quasi-static strength equivalent to measurements conducted at a chosen constant penetration velocity (industry standard for Cone Penetration Testing: 2 cm/s). The strain rate factor chosen for this study, f_{sr}, is based on an empirical relation between the dynamic penetrometer penetration velocity v, which was determined from the first integration of the deceleration-time profile, and a constant penetration rate v_{ref} (Dayal and Allen 1975):

$$f_{sr} = 1 + K \log(v/v_{ref}) \quad (2.4)$$

where K is an empirical constant that can be assumed to range from 1.0-1.5 (Stoll et al. 2007; Stark et al. 2012b; Stephan et al. 2015). K= 1.25±0.25 was used in this study to account for the range of suggested values. An equivalent of quasi-static bearing capacity *qsbc* can then be estimated using:

$$qsbc = q_{ud} / f_{sr} \quad (2.5)$$

In this study, the deceleration, and estimated *qsbc*, was utilized to develop a regional soil classification scheme, and to derive a sediment map. Furthermore, soil layering was derived from the *qsbc*-penetration depth profiles (Figure 2.3). The penetration depth here was determined from the second integration of the deceleration-time profile. The change in the slope of the *qsbc* profile

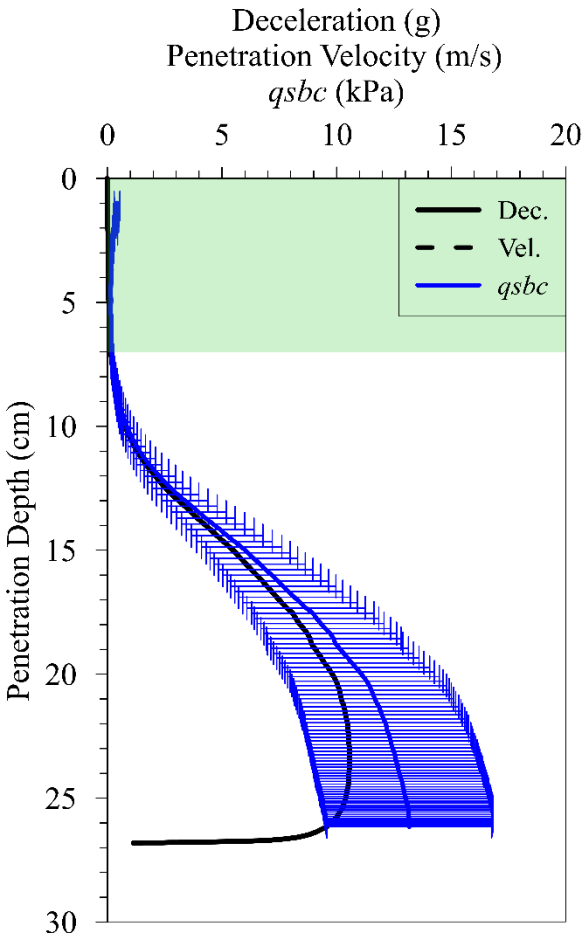

Figure 2.3. An example of the measured deceleration (black solid line), the derived values for the impact and penetration velocities (black dashed line), and the estimated *qsbc* profile (blue line including uncertainty following from the choice of strain rate factor). The green shaded area highlights a soft sediment top layer. The profile was measured along transect 15 at a distance of 600 m from the shoreline.

indicates a change in the soil behavior or a different soil type (Stark et al. 2012). The results were compared to existing sediment information (e.g. Wright 1972; Armentrout 1980). No large volume sediment samples were obtained, but sediment traces were found upon recovery of the penetrometer after each drop were characterized, and served as groundtruthing.

2.4.3 Soil classification

Stoll and Akal (1999) and Stoll et al. (2007) classified sediments using expendable bottom penetrometer (*XBP*) deceleration measurements. They found that the presence of coarse-grained sediments led to decelerations of more than 60 g, while decelerations of less than 20 g were measured in areas of soft clay. Mulukutla et al. (2011) proposed the Firmness Factor (*FF*) to characterize sediments based on penetrometer deceleration records :

$$FF = \frac{a_{max}}{v_i \, g \, t_p} \tag{2.6}$$

where a_{max} is maximum acceleration, v_i is impact velocity, and t_p is the total penetration time. The minimum values of *FF* for fine sand and maximum for coarse silt ranged between 10.5 and 70 m^{-1} for an impact velocity between 4.86 and 9.16 m/s. In Yakutat Bay, 50 deployments featured an impact velocity of 4.9-6.2 m/s, being within the range investigated by Mulukutla et al. (2011). These two classification schemes, in addition to sediment traces noticed on the penetrometer after each drop, and the available literature about the surficial sediments in Yakutat Bay were utilized to generate a regional soil classification scheme for the sediments in Yakutat Bay based on the surface sediment distribution map by Wright (1972). Armentrout (1980) extracted no samples in the focus areas of this study. Therefore, only Wright (1972) was considered for the soil classification system. However, the regions close to Disenchantment Bay were potentially affected by the introduction of a large amount of fine sediments during outburst floods in 1986 and 2002 following the failure of the ice and sediment dams at the entrance of Russell Fjord (Mayo 1989; Cowan et al. 1996). As the measured sediment strength likely represented a mixture of the sediments introduced by these events with the gravelly mixture documented by Wright (1972) for these regions, these deployments were not considered for the development of the local soil classification scheme.

2.4.4 Analysis of pore water pressure measurements

Most portable free fall penetrometers do not carry a pressure transducer, and there is still little information and data on the pore water pressure (PWP) response of high velocity (>1 m/s) impact penetrometers. In this study, an attempt was made to utilize the measured PWP response during

impact, and for the period when the penetrometer rested in the sediment (on the order of seconds to tens of seconds), for further interpretation of the soil mechanical properties of the tested sediments. For this, only the deployments with a penetration depth of more than 15 cm were considered to ensure full embedment for the pressure sensor in the sediments.

During the free fall of the probe through water, the pressure gauge read values less than the hydrostatic pressure due to the Bernoulli effect. Accordingly, the water depth *h* was determined as following:

$$h = h_i + \frac{v_i^2}{2g} \tag{2.5}$$

where h_i is the uncorrected water depth based on measured pressure, and v_i is the impact velocity. *h* was compared to single beam echo sounder measurements. During penetration into the sediment such a direct correction is difficult, due to the different physical characteristics of the sediments, and the generation of excess pore water pressure by the probe (see more detail in the Discussion section).

2.4.5 Field surveys

The *BlueDrop* was deployed 149 times in four days of surveying in May and July 2014, and August 2015. One deployment took about 1-2 minutes; survey times are mostly accounted to transits. The deployments covered two focus areas in Yakutat Bay. These areas were identified as the most interesting, based on existing sediment information. Areas of known rock outcrops and water depths in excess of 100 m were avoided. The latter deeper areas are known to be characterized by soft and fine sediments, and are unlikely subjected to significant sediment remobilization processes. The first focus area included 50 deployments distributed along nine transects starting from near the bay entrance to the mouth of Disenchantment Bay in the Northwest of Yakutat Bay (Figure 2.1). The transects are approximately perpendicular to the shore with 4-7 deployments per transect, except the last transect which featured only two deployments. One of the survey targets here was to identify and map the transition from coarse sandy shoreline sediments to the finer glacier material. The second focus area is located in Monti Bay at the southeastern side of Yakutat Bay, close to Yakutat City. Here, the probe was deployed at 99 locations along 7 transects (transects 10-16) in addition to distributed deployments in different locations in Monti Bay (Figure

2.1). The transects in this region differ in the number of deployments, with transect 10 (between Khantaak Island and the mainland) being the longest with 37 deployments. Particularly, changes of sediment type, characteristics and dynamics between the shorelines of the islands, and with regard to the rather complex bathymetry were of interest in this area.

2.5 Results

Impact velocities (v_i) varied depending on the water depth (h = 2-48 m) between 2.3-6.2 m/s. The variation in the impact velocity was relatively large at water depths < 3 m, due to changes in the deploying height above the water surface. The recorded maximum velocity reached 6.2 m/s at a water depth of about 5 m, approaching the theoretical terminal velocity of the probe in seawater. With increasing water depths, the rope drag (braided rope ~5 mm in thickness) caused a reduction of the impact velocity. The minimum impact velocity was 2.3 m/s at a water depth of 46 m.

A loose sediment top layer (LSTL) was defined by small deceleration values (<1 g), and confirmed by small *qsbc* values (< 1 kPa; see green shaded area in Figure 2.3) over a layer of stronger sediments. Such layering can reflect loose or soft sediments on top of denser sediments, or on top of sediments of a stiffer type (e.g., mud on sand). The detected thickness of this loose sediment layer varied between 5.3-18.4 cm with an average value of 8.2 cm and standard deviation of 3.25 cm at the northwestern side of the bay (Figure 2.4a). The thickest loose top layers (>15 cm) were found along transect 6 (purple stars in Figure 2.4a) near the mouth of the Kame and Sudden Streams discharging from Malaspina Glacier (Figure 2.1). Transects 1 to 5 showed an approximately constant top layer thickness (~6.6 cm), and a slight increase in top layer thickness at a distance greater than 1500 m from the shoreline (Figure 2.4a). Transects 7-9, located at the western side of the entrance to Disenchantment Bay, were short, and a varying top layer thickness was observed reaching over 10 cm (Figure 2.4a). At the southeastern side of the bay, the thickness of the top layer reached 3.0-12.0 cm with an average value of 7.1 cm and standard deviation of 1.51 cm (Figure 2.4b). The maximum values were measured along transects 15 and 16 near the Yakutat shipyard. Variations along transects were noticeable at this side of the bay, especially along transects 10 and 12.

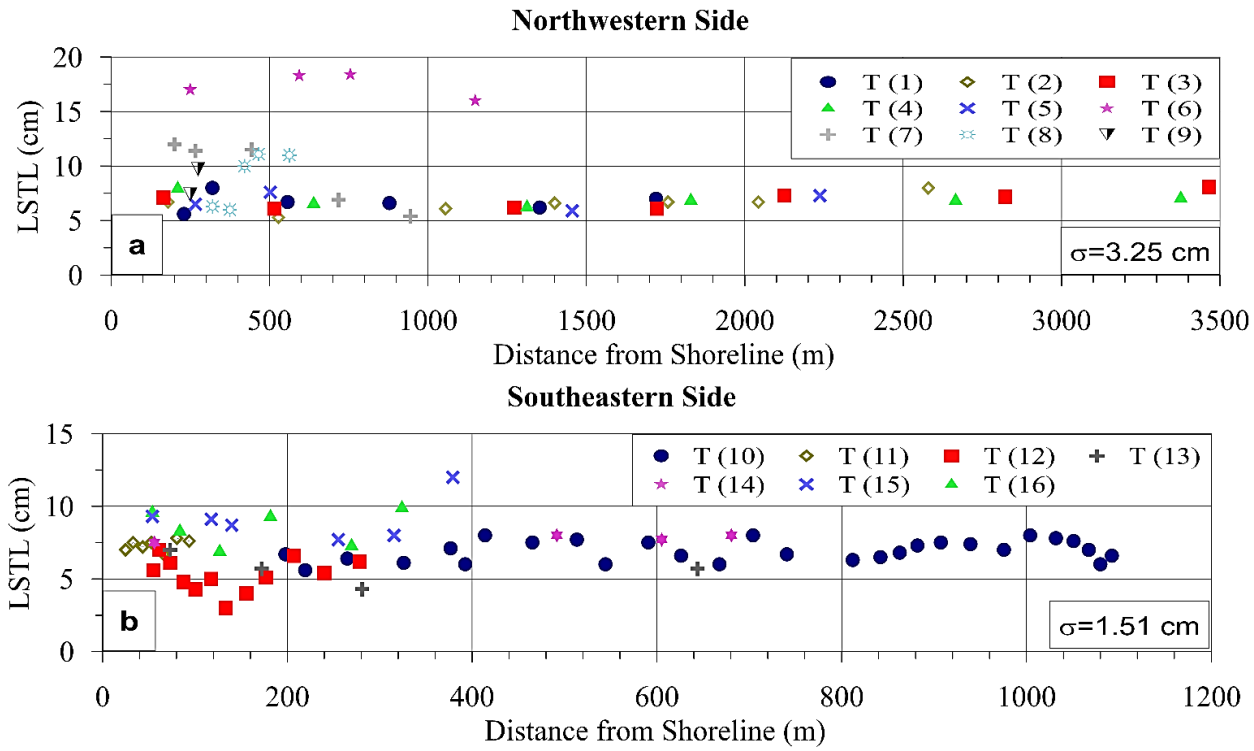

Figure 2.4. Loose sediment top layer thickness (LSTL) with distance from the shoreline along the 16 transects. σ is the standard deviation for the LSTL thickness in each side of the

The measured maximum deceleration reflected the local sediment type. In general, larger decelerations were observed near the shoreline decreasing offshore. This is consistent with sandy to gravelly beach sediments in many areas, and the expectation of fine sediment deposition at deeper water depths. The penetrometer maximum deceleration values reached between 7.5-84.1 *g* at the northwestern side of the bay, and between 3.7-74.4 *g* at the southeastern side of the bay. This led to estimates of the maximum *qsbc* ranging between 9-107 kPa and between 5-95 kPa at penetration depths of 10-42 cm and 10-39 cm, respectively. In accord with the measured maximum deceleration values, the estimates of the maximum *qsbc* were also characterized by a decrease with increasing distance from the shore and water depth (Figure 2.5). Particularly, the northwestern side of the bay featured an overall decrease in sediment strength with increasing distance from the shoreline. This trend was particularly strong at the entrance to Disenchantment Bay and decreased noticeably with distance from Disenchantment Bay alongshore (Figure 2.5a). A gradient was determined for the change of the *qsbc* with the distance from shoreline. The *qsbc* was decreasing in direction offshore with -0.1 kPa/m along transects 1-7, -0.25 kPa/m along transect 8, and in

excess of -1 kPa/m along transect 9. The latter may be biased by a limited number of two deployments along transect (Figure 2.5a).

The southeastern side of the bay was characterized by mostly soft sediments (*qsbc* < 50 kPa for 86% of the deployments here) except for the nearshore zone along transects 10, 11 and 12 (Figure 2.5b). The sediment strength decreased rapidly at distances of 50-100 m from the shoreline instead of the gradual decrease observed at the northwestern side of the bay. It should be emphasized that transect 10 is located between two land masses (Khantaak Island and the mainland; Figure 2.1), and that the resulting *qsbc* values for the deployment at a distance less than 200 m were neglected due to the high values (> 300 kPa) and negligible penetration depths which likely result from the presence of coarse gravel and cobbles.

2.5.1 Soil classification

The deceleration values were compared to the sediment type on the sediment distribution map suggested by Wright (1972) (Figure 2.6). In the Northwest of the bay, three deployments were located in a zone classified as clay. The maximum decelerations of the penetrometer in these

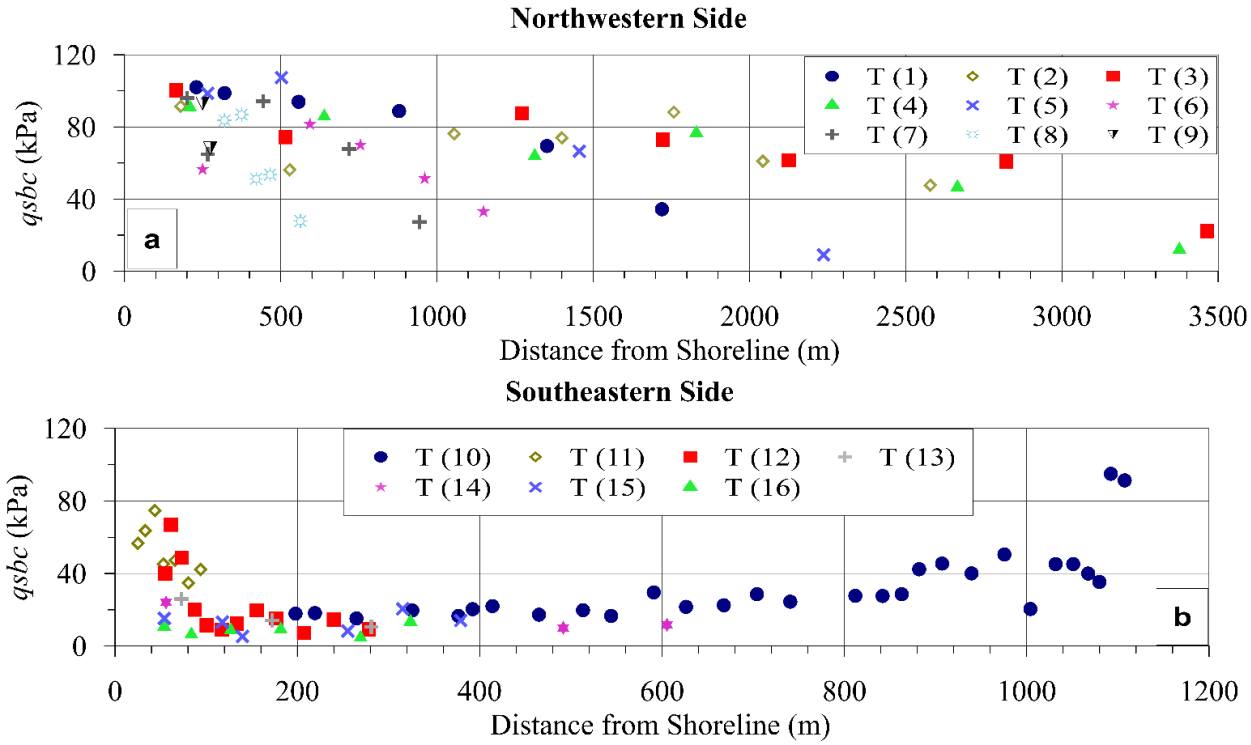

Figure 2.5. The *qsbc* versus the distance from the shoreline along the measured transects.

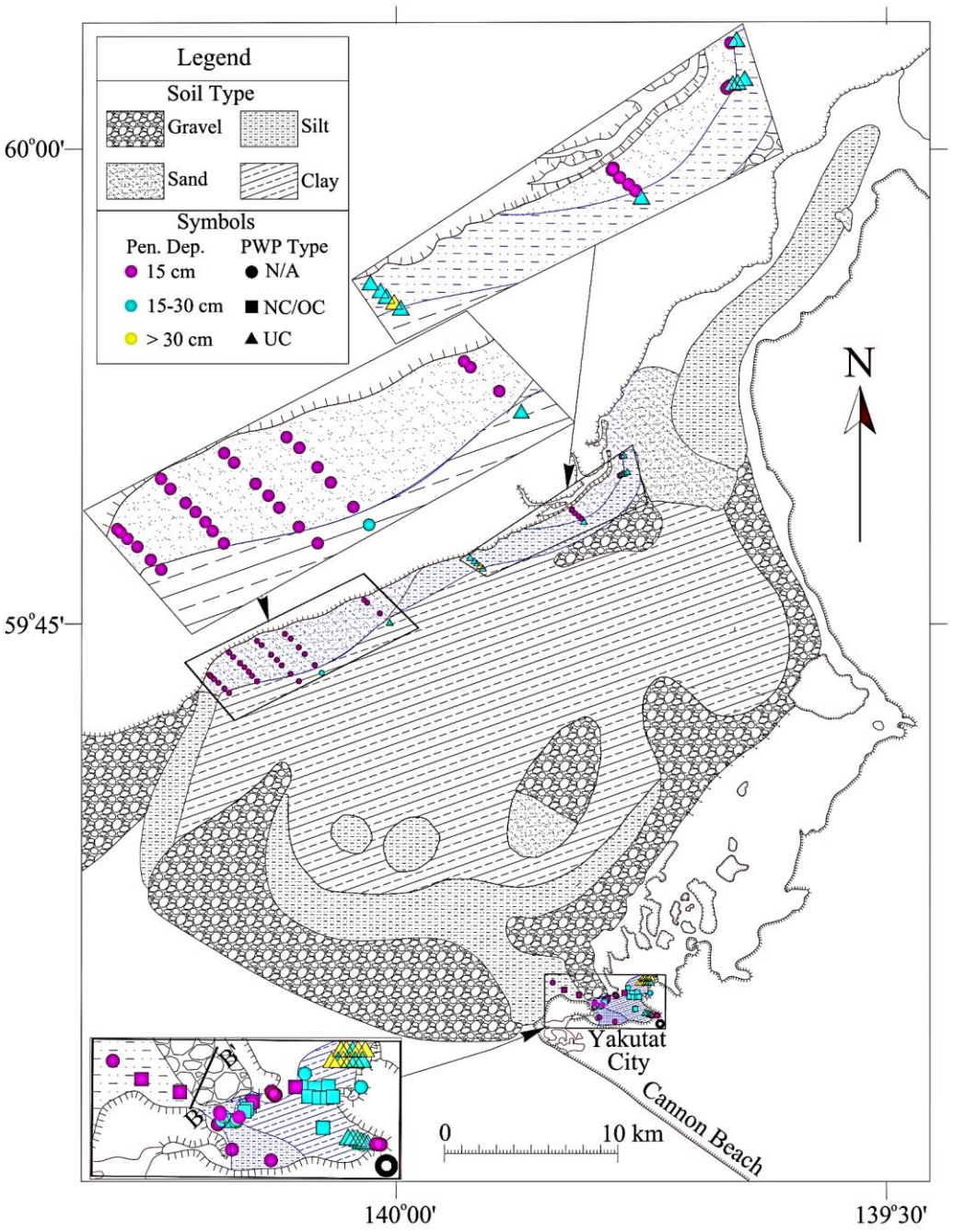

Figure 2.6. Sediment distribution map for Yakutat Bay modified after Wright (1972). PFFP deployment locations are represented by colored symbols. The color scale of the symbols show the penetration depth while the blue hatch indicates the suggested sediment type based on the PFFP measurements. The pore pressure response types are reflected in the symbol shape, and were grouped as normally consolidated or overconsolidated "NC/OC", underconsolidated "UC", or not considered for the pore pressure analysis "N/A".

locations ranged between 9.8-24.9 *g*. At the southeastern side of Yakutat Bay, six deployments were located in a zone classified as silt (Wright 1972). The measured deceleration values for these deployments ranged between 25.5-51.9 *g*. Accordingly, an arbitrary value of 25 *g* was considered to differentiate between the clayey and silty sediments. The deployments along transect 8 and 9 (i.e. at Disenchantment Bay mouth) exhibited deceleration values between 21-73 *g*, but the map indicates gravel in these locations. In this case, the comparison to Wright (1972) may not be applicable anymore due to the effect of the outburst floods in 1986 and 2002. None of the deployment locations fell into sand zones in the sediment distribution map. However, the sand was clearly abundant in the Northwestern nearshore zone.

In Yakutat Bay, 50 deployments achieved an impact velocity within the range used by Mulukutla et al. (2011) for classification using *FF*. For the deployments with *FF* =10.5-70 m^{-1}, the maximum deceleration ranged between 31.5 and 70 *g*. Based on these values, the value suggested by Stoll et al. (2007), the sediment map by Wright (1972), and field visual observations, a range of (50-60 *g*) with an average arbitrary value of 55 *g* was suggested as a threshold deceleration value for sand in the investigated region.

A regional soil classification model was developed from the above described considerations (Figure 2.7), and was used to complement the sediment map by Wright (1972) (blue hatch, Figure 2.6), and to identify changes in surficial sediment distributions such as the more recent fine sediment deposits at the entrance of Disenchantment Bay.

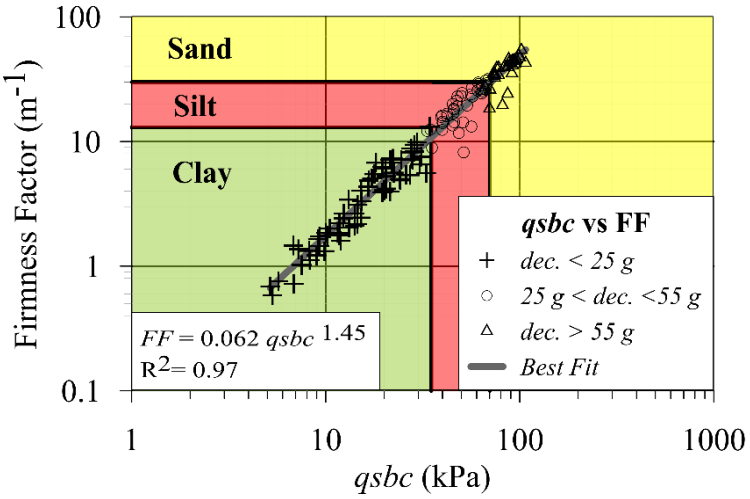

Figure 2.7. Firmness factor (after Mulukutla et al. 2011) vs. *qsbc* in the proposed soil classification scheme: clay (green), silt (red), sand (yellow).

2.5.2 Pore water pressure (PWP) response

Fifty-nine percent of the deployments were rejected from PWP analysis due to either a damped or delayed PWP response, likely being associated to a lack of filter ring saturation (27 %), or due to insufficient penetration depth (<15 cm) (32 %).

Reduced (P_{0-}) and elevated (P_{0+}) PWP responses were measured in relation to the estimated hydrostatic pressure (P_0) during penetration (Figure 2.8). Here, P_0 refers to the pressure as measured at the seabed-water interface, plus the projected hydrostatic pressure increase with regard to penetration depth (Figure 2.8, dashed lines). Therefore, it does not consider the Bernoulli effect. P_{0-} was observed directly after the embedment of the pressure sensor into the soil for about 88 % of the deployments. This reduction in the pressure was followed by an increase of pore pressure with continuing penetration to a value higher than the projected reference pressure (P_{0+}) (Figure 2.8a). Seventeen deployments (11 %) were characterized by P_{0+} directly after impact followed by a decrease to P_{0-} (Figure 2.8b). Two deployments (~1 %) in the southeast of Yakutat Bay were characterized by consistently P_{0+} during penetration (Figure 2.8c).

The excess PWP was calculated by subtracting the hydrostatic pressure (P_0) from the measured PWP. The excess PWP was compared to the effective stress considering submerged unit weights of 9.0 kN/m^3 for sand, 7.5 kN/m^3 for silt and 6 kN/m^3 for clay. Three main response types were observed: (1) The excess PWP was predominantly negative, suggesting sediment dilation, and less than the effective stress (Figure 2.9a). This response type was mostly observed in sandy sediments. (2) The excess PWP exceeded the effective stress before or at the maximum dynamic force (which coincides with the maximum *qsbc*) (Figure 2.9b). (3) The excess PWP exhibited a delayed increase in excess PWP, i.e. the excess PWP exceeded the effective stress after the maximum dynamic force (Figure 2.9c). The excess PWP at the maximum dynamic force seemed to correlate to the maximum deceleration (or soil type) (Figure 2.10a). Additionally, the difference between the excess PWP and effective stress at the maximum dynamic force was plotted with regard to the soil classification (Figure 2.10b). For the deployment in clayey sediments, the excess PWP was positive in 91 % of the deployments, indicating a contractive soil behavior during penetration, and exceeded the effective stress in 71 % of the deployments. The excess PWP response in sand was mostly negative (91 % of the deployment in sand) with only 3 deployments achieving positive excess PWP (<1 kPa), reflecting overall a dilative soil behavior. Similarly, the excess PWP

response was negative in most of the deployments in silt (69 % of the deployments in silt), and the excess PWP was less than the effective stress in most of the deployments (88 % of the deployments in silt).

No PWP dissipation measurements (as done by Stegmann et al. 2006; Seifert et al. 2008; Kopf et al. 2009; Chow et al. 2014; Stark et al. 2015) were intended during surveying to keep measurements as time-efficient as possible. Thus, PWP recordings of the penetrometer at rest were on the order of seconds. Nevertheless, three main behaviors were observed (Figure 2.11): The first

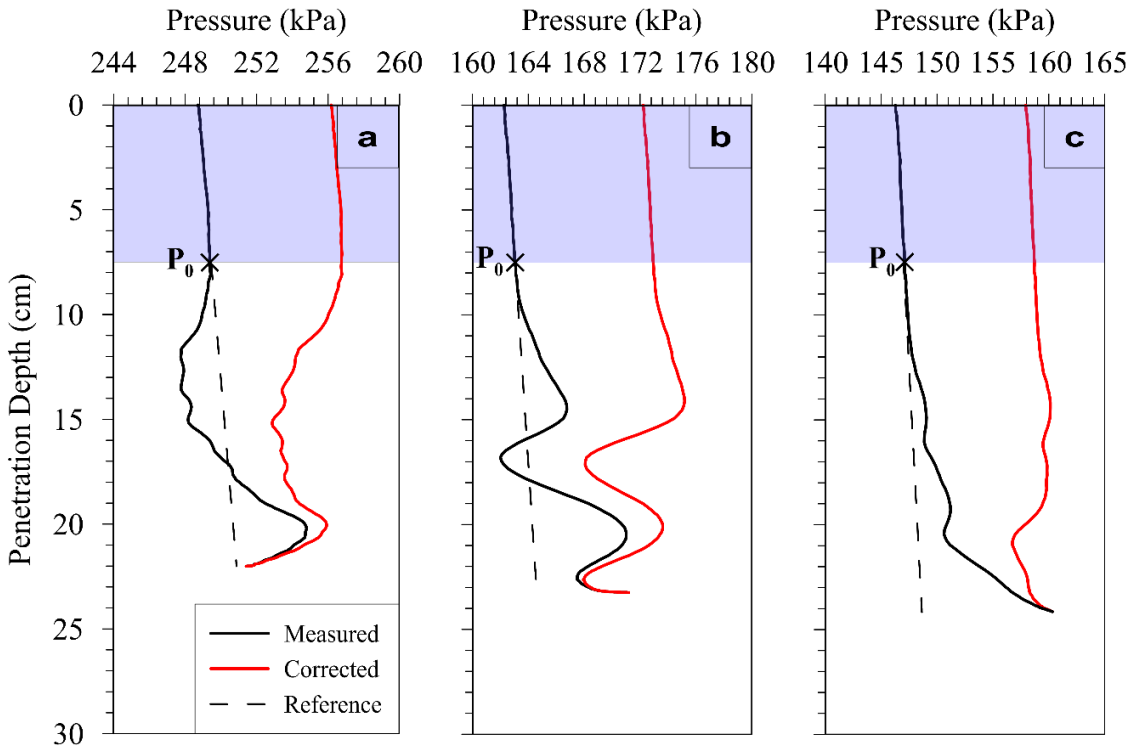

Figure 2.8. The measured pressure sensor reading during impact and penetration (black solid line). The penetration depth is given with regard to position of the cone's tip. The blue shaded area indicates the penetration depth at which the tip but not the pore pressure inlets have entered the sediment, and P_0 shows the value of the measured pressure at the seabed-water interface. The red solid line gives the pressure corrected for the Bernoulli effect. The dashed line represents a reference line at $P_0 + P_{hyd}$. a) Reduced followed by elevated pressure with increasing sediment depth, b) Elevated pressure at the beginning of penetration followed by a reduction during penetration, c) Elevated pressure during penetration and over the full penetration.

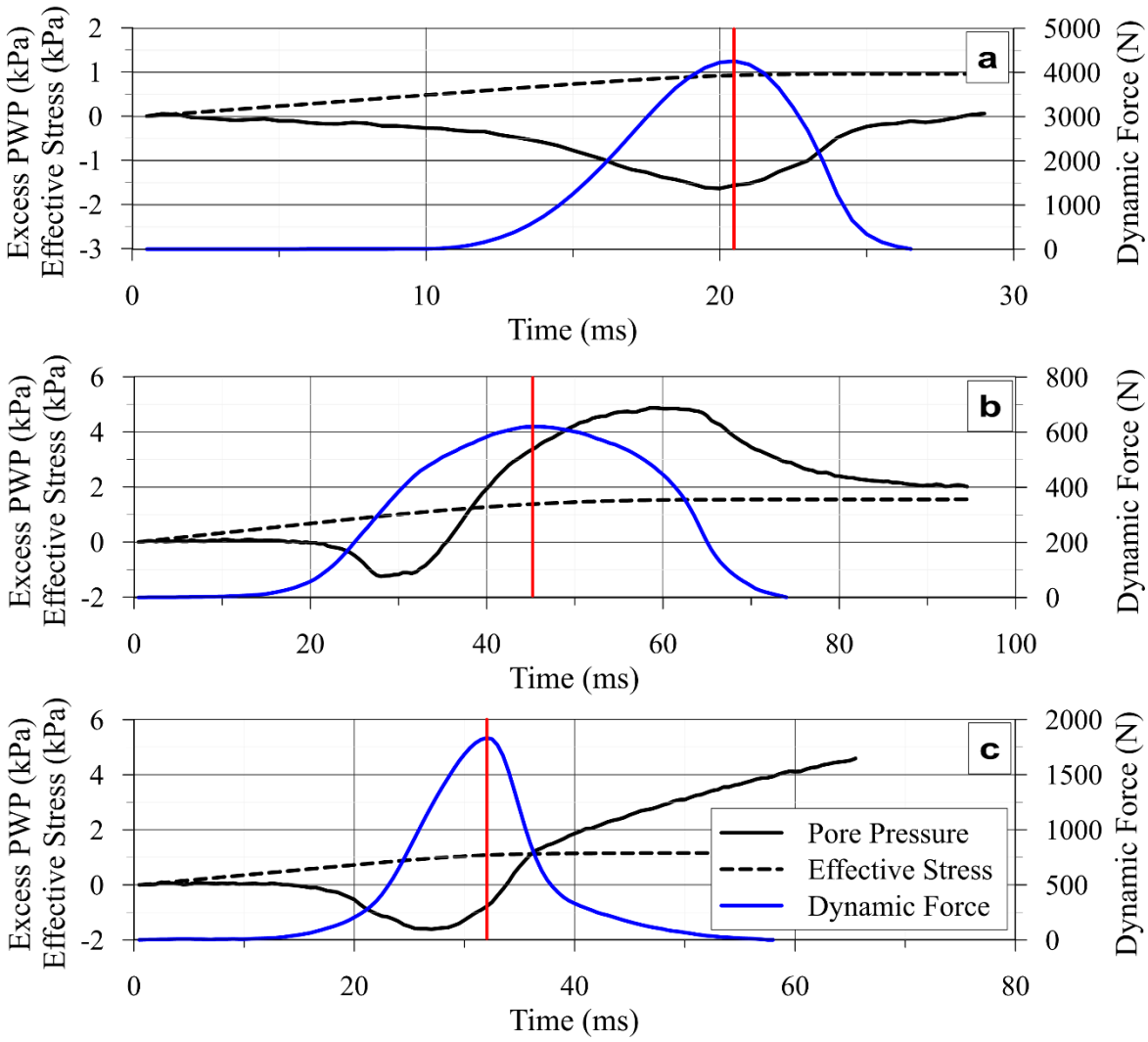

Figure 2.9. The excess PWP with time during impact and penetration (black solid line) compared to the approximated effective stress (black dashed lines). The blue solid lines show the dynamic force calculated from the measured deceleration. The vertical red lines indicate the position of the maximum dynamic force. a) the excess PWP is negative , b) the excess PWP exceeded the effective stress before the maximum dynamic force , c) the excess PWP exceeded the effective stress after the maximum dynamic force.

type was associated to sandy soils (Figure 2.11a) and was characterized by a rapid increase in the PWP until reaching a constant value. This constant value was mostly within less than ~1 m difference from the water depth as measured by the single beam echo sounder (94 % of the deployments with available echo sounder data), and the measured seabed surface pressure after application of the Bernoulli correction (89 %). The second PWP response type showed a gradual

increase in PWP (Figure 2.11b). The PWP for this type reached values in excess of the estimated hydrostatic pressure for some of the deployments (~5 % of the analyzed deployments), while in other deployments the penetrometer was retrieved before reaching the hydrostatic value (~17 %). If excess pore pressure values were measured, the penetrometer was retrieved before a dissipation of the excess pore pressure was observed (i.e., elevated pressures would diffuse to estimated hydrostatic pressure). This response type was mostly correlated to silt or clay in the northwestern side of the bay in addition to locations classified as clayey soils in the southeastern side of the bay. The third response type (Figure 2.11c) was distinguished by a peak of the PWP during penetration followed by an approximately constant, equaling or less than the estimated hydrostatic PWP for the penetrometer at rest. This type was found for the silty and clayey soils in the southeastern side of Yakutat Bay.

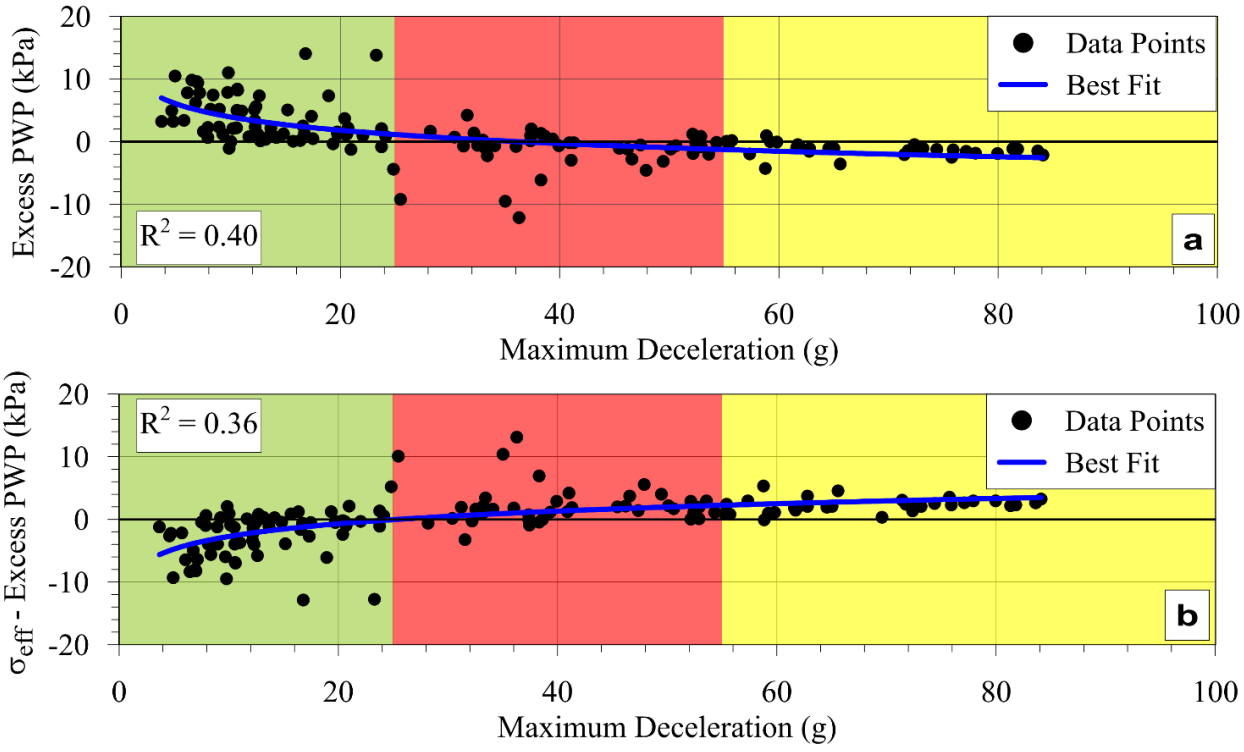

Figure 2.10. a) The excess PWP at the maximum dynamic force versus the measured maximum deceleration, b) the effective stress minus the excess PWP at the maximum dynamic force versus the measured maximum deceleration. The green, red and yellow shadings show the ranges of the deceleration for clay, silt and sand, respectively, based on the proposed classification scheme.

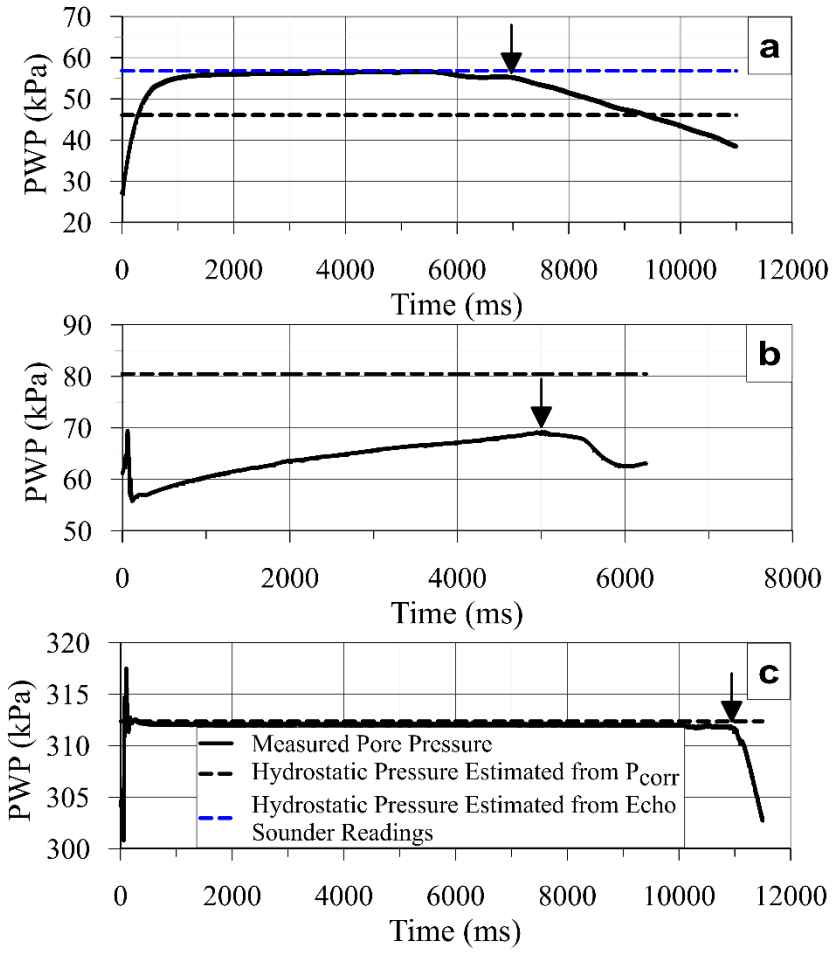

Figure 2.11. Pore pressure behavior types observed while the penetrometer was at rest in the sediments. Black solid lines show the measured PWP, black dashed lines show the hydrostatic pressure considering the Bernoulli effect, while the blue dashed line shows the calculated pressure based on the echo sounder water depth. The sudden change of the pressure values at the beginning represent the change of the pore water pressure during of the pore water pressure sensor penetration (i.e. shown in Figure 2.8). The arrows show the points at which the device was retrieved. The response type (a) was found mainly in sandy sediments while the response types (b and c) were found in both silty and clayey sediments.

2.6 Discussion

A regional sediment classification scheme was developed based on some penetrometer deployments that overlapped with existing sediment type maps in addition to the traces noticed on

the penetrometer after each drop and the existing classification schemes in literature. Using this sediment classification scheme, some gaps of the existing sediment map were filled, and areas impacted by specific large sediment deposition events were identified (Figure 2.6). Although the time difference between the sediment distribution map by Wright (1972) and the deployments used to create the classification scheme was large (at least 42 years), different factors support the proposed development of the regional sediment classification scheme:

(i) Previous classification schemes (including the suggested threshold values for the relevant impact velocities) from the literature were utilized as a guideline.
(ii) Sediment traces on the *BlueDrop* served a visual description of the sediment type.
(iii) Ebb tidal currents directed towards the western shore prevent sediment deposition from ice floats at the eastern side of Yakutat Bay (Tarr and Butler 1909).
(iv) Deployments in the areas largely affected by major sedimentation events, such as outburst floods in 1986 and 2002, were not considered for the development of the classification scheme.
(v) Deployments used to develop the classification scheme at the Northwester side were located at a minimum distance of 8.5 km from regions of high sedimentation rates. An overall agreement between Wright (1972) and Armentrout (1980) for the used deployments support this. For the single deployment where Wright (1972) contradicts Armentrout (1980), sediment traces showed clay.
(vi) Only 9 deployments were used to create the classification scheme. This allowed using the observed traces at other deployment locations to validate the classification scheme. The results were generally consistent with retrieved sediment traces, and local knowledge.

The direct application of the derived soil classification scheme to other sites, or penetrometers, must be considered carefully. Different factors affect the soil response to a penetrating object, such as: the penetrometer mass, the tip shape and size, the penetration velocity, and the dynamic soil behavior including pore pressure response (Mulukutla et al. 2011; Stark et al. 2009). While some of these issues were addressed by estimating *qsbc*, the current approach still includes empirical parameters that have been derived for certain soils and penetrometers. Since in this study all the investigations were carried out using the same penetrometer with the same conical tip, the effect of the change in the penetrometer characteristics was removed. The average impact velocity was 4.4 m/s with a standard deviation of 0.9 m/s. This narrow range of the impact velocity limited the

effect of the impact velocity variation. These facts encouraged the use of the classification scheme by Stoll et al. (2007) and Mulukutla et al. (2011) as guidelines for the development of a regional classification scheme. While this specific classification scheme may not be directly transferable to other sites or devices, it demonstrated that such a model can be quickly developed with limited previous knowledge of the sediments.

Cross-shore transects suggested that more details can be derived than just a classification of the main sediment types. Gradual changes in sediment strength with distance from the shore likely expressed a gradual mixing of sediments, in comparison to the observed more abrupt transitions at the Southeastern side. Stark et al. (2016) documented that variations of sand content in muddy samples, as well as of median grain size are reflected in the estimates of *qsbc*. This suggested that the gradual change in *qsbc* at the Northwestern side expressed a well gradually mixed transition zone from sandy nearshore sediments (on average 1.5 km cross-shore) to finer deep water sediments, and that this transition zone varied in cross-shore width depending on the seabed slope and local hydrodynamic forcing. A direct correlation to median grain size or sand content could not be established based on the existing data set.

The outflow area of the Kame and Sudden Streams (see transect 6) suggested the deposition of fine sediments from these streams (Tarr and Butler 1909). Particularly, thick loose sediment top layers pointed at most recent and likely ongoing sediment deposition (Figure 2.5). This was supported by observations of turbid water with high concentrations of suspended sediment in this area, while the water was generally very clear in the other survey areas. At the mouth of the Disenchantment Bay, the gradual decrease of sediment strength was significantly stronger, suggesting a much narrower sandy-gravelly nearshore zone. This observation is in disagreement with the sediment distribution map by Wright (1972), and can be explained with two large sediment deposition events that occurred between the survey by Wright (1972) and the here presented study. Two large outburst flood events in 1986 and 2002 resulted in the deposition of about 12 and 7 million cubic meter of mud and fine sand, respectively, and covered native sediments with a blanket of fine soils (Cowan et al. 1996; Trabant et al. 2003; Willems et al. 2011). This explained the difference between the results of the two surveys, and suggested that those introduced sediments are –if at all- only slowly eroding.

The archipelago of islands at the southeastern side of the Yakutat Bay inlet forms a buffer that

protects Monti Bay from the Pacific's wave energy that continually affects Yakutat Foreland shores (Tarr and Butler 1909). The sediments at this side of the bay were soft and mostly in the clay range. Exceptions were found at the entrance of Monti Bay and near the shoreline along transects 10 and 11. At the entrance of Monti Bay, the deceleration signature suggested that the sediments were mostly silt with a relatively high resistance against the penetrometer. This agrees with observations of coarse sandy to gravelly sediments at the shores. Jordan (1962) reported slumps, recessions and uplifts at these locations caused by the earthquakes, potentially introducing coarser material. According to local residents, a recent earthquake caused slumps in the same region. The deployments in transects 15 and 16 (i.e. next to Yakutat Shipyard) showed irregularities in the deceleration profile which might be due to the presence of organics probably as a result of vegetation or organic waste materials.

Loose top sediment layers of varying thickness were observed in all of the investigated zones. Such layers can result from the remobilization of the top sediment layer by hydrodynamics, existence of a recently deposited sediment layer, vertical layers of different sediment types, or from the abundance of plants (Stark and Kopf 2011). Unfortunately, the penetrometer record alone does not allow to determine the governing process, but the local hydrodynamic conditions in some spots, and known sediment deposition events in others suggest that the soft sediment top layers can be associated to sediment remobilization and deposition processes. The irregularities observed in the deceleration profiles of the deployments in Monti Bay indicated the presence of vegetation, based on comparison to findings by Stark and Wever (2009) and Stark et al. (2015).

The measured pressure before impact with correction for the Bernoulli effect was applied to find the water depth at the deployment locations. The corrected values, h, were in good agreement with the estimates from the echo sounder (in the range of uncertainty of the sounder). At shallow water depths ($\lesssim$ 12 m), the penetrometer seemed to underestimate the water depth. Sandven (2010) discussed the issue of insufficient saturation of pore water pressure filters during Cone Penetration Testing, and pointed out that this issue occurs mostly in shallow water depths (< 8 m) at which the hydrostatic pressure is low. During the Yakutat surveys, the pore pressure filter ring was saturated in water for approximately 12 hours prior to the survey. To improve pore pressure measurements in shallow water depths in the future, mineral oil may represent a more reliable saturation fluid (Sandven 2010).

The PWP response for 98 % of the analyzed deployments showed a decrease in the PWP values during the penetration followed by an increase in the PWP before or after the penetrometer came to a halt (Figure 2.8a and 2.8b). The dilative behavior of soil, the displacement of soil and fluids during the penetrometer impact, and the change of the penetrated material density (i.e. water versus soil) are possible explanations for this behavior (e.g. Stoll et al. 2007; Kopf et al. 2009; Mulukutla et al. 2011). Seifert et al. (2008) found that the presence of sand and silt causes a decrease in the PWP to sub-hydrostatic at sites which were mostly dominated by fine sediments. Accordingly, the abundance of silt is a possible explanation for this behavior (Wright 1972; Carlson et al. 1977; Armentrout 1980; Cowan et al. 1996). Seifert et al. (2008) also suggested the availability of microbial gas and the lack of saturation as possible explanations for reduction of the PWP. Carlson et al. (1980) mapped the gas charged sediments in the Eastern Gulf of Alaska, and indicated that Yakutat Bay sediments are gas-free. A lack of saturation is unlikely here, as the deployments in shallow water depths pointed more clearly at this issue, and were removed from the analysis accordingly.

The excess PWP response at the maximum dynamic force showed positive excess PWP in clay, and negative excess PWP in sand (Figure 2.10). The highest negative excess PWP was found for deployments in silt which is similar to the findings by Mulukutla et al. (2011). This can be explained by the dilative nature of some types of silt (Duncan et al. 2014). Furthermore, the observed dilative behavior in sand matched well the observations by Stoll et al. (2007) during laboratory experiments of free fall penetrometers at similar speeds.

Three different types of pore pressure responses were observed after the penetrometer came to a halt (Figure 2.11). The first PWP response type was the dominant type in the soils classified as sand. In such soils of high permeability, the PWP is expected to return quickly to the hydrostatic value after the penetrometer comes to a stop (Stoll et al. 2007). The PWP did indeed equilibrate quickly to a constant value. This value was in agreement with the single beam echo sounder measurements plus embedment depth for the deployments where reliable sounder measurements were available, but exceeded the estimated hydrostatic pressure based on the pressure gauge measurements at the point of impact and correction for the Bernoulli effect and embedment depth. This issue was encountered at shallow water depths, and still, a lack of saturation of the filter ring (gas bubbles in filter ring) is a likely explanation. A competing explanation would be an error in

identification of the point of impact, but the sensitivity was tested, and let to negligible impacts here.

The second and third response types were found at locations which were classified as silt or clay based on the proposed classification scheme. These soils were found mostly at water depth greater than 10 m. Accordingly, a lack of saturation was not expected (Sandven 2010), being confirmed by the good agreement between estimated water depth and the measurement of the echo sounder (Figure 2.11).

The PWP type (b) showed an increase in the PWP after the penetrometer came to a halt (Figure 2.11b). The increase continued until reaching a value higher than the calculated hydrostatic pressure for the sufficiently long deployments. Different reasons can explain this behavior such as dilative behavior of the overconsolidated sediments, and presence of high organic content (Seifert et al. 2008). Considering the region's sedimentation rates, the penetration depth and the age of the deposit in some locations with type (b) behavior (e.g. the recent deposits in Disenchantment Bay after 1986 and 2002 outburst floods), the soil is unlikely to be heavily overconsolidated. The soils organic-carbon content in Yakutat Bay is low, less than 0.8 % (Armentrout 1980). Accordingly, the organic content is also unlikely the main reason behind the observed delay in the PWP increase after penetration. Another, and the most probable, explanation for this behavior is that the sediments are lightly consolidated (Seifert et al. 2008). The presence of this PWP response type in the relatively high sedimentation rate regions (i.e. the northwestern side Yakutat Bay) supports this assumption. This agrees with Sangrey et al. (1979) who found that, for one sample, the overconsolidated ratio of the sediments in Yakutat Bay is 0.22. Another explanation to the observed PWP response must be considered for deployments near the populated areas in Monti Bay. The disposal of organic waste into the water might have led to an increase of the soil organic content. The irregularities in the deceleration signature support an increasing in the soil organic content at these location (Stark et al. 2015), and specifically since the deployments with this behavior where found along transect 12 which is near Yakutat Fisheries Dock and along transects 15 and 16 which are near the Yakutat shipyard. The continuous movement of boats can also cause disturbances and mixing of the top soil which can also cause a decrease of the degree of consolidation for these sediments.

The PWP response type (c) showed approximately constant and hydrostatic pressure values for the

PWP after the penetrometer came to halt (Figure 2.11). This response type was observed in silt and clay at the southeastern side of Yakutat Bay (i.e. Monti Bay). Possible explanations here are that the sediment is highly permeable, or stiff enough to allow the formation of a crater and/or fissures during penetration. Jordan (1962) noticed an average change of about 10 m for the depth of Monti Bay between 1892 and 1941 yielding an average sedimentation rate of about 0.2 m/yr. Figure 2.12 shows an example for the water depth measured in 1892, 1941 and 1958 by Jordan (1962), along profile B-B' shown in Figure 2.6, in addition to the water depth in 2005 extracted from the bathymetry map by Caldwell et al. (2011). Despite changes in resolution between the two sources it can be concluded that there is a continuous change in the water depth without any trend of continuous filling or erosion but rather random variation. Specifically, earthquakes have caused slumps, uplift and probably slope stability failures. This makes calculating the deposition rate based on these profiles not representative (Jordan 1962; Molnia 1979). Given these factors and considering that the penetration depths did not exceed 34 cm for the deployments with this PWP response type, the soil is likely normally consolidated to lightly overconsolidated within the penetrated depth. However, coarse sediment deposits from slumps and earthquakes may increase the permeability of sediments in this area.

Although the penetration rate in the case of the PFFP is more than 50 times the standard penetration rate for the CPT test, the excess PWP at the maximum dynamic force agreed well with the expected behavior during CPT penetration (e.g. Robertson and Campanella 1983; Lunne et al. 1997).

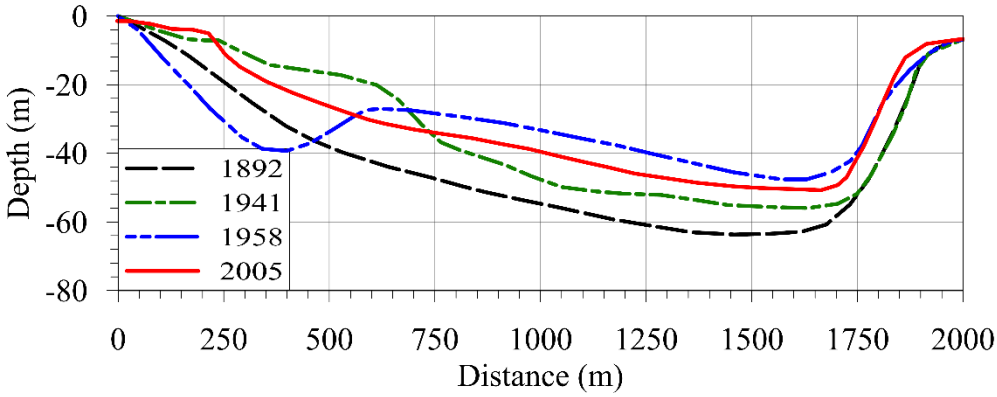

Figure 2.12. The change of water depth along one of Jordan (1962) profiles which shown in Figure (2.6) (B-B'). The figure shows also the water depth in 2005 extracted from the bathymetry map after Caldwell et al. (2011).

Attention must be drawn to the fact that the sand response to CPT is mainly drained while it was found that the sediment response during PFFP penetration is mainly undrained, even in the sandy sediments (Lucking et al. 2017). Nevertheless, the results suggested the possibility of using the excess PWP from PFFP for a quantitative sediment characterization, and may encourage the development of a soil behavior chart as introduced by Robertson (1990) for CPT.

2.7 Conclusions

The use of free fall penetrometers provides an economic, safe and rapid option for investigating the surficial seabed layers in areas of difficult access and logistic restrictions. A regional classification scheme based on the maximum deceleration of the probe during penetration, and estimated quasi-static bearing capacity was derived which can be used for future investigations in the region or as a guideline for other areas. The classification scheme was developed using only visual field observations, and the available literature from the region, in addition to the penetrometer results. It served the assessment of the area's current sediment distribution and sedimentation history.

Few portable free fall penetrometers offer pore pressure measurements. The excess pore water pressures during impact correlated to the sediment type. Positive excess pore water pressures were observed for the deployments in clay, and negative excess pore water pressures were measured for most of the deployments in silt and sand, reflecting a dilative behavior. The pore pressure response at rest was evaluated with regard to the sediment's state of consolidation. The results offered complementary insights into the in-situ sediment characteristics. The study represents a first attempt to use the pore pressure response data of the penetrometer at rest over a period of only few seconds to study the sediment behavior. This short measurement period leads to some uncertainty as the pore pressure response may still change after 2-10 seconds of the penetrometer at rest (Chow et al. 2014). A longer time of observation will be considered for future investigations if the environmental conditions allow. Controlled tests in a calibration chamber would provide insight into the pore water pressure response during and after the free fall penetrometer penetration, considering different sediment characteristics and consolidation states, and are planned for the near future.

Overall, the results allowed to map sediment types, and to get a rapid assessment of the sediment strength and state of consolidation. Furthermore, areas impacted by most recent sediment deposition events related to the seismic or glacier activity of the region were clearly identified.

2.8 Acknowledgments

This study was funded by the Institute for Critical Technology and Applied Science (ICTAS) at Virginia Tech. The authors appreciate the assistance of Fred Falcone and Brandon Quinn during the field investigations. The authors also acknowledge on-site support by the City and Borough of Yakutat, and specifically, Rhonda Coston, the harbor master, and Bill Lucy, and by Bill Staby of Resolute Marine Energy. The authors also appreciate the support by Chris Zobel (Pamplin School of Business, Virginia Tech).

2.9 References

Armentrout, J. 1980. Surface Sediments and Associated Faunas of Upper Slope, Shelf and Bay Environments Yakataga-Yakutat Area, Northern Gulf of Alaska. *Pacific Coast Paleogeography Symposium 4: Quaternary Depositional Environments Of The Pacific Coast*. 241–255.

Aubeny, C. P., and H. Shi. 2006. Interpretation of Impact Penetration Measurements in Soft Clays. J. Geotech. Geoenvironmental Eng. **132**: 770–777. doi:10.1061/ ASCE 1090-0241 2006 132:6 770

Bauer, M. A., G. L. Pavlis, and M. Landes. 2014. Subduction geometry of the Yakutat terrane, southeastern Alaska. Geosphere **10**: 1161–1176. doi:10.1130/GES00852.1

Boulton, G. S., and K. E. Dobbie. 1993. Consolidation of sediments by glaciers: relations between sediment geotechnics , soft-bed glacier dynamics and subglacial ground-water flow. J. Glaciol. **39**: 26–44.

Burns, S., and P. Mayne. 1998. Monotonic and dilatory pore-pressure decay during piezocone tests in clay. Can. Geotech. J. **35**: 1063–1073. doi:10.1139/t98-062

Caldwell R.J., B.W. Eakins, and E. Lim. 2011. Digital elevation models of Yakutat, Alaska: procedures, data sources and analysis. NOAA Technical Memorandum NESDIS NGDC-41.

Carlson, P. R., B. F. Molnia, S. C. Kittelson, and J. Hampson, J.C. 1977. Map of distribution of bottom sediments on the continental shelf, northern Gulf of Alaska.

Carlson, P. R., B. F. Molnia, J. Hampson, P. Austin, and T. J. Atwood. 1978. Post-deglaciation sedimentation in Yakutat Bay, Alaska. Transactions-American Geophysical Union, **59**: 296-296.

Carlson, P. R., B. F. Molnia, and M. C. Wheeler. 1980. Seafloor geologic hazards in OCS lease area 55, eastern Gulf of Alaska. *12th Offshore Technology Conference* 593–598. doi:10.4043/3914-MS

Chow, S. H., C. D. O'Loughlin, and M. F. Randolph. 2014. Soil strength estimation and pore pressure dissipation for free-fall piezocone in soft clay. Géotechnique **64**: 817–827. doi:DOI 10.1680/geot.14.P.107

Cowan, E. A., J. Cai, R. D. Powell, J. D. Clark, and J. N. Pitcher. 1997. Temperate glacimarine varves; an example from Disenchantment Bay, Southern Alaska. J. Sediment. Res. **67**: 536–549. doi:10.1306/D42685C7-2B26-11D7-8648000102C1865D

Cowan, E. A., P. R. Carlson, and R. D. Powell. 1996. The Marine Record of the Russell Fiord Outburst Flood, Alaska, U.S.A. Ann. Glaciol. **22**: 194–199. doi:http://dx.doi.org/10.3198/1996AoG22-1-194-199

Dayal, U., and J. H. Allen. 1973. Instrumented Impact Cone Penetrometer. Can. Geotech. J. **10**: 397–409. doi:10.1139/t73-034

Dayal, U., and J. H. Allen. 1975. The Effect of Penetration Rate on the Strength of Remolded Clay and Sand Samples. Can. Geotech. J. **12**: 336–348. doi:10.1139/t75-038

Dean, E. T. R. 2010. Offshore geotechnical engineering principles and practice, Thomas Telford.

Duncan, J. M., S. G. Wright, and T. L. Brandon. 2014. Soil strength and slope stability, John Wiley & Sons.

Hayes, M. O., C. H. Ruby, M. F. Stephen, and S. J. Wilson. 1976. Geomorphology of the Southern Coast of Alaska. *Proceedings of 15th Conference on Coastal Engineering, Honolulu, Hawaii, 1976.* 1992–2008.

Jordan, G. F. 1962. Redistribution of sediments in Alaskan bays and inlets. Geogr. Rev. **52**: 548–558. doi:10.1038/126199a0

Kopf, A., S. Stegmann, G. Delisle, B. Panahi, C. S. Aliyev, and I. Guliyev. 2009. In situ cone penetration tests at the active Dashgil mud volcano, Azerbaijan: Evidence for excess fluid

pressure, updoming, and possible future violent eruption. Mar. Pet. Geol. **26**: 1716–1723. doi:10.1016/j.marpetgeo.2008.11.005

Lucking, G., N. Stark, T. Lippmann, and S. Smyth. 2017. Variability of in situ sediment strength and pore pressure behavior of tidal estuary surface sediments. Geo-Marine Lett. 1–16. doi:10.1007/s00367-017-0494-6

Lunne, T., P. K. Robertson, and J. J. M. Powell. 1997. Cone Penetration Testing in Geotechnical Practice,.

Mayne, P. W. 2001. Stress-strain-strength-flow parameters from enhanced in-situ tests. International Conference on In-Situ Measurement of Soil Properties & Case Histories [In-Situ 2001]. Bali, Indonesia: 27–48.

Mayo, L. R. 1989. Advance of Hubbard glacier and 1986 outburst of Russell Fiord, Alaska, U.S.A. Ann. Glaciol. **13**: 189–194.

Molnia, B. 1979. Sedimentation in coastal embayments, northeastern Gulf of Alaska. *11th Offshore Technology Conference*. 665–670. doi:10.4043/3435-MS

Molnia, B. F., and J. R. Hein. 1982. Clay Mineralogy of a Glacially Dominated, Subarctic Continental Shelf: Northeastern Gulf of Alaska. J. Sediment. Res. **52**: 515–527. doi:10.1306/212F7F90-2B24-11D7-8648000102C1865D

Mulukutla, G. K., L. C. Huff, J. S. Melton, K. C. Baldwin, and L. A. Mayer. 2011. Sediment identification using free fall penetrometer acceleration-time histories. Mar. Geophys. Res. **32**: 397–411. doi:10.1007/s11001-011-9116-2

Previsic, M., and Bedard, R. 2009. Yakutat Conceptual Design, Performance, Cost and Economic Wave Power Feasibility Study. Tech. Report No. EPRI-WP-006-Alaska.

Robertson, P. K., and R. G. Campanella. 1983. Interpretation of cone penetration tests. Part II: Clay. Can. Geotech. J. **20**: 734–745. doi:10.1139/t83-079

Robertson, P. K. 1990. Soil classification using the cone penetration test. Can. Geotech. J. **27**: 151–158. doi:10.1139/t90-014

Robertson, P. K., J. P. Sully, D. J. Woeller, T. Lunne, J. J. M. Powell, and D. G. Gillespie. 1992. Estimating coefficient of consolidation from piezocone tests. Can. Geotech. J. **29**: 539–550. doi:10.1139/t92-061

Sandven, R. 2010. Influence of test equipment and procedures on obtained accuracy in CPTU. *2nd International Symposium on Cone Penetration Testing*. 26. Huntington Beach, CA.

Edited by Mitchell et al.

Sangrey, D. A., E. C. Clukey, and B. F. Molnia. 1979. Geotechnical Engineering Analysis Of Underconsolidated Sediments From Alaska Coastal Waters. *Offshore Technology Conference*. doi:10.4043/3436-MS

Seifert, A., S. Stegmann, T. Mörz, M. Lange, T. Wever, and A. Kopf. 2008. In situ pore-pressure evolution during dynamic CPT measurements in soft sediments of the western Baltic Sea. Geo-Marine Lett. **28**: 213–227. doi:10.1007/s00367-008-0102-x

Stark, N., A. Kopf, H. Hanff, S. Stegmann, and R. Wilkens. 2009. Geotechnical investigations of sandy seafloors using dynamic penetrometers. Oceans 2009. 1–10. Biloxi, MS

Stark, N., and Wever, T.F. 2009. Unraveling subtle details of expendable bottom penetrometer (XBP) deceleration profiles. Geo-Marine Letters, **29**(1): 39–45. doi:10.1007/s00367-008-0119-1.

Stark, N., H. Hanff, C. Svenson, V. B. Ernstsen, A. Lefebvre, C. Winter, and A. Kopf. 2011. Coupled penetrometer, MBES and ADCP assessments of tidal variations in surface sediment layer characteristics along active subaqueous dunes, Danish Wadden Sea. Geo-Marine Lett. **31**: 249–258. doi:10.1007/s00367-011-0230-6

Stark, N., and A. Kopf. 2011. Detection and quantification of sediment remobilization processes using a dynamic penetrometer. *IEEE/MTS Oceans 2011*. 1–9.

Stark, N., R. Wilkens, V. B. Ernstsen, M. Lambers-Huesmann, S. Stegmann, and A. Kopf. 2012. Geotechnical Properties of Sandy Seafloors and the Consequences for Dynamic Penetrometer Interpretations: Quartz Sand Versus Carbonate Sand. Geotech. Geol. Eng. **30**: 1–14. doi:10.1007/s10706-011-9444-7

Stark, N., B. Quinn, K. Ziotopoulou, and H. Lantuit. 2015. Geotechnical investigation of pore pressure behavior of muddy seafloor sediments in an arctic permafrost environment. The ASME 2015 34th International Conference on Ocean, Offshore and Arctic Engineering (OMAE2015). ASME. 1–10. doi:10.1115/OMAE2015-41583

Stark, N., Radosavljević, B., Quinn, B.M., and Lantuit, H. 2016. Application of a portable free-fall penetrometer for the geotechnical investigation of the Arctic nearshore zone. Canadian Geotechnical Journal, (ja): 1–16. doi:10.1139/cgj-2016-0087.

Stegmann, S., T. Morz, and A. Kopf. 2006. Initial results of a new free fall cone penetrometer (FF- CPT) for geotechnical in situ characterisation of soft marin sediments. Nor. J. Geol. **86**: 199–208

Steiner, A., A. J. Kopf, J.-S. L'Heureux, S. Kreiter, S. Stegmann, H. Haflidason, and T. Moerz. 2013. In situ dynamic piezocone penetrometer tests in natural clayey soils—a reappraisal of strain-rate corrections. Can. Geotech. J. **51**: 272–288. doi:10.1139/cgj-2013-0048

Stephan, S., N. Kaul, and H. Villinger. 2015. Validation of impact penetrometer data by cone penetration testing and shallow seismic data within the regional geology of the Southern North Sea. Geo-Marine Lett. **35**: 203–219. doi:10.1007/s00367-015-0401-y

Stoll, R. D., and T. Akal. 1999. XBP - Tool for rapid assessment of seabed sediment propertie. Sea Technol. **40**: 47–51.

Stoll, R. D., Y. F. Sun, and I. Bitte. 2007. Seafloor properties from penetrometer tests. IEEE J. Ocean. Eng. **32**: 57–63. doi:10.1109/JOE.2007.890943

Tarr, R. S., and B. S. Butler. 1909. The Yakutat Bay region, Alaska; physiography and glacial geology: U.S. Geol. Surv. Prof. Pap. **64**: 183p.

Tarr, R. S., and L. Martin. 1912. Earthquakes at Yakutat Bay, Alaska, in September 1899. U.S. Geol. Surv. Prof. Pap. **69**: 133.

Terzaghi, K. 1943. Theoretical soil mechanics, Wiley, New York.

Trabant, D. C., R. S. March, and D. S. Thomas. 2003. Hubbard Glacier, Alaska: Growing and advancing in spite of global climate change and the 1986 and 2002 Russell Lake outburst floods. U.S. Geol. Surv. Fact Sheet 1–3.

Twenhofel, W. S. 1952. Recent shore-line changes along the Pacific coast of Alaska. Am. J. Sci. **250**: 523–548. doi:10.2475/ajs.250.7.523

Ullrich, A. D., E. A. Cowan, S. D. Zellers, J. M. Jaeger, and R. D. Powell. 2009. Intra-annual Variability in Benthic Foraminiferal Abundance in Sediments of Disenchantment Bay, an Alaskan Glacial Fjord. Arct. Antarct. Alp. Res. **41**: 257–271. doi:10.1657/1938-4246-41.2.257

Willems, B. A., R. D. Powell, E. A. Cowan, and J. M. Jaeger. 2011. Glacial outburst flood sediments within Disenchantment Bay, Alaska: Implications of recognizing marine jökulhlaup deposits in the stratigraphic record. Mar. Geol. **284**: 1–12. doi:10.1016/j.margeo.2011.03.004

Wright, F. F. 1972. Marine geology of Yakutat Bay, Alaska. U.S. Geol. Surv. Prof. Pap. 800-B: B9–B15.

Chapter 3: In-Situ Geotechnical Early Site Assessment of a Proposed Wave Energy Converter Site, Yakutat, Alaska, Using a Portable Free-Fall Penetrometer

The contributions of authors to the composition of this manuscript are delineated as follows:

Ali Albatal:

- Conducted the literature review; performed all analyses; prepared figures and tables; wrote the draft manuscript.
- Addresses the comments and suggestions of the coauthor in developing a draft manuscript.
- Addressed the reviewers' comments and prepared the final version of the manuscript.

Nina Stark:

- Planned, supervised and participated in the field surveys.
- Supervised the study.
- Reviewed and edited the draft manuscript.
- Reviewed and edited the response to reviewers' comments and final version of the manuscript.

In-Situ Geotechnical Early Site Assessment of a Proposed Wave Energy Converter Site, Yakutat, Alaska, Using a Portable Free-Fall Penetrometer

Ali Albatal and Nina Stark

Published by the American Society of Civil Engineers (ASCE) as part of the Proceedings of Geo-Chicago 2016: Sustainable Geoenvironmental Systems, August 14-18, 2016, Chicago, IL

Reference:

Albatal, A., and Stark, N. (2016). "In Situ Geotechnical Early Site Assessment of a Proposed Wave Energy Converter Site in Yakutat, Alaska, Using a Portable Free-Fall Penetrometer." Geo-Chicago 2016, Chicago, IL, 429–438. DOI: 10.1061/9780784480137.041.

Relevant Appendices:

Appendix C: Comparison between nearshore zones of Cannon Beach, AK and the USACE's Field Research Facility Beach, NC

3.1 Abstract

Wave energy converters (WECs) are promising techniques with regard to the production of sustainable energy. However, the geotechnical and sedimentological site assessment, and the resulting foundation or anchoring design, can still represent a major challenge due to the energetic environmental conditions in the targeted areas. Most recently, portable free-fall penetrometers were suggested for the early site assessment of WEC projects as an innovative cost-effective method to investigate the uppermost layers of the seabed with regard to sediment strength and possible sediment transport processes. In this study, early site assessment was conducted at a proposed WEC site near Cannon Beach, Yakutat, Alaska, using the free fall penetrometer *BlueDrop*. 151 deployments were performed in water depths of 3-40 m during three survey days in May and July, 2014. The results suggested an average quasi-static bearing capacities of 125 ± 18 kPa (normalized for a constant penetration velocity of 2 cm/s) at the uppermost seafloor surface, generally increasing with distance to the shore and water depth. A loose top layer of reworked sediments of up to 4 cm in thickness was detected, indicating moderate sediment remobilization processes. Lower strength and abundance of loose sediment top layers were particularly observed at water depths less than about 15 m.

3.2 Introduction

Ocean energy is one of the most promising sources for the harvesting of renewable energy. The world's oceans offer a large amount of energy in the form of waves, tides, currents and heat (Ghosh and Prelas 2011). This energy potentially covers more than the world's need of power, and the interest of using it is continuously increasing (Pelc and Fujita 2002). Oceans around the world produce up to 10 TW of wave energy (Muetze and Vining 2006). Depending on the wave height, one wave can transmit more than 50 kW per meter length of the wave front (Muetze and Vining 2006; Cornett 2009; Letcher 2014). Considering this amount of energy, researchers and developers are racing to produce the most efficient and reliable designs of wave energy converters (WECs). Alaska is well-known for energetic wave conditions. With a wave power density of about 1,570 TWh/yr, Alaska's continental shelf contains about 60% of the U.S. wave power density (EPRI 2011). Motivated by this potential and the region's demand for an alternative energy source to

fossil fuels, Alaska became a target area for the harvesting of wave energy in the U.S. In this framework, Yakutat, Alaska, was identified as an area of interest (EPRI 2009).

In order to secure an efficient wave energy production, it is essential to choose an appropriate location to deploy the WECs. The potential energy production, the environmental impact, and particularly for bottom-mounted WECs, the seabed stability and sediments dynamics should be considered to determine the appropriate deployment location (Falnes and Løvseth 1991; Cornett 2009; Stark et al. 2014). An energetic environment can jeopardize the stability of the foundation, the mooring and the cable systems, increasing the need for a detailed site assessment (Muetze and Vining 2006). However, the seabed investigation can represent a major challenge at sites characterized by strong hydrodynamics, with regard to the field activities as well as to the associated costs (Letcher 2014; Stark et al. 2014). In addition to the cost of equipment, labor, and the data processing and interpretation, an equipped vessel for the purpose of offshore site investigation can cost up to $500,000 per day even if only shallow water depths are targeted (Randolph et al. 2005). Thus, budget restrictions, particularly at early stages of such projects, can prohibit the site assessment of the seabed with conventional strategies. This can lead to delays, or even cancellations of projects.

Portable free fall penetrometers (PFFP[2]) have been suggested as an economic and rapid method to investigate the seabed's uppermost sediment layers (Colp et al. 1975; Dayal 1980; Stoll and Akal 1999; Stark and Kopf 2011). The basic idea is to estimate the soil bearing resistance (or even shear strength) by measuring the deceleration of a soil impacting and penetrating probe based on semi-empirical equations and for different penetration depths reached (Dayal 1980; Aubeny and Shi 2006; Stark et al. 2012a).

This article is focusing on the in-situ geotechnical characterization of the seabed surface and the sediment dynamics in the vicinity of a proposed deployment location of a bottom mounted WEC near Cannon Beach in Yakutat, Alaska. The PFFP *BlueDrop* was suggested for the preliminary site characterization of the uppermost seabed layers at the targeted location and the surrounding area (Stark et al. 2014). During two surveys in May and July 2014, a characterization of sediment type, evaluation of surficial seabed strength and mapping of areas of potential sediment remobilization was conducted. Sediment dynamics were the focus of the investigation, as they may

[2] Modified from FFP in the original manuscript to be consistent with the other manuscript in this dissertation

affect scour processes as well as the functionality of the proposed bottom-mounted device. The study also served as a demonstration of how portable free-fall penetrometers can be applied in the framework of early site assessment of WECs, and contributed to a larger geotechnical characterization of the geologically complicated area (Stark et al. 2014).

3.3 Regional Context

Yakutat is enclosed by glaciers and mountains, and is disconnected from a wider electric grid. It is located at the entrance of Yakutat Bay in the Gulf of Alaska, about 360 km northwest of Juneau (Figure 3.1). A WEC near Cannon Beach was suggested to reduce the dependency on diesel as a source of energy. The new developments of bottom mounted WECs is particularly encouraging for sites such as Yakutat which feature challenges for surface-piercing devices such as the abundance of driftwood and possibly ice.

The average measured significant wave height was about 2-2.5 m with an average dominant wave period of about 9.9 s in 2008, producing an average power density of about 22 kW/m at a water depth of 13 m (EPRI 2009; NDBC 2015).

Ruby (1977) studied the variation of the sediment particle size along the beach face between Yakutat Bay and Dry Bay which is 80 km southeast Cannon Beach (Figure 3.1). The sediments at Cannon Beach were identified as fine quartz sand and rock fragments with a mean particle size ranging from 0.2-0.3 mm, and were classified as poorly graded fine sand according to the Unified Soil Classification System (USCS) (ASTM D2487). The finer fractions were found at the upper beach face, while coarser particles were mostly abundant in the lower intertidal zone (Ruby 1977). However, a full description of the regional sediment processes is still lacking (EPRI 2009; Stark et al. 2014).

3.4 Method

The portable free-fall penetrometer *BlueDrop* (Figure 3.2) can be deployed in water depths of up to 200 m (Stark et al. 2014). The device has an approximately streamlined shape, and has a mass of 7.71 kg. The total length of the device is 63.1 cm (Figure 3.2). The main body and tail are made

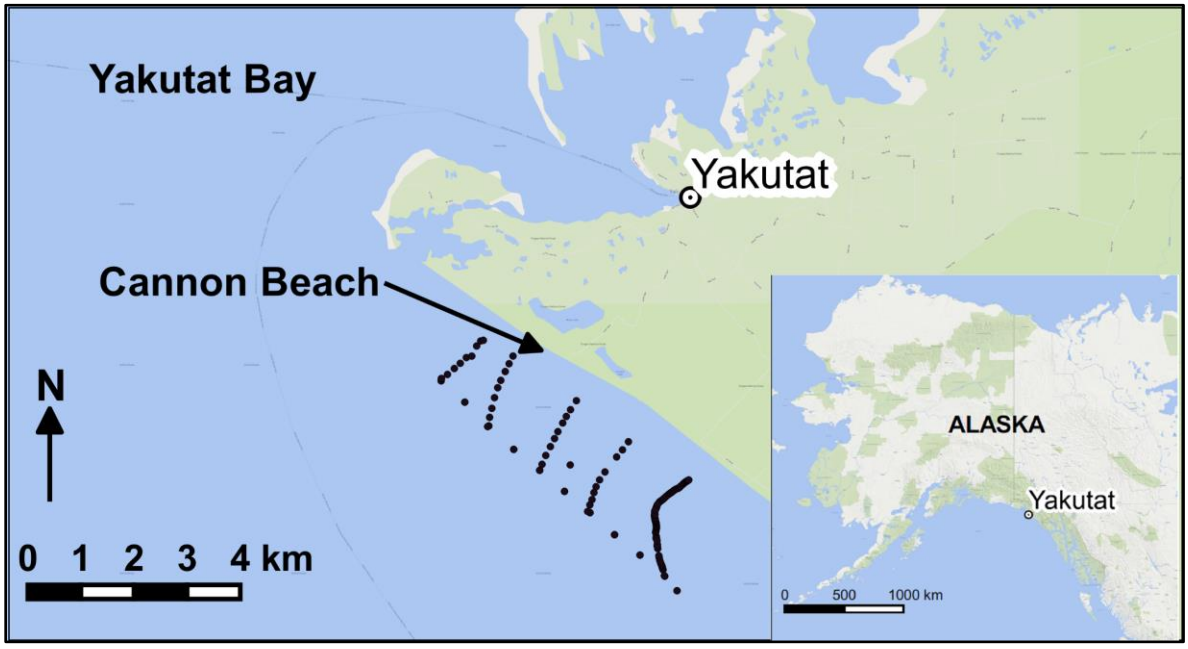

Figure. 3.1. Location of Cannon Beach in Yakutat, AK. Yakutat City coordinates are 59.5469° N, 139.7272° W. The black dots represent the penetrometer deployments locations.

of aluminum while the tip is made of steel. The body contains batteries, a pressure transducer behind the tip (i.e. u_2 location) which measures up to about 2 MPa with an accuracy of ± 4.67x10-4 kPa, five vertical microelectromechanical systems (MEMS) accelerometers recording at 2 kHz, with capacities ranging from ± 1.7-250 *g* (with *g* being the gravitational acceleration) and two 3-dimensional MEMS accelerometers with capacities up to ± 55 *g*. The device records continuously during free fall through the water column and during the soil penetration. The impact and penetration velocity and penetration depth was derived from the first and second integration of the deceleration-time profile, respectively, during impact and penetration into the soil (Dayal and Allen 1973, Stoll and Akal 1999; Stark and Wever 2009). The sediment resistance force was calculated using Newton's second law, and an equivalent of quasi-static bearing capacity *qsbc* (normalized for a constant penetration velocity of 2 cm/s) was estimated, based the approach described by Stark et al. (2012a) and the strain rate correction suggested by Dayal and Allen (1973). The water depth was estimated using the measured hydrostatic pressure at impact, because available bathymetric maps are of coarser resolution than the deployment grid.

The PFFP *BlueDrop* was deployed 151 times in a water depth ranging from 3-40 m during three survey days in May and July 2014. The deployment locations covered generously the proposed

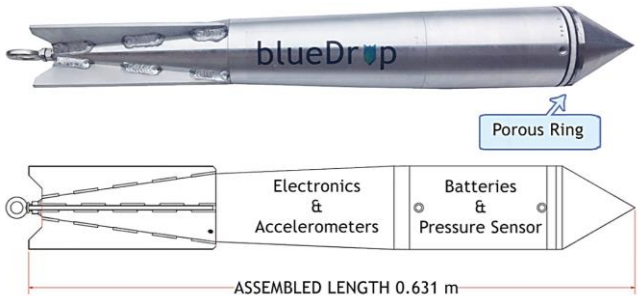

Figure. 3.2. The FFP *BlueDrop* (from www.bluecdesigns.com).

WEC deployment area to enable an assessment of the general geotechnical and morphological characteristics. They included five transects approximately perpendicular to the shore and a shore parallel transect (Figure 3.1). In addition to the penetrometer surveys, sediment grab sampling was attempted using a small, hand-deployed Van-Veen grab sampler. Unfortunately, the recovered volumes of sediment were insufficient for further analysis. Three representative samples were retrieved at Cannon Beach during low tide using a shovel. However, the here presented study was focused on the *BlueDrop* deployments.

3.5 Results

The water depth based on the *BlueDrop* results ranged between 2.9-39.5 m, being in accord with expected water depths and the available soundings of a single beam echo sounder (Figure 3.3). The resulting bathymetric contour map indicated shore parallel shoals crossing transects 2 and 3, possibly representing submerged sand bars (Figure 3.3).

The measured maximum decelerations ranged between 20-72 g ± 1.56x10-5 g with an average of about 46 g. The resulting maximum *qsbc* reached in the penetrated sediment depths (being ≤ 11 cm) 40-215 ± 5-32 kPa with an average of about 125 ± 18 kPa. Deployment duplicates at approximately the same location showed a good agreement (Figure 3.4). The lowest values of the *qsbc* (< 50 kPa) were observed at a distance of about 600-800 m from the shoreline while the highest values of the *qsbc* (> 200 kPa) were observed at distances of about 1.2 and 2.1-2.2 km from the shoreline, respectively. Generally, a trend of increasing *qsbc* with increasing water depth and distance to the shoreline was observed, particularly up to a distance of 2000 m from the shoreline (Figure 3.5).

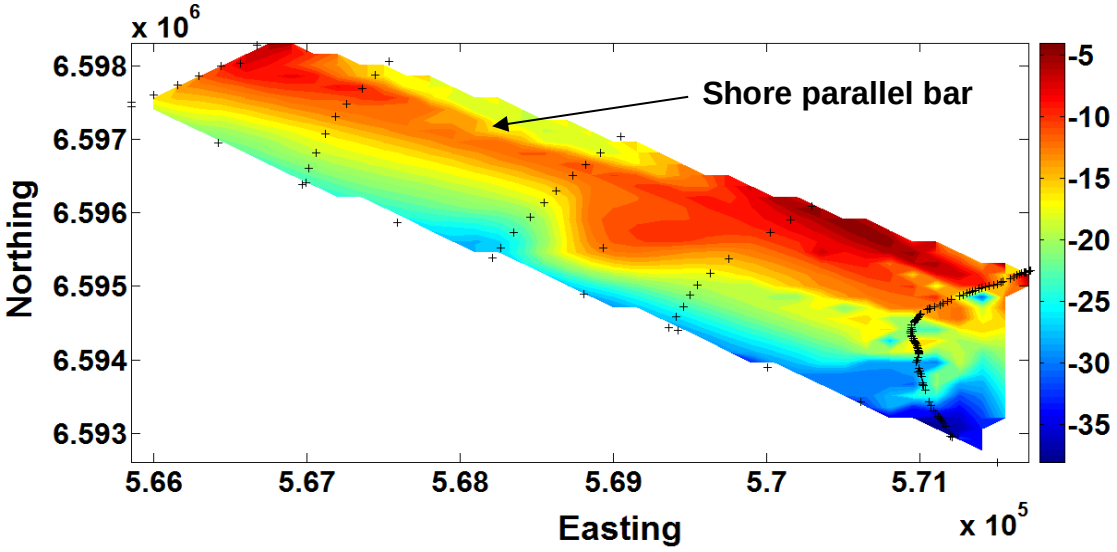

Figure. 3.3. The bathymetry of the survey area based on the *BlueDrop* deployments (crosses). The numbers 1 through 5 indicate the transect numbers. The arrow indicates a possibly shore parallel bar between transects 2 and 3.

The impact velocity varied between 2.8-5.4 m/s with an average impact velocity of 4.4 m/s. The penetration depth reached between 4-11 cm with an average value of ~6 cm. A trend of decreasing penetration depth with increasing distance from the shore, and water depth, was observed. This trend seemed to be more pronounced at water depths less than about 15 m.

A loose sediment top layer opposing a low resistance against the penetrometer was identified in 99% of the deployments (see Figure 3.4 upper 1 cm), representing a thin layer of likely mobile sediments. The maximum thickness of this layer was 4 cm, and was detected at the location of the shore parallel bar, indicating ongoing sediment remobilization processes here. As shown in Figure 3.6, which shows the variation of the loose sediment top layer thickness along transect 5, the thickness of this layer decreases with distance from the shore.

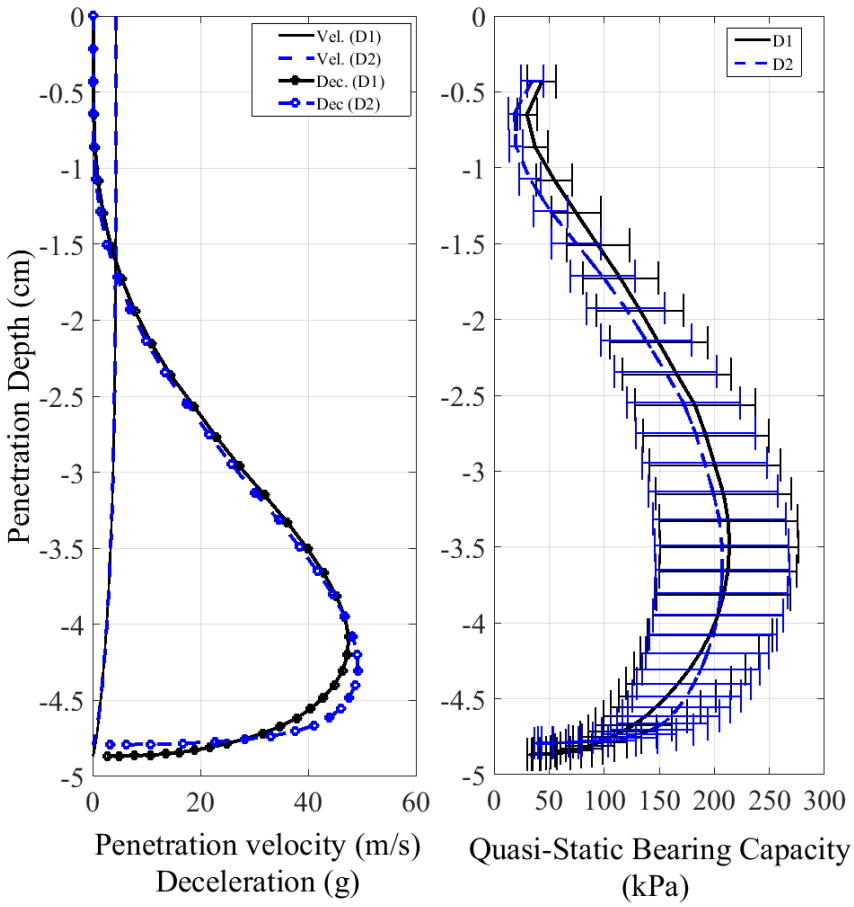

Figure. 3.4. The deceleration-depth and penetration velocity-depth (left), and *qsbc*-depth (right) profiles for two deployments (D1-black lines; D2-blue lines) at approximately the same location. The error bars represent the uncertainty ranges resulting from the strain rate factor of 1-1.5. The *qsbc* values at a sediment depth of < 0.6 cm were impacted by deviations following the calculation approach and were neglected here.

3.6 Discussion

The presented study aimed at a cost-effective geotechnical early-site investigation of seabed characteristics and sediment dynamics at a location of a proposed bottom mounted WEC, in order to contribute to the choice of the most suitable WEC deployment area. Using the PFFP *BlueDrop* allowed an economical and rapid characterization of the seabed surface. Deployment duplicates at approximately the same locations showed a high consistency (Figure 3.4). The results indicated the abundance of a thin and loose sediment top layer likely associated to wave-driven

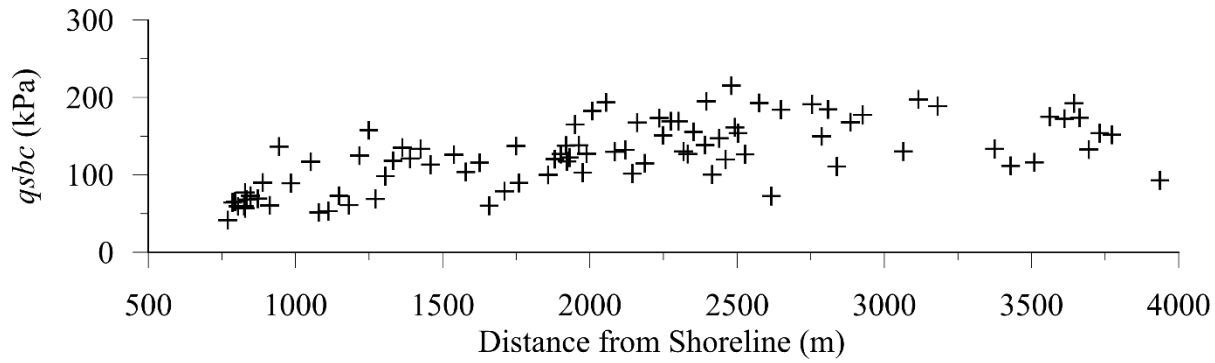

Figure. 3.5. Estimated *qsbc* with the distance from shoreline for transect 5. The figure shows an increase of *qsbc* with the increase of the distance from the shoreline to a distance of about 2000 m from the shoreline.

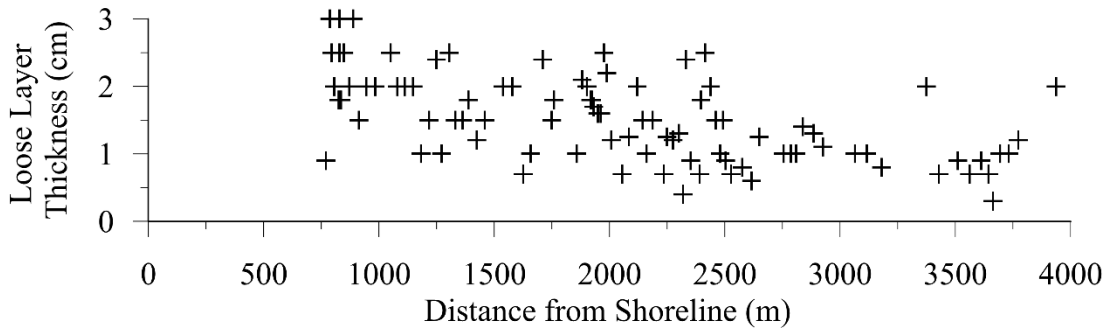

Figure. 3.6. The loose sediment top layer thickness along transect 5 showing the decrease of its thickness with the increase of the distance from the shoreline.

sediment remobilization processes (Stark and Kopf 2011). This layer reached a thickness of 4 cm at the shore parallel bar, suggesting ongoing morphodynamics. The layer became less significant with further distance from the shore and larger water depth as expected from sediment remobilization due to wave action (Nichols 2009).

The resistance of the soil against impact and penetration of an object depends on the penetrometer geometry, the impact velocity and the soil properties (Mulukutla et al. 2011, Stark et al. 2012b). Although the small penetration depth is a disadvantage when using PFFPs in sandy seabeds, it was possible to derive a first estimate for the soil bearing capacity and the sediment stiffness at the uppermost layers of the seabed surface (Stark et al 2012a). 92% of the impact velocity values ranged between 3.5 - 5.4 m/s. This would allow to classify the soil based on the penetration depth

(on average 6 cm) and maximum deceleration (on average 46 *g*), confirming a consistently sandy seabed in the tested area based on approaches presented by Stoll and Akal (1999); Mulukutla et al. (2011); Stark and Kopf (2011). However, the measured variations in deceleration values indicated a variability in the density of the sandy soils from loose to dense sands (Akal and Stoll 1995). The decrease of the penetration depth with the increase of the water depth was affected by the decrease of the impact velocity due to the increase of the rope drag force, and by the decrease of the loose mobile layer thickness (Stark et al. 2014).

The estimated *qsbc* suggested an increasing density with distance from the shore until reaching 2000 m and with water depth of up to 15 m (Figure 3.5). This may be related to the decreasing impact of waves on the seabed with the increase in the water depth. With less wave-related sediment remobilization, the particles have a larger chance to settle and form denser layers (Stark and Kopf 2011).

Uncertainties in *qsbc* followed the calculation procedure, and specifically the estimate of the strain rate factor (Stark et al 2012a; Steiner et al. 2014). However, the observed scattering of the *qsbc* values exceeded the uncertainty due to the strain rate factor range. A reason for that can be changes of the seabed slope and small-scale morphological features. Compared to the horizontal surface, a sloped surface causes a reduction in the bearing capacity (Castelli and Motta 2010). The distance between the deployments is too large to detect small seabed bedforms, but it can be expected to find wave-induced ripples in the shallow areas and even in the deeper parts of the tested area where the ripples may have formed during large storm events in the past (Quick 1982; Mogridge et al. 1994). Such small seabed formations may have caused a variation in the seabed slope and strength at the impact location (Stark et al. 2012b). This would have led to variation in the values of the *qsbc* even for the same soil characteristics. In addition to the sloped surface, these formations are usually associated with a sediment-sorting pattern of changes in sediment particle sizes between the ripples' crests and the troughs (Foti and Blondeaux 1995; Balasubramanian et al. 2008). This can cause a change in the *qsbc* results due to the change in the sediment characteristics (Mulukutla et al. 2011, Stark et al. 2012b). However, the effect of the sorting might be small due to the small range of the particle sizes. An evidence for that is the good agreement between most of the duplicated deployments (Figure 3.4). Other reasons that may explain the observed deviations are longshore variations in hydrodynamics (e.g. occasional development of rip currents) and their

impact on seabed mobilization, or the abundance of localized gravel at some locations due to the availability of rock fragments in the seabed as described by Ruby (1977).

The results showed high bearing capacity values for the seabed surface in comparison to Stark et al. (2012a), for example, who tested quartz sands in the same size range in the North Sea. This was an encouraging finding for the possibility of deploying a WEC in this area. Although only the uppermost seafloor layers were tested, the estimated values may serve as an indication for deeper sediment depths. However, this is based on the assumption that the uppermost tens of meters of the seabed are composed of the same material. This can be investigated using technologies such as chirp sonar (LeBlanc et al. 1991). The results of this survey can help in choosing priority locations, which would then be subject to a detailed site investigation, including more comprehensive field tests such as, e.g., cone penetrometer testing (CPT), vane shear tests, and/or acquisition of soil samples and cores (Stark et al. 2014).

Scour around the foundation and high amounts of suspended sediments may represent concerns in this case. Finding a shore parallel bar was an important evidence for sediment dynamics in the area, particularly at shallower water depths. However, the current results are not sufficient to get a full picture of the sediment remobilization processes and more investigations are required to assess possible risks associated to scour, as well as larger sediment relocation mechanisms. This is because (i) the bar was only identified crossing only two transects, raising a question about the stability of this bar and if there is a continuous formation and migration of bars in the region. (ii) The contour map included a significant amount of interpolation due to the limited number of transects. A hydrographic survey using e.g. a multi beam echo sounder would give significantly more detail about the local morphology. (iii) The results of the deployments represented a snapshot in time while continuous monitoring or periodic surveying is required to get a full picture of the sediments dynamics (Stark and Kopf 2011). It should also be mentioned that both surveys were conducted during calm to moderate wave conditions. Cannon Beach is classified as an erosional beach, and the sediment remobilization is expected to increase significantly under storm conditions (Ruby 1977; Nichols 2009).

3.7 Conclusions

The impact of the wave action on the proposed WEC area near Cannon Beach was evident. The change of the seabed's geotechnical characteristics with the change of the water depth was likely related to wave action. Deeper water depths were associated with (i) a decrease in the penetration depth, (ii) an increase in the *qsbc*, and (iii) a decrease in the loose mobile layer thickness. Nevertheless, significant scattering was also obvious in the *qsbc* versus water depth record. Different explanations such as small-scale morphological features, changes in seabed slope, longshore differences in hydrodynamics, or local abundance of gravel must be considered.

The results of the *BlueDrop* deployments showed that the seabed surface in the proposed WEC location is characterized by high bearing capacities, being encouraging to move on to the detailed site characterization. Another survey was conducted in August 2015 focusing on the collection of sediment samples to verify the promising results via laboratory tests. The noticeable indications for ongoing sediment transport processes emphasized the need to investigate the risk of scour and impacts through large amounts of suspended sediments.

3.8 Acknowledgments

This study was funded by the Institute for Critical Technology and Applied Science at Virginia Tech. The authors thank Brandon Quinn for his assistance during the field investigation. The authors also appreciate the support by Resolute Marine Energy Ltd, and Chris Zobel (Pamplin School of Business, Virginia Tech). On-site support through the City and Borough of Yakutat, and specifically, Rhonda Coston and Bill Lucy is highly appreciated. The authors also acknowledge technical support through Steven Smyth and the BlueCDesigns Ltd team.

3.9 References

Aubeny, C.P. and Shi, H. (2006). "Interpretation of impact penetration measurements in soft clays." J. Geotechnical and Geoenv. Eng., 132(6), 770-777.

Akal, T. and Stoll, R. D. (1995). "An expendable penetrometer for rapid assessment of seafloor parameters." Proc. MTS/IEEE OCEANS'95. Challenges of Our Changing Global Env. Conference, 3, 1822-1826.

Balasubramanian, S., Voropayev, S.I., and Fernando, H.J.S. (2008). "Grain sorting and decay of sand ripples under oscillatory flow and turbulence." J. of Turbulence, 9(17), 1-19.

Castelli, F., and Motta, E. (2010). "Bearing capacity of strip footings near slopes." Geotechnical and Geological Eng., 28(2), 187-198.

Colp, J.L., Caudle, W.N., and Schuster, C.L. (1975). "Penetrometer system for measuring in situ properties of marine sediment." Proc. IEEE Ocean 75 Conference, San Diego, CA, 405-411.

Cornett, A.M. (2009). "A global wave energy resource assessment." Sea Technology, 50(4), 59-64.

Dayal, U., and Allen, J.H. (1973). "Instrumented impact cone penetrometer." Canadian Geotechnical J., 10(3), 397-409.

Dayal, U. (1980). "Free fall penetrometer: a performance evaluation." Applied Ocean Research, 2(1), 39-43.

EPRI (Electric Power Research Institute) (2009). Yakutat conceptual design, performance, cost and economic wave power feasibility study. Tech. Report No. EPRI-WP-006-Alaska

EPRI (Electric Power Research Institute) (2011). Mapping and assessment of the US ocean wave energy resource. Tech. Report No. 1024637. Palo Alto, CA.

Falnes, J., and Løvseth J. (1991). "Ocean wave energy." Energy Policy, 19(8), 768-775.

Foti, E., and Blondeaux, P. (1995). "Sea ripple formation: the heterogeneous sediment case." Coastal Eng., 25(3), 237-253.

Ghosh, T.K., and Prelas M.A. (2011). Energy Resources and Systems: Volume 2: Renewable Resources. Springer, New York, NY.

LeBlanc L.R., Mayer, L., Rufino, M., Schock, S.G., and King, J. "Marine sediment classification using the chirp sonar." J. Acoustical Soc. of America, 91(1), 107-115.

Letcher, T.M. (2014). Future Energy: Improved, Sustainable and Clean Options for Our Planet. Second Edition, Elsevier, Boston, MA.

Mogridge, G.R., Davies, M.H., and Willis, D.H. (1994). "Geometry prediction for wave-generated bedforms." J. Coastal Eng., 22(3), 255-286.

Muetze, A. and Vining, J. (2006). "Ocean wave energy conversion-a survey." Proc., Industry Applications Conference, 2006. Conference Record of the 2006 IEEE 41st IAS Annual Meeting. 3, 1410-1417.

Mulukutla, G.K., Huff, L.C., Melton, J.S., Baldwin, K.C., and Mayer, L.A. (2011). "Sediment identification using free fall penetrometer acceleration-time histories." Marine Geophysical Research, 32(3), 397-411.

NDBC (National Data Buoy Center) (2015). "Station 46083-historical data." <http://www.ndbc.noaa.gov/station_page.php?station=46083> (June 22, 2015).

Nichols, G. (2009). Sedimentology and Stratigraphy. John Wiley & Sons, West Sussex, UK.

Pelc, R. and Fujita, R.M. (2002). "Renewable energy from the ocean." Marine Policy 26(6), 471–479.

Quick, M.C. (1982). "Wave-induced sand ripples." Canadian J. of Civil Eng. 9(2), 285-295.

Randolph, M., Cassidy, M., Gourvenec, S. and Erbrich, C. (2005). "Challenges of offshore geotechnical engineering." Proc., Int. Conference on Soil Mech. and Geotechnical Eng., ISSMGE, Osaka, Japan, 16(1), 1-123.

Ruby, C.H. (1977). Coastal morphology, sedimentation and oil spill vulnerability, northern Gulf of Alaska. Tech. Report No. 15-CRD, University of South Carolina.

Stark, N., and Wever, T.F. (2009). "Unraveling subtle details of expendable bottom penetrometer (XBP) deceleration profiles." Geo-Marine Letters, 29(1), 39-45.

Stark, N. and Kopf, A. (2011). "Detection and quantification of sediment remobilization processes using a dynamic penetrometer." Proc. IEEE/MTS Oceans 2011 Conference, Waikoloa, HI.

Stark, N., Wilkens, R., Ernstsen, V.B., Lambers-Huesmann, M., Stegmann, S., and Kopf, A. (2012a). "Geotechnical properties of sandy seafloors and the consequences for dynamic penetrometer interpretations: quartz sand versus carbonate sand." J. Geotechnical and Geological Eng., 30(1), 1-14.

Stark, N., Coco, G., Bryan, K.R., and Kopf, A. (2012b). "In-situ geotechnical characterization of mixed-grain-size bedforms using a dynamic penetrometer." J. Sedimentary Research, 82(7), 540-544.

Stark, N. Hay, A.E. and Trowse, G. (2014). "Cost-effective geotechnical and sedimentological early site assessment for ocean renewable energies." Proc. IEEE/MTS Oceans 2014 Conference, St. John's, NL.

Steiner, A., Kopf, A. J., L'Heureux, J. S., Kreiter, S., Stegmann, S., Haflidason, H., and Moerz, T. (2014). "In situ dynamic piezocone penetrometer tests in natural clayey soils—a reappraisal of strain-rate corrections." Canadian Geotechnical J., 51(3), 272-288.

Stoll, R.D., and Akal, T. (1999). "XBP-tool for rapid assessment of seabed sediment properties." Sea Technology, 40 (2), 47-51.

Chapter 4: Estimating in-situ relative density and friction angle of nearshore sand from portable free fall penetrometer tests

The contributions of authors to the composition of this manuscript are delineated as follows:

Ali Albatal:

- Participated in one of the three field surveys (August 2015) conducted in Yakutat Bay.
- Initiated the idea, reviewed the literature; performed all analyses; prepared figures and tables; wrote the draft manuscript.
- Conducted the laboratory tests.
- Addresses the comments and suggestions of the coauthors in developing a draft manuscript.

Nina Stark:

- Planned, supervised and participated in the three field surveys.
- Helped finalizing the idea.
- Supervised the study.
- Reviewed and edited the draft manuscript.

Bernardo Castellanos

- Reviewed and edited the draft manuscript.
- Supervised the laboratory tests.

Estimating in-situ relative density and friction angles of nearshore sand from portable free fall penetrometer tests

Ali Albatal, Nina Stark and Bernardo Castellanos

The authors of the following manuscript intend to submit it to the Canadian Geotechnical Journal.

Relevant Appendices:

Appendix B: Laboratory tests Cannon Beach sand

4.1 Abstract

The in-situ relative density and friction angle of sand in the nearshore zone of Cannon Beach, Yakutat, Alaska, were estimated from the deceleration measured by a portable free fall penetrometer (PFFP) at 72 test locations. A correlation between the relative density and PFFP's maximum deceleration was developed from controlled PFFP deployments into a representative sand of different relative densities. Two general approaches were tested to derive the in-situ friction angles: (1) a correlation between relative density and friction angle, and (2) bearing capacity theory. For the former, laboratory vacuum triaxial tests were performed to adjust an existing correlation between relative density and friction angle for the tested nearshore sediments. In-situ friction angles were then determined using this adjusted correlation, and the field relative densities estimated from the initially developed correlation with the maximum deceleration of the PFFP. Results showed that the in-situ relative density varies between 32-90% while the friction angle varies between 44°-57°. Two bearing capacity based methods suitable for shallow penetrations were tested. For this approach, equivalents of static cone resistance were determined from the measured decelerations considering the strain rate effect. A range of strain rate empirical coefficients K=0.1-1.5 was tested and discussed. A K value between 0.2 and 0.4 yielded matching results between the two approaches. In summary, the estimated in-situ friction angles agree well with expected values and may be applied for problems of sediment transport or early site assessment.

4.2 Introduction

The friction angle is an important parameter for the analysis of many nearshore and offshore problems including: erosion and scour calculations, prediction of sediment transport and estimating the seabed sediments' bearing capacity and shear strength. The friction angle of nearshore sand, or the corresponding angle of repose (more commonly used for sediment transport problems), is often assumed to range between 30°-33°, or is estimated using empirical relationships from controlled flume experiments (e.g., Bagnold 1973, Kirchner et al. 1990, Buffington et al. 1992, Ghazavi et al. 2008, Ibsen et al. 2012). Flume experiments often struggle to re-establish fully in-situ soil conditions (e.g., sediment density and grain size distribution), particularly if they feature dynamic sediment remobilization processes. Therefore, a method to

estimate friction angles in-situ would make an important contribution to applications related to sediment transport and geotechnical site investigations, particularly in sandy nearshore zones.

Lightweight and portable free fall penetrometers (PFFPs) provide an economic method to characterize the surficial nearshore sediments (Stark 2016). Furthermore, PFFPs have proven to be deployable in energetic nearshore conditions under which heavier equipment would represent a risk to the instruments and surveyors. A number of researchers have investigated approaches to determine the undrained shear strength of clayey sediments based on semi-empirical equations or numerical modeling from PFFP deceleration-depth measurements (e.g., Aubeny and Shi 2006, Abelev et al. 2009a, 2009b, Nazem et al. 2012, Steiner et al. 2014, Morton et al. 2015). However, literature on the analysis of PFFP deployments in sandy sediments is still limited to determining the dynamic cone resistance, or an equivalent cone resistance estimated from the deceleration measurements (e.g., Akal and Stoll 1995, Stoll et al. 2007, Stark et al. 2009, 2012, Stephan et al. 2015, Lucking et al. 2017). The small number of PFFP studies in sandy environments results from the limited penetration depth into sandy sediments (often < 20 cm). Another issue is the typically undrained behavior of sand during the fast penetration rate of the PFFP (~2.8-5.4 m/s), making the determination of the friction angle, a drained parameter, challenging and subject to uncertainties (Seed and Lundgren 1954, Steiner et al. 2014, Lucking et al. 2017). Nevertheless, the interest in surficial seabed data in sandy nearshore environments has increased with regard to (i) the determination of more accurate input parameters for sediment transport and erosion models, as well as to (ii) site reconnaissance and early site assessment for ocean renewable energy in remote locations. With sandy soils being common on beaches and in energetic nearshore environments (U.S. Army Shore Protection Manual 1974), both of these fields would benefit from estimates of friction angles, and/or relative density. Conventional cone penetration testing and even sediment coring, e.g., vibrocoring, struggle to assist in these applications due to issues to resolve or preserve the uppermost seabed surface conditions, and/or due to budget restrictions and associated limitations in spatial resolution. Thus, estimating friction angles and relative density of sands from PFFP could provide unique and affordable second order approximation.

The friction angle of sand can be determined using the relative density as an intermediate parameter (Schmertmann 1975). Different correlations and charts are available in the literature to estimate the friction angle directly from the relative density, or in combination with other known parameters like the grain size and confining pressure (e.g., Meyerhof 1956, Schmertmann 1975,

1978, Duncan et al. 2014). Therefore, attempts have been made to estimate relative density from PFFP measurements. Akal and Stoll (1995) deployed the eXpendable Bottom Penetrometer (*XBP*) in a fine sand at different relative densities, and found that the probe's maximum deceleration increased with the relative density. Orenberg et al. (1996) used a semi-empirical correlation to determine the field relative density of sand in different locations in the Gulf of Mexico, using the eXpendable Doppler Penetrometer (*XDP*). The results of their studies were in agreement with cone penetration test (CPT) results.

The quality of the free fall penetrometer data analysis method is commonly assessed by comparing the calculated equivalent cone resistance with the cone resistance obtained from CPT tests (e.g., Bowman et al. 1995, Steiner et al. 2014, Stephan et al. 2015). Although this strategy can hardly be directly applied as CPT data from surface sediments under energetic conditions are difficult to obtain, and it is subjected to its own uncertainties, it might still be valid to use of methods developed originally for CPT analysis to estimate the sand friction angle from PFFP results. The first method used in this paper is the one developed by Durgunoglu and Mitchell (1973). This method was proved to provide good results for both shallow and deep penetrations (e.g., Baldi et al. 1982; Schmertmann 1982; Robertson and Campanella 1983; Yu 2013). The second method used was developed by Meyerhof (1961). This method was used by Dayal (1980) to estimate the bearing capacity for a free fall penetrometer measurement. Dayal (1980) found a good agreement between the estimated values and the achieved values in the laboratory.

In summary, the overarching research goal of this study is to test the following two methods to estimate the in-situ friction angle of nearshore sand from PFFPs deceleration-time records: (1) Durgunoglu and Mitchell's and Meyerhof's methods, and (2) an indirect approach utilizing estimates of relative density from the penetrometer deceleration records. This goal also required to investigate the relationship between the relative density of sands and the PFFP deceleration records, as well as to discuss the need for strain rate corrections.

4.3 Methods

4.3.1 Field Measurements and Data Analysis

Field data was collected in May and July 2014, and in August 2015, in the nearshore zone off

Cannon Beach, Yakutat, Alaska (Figure 4.1). Cannon Beach is an erosional sandy beach composed of poorly graded sand with a mean particle size of 0.2-0.4 mm (Ruby 1977). The sand has a uniform grain size with small variations across the shore. Deployments were carried out at one hundred and fifty-one locations in water depths between 3 m and 40 m using the PFFP *BlueDrop*. Furthermore, 57 sediment samples were collected from Cannon Beach. This penetrometer dataset was initially presented by Albatal and Stark (2016) with the purpose of measuring spatial differences in surficial sediment strength associated to wave-driven sediment transport processes. The authors proposed that the observed spatial variations reflect differences in relative density associated to local erosion and sediment re-deposition, and potential bedform evolution, migration, and destruction. The estimate of relative densities, and even more so, in-situ friction angles, would allow to investigate this hypothesis further in the context of sediment transport models. This also motivated the use of this data set for this study, in addition to the fact that the site offers limited impacts from sediment grain size variations, or recent engineering activities.

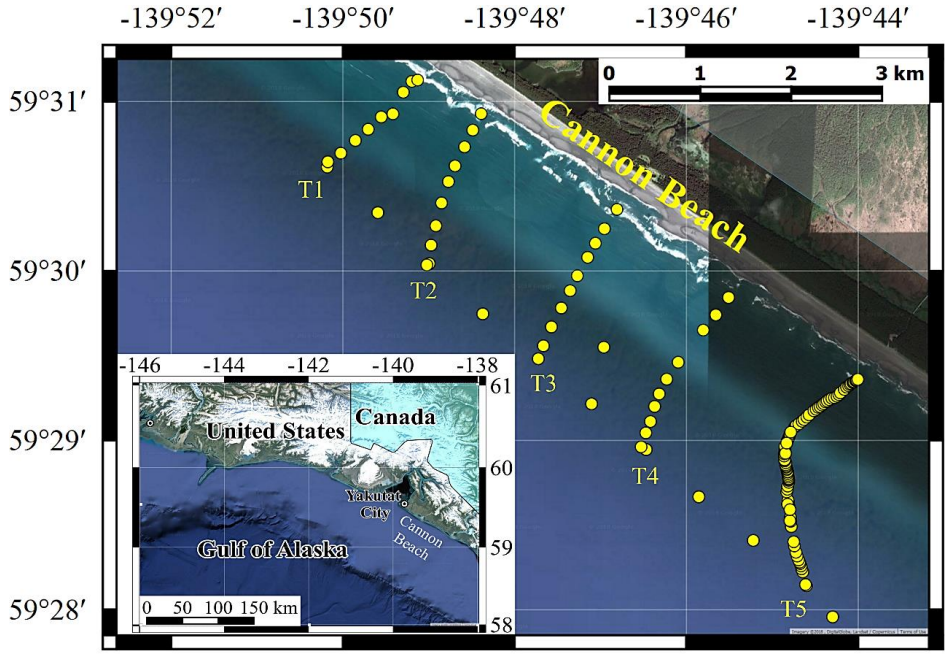

Figure 4.1. Google™ Earth (2018) image shows the location of Cannon Beach, Yakutat, AK. The yellow dots indicate the PFFP deployment positions with T1-T5 representing the cross-shore transect numbers from Albatal and Stark (2016).

4.3.1.1 Portable Free fall Penetrometer

The PFFP *BlueDrop* measures vertical accelerations/decelerations up to ±250 g (where g is the gravitational acceleration) and pore pressures up to 2 MPa, at a sampling rate of 2 kHz. The device is 63.1 cm in length, 8.75 in diameter, and weighs ~7.7 kg using the 60º conical tip option (Stark et al. 2014). The penetration velocity and depth were determined by the first and second integration of the deceleration, respectively. The procedure presented by Stark et al. (2011, 2012) was used to calculate an equivalent cone resistance $q_{c,eq}$:

Upon impact, the force resisting the penetrometer penetration (F) can be estimated using Newton's second law:

$$F = ma - F_b \tag{4.1}$$

where m is the penetrometer mass, a is the measured acceleration (deceleration in the case of sediments penetration), and F_b is the buoyancy force in salt water. Stark et al. (2016) found that neglecting the soil buoyance results in an error of about 1% in the sediment's resistance for penetration depths less than 20 cm. The achieved penetration depth for all deployments was less than 20 cm so the soil buoyance was neglected for this paper. Any impact of drag force or skin friction was also neglected, because of the penetrometer's shape which reduces the drag force in addition to the limited penetration depth (Aubeny and Shi 2006, Stark et al. 2012). Moreover, the use of an unworn cone limits the skin friction effect (DeJong et al. 2001). Considering those assumptions and the cone area A, the dynamic bearing resistance q_d can be determined from the resistance force F as follows:

$$q_d = F/A \tag{4.2}$$

To account for strain rate effects, and thus, to determine an equivalent of static resistance $q_{c,eq}$, a strain rate correction, f_{sr}, needs to be applied (Dayal and Allen 1973, Stark et al. 2011, 2012, Steiner et al. 2014):

$$q_{c,eq} = q_d/f_{sr} \tag{4.3}$$

A commonly used strain rate factor coefficient for the case of sandy soil is expressed as a logarithmic function (e.g., Stoll et al. 2007, Stark et al. 2009, 2012, Stephan et al. 2015):

$$f_{sr-log} = 1 + K \log_{10}(v_{dyn}/v_{ref}) \tag{4.4}$$

where v_{dyn} is the dynamic penetration velocity which can be determined by integrating the measured deceleration, v_{ref} is a chosen reference penetration velocity (0.02 m/s being the standard velocity for the cone penetration tests according to ASTM 5778), and K is a dimensionless empirical coefficient. The value of K is soil dependent (True 1976), and different K values have been used in the literature with values ranged between 0.0-1.5 (Table 4.1). However, the most commonly used values range between 1-1.5 for similar PFFPs based on laboratory and field experiments (Stoll et al. 2007; Stark et al. 2012, 2017; Stephan et al. 2015). Accordingly, an average initial K value of 1.25 will initially be considered, and discussed later on in the article (see results and discussion).

Stephan (2015) investigated the use of the inverse hyperbolic sine strain rate correction equation for sandy sediments. Randolph (2004) formulated this equation originally for clayey soils. Stephan compared the inverse hyperbolic sine equation to the logarithmic equation in sandy sediments, and found that they get qualitatively similar results with the equivalent cone resistance values obtained using the inverse hyperbolic sine equation being lower than those obtained using the logarithmic equation by up to 20% for K=1.5. In accord with the formulations of the strain rate correction, this difference decreased with a decrease of K. An advantage of inverse hyperbolic sine equation is the behavior of the function for $v_{dyn} < v_{ref}$, for which the value of f_{sr} converges towards f_{sr}=1, while the logarithmic equation results in a static resistance higher than the dynamic resistance. Steiner et al. (2014) also compared the inverse hyperbolic sine equation to the logarithmic equation in clayey sediments, and argued that the inverse hyperbolic sine strain rate correction equation gives more accurate results. In this study, both expressions will be tested, and the applicability of the inverse hyperbolic sine strain rate equation to sandy soils will be briefly discussed in the framework of a general discussion of the strain rate correction. The inverse hyperbolic sine strain rate equation is formulated as follows:

$$f_{sr-asinh} = 1 + \frac{K}{\ln(10)} \, sinh^{-1}\left(\frac{v_{dyn}}{v_{ref}}\right). \tag{4.5}$$

Table 4.1. The strain rate empirical coefficient *K* values used in literature

Sand Mineralogy	Max. Velocity (m/s)	*K*	Reference
Quartz sand	0.8	0.0	Dayal and Allen (1975)
	5.0	0.8-1.5	Stoll et al. (2007)
	10.0	1.0-1.5	Stark et al. (2009, 2012, 2017)
	4.6	1.5	Stephan et al. (2015)
	5.0	1.0-1.5	Lucking et al. (2017)
Carbonate sand	10.0	1.0-1.5	Stark et al. (2012)

4.3.1.2 Sampling

Fifty-seven samples were collected along five shore-normal transects. The transect locations were chosen to be as close as possible to the PFFP deployment locations shown by Albatal and Stark (2016). The samples covered the area between the base of the berm to the lower intertidal zone with 11 or 12 samples in each transect. A cubic box of known volume was used for sampling so that the field total unit weight could be calculated. The 0.87 cm^3 cube has a side length of 0.95 cm and an edge thickness of about 0.2 cm. The transparent cubic box was carefully pushed into the sediments. The box and the collected sediment were retrieved with an underlying plate to avoid loss or disturbance of the soil. The total unit weight of the samples ranged between 15.4 kN/m^3 and 20.6 kN/m^3 with an average value of 18.1 kN/m^3 while the average dry and saturated unit weights calculated based on the retrieved samples water content were 16.2 kN/m^3 and 20.1 kN/m^3, respectively. Sampling at the PFFP deployment locations was attempted as well, but a small-size grab sampler did not allow to collect samples of sufficient volume due to the high wave action. However, the little sediment collected allowed to confirm that the sediments were similar to the ones sampled in the intertidal zone.

4.3.2 Laboratory Tests

4.3.2.1 Grain Size Analysis

Grain sizes were determined following the procedures presented in ASTM D6913 and the sediment was classified according to the Unified Soil Classification System (ASTM D2487).

4.3.2.2 Shear Strength Tests

To simulate the shallow penetration depths and variations of soil density, tests were carried out under low confining pressures and at different relative densities. The samples were prepared using the sand raining method. Sand was rained from a hopper with a perforated base through a cylindrical pipe that contains a diffuser (two sieves separated by a distance *S*), and collected using a split mold (Figure 4.2). Eid (1987) divided the parameters that affect the relative density and uniformity of the sample into conditional and unconditional parameters. The conditional parameters are the distance between the hopper and diffuser (*R*), the space between the two sieves of the diffuser (*S*), the length between the diffuser and the sample (*H*) (Figure 4.2), and the particle size. According to Eid (1987), the effect of the conditional parameters can be neglected when $R \geq$ 45 cm, $S \approx 10$ cm, and $H > 50$ cm. Therefore, the conditional parameters were kept constant at R = 45 cm, S = 10 cm and H = 55 cm. By varying the unconditional parameters (the perforated base opening size and the diffuser sieves opening size), the sand samples can then be prepared at different relative densities. The perforated base opening sizes used were ranging between 2.2 mm and 11.3 mm (Figure 4.2c). This configuration allowed the preparation of samples at relative densities of 0 %, 15 %, 40 % and 75%, and with a maximum standard deviation of 1.42%.

One objective of the presented study is to estimate the sand friction angle at low confining pressures to simulate the small penetration depths when using PFFPs. The available conventional triaxial tests did not allow to test the sand under such low confining pressures (i.e. <10 kPa). The vacuum triaxial test has been suggested as a suitable method for such cases (Melzer 1974; Desai et al. 1992). The test specimen dimensions were 7.1 cm diameter and 15.2 cm in height. Three sets of vacuum triaxial tests were performed under confining pressures of 1.70 kPa, 3.45 kPa and 6.89 kPa. A significant effect from the membrane was expected when testing sand in triaxial devices especially under such small confining pressures (Ponce and Bell 1971; Melzer 1974). This effect

was reduced by about 50% using a special membrane with a thickness of 0.15 mm in comparison to a conventional membrane (0.30 mm). The most significant membrane effect (20%) was found at a low confining pressure of 1.72 kPa and 0% relative density. This value was less than the values reported by Melzer (1974), equaling 30% of the deviator stress at a confining pressure of 3.5 kPa. At higher confining pressures and densities, the membrane effect was generally smaller, and reached a value as low as 0.9% of the deviator stress at a confining pressure of 6.89 kPa and a relative density of 75%.

Since the vacuum triaxial tests were performed on dry samples, direct shear tests were performed on saturated and dry samples in order to estimate the effect of the saturation on the friction angle following the ASTM D3080 procedure. To ensure full saturation, samples were soaked overnight under the required normal stress before shearing.

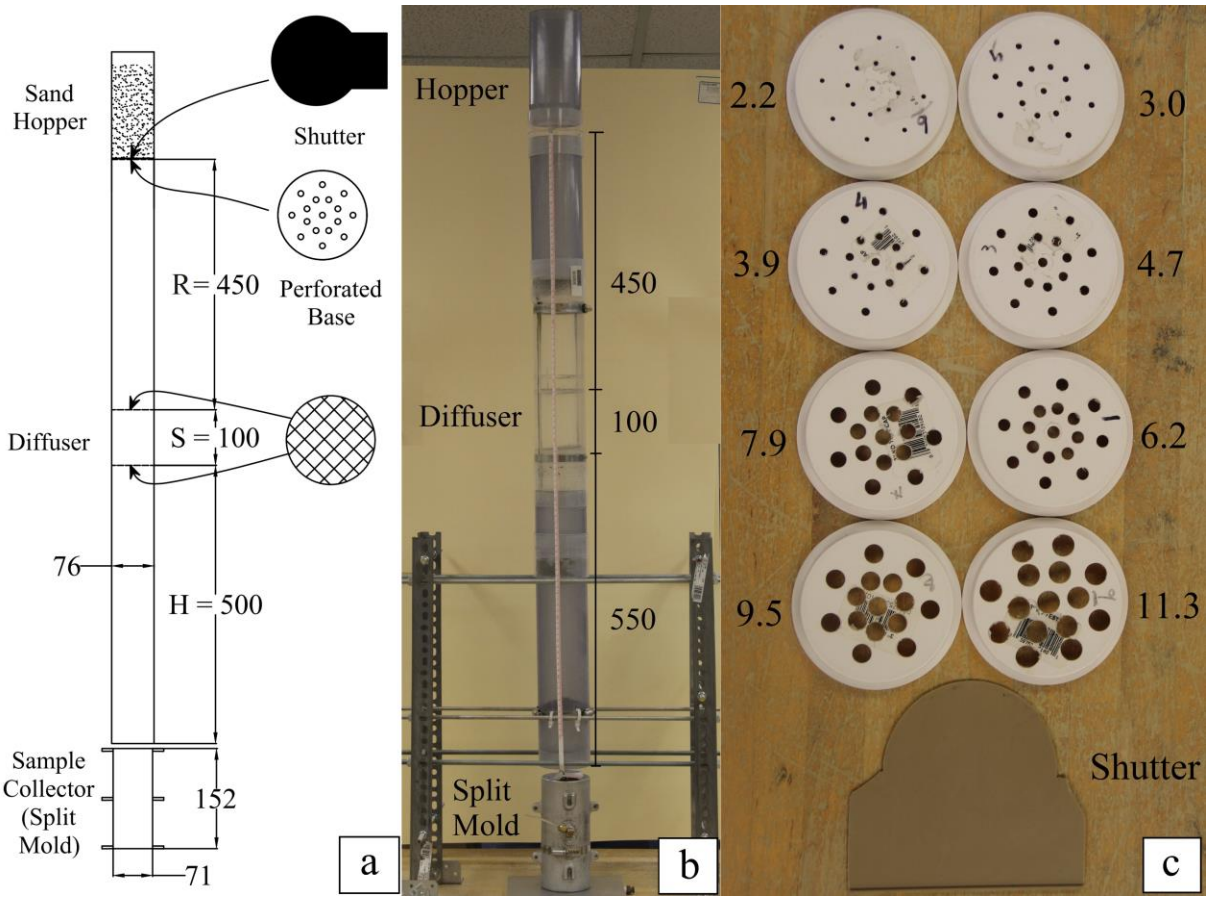

Figure 4.2. a) and b) Sand raining system used to prepare samples at different relative densities (modified after Eid 1987). c) Perforated bases used to change the soil density (numbers show the opening diameter size). All dimensions are in mm.

4.3.2.3 Relative Density from Portable Free Fall Penetrometer Deployments

In order to estimate the field relative density, the PFFP *BlueDrop* was deployed into saturated sand prepared at different relative densities in the laboratory. The laboratory setup described in Bilici and Stark (n.d.) was used for this purpose. The PFFP was dropped from a chosen height into a 40 cm height sand sample formed in a steel cylindrical barrel with a diameter of 81 cm. The water level inside the barrel was 40 cm above the sediment surface. The quantity of the sand collected at Cannon Beach was not sufficient for this test configuration. Therefore, a local quartz sand with a matching grain size distribution was used. The sand was compacted manually in layers of 4-5 cm with different compaction efforts to achieve the desired relative densities. Three relative densities were achieved: loose, medium dense and dense with final relative densities of 23%, 45% and 70%, respectively. Three tests were performed at each sample. Impact velocities similar to the field values (average of 4.7 m/s for the deployments used in this study) were targeted in order to avoid bias from strain rate effects. The impact velocity for the deployments in the laboratory ranged between 4.9-5.0 m/s. Finally, a correlation between the relative density of sand and the penetrometer deceleration records for an impact velocity of about 5 m/s was derived.

4.3.3 Estimating the Friction Angle of Sand from Field Measurements

The in-situ friction angle was estimated from the maximum deceleration using three different approaches (Figure 4.3).

4.3.3.1 Durgunoglu and Mitchell (1973) theory, ϕ'_{DM} ($\phi'_{DM\text{-}log}$ and $\phi'_{DM\text{-}asinh}$)

Durgunoglu and Mitchell (1973) developed a bearing capacity theory for the purpose of characterizing the soil at shallow and deep penetration depths using the static cone penetration tests. This method was originally developed to assess the characteristics of the topmost lunar soil using a hand held self-recording penetrometer as a part of the Apollo 15 and Apollo 16 missions. The method distinguishes between a shallow and a deep penetration, and proved to provide good results for both shallow and deep penetrations (Mitchell and Lunne 1978; Villet and Mitchell 1981; Baldi et al. 1982; Schmertmann 1982; Bellotti et al. 1983; Lunne and Christoffersen 1983; Robertson and Campanella 1983; Yu and Mitchell 1998; Yu 2013). The shallow penetrations achieved by the PFFP in this study match the penetration depths for which the Durgunoglu and

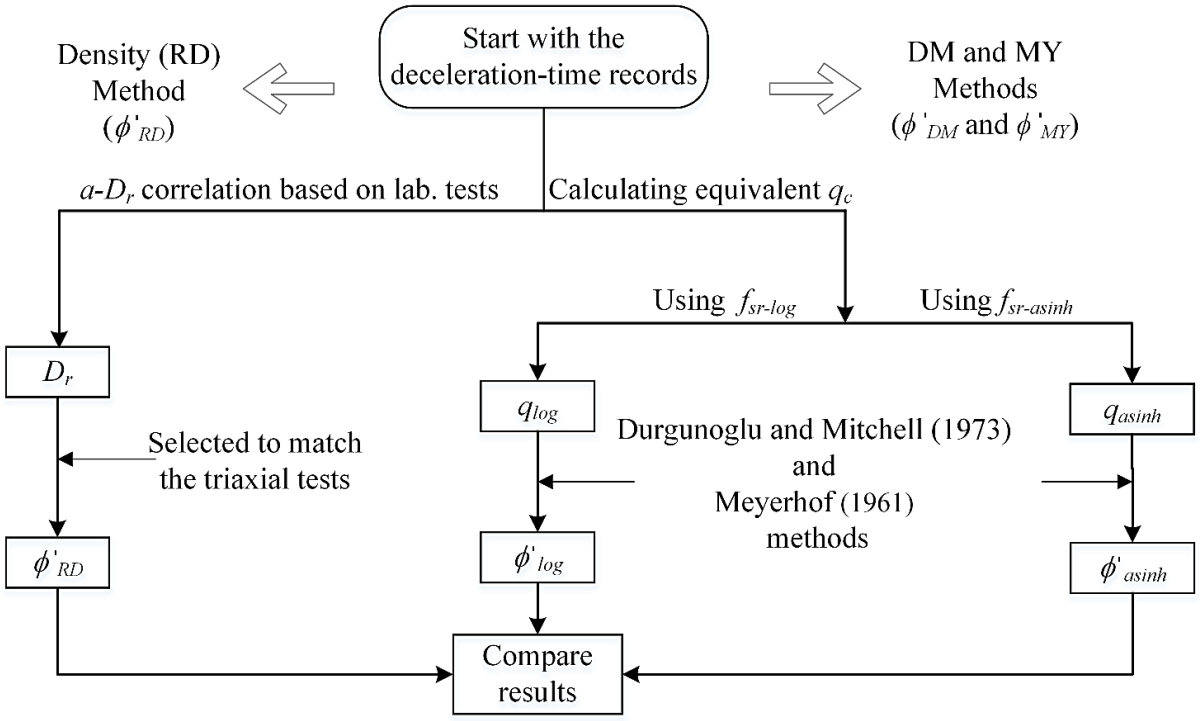

Figure 4.3. Flowchart for the analysis process to determine the sand friction angle based on the *BlueDrop* results. The dashed line represents a weakness point for the used approach (see discussion).

Mitchell bearing capacity theory was developed. For cohesionless soils, the cone resistance can be represented by:

$$q_c = \gamma_s B N_{\gamma q} \xi_{\gamma q}. \tag{4.6}$$

where γ_s is the submerged unit weight of soil, B is the penetrometer diameter, $N_{\gamma q}$ is the bearing capacity factor which includes both friction and surcharge factors (N_γ, N_q), and $\xi_{\gamma q}$ is a shape factor. The values of $N_{\gamma q}$ depends on the effective friction angle ϕ', cone roughness δ/ϕ', the penetration depth normalized to the penetrometer diameter D/B, and the penetrometer tip angle α. The friction angle was determined iteratively from the equivalent cone resistance $q_{c,eq}$ using the procedure described in detail by Durgunoglu and Mitchell (1973) which can be summarized as follows:

1. Assume: $q_c = q_{c,eq.}$
2. Determine $N_{\gamma q}$ $\xi_{\gamma q}$ from the known values $q_{c,eq}$, γ_s and B using Equation 4.6.
3. Estimate a reasonable value for ϕ'.

4. Using Figure 4.4a (or the set of equations given in Durgunoglu and Mitchell (1973) for different *D/B*), determine $N_{\gamma q}$ for the estimated ϕ'. This figure is applicable for a cone tip angle of 60°, the same tip angle used for the *BlueDrop*, and for a cone roughness of 0.5 which is a reasonable assumption for δ/ϕ' between steel cones and soil (Durgunoglu and Mitchell 1975a; Mitchell and Lunne 1978; Schmertmann 1982).
5. Determine the shape factor $\xi_{\gamma q}$ for the estimated ϕ' using the following equation:

$$\xi_{\gamma q} = 0.6 + \frac{1.5}{1 + 1.5/(0.6 + tan^6\phi')} \tag{4.7}$$

6. Repeat Steps 4 thru 5 for other values of ϕ' (e.g., increment of 1º).
7. Plot the assumed values of ϕ' versus the corresponding $N_{\gamma q}$ $\xi_{\gamma q}$ (Figure 4.4b, solid line)
8. Determine the actual ϕ' from the known value of $N_{\gamma q}$ $\xi_{\gamma q}$ (Figure 4.4b, dashed line).

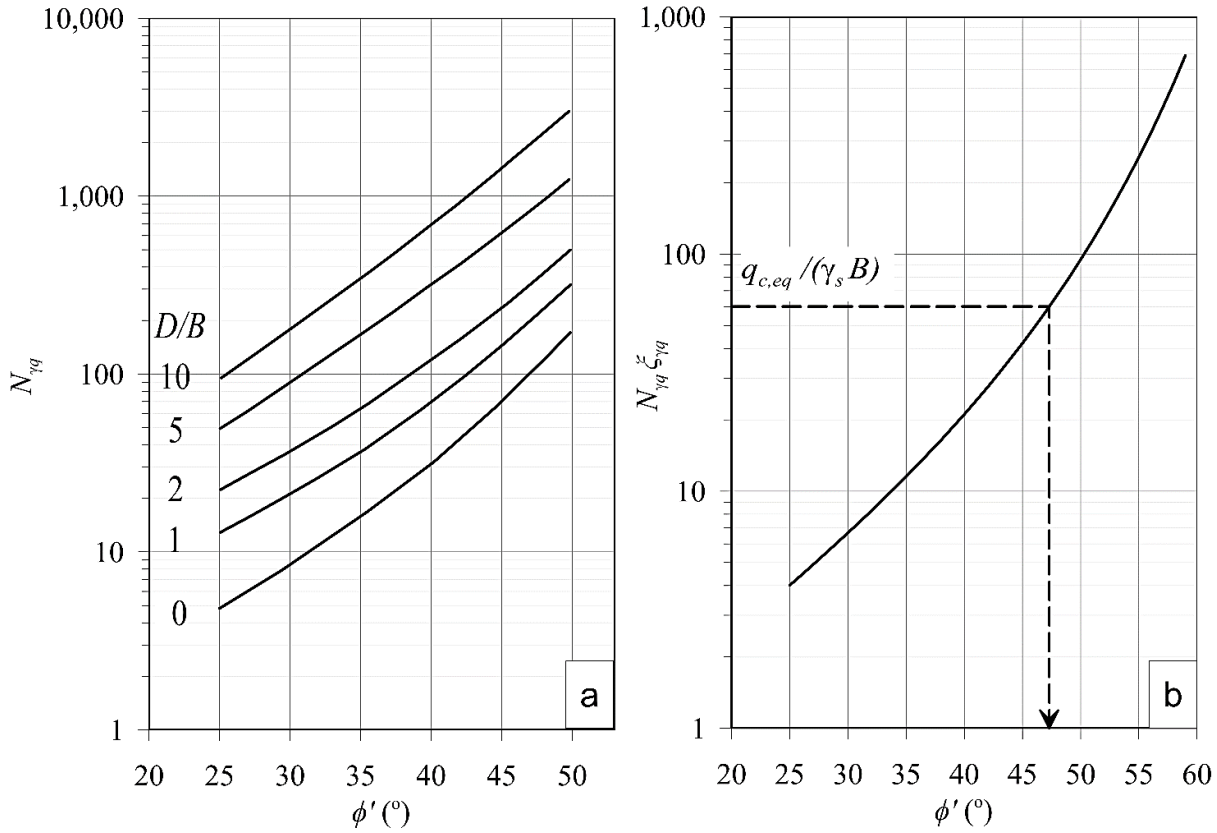

Figure 4.4. a) Bearing capacity factor for 60º tip cone, δ/ϕ=0.5 and different relative penetration depths (Durgunoglu and Mitchell 1973), b) An example for determining the friction angle using the iterative procedure.

4.3.3.2 Meyerhof (1961) bearing capacity method, ϕ'_{MY} ($\phi'_{MY\text{-}log}$ and $\phi'_{MY\text{-}asinh}$)

Meyerhof (1961) developed a bearing capacity method to estimate the bearing capacity q_r of conical tip piles. This method was used by many researchers to estimate the friction angle of sand from CPT test measurements (e.g., Mitchell and Lunne 1978, Lunne and Christoffersen 1983). Dayal (1980) compared the bearing capacity estimated using Meyerhof's method to the bearing capacity calculated based on free fall penetrometer measurements and found a good agreement between the results. For cohesionless soil, the bearing capacity equation can be written as:

$$q_r = p_o N_{qr} + \frac{1}{2}\gamma B N_{\gamma r} \tag{4.8}$$

where p_o is the horizontal pressure ($p_o = K_b \gamma D$, where K_b is an earth pressure factor and equals to 0.5 for sand), and N_{qr} and $N_{\gamma r}$ are bearing capacity factors that can be determined from Figure 4.5 for shallow depths. Meyerhof distinguished between a perfectly smooth cone versus a fully rough cone. Meyerhof (1961) suggested using a linear interpolation for all cone roughnesses in between, which is considered as a shortcoming of this method (Durgunoglu and Mitchell 1973). To follow Meyerhof (1961) here, the average value of N_{qr} and $N_{\gamma r}$ between perfectly smooth and perfectly rough base was used (Figure 4.5). To determine the friction angle from $q_{c,eq}$, the bearing capacity was plotted versus the bearing capacity factors, N_{qr} and $N_{\gamma r}$ for a tip angle α = 60˚. The friction angle was then determined by trial and error using Equation 4.8.

4.3.3.3 Density Method ϕ'_{RD}

The field friction angles of sand were determined using estimates of the relative density and considering the confining pressure represented by the penetration depth. The field relative densities were estimated based on a deceleration-relative density correlation derived from the laboratory tests results (see the results section). The estimates of the relative density were used to determine the friction angle using the method presented by Duncan et al. (2014). These researchers proposed a correlation to estimate the friction angle of sand based on the relative density, confining pressure and gradation.

$$\phi' = A^* + B^*(D_r) - [C^* + D^*(D_r)] \log(\sigma'_N / P_a) \tag{4.9}$$

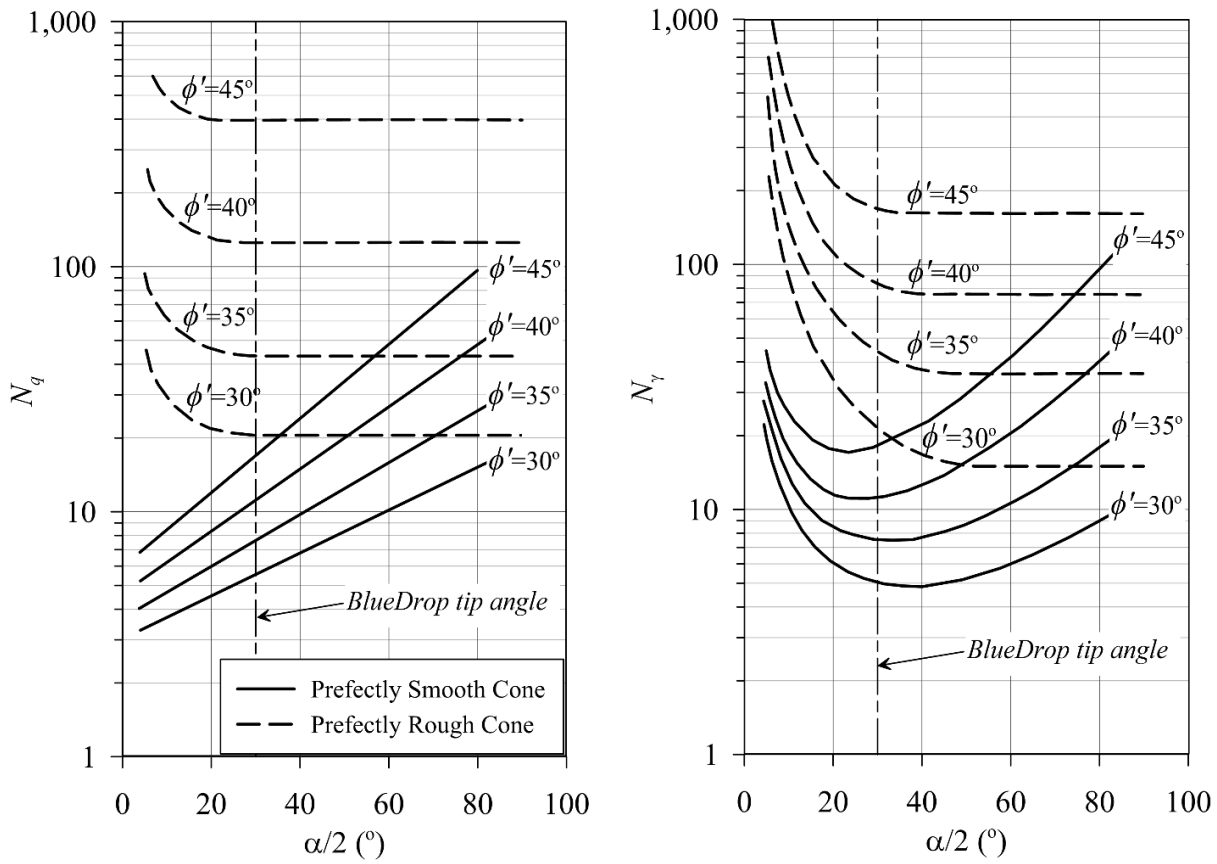

Figure 4.5. Shallow penetration bearing capacity factors by Meyerhof (1961) for perfectly smooth cones (solid lines) and perfectly rough cones (dotted lines).

where σ'_N is the normal stress, and P_a is the atmospheric pressure. For poorly graded sand, Duncan et al. (2014) found that the constants A^*, B^*, C^* and D^* were to be equal to 34, 10, 3 and 2, respectively. These values were modified for the Cannon Beach (offshore) sands based on the vacuum triaxial tests performed (see the results section). Considering the penetration depth and estimated relative density, Equation 4.9 was used to determine the expected friction angle based on relative densities derived from the deceleration measurements.

4.4 Results

4.4.1 Grain Size Analysis

Cannon Beach's sand was classified as poorly graded sand according to the unified soil classification system (ASTM D2487) with generally small variations in the particle size between

the samples (Figure 4.6). The median grain size D_{50} for the shown samples ranged between 0.31-0.39 mm, while the coefficient of curvature *Cc* and coefficient of uniformity *Cu* varied between 0.92-1.19 and 1.60-2.04, respectively. A relatively smaller particle size was measured for the samples at the base of the berm (transition from intertidal to subaerial zone), which are the least affected by the water processes. Overall, the sediment grain size is in agreement with those reported by Ruby (1977).

4.4.2 Soil behavior during the PFFP penetration

For all the 151 deployments, the impact velocity of the penetrometer ranged between 2.8-5.4 m/s with an average of 4.4 m/s and standard deviation of 0.6 m/s. These velocities were used to assess

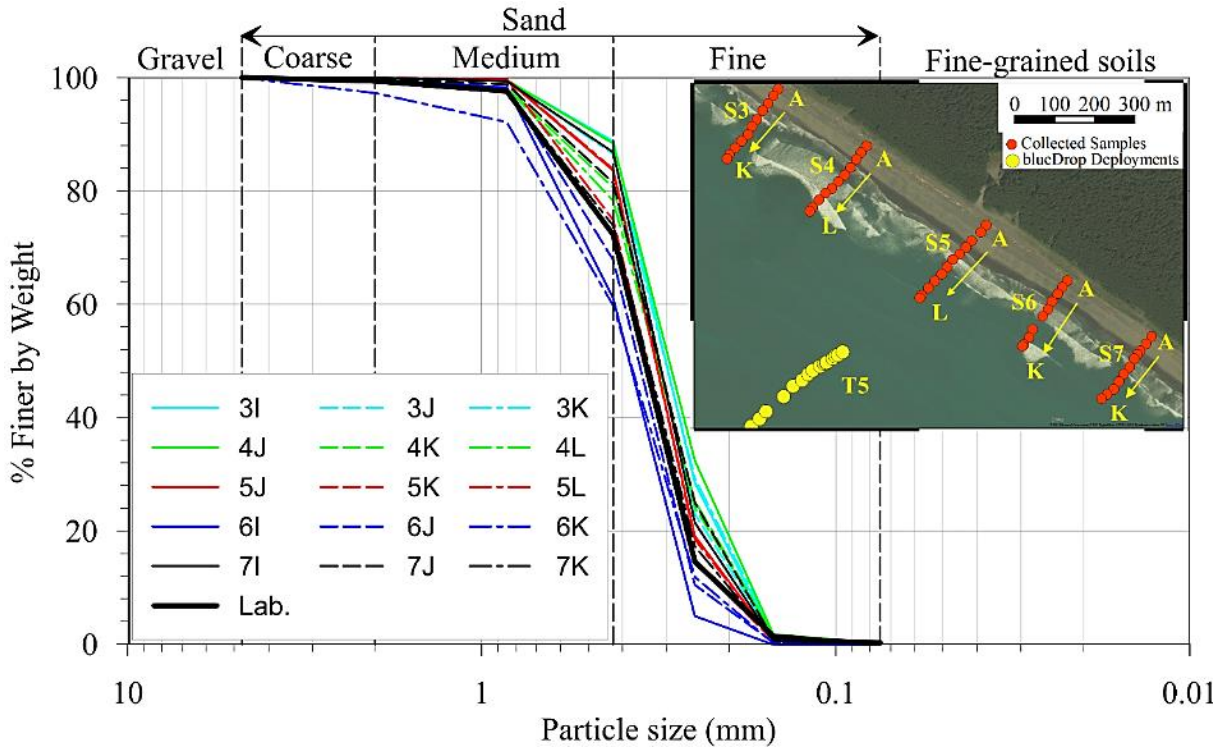

Figure 4.6. The grain size distribution for the last three samples closest to the low water line of each transect collected from the lower intertidal zone. Transects were labeled S3 thru S7 in the area of this study. Along each transect, sample locations were denoted as A-L, with A starting at the berm and L or K being the closest to the water. The figure also shows the grain size distribution for the sand used in the laboratory to correlate the relative density to the maximum deceleration (bold black line).

whether the soil response is undrained, partially drained, or drained based on the "non-dimensional dynamic velocity", *V*, suggested by Randolph (2004) and Randolph and Hope (2004), and used by Steiner et al. (2014) for a free fall penetrometer:

$$V = \frac{v_{dyn}\, B}{c_v} \tag{4.10}$$

where B is the penetrometer diameter, and c_v is the coefficient of consolidation. The sediment response is fully undrained if $V > 30$, partially drained if $30 \geq V > 0.3$, and fully drained if $V \leq 0.3$ (Steiner et al. 2014). Considering the expected c_v for fine sand reported by Duncan et al. (2014), ranging from 1.075×10^{-4} to 1.075×10^{-2} m^2/s, the minimum penetration velocity at which the sand response is fully undrained ranges between 0.04-3.70 m/s for the used penetrometer diameter of 8.75 cm (Figure 4.7a). A consolidation test was conducted on a sand sample from Cannon Beach

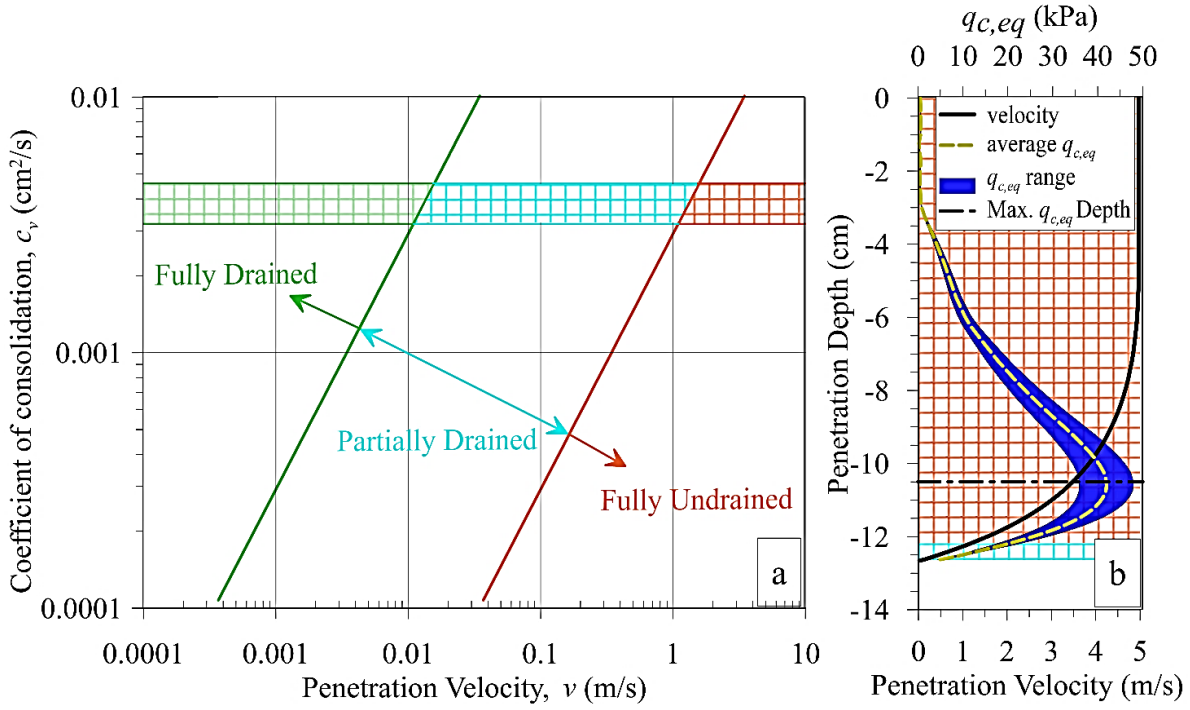

Figure 4.7. a) The penetration velocity *v* ranges at which the sand behavior is fully undrained, partially drained and fully drained for fine sand. The c_v range is for fine sand according to Duncan et al. (2014), and the hatched area indicates the range of c_v as determined for Cannon Beach's sand. b) A typical deployment profile with the fully undrained and partially drained zones being indicated by the hatched areas. The horizontal centerline marks the depth of maximum $q_{c,eq}$.

and resulted in c_v ranging between 3.2×10^{-3} m^2/s and 4.6×10^{-3} m^2/s. Accordingly, the sediment response is fully undrained if the penetration velocity is larger than 1.10 m/s, and fully drained if the penetration velocity less than 0.01 m/s (hatched area in Figure 4.7a). A typical deployment profile is shown in Figure 4.8b. It shows that the sand response is mostly undrained, and that the response at penetration depths between the seabed surface and the depth of the maximum $q_{c,eq}$ can be considered fully undrained.

4.4.3 Shear Strength

Although it was found that the soil response during the PFFP penetration is mostly fully undrained, it is common to determine the drained strength parameters from undrained tests as well as from transient loading in which the sample is subjected to a rapid loading (eg., Seed and Lundgren 1954; Seed and Lee 1967; Yamamuro and Lade 1993). Samples collected from the lower intertidal zone were selected for the vacuum triaxial testing to ensure that variations in particle size had no influence on the results. Some fluctuations in the vacuum pressure were observed during the tests. A maximum variation of about ± 0.03 kPa was allowed. Tests with higher variations were discarded. As expected, the secant friction angles for the sand increased with increasing the relative

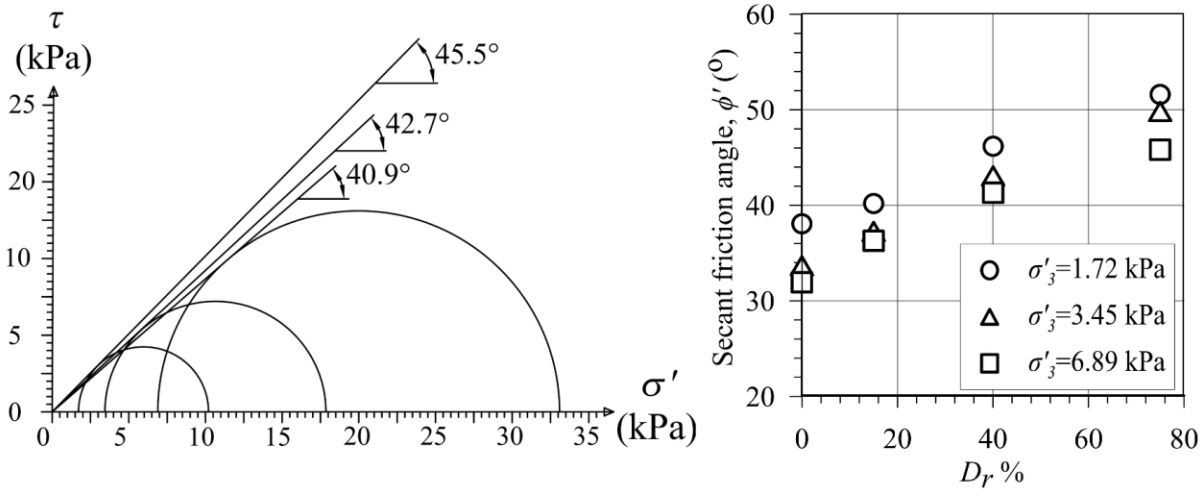

Figure 4.8. Example results for the secant friction angle of Cannon Beach sand tested at different confining pressures in vacuum triaxial test, at initial relative density of 40% (left panel). Results from vacuum triaxial tests at different relative densities and confining pressures (right panel).

density and decreased with increasing the confining pressure (Figure 4.8). The highest secant friction angle (51.6°) was found at a confining pressure of 1.72 kPa and 75% relative density. The lowest secant friction angle (32.0°) was found at a relative density of 0% and confining pressure of 6.89 kPa.

Based on the vacuum triaxial tests results, the constants A^*, B^*, C^* and D^* in Equation 4.9 were obtained to represent the Cannon Beach samples. A good agreement between the measure secant friction angle and the calculated from Equation 4.9 was obtained using values of A^*=34, B^*=10, C^*=2, and D^*=5 (Figure 4.9).

The friction angles of the sand were also obtained using direct shear tests (Figure 4.10). Controlled by the capability of the available devices, the normal pressures used for the direct shear test were 24.8, 48.8, and 72.8 kPa. Considering the secant friction angle for each normal stress, the saturated friction angles were between 0.43º-1.12º smaller than the dry samples. Using the Mohr's-Coulomb failure criterion, the friction angle of the saturated samples (32.7°) was smaller than the obtained from dry samples (33.6°) by 0.9° (Figure 4.10).

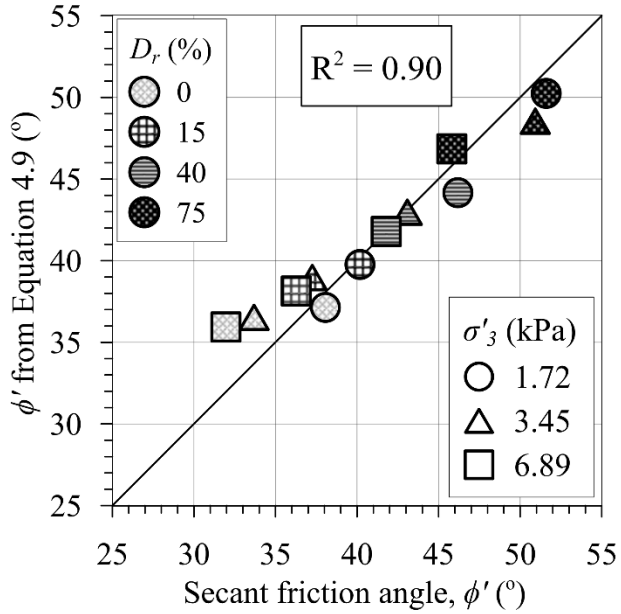

Figure 4.9. Relationship between the secant friction angle from the vacuum triaxial tests and the estimated friction angles using Equation 4.9 and the modified constants. The symbol shape shows the confining pressure while the symbol hatch shows the initial relative density.

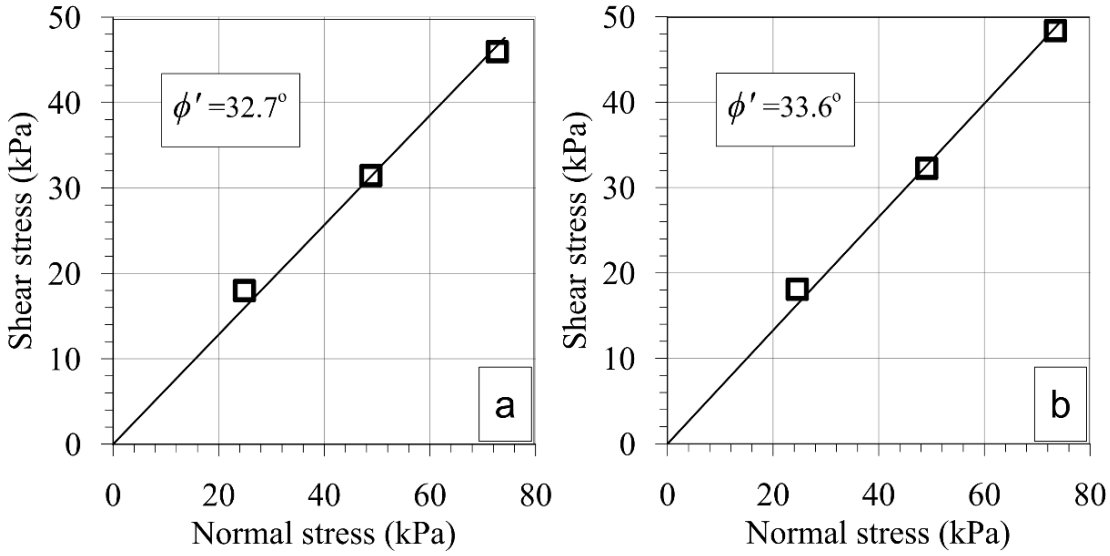

Figure 4.10. Direct shear test for saturated samples (left), and for dry samples (right).

4.4.4 Estimating friction angles from the Free Fall Penetrometer measurements

Friction angles were estimated for 72 deployments, using the three approaches described in the methods section. In order to minimize the effect of the strain rate variation (see the discussion section), deployments with little variation in impact velocity (4.1-5.4 m/s with an average of 4.7 m/s and a standard deviation of 0.35 m/s) were chosen for analyses. Moreover, the selected deployments represented the full range of the achieved decelerations (25-72 *g*) in the field.

4.4.4.1 Durgunoglu and Mitchell (1973) ϕ'_{DM} ($\phi'_{DM\text{-}log}$ and $\phi'_{DM\text{-}asinh}$)

A strain rate equation coefficient *K* of 1.25, which represents the average value of the commonly used strain rate coefficient range in the literature for similar devices, was used to determine the in-situ friction angles. For the whole range of the achieved decelerations in the field (25-72 *g*), affected by the variation in the relative density along the profile, the calculated using the DM method ranged between $\phi'_{DM\text{-}log}$ = 38.3°-51.5° using the logarithmic strain rate equation, and between $\phi'_{DM\text{-}asinh}$ = 37.5°-51.0° using the inverse hyperbolic sine strain rate equation. The friction angles calculated using the logarithmic equation were on average 0.63º greater than those calculated using the inverse hyperbolic sine, with a standard deviation of 0.05º. Using the whole

range of the commonly used *K* values in the literature (i.e. *K* = 1-1.5) contributed to uncertainties in the estimated friction angles between ±0.8°and ±1.4º with an average of ± 1.0º for both strain rate correction methods.

4.4.4.2 Meyerhof (1961) method ϕ'_{MY}

For all the considered deployments, the friction angles calculated using Meyerhof's method ranged between $\phi'_{MY\text{-}log}$ = 40.7°-52.9° using the logarithmic strain rate equation, and between $\phi'_{MY\text{-}asinh}$ = 40.1°-52.0° using the inverse hyperbolic sine strain rate equation. Using Meyerhof's method, the friction angles derived from the logarithmic equation were on average by 0.67º larger than the ones calculated using the inverse hyperbolic sine, with a standard deviation of 0.14º.

4.4.4.3 Density Method ϕ'_{RD}

Based on the laboratory tests, peak decelerations of 20-21 *g*, 32-33 *g*, and 46-51 *g* were found to correspond to relative densities of 23%, 45% and 70%, respectively (Figure 4.11). Considering these results, a correlation was developed between the measured maximum deceleration (*a*) and sand the relative density (D_r):

$$D_r = 14.66 \times 10^{-3} a^2 + 2.66\, a - 25.17 \tag{4.11}$$

Equation 4.11 was then used to estimate the field relative density from the measured deceleration values. The field relative densities estimated using Equation 4.11, ranged between 32-90%. Applying the resulting relative density values, and knowing the achieved penetration depth, the in-situ friction angles were estimated using the density method (i.e. Equation 4.9), yielding friction angles of ϕ'_{RD} = 44°-57°.

4.4.4.4 Comparing the different methods

The friction angles obtained using the density method, $\phi'_{RD,}$ were overall greater than the friction angles calculated from the two bearing capacity approaches, ϕ'_{DM} and ϕ'_{MY}. Using a strain rate coefficient *K* of 1.25 for the bearing capacity methods, ϕ'_{RD} was on average 4.8° greater than ϕ'_{DM}

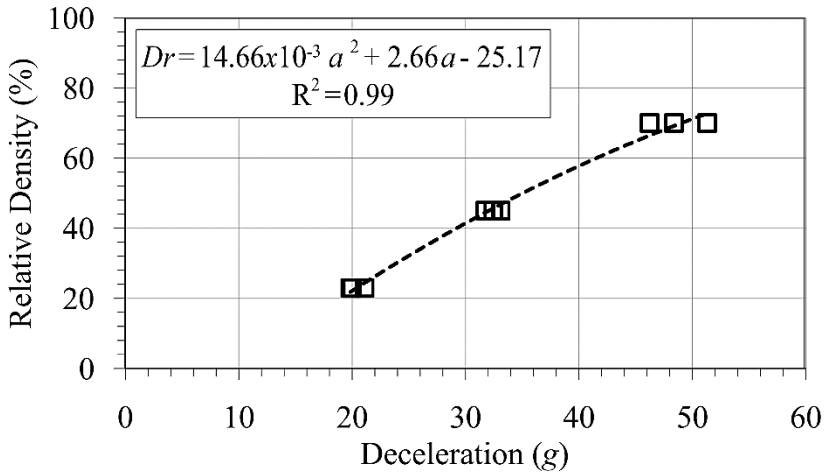

Figure 4.11. The relative density versus maximum deceleration for the tests performed in the laboratory.

using the logarithmic strain rate equation, and 5.5° greater than ϕ'_{DM} using the inverse hyperbolic sine strain rate equation (Figures 4.12a and 4.12b). Relatively smaller deviations were found using Meyerhof's method where ϕ'_{RD} was on average 4.2° greater than ϕ'_{MY} using the logarithmic strain rate equation, and 5.0° greater than ϕ'_{MY} using the inverse hyperbolic sine strain rate equation (Figures 4.12c and 4.12d).

Two adjustments were tested to investigate potential impacts on the results, and causes for deviations. First, since the vacuum triaxial tests, which were used to calibrate the density method, were conducted on dry samples, and it was found that the dry sand friction angle is on average ~1° more than the saturated samples, the expected friction angle using the density method ϕ'_{RD} was reduced by 1°. Second, the used strain rate factor coefficient was the average value of the commonly used values in the literature (i.e., K=1.25). Accordingly, the lower bound value for the strain rate factor coefficient K value of 1.0 was tested, instead of 1.25, in the analyses. Additionally, since the logarithmic strain rate equation gave better results than the inverse hyperbolic sine strain rate equation, compared to the density method (Figure 4.12), the logarithmic equation was chosen for further analyses. With these considerations, the resulting best-fit line showed that ϕ'_{RD} was on average 2.9° greater than ϕ'_{DM}, and 2.1° greater than ϕ'_{MY}.

Significantly lower than 1.0 K values have been proposed in the literature for sands (Table 4.1). Accordingly, a strain rate factor coefficient K values of 0.1-1.0 were tested for the logarithmic

expression in order to find the strain rate coefficient *K* value that gives matching results between the two approaches. The best fit was found using a *K* value of 0.2 for DM method and 0.4 for Meyerhof's method where ϕ'_{RD} was on average equal to ϕ'_{DM} and ϕ'_{MY} (Figure 4.12).

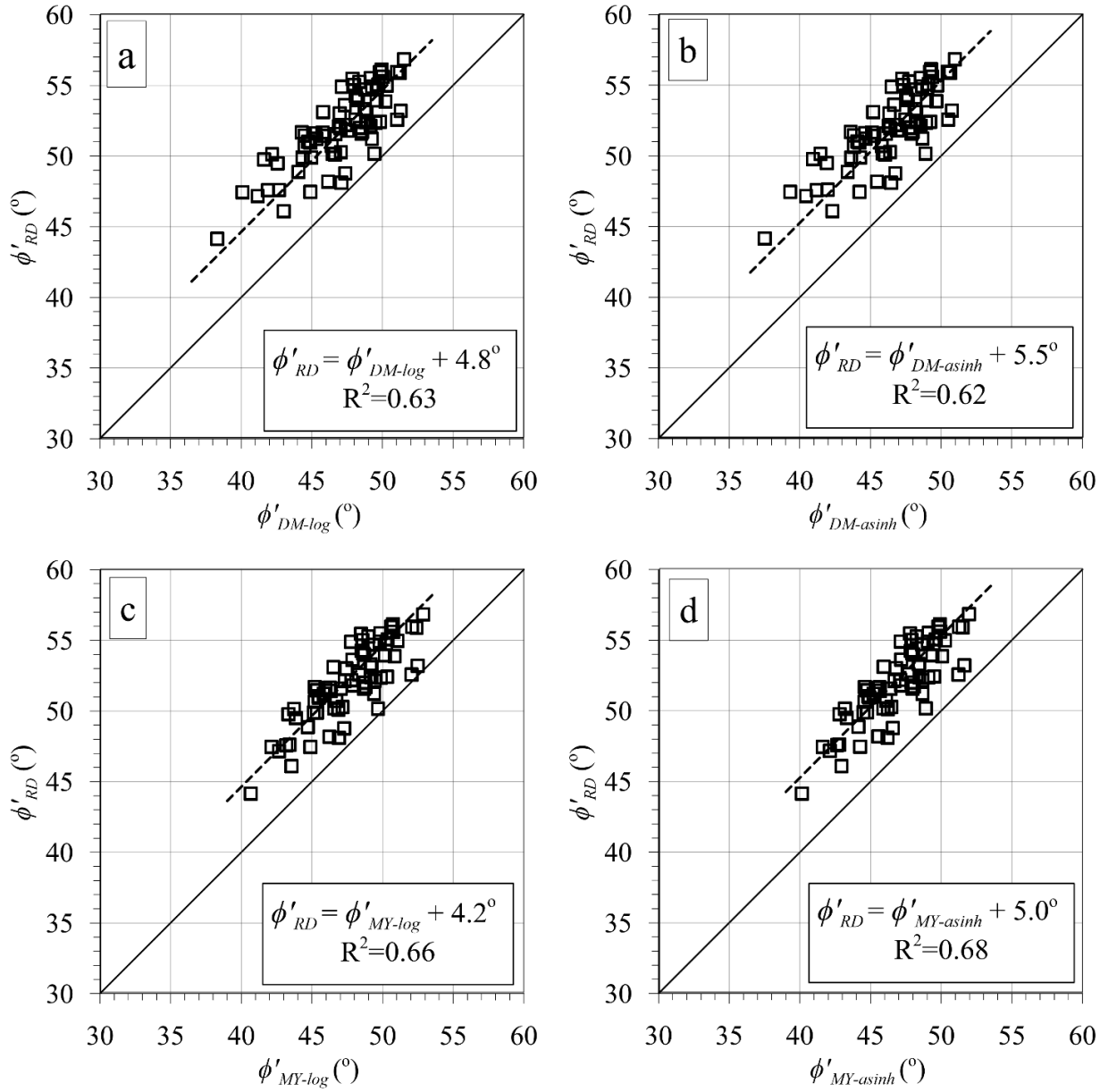

Figure 4.12. The relationship between the friction angles calculated using DM and MY methods and the calculated friction angles using the density method, using the logarithmic equation (left) and inverse hyperbolic sine (right).

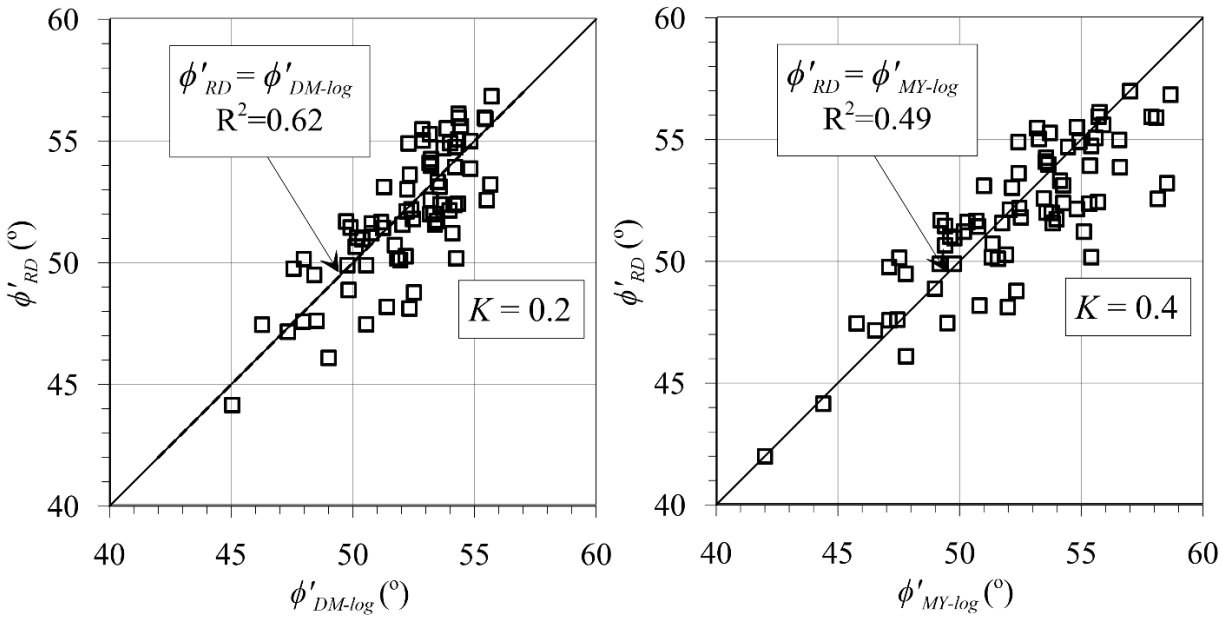

Figure 4.13. The relationship between the calculated friction angle using the density method versus DM method (left) and Meyerhof's method (right) after the modifications and using the best fit for *K*.

The calculated in-situ friction angles were found correlated to the Firmness Factor (*FF*) proposed by Mulukutla et al. (2011) which is formulated as:

$$FF = \frac{a_{max}}{g\ t_p\ v_i} \tag{4.12}$$

where a_{max} is the maximum acceleration (deceleration during the sediment penetration), t_p is the total penetration time and v_i is the impact velocity. Here, ϕ'_{DM} was calculated using the logarithmic strain rate equation. The best-fit line for the correlation between the friction angle and the firmness factor is a power function (Figure 4.14) that can be formulated as follows:

$$\phi'_{DM-log} = 39.7\ FF^{0.08} \tag{4.13}$$

$$\phi'_{MY-log} = 35.9\ FF^{0.12} \tag{4.14}$$

Such correlation can be useful to get a quick first estimate for the friction angle value due to its simplicity.

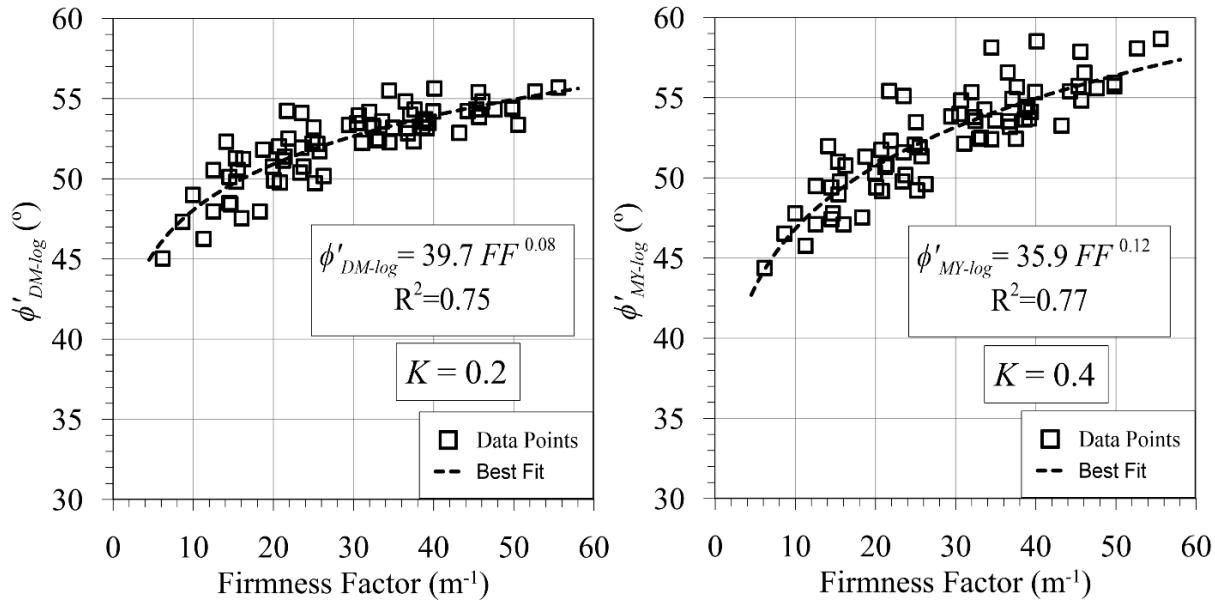

Figure 4.14. The relationship between the firmness factor and the calculated friction angle, using DM method (left) and Meyerhof's method (right).

4.5 Discussion

The curvature of the failure envelope of sand represents an important factor at low confining pressures (or small penetration depths) due to the dilative behavior of sand at these pressures (Lee and Seed 1967). This curvature can be represented practically using secant friction angles (Terzaghi et al. 1996; Duncan et al. 2014). The secant friction angle is defined as the angle between the abscissa and the line tangent to Mohr's circle and passes through the origin for each test separately. Using this method, the downward curvature is represented by a decrease in secant friction angle with the increase of the confining pressure (Figure 4.8). The obtained secant friction angles from the vacuum triaxial tests for Cannon Beach sands had deviations between 0.3º to 4.9º, with an average of 2.1º, when compared to the friction angle estimated using Duncan et al. (2014) formula and constants for the confining pressures and relative densities from the vacuum triaxial tests (Figure 4.15). Although the formula by Duncan et al. (2014) was developed based on the laboratory tests reported by Marachi et al. (1969) and Becker et al. (1972), which were performed under a minimum confining pressure of about 70 kPa in addition to the different sand origin, the scatter of the secant friction angles obtained from the vacuum triaxial tests is within the scatter of

Duncan's et al. (2014) results (Figure 4.15). This supports the applicability of Duncan et al. (2014) to Cannon Beach sands.

The first estimates of friction angles ϕ'_{DM} and ϕ'_{MY} using K~1.25 were in general smaller than ϕ'_{RD}. However, many previous studies for estimating the friction angle of sand from standard cone penetration testing showed that Durgunoglu and Mitchell's (1973) and Meyerhof's (1961) bearing capacity methods tend to underestimate the friction angle compared to the laboratory tests. Villet and Mitchell (1981) found that Durgunoglu and Mitchell (1973) provide good lower bound values for the friction angles compared to triaxial test results. Other investigators reported that Durgunoglu and Mitchell's theory tends to underestimate the friction angle of sand due to neglecting the sand compressibility (Baldi et al. 1981; Eid 1987). Robertson and Campanella (1983) reported that Durgunoglu and Mitchell's (1973) theory underestimates the friction angle by ~2°. Baldi et al. (1986) also reached a similar finding, and reported that Durgunoglu and Mitchell's (1973) method resulted in sand friction angles 2.4-2.6° less than triaxial tests, for relative densities

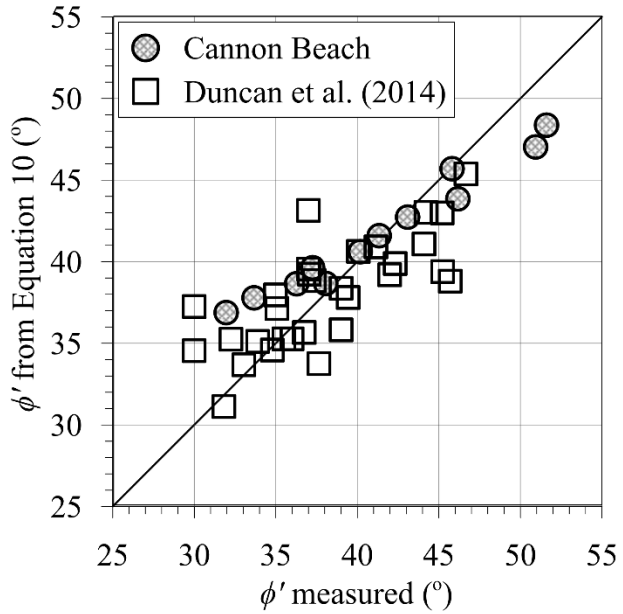

Figure 4.15. The secant friction angles for Cannon Beach's sand estimated using Equation 9 and Duncan's et al (2014) constants (hatched circular symbols) in addition to the secant friction angles Duncan's et al (2014) used to develop their equation (square symbols).

between 45-95%, considering the curvature in the failure envelope. Mitchell and Lunne (1978) and Lunne and Christoffersen (1983) documented that Meyerhof (1961) method tends to underestimate the friction angle compared to the triaxial test. However, the difference shown in this study (Figure 4.12) was higher than reported in the literature. This might be due to two factors: First, the sand was tested dry, which resulted in higher friction angles compared to the saturated samples (Figure 4.11). However, this effect is expected to be small given that the direct shear tests on dry and saturated samples showed that the friction angles determined using dry samples were only 0.43º-1.12º higher than those determined using saturated samples. Second, the initially used strain rate coefficient (K~1.25) was obtained for different soils and penetrometers and might not be the best fit for Cannon Beach sand and/or the *BlueDrop*.

Sand exhibits a higher resistance, compared to static loading, due to the increase in shear strength and the development of negative pore water pressures caused by the dilative behavior of sand (Seed and Lundgren 1954). Such negative pore pressures under initial shearing were indeed observed for *BlueDrop* impacts into sand (Lucking et al. 2017; Albatal and Stark 2017). For uniform sand, this dilation can occur even if the sand is in a loose state (Ottesen-Hansen and Gislason 2007). Different strain rate coefficients have been used in the literature for sandy sediments with values ranging from 1 (K coefficient of zero, for penetration velocity up to 0.8 m/s) (Dayal et al. 1975) to values of 3-5 (K coefficient of 0.8-1.5, at impact velocities > 3 m/s) (Stoll et al. 2007; Stark et al. 2012; Stephan et al. 2015). On the other hand, laboratory drained triaxial tests using a load that strikes at 3 m/s velocity on saturated dense sands samples by Seed and Lundgren (1954) showed an increase of 40% in the shear strength increase compared to the static tests (corresponding to K value of about 0.2 using a reference velocity of 0.02 m/s). Yamamuro et al. (2011) also found similar results with an increase of 30% in the principal stress ratio at a strain rate of 1750% /s (3.1 m/s velocity). Moreover, even for the same soil, the strain rate effect varied with the variation in the relative density where dense sand is more susceptible to the change in the strain rate than loose sand (Seed and Lundgren 1954). Accordingly, the lowered values of the strain rate coefficient (i.e. K= 0.2 for the DM method, and of K=0.4 for the MY) seem reasonable (i.e., a better agreement with the triaxial test results). This encourages more research in this direction, and a review of the application of strain rate factors when testing in sandy environments. However, it should be noted here that the strain rate is soil dependent rather than an analysis method dependent. Accordingly, an average value of K=0.3 can be considered for both methods. Using

K=0.3, the deviations in the friction angle from the values calculated using K= 0.2 were between +0.6° and +0.9° with an average value of +0.7° for the DM method. Using MY method, the deviations from the values determined using K=0.4 were between -0.7° and -1.3° with an average of -1.0°.

Overall, all of the proposed and tested methods yielded promising results, and suggested that estimating friction angles from PFFP is feasible. An advantage of the use of the methods yielding ϕ'_{DM} and ϕ'_{MY} is their applicability regardless of the variation in the relative density and particle size. The same applies to the use of the Firmness Factor. Accordingly, the proposed correlations between the friction angle and firmness factor may be applicable at other sites. This hypothesis will be tested in the near future on deployments from other locations.

Initial data are presented relating relative density to PFFP deceleration measurements directly. In a controlled environment, three tests for three different relative densities were carried out, respectively, in a sand of similar mineralogy and grain size distribution as the Cannon Beach sand. The results stood out regarding the repeatability of the results, and an excellent correlation between relative density and maximum deceleration, with R^2= 0.99, was obtained. While the tests here were only performed for one specific sediment type, and served the purpose to use the method by Duncan et al. (2014) to derive in-situ friction angles, the results are encouraging regarding estimates of relative density.

Allowing the applicability of the DM and MY methods to determine the sand friction angles, may enable to use Duncan et al. (2014) Equation 4.9 as a second method to determine the relative density based on the friction angle and penetration depths. As shown in Figure 4.16, the relative density was back-calculated from $q_{c,eq}$ utilizing the estimated friction angles using DM and MY methods and using Duncan's (2014) equation (i.e. Equation 4.9). However, field data including relative density, or calibration chamber tests, are required to validate the results. A semi-empirical correlation was used by Orenberg et al. (1996) to estimate the relative density of sand from the eXpendable Doppler Penetrometer (*XDP*). However, our attempts to access background information for this method were unsuccessful.

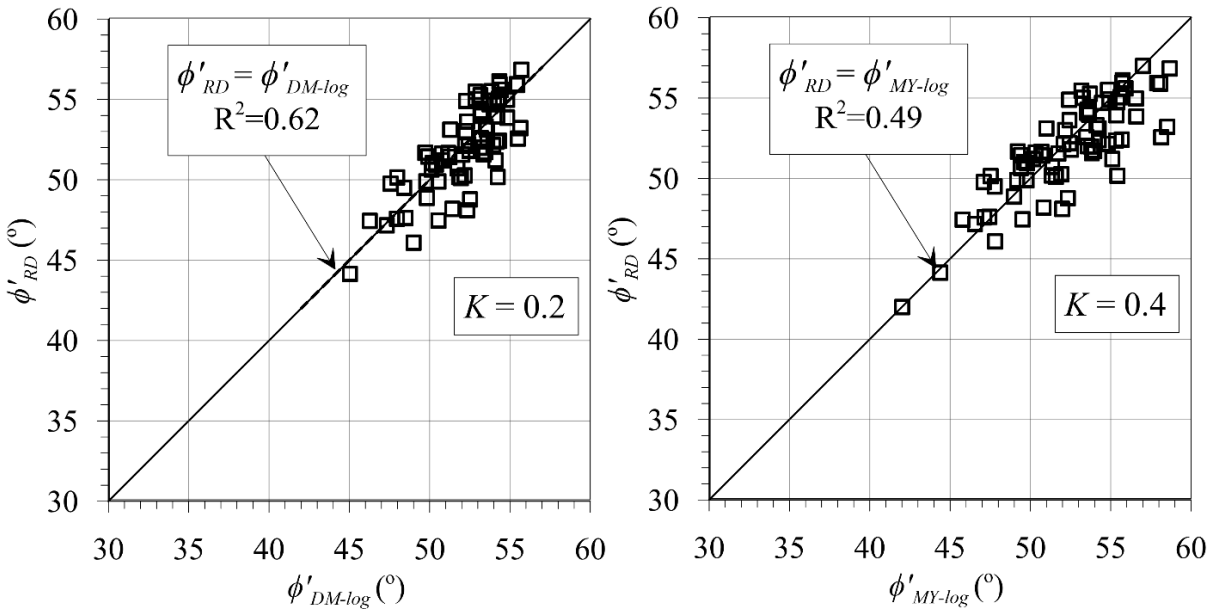

Figure 4.16. The relationship between the relative density estimated using Akal and Stoll (1995) findings versus the calculated relative density back calculated from $q_{c,eq}$ using DM method (left) and Meyerhof's method (right).

4.6 Conclusions

Friction angles of nearshore sands were estimated using three approaches: bearing capacity theory by (1) Durgunoglu and Mitchell (1973, 1975a), and by (2) Meyerhof (1961) using the penetrometer deceleration records, and (3) from estimates of relative density from the penetrometer deceleration records using Duncan et al. (2014) equation. The coefficients used in the correlation by Duncan et al. (2014) were slightly modified based on vacuum triaxial tests of site-specific sediments at different confining pressures and relative densities. The logarithmic and inverse hyperbolic sine strain rate equations were used to calculate an equivalent cone resistance from the deceleration-time measurements, and a range of the strain rate empirical coefficient K between 0.1-1.5 was tested. Because the vacuum triaxial tests were performed for dry samples, direct shear tests were conducted to test the effect of saturation on the friction angles. The following conclusions can be drawn:

1- Using a strain rate coefficient of K = 1, the friction angles obtained using the density method ϕ'_{RD} were by 2.9° greater than the friction angles using Durgunoglu and Mitchell

(1973) method, ϕ'_{DM}, and by 2.1° using Meyerhof (1961) method, $\phi'_{MY,}$ which agrees with previous findings in the literature.

2- The friction angles calculated using Durgunoglu and Mitchell (1973, 1975a), and Meyerhof (1961) (i.e. ϕ'_{DM} and ϕ'_{MY}) represented a good lower bound in comparison to the values estimated using Duncan's method based on the laboratory experiment supported density method using a strain rate coefficient K=1.25.
3- The logarithmic equation and a strain rate coefficient K = 0.2 using Durgunoglu and Mitchell (1973) method, and K = 0.4 using Meyerhof (1961) method yielded the best strain rate correction to match the density method.
4- The logarithmic strain rate equation yielded better results than the inverse hyperbolic sine strain rate equations compared to the density method.
5- The direct shear tests showed that sediment saturation led to a decrease in friction angle of ~1° compared to dry samples.
6- In-situ relative density across the nearshore (water depths 4-25m) was estimated to range between 32-90%, resulting in friction angles ranging from 44° to 57°.
7- The friction angles were found to correlate well to the firmness factor. Correlations between the friction angle and firmness factor were proposed based on the results.

The results were in line with many publications that used the Durgunoglu and Mitchell (1973, 1975a) and Meyerhof (1961) methods to estimate the friction angle of sands using the static cone resistance (e.g., Villet and Mitchell 1981, Baldi et al. 1986, Lunne and Christoffersen 1983). The results are promising, and more testing in other areas is planned in the near future. The estimated in-situ friction angles suggest potentially significantly higher and more variable in-situ friction angles than most generally applied values for sediment transport, or early site assessment applications (e.g., Bagnold 1973, Kirchner et al. 1990, Buffington et al. 1992). This highlights the potential relevance for the here presented method. The results of this study can be used to get a second order approximation for the sand's field strength parameters and validation is always recommended using site-specific tests.

4.7 Acknowledgments

The study was funded by the Institute for Critical Technology and Applied Science (ICTAS) at Virginia Tech. The authors thank Fred Falcone and Brandon Quinn for the assistance during the field investigations. The authors appreciate the on-site support of the City and Borough of Yakutat, specifically, Rhonda Coston, the harbormaster and Bill Lucy, and of Bill Staby from Resolute Marine Energy. The authors also acknowledge the support of Thomas Brandon, Chris Zobel and Thomas Barham.

4.8 References

Abelev, A., Tubbs, K., and Valent, P. 2009a. Numerical investigation of dynamic free-fall penetrometers in soft cohesive marine sediments using a finite difference approach. In OCEANS 2009, MTS/IEEE Biloxi - Marine Technology for Our Future: Global and Local Challenges. IEEE, Biloxi, MS, USA. pp. 1–10. doi:10.23919/OCEANS.2009.5422350.

Abelev, a., Simeonov, J., and Valent, P. 2009b. Numerical investigation of dynamic free-fall penetrometers in soft cohesive marine sediments using a finite element approach. In OCEANS 2009, MTS/IEEE Biloxi - Marine Technology for Our Future: Global and Local Challenges. IEEE, Biloxi, MS, USA. pp. 1–8. doi:10.23919/OCEANS.2009.5422351.

Akal, T., and Stoll, R.D. 1995. An expendable penetrometer for rapid assessment of seafloor parameters. In OCEANS 1995. MTS/IEEE, Challenges of Our Changing Global Environment. IEEE, San Diego, CA. pp. 1822–1826. doi:10.1109/OCEANS.1995.528858.

Albatal, A., and Stark, N. 2016. In Situ Geotechnical Early Site Assessment of a Proposed Wave Energy Converter Site in Yakutat, Alaska, Using a Portable Free-Fall Penetrometer. In Geo-Chicago 2016. Chicago, IL. pp. 429–438. doi:10.1061/9780784480137.041.

Albatal, A., and Stark, N. 2017. Rapid sediment mapping and in situ geotechnical characterization in challenging aquatic areas. Limnology and Oceanography: Methods, 15(8): 690–705. doi:10.1002/lom3.10192.

ASTM D2487-11. Standard Practice for Classification of Soils for Engineering Purposes (Unified Soil Classification System). ASTM International, West Conshohocken, PA.

ASTM. D3080/D3080M-11. Standard Test Method for Direct Shear Test of Soils Under Consolidated Drained Conditions. ASTM International, West Conshohocken, PA.

ASTM D5778-2012. Standard Test Method for Electronic Friction Cone and Piezocone Penetration Testing of Soils. ASTM International, West Conshohocken, PA.

ASTM D6913/D6913M 2017. Standard Test Methods for Particle-Size Distribution (Gradation) of Soils Using Sieve Analysis. ASTM International, West Conshohocken, PA.

Aubeny, C.P., and Shi, H. 2006. Interpretation of Impact Penetration Measurements in Soft Clays. Journal of Geotechnical and Geoenvironmental Engineering, 132(6): 770–777. doi:10.1061/(ASCE)1090-0241(2006)132:6(770).

Bagnold, R.A. 1947. Sand Movement by Waves: Some Small-Scale Experiments with Sand of Very Low Density. Journal of the Institution of Civil Engineers, 27(4): 447–469. ICE Publishing. doi:10.1680/ijoti.1947.13608.

Bagnold, R.A. 1973. The Nature of Saltation and of "Bed-Load" Transport in Water. In Proceedings of the Royal Society of London. A. Mathematical and Physical Sciences. pp. 473–504. doi:10.1098/rspa.1973.0038.

Baldi, G., Bellotti, R., Ghionna, V., Jamiolkowski, M., and Pasqualini, E. 1981. Cone resistance of a dry medium sand. In 10th International Conference on Soil Mechanics and Foundation Engineering. Stockholm, Sweden. p. 427–432.

Baldi, G., Bellotti, R., Ghionna, V., Jamiolkowski, M., and Pasqualini, E. 1982. Design parameters for sands from CPT. In Proceedings of the 2nd European Symposium on Penetration Testing, ESOPT. Amsterdam. pp. 425–432.

Baldi, G., Bellotti, R., Ghionna, V., Jamiolkowski, M., and Pasqualini, E. 1986. Interpretation of CPTs and CPTUs; 2nd part: drained penetration of sands. In Proceedings of the Fourth International Geotechnical Seminar. Singapore. pp. 143–156.

Becker, E., Chan, C.K., and Seed, H.B. 1972. Strength and deformation characteristics of rockfill materials in plane strain and triaxial compression tests. In Report No. TE-72-3, Dept. of Civil Engineering, University of California, Berkeley. Berkeley, CA.

Bellotti, R., Ghionna, V.N., Jamiolkowski, M., Manassero, M., and Pasqualini, E. 1983. Evaluation of sand strength from CPT. In Soil and rock investigations by in situ testing.

Paris, France. pp. 195–203.

Bilici, C., and Stark, N. (n.d.). Performance of a Novel Sediment Sampler as an Add-on Unit for Portable Free Fall Penetrometers: Combining in situ geotechnical testing with sediment sampling. Limnol. Oceanogr. Methods (In Revew).

Bowman, L., March, R., Orenberg, P., True, D., and Herrmann, H. 1995. Evaluation of dropped versus static cone penetrometers at a calcareous cohesive site. In OCEANS'95. MTS/IEEE. Challenges of Our Changing Global Environment. IEEE, San Diego, California. pp. 1846–1858. doi:10.1109/OCEANS.1995.528862.

Buffington, J.M., Dietrich, W.E., and Kirchner, J.W. 1992. Friction angle measurements on a naturally formed gravel streambed: Implications for critical boundary shear stress. Water Resources Research, 28(2): 411–425. doi:10.1029/91WR02529.

Shore protection manual 1974. US Army Corps of Engineers, Coastal Engineering Research Center, Washington, DC.

Dayal, U. 1980. Free fall penetrometer: a performance evaluation. Applied Ocean Research, 2(1): 39–43. doi:10.1016/0141-1187(80)90046-2.

Dayal, U., and Allen, J.H. 1973. Instrumented Impact Cone Penetrometer. Canadian Geotechnical Journal, 10(3): 397–409. doi:10.1139/t73-034.

Dayal, U., Allen, J.H., and Jones, J.M. 1975. Use of an Impact Penetrometer for the Evaluation of the In-Situ Strength of Marine Sediments. Marine Geotechnology, 1(2): 73–89. doi:10.1080/10641197509388155.

DeJong, J.T., Cargill, P.E., and Frost, J.D. 2001. Effect of Surface Texturing on CPT Friction Sleeve Measurements. Journal of Geotechnical and Geoenvironmental Engineering, 127(2): 158–168. American Society of Civil Engineers. doi:10.1061/(ASCE)1090-0241(2001)127:2(158).

Desai, C.S., Saadatmanesh, H., and Allen, T. 1992. Behavior of Compacted Lunar Simulants Using New Vacuum Triaxial Device. Journal of Aerospace Engineering, 5(4): 425–441. ASCE. doi:10.1061/(ASCE)0893-1321(1992)5:4(425).

Duncan, J.M., Wright, S.G., and Brandon, T.L. 2014. Soil strength and slope stability. John Wiley & Sons, Hoboken, NJ.

Durgunoglu, H.T., and Mitchell, J.K. 1973. Static penetration resistance of soils. Research report number NASA-CR-133460, prepared for NASA Headquarters, Washington, D.C. Available from https://ntrs.nasa.gov/search.jsp?R=19730019713.

Durgunoglu, H.T., and Mitchell, J.K. 1975a. Static penetration resistance of soils : I- analysis. In ASCE Specialty Conference on in-situ Measurement of Soil Parameters. Raleigh, NC. pp. 151–171.

Durgunoglu, T.H., and Mitchell, J.K. 1975b. Static penetration resistance of soils: II - Evaluation. In ASCE Specialty Conference on in-situ Measurement of Soil Parameters. Raleigh, NC. pp. 172–189.

Eid, W.K. 1987. Scaling effect in cone penetration testing in sand. Ph.D. thesis, Virginia Polytechnic Institute and State University, Blacksburg, VA.

Ghazavi, M., Hosseini, M., and Mollanouri, M. 2008. A comparison between angle of repose and friction angle of sand. In The 12th International Conference of International Association for computer Methods and Advances in Geomechanics (IACMAG). Citeseer, Goa, India. pp. 1272–1275.

Kirchner, J.W., Dietrich, W.E., Iseya, F., and Ikeda, H. 1990. The variability of critical shear stress, friction angle, and grain protrusion in water-worked sediments. Sedimentology, 37(4): 647–672. Blackwell Publishing Ltd. doi:10.1111/j.1365-3091.1990.tb00627.x.

Ibsen, L.B., Barari, A., and Larsen, K.A. 2012. Modified vertical bearing capacity for circular foundations in sand using reduced friction angle. Ocean Engineering 47: 1–6. doi:https://doi.org/10.1016/j.oceaneng.2012.03.003.

Lambe, T.W., and Whitman, R. V. 1969. Soil mechanics. John Wiley & Sons.

Lee, K.L., and Seed, H.B. 1967. Drained strength characteristics of sands. Journal of Soil Mechanics and Foundations Division, SM6: 117–141.

Lucking, G., Stark, N., Lippmann, T., and Smyth, S. 2017. Variability of in situ sediment strength and pore pressure behavior of tidal estuary surface sediments. Geo-Marine Letters,: 1–16. doi:10.1007/s00367-017-0494-6.

Lunne, T., and Christoffersen, H.P. 1983. Interpretation of Cone Penetrometer Data for Offshore Sands. In Offshore Technology Conference. Offshore Technology Conference, Houston,

TX. pp. 181–188. doi:10.4043/4464-MS.

Marachi, N.D., Chan, C.K., Seed, H.B., Duncan, and M., J. 1969. Strength and deformation characteristics of rockfill materials. Report No. TE 69-5, University of California, Berkeley.

Melzer, K.-J. 1974. Methods for investigating the strength characteristics of a lunar soil simulant. Géotechnique, 24(1): 13–20. doi:10.1680/geot.1974.24.1.13.

Meyerhof, G.G. 1956. Penetration tests and bearing capacity of cohesionless soils. Journal of the Soil Mechanics and Foundations Division, 82(1): 1–19. ASCE.

Meyerhof, G.G. 1961. The ultimate bearing capacity of wedge-shaped foundations. In International Conference on Soil Mechanics and Foundation Engineering. pp. 105–109.

Mitchell, J.K., and Lunne, T.A. 1978. Cone resistance as measure of sand strength. Journal of the Geotechnical Engineering Division, 104(7): 995–1012.

Morton, J.P., O'Loughlin, C., and White, D. 2015. Centrifuge modelling of an instrumented free-fall sphere for measurement of undrained strength in fine-grained soils. Canadian Geotechnical Journal, 929: 918–929. doi:10.1139/cgj-2015-0242.

Mulukutla, G.K., Huff, L.C., Melton, J.S., Baldwin, K.C., and Mayer, L.A. 2011. Sediment identification using free fall penetrometer acceleration-time histories. Marine Geophysical Research, 32(3): 397–411. doi:10.1007/s11001-011-9116-2.

Nazem, M., Carter, J., Airey, D., and Chow, S. 2012. Dynamic analysis of a smooth penetrometer free-falling into uniform clay. Géotechnique, 62(10): 893–905. doi:10.1680/geot.10.P.055.

Orenberg, P., True, D., Bowman, L., Herrmann, H., and March, R. 1996. Use of a Dropped Dynamic Penetrometer in Cohesionless Soil. In Offshore Technology Conference. Offshore Technology Conference. pp. 639–648. doi:10.4043/8027-MS.

Ottesen-Hansen, N.-E., and Gislason, K. 2007. Soil reactions in saturated sand caused by impulsive loads. Journal of Waterway, Port, Coastal, and Ocean Engineering, 133(1): 39–49. doi:10.1061/(ASCE)0733-950X(2007)133:1(39).

Ponce, V.M., and Bell, J.M. 1971. Shear strength of sand at extremely low pressures. Journal of Soil Mechanics & Foundations Division, SM4: 625–638.

Randolph, M.F. 2004. Characterisation of soft sediments for offshore applications. In 2nd International Conference on Site Characterisation, Porto, Portugal. pp. 209–231.

Randolph, M.F., and Hope, S. 2004. Effect of cone velocity on cone resistance and excess pore pressures. In International Symposium on Engineering Practice and Performance of Soft Deposits. Yodagawa Kogisha Co., Ltd. pp. 147–152.

Robertson, P.K., and Campanella, R.G. 1983. Interpretation of cone penetration tests. Part I: Sand. Canadian Geotechnical Journal, 20(4): 718–733. doi:10.1139/T07-109.

Ruby, C.H. 1977. Coastal morphology, sedimentation and oil spill vulnerability, northern Gulf of Alaska. Columbia, SC.

Schmertmann, J. 1982. A method for determining the friction angle in sands from the Marchetti dilatometer test (DMT). In 2nd European Symposium on Penetration Testing. Amsterdam. pp. 853–861.

Schmertmann, J.H. 1975. Measurement of in situ shear strength. In Proceedings, ASCE Spec. Conference on In Situ Measurement of Soil Properties, Raleigh, NC, 1975. pp. 57–138.

Schmertmann, J.H. 1978. Guidelines for Cone Penetration Test: Performance and Design. Federal Highway Administration Report Number FHWA-TS-78-209, Washington, DC.

Seed, H.B., and Lundgren, R. 1954. Investigation of the effect of transient loading on the strength and deformation characteristics of saturated sands. In ASTM International. ASTM. pp. 1288–1306.

Srivastava, S., Srinivasan, V., and Ghosh, P. 2016. Effective utilization of dynamic penetrometer in determining the soil resistance of the reconstituted sand bed. Japanese Geotechnical Society Special Publication, 2(7): 331–334. doi:10.3208/jgssp.OTH-30.

Stark, N. 2016. Geotechnical Site Investigation in Energetic Nearshore Zones: Opportunities & Challenges. Australian Geomechanics Journal, 51(4): 95–107.

Stark, N., Hanff, H., Svenson, C., Ernstsen, V.B., Lefebvre, A., Winter, C., and Kopf, A. 2011. Coupled penetrometer, MBES and ADCP assessments of tidal variations in surface sediment layer characteristics along active subaqueous dunes, Danish Wadden Sea. Geo-Marine Letters, 31(4): 249–258. doi:10.1007/s00367-011-0230-6.

Stark, N., Hay, A.E., and Trowse, G. 2014. Cost-effective Geotechnical and Sedimentological

Early Site Assessment for Ocean Renewable Energies. 2014 Oceans - St. John's,: 1–8.

Stark, N., Kopf, A., Hanff, H., Stegmann, S., and Wilkens, R. 2009. Geotechnical investigations of sandy seafloors using dynamic penetrometers. In Oceans 2009. Biloxi, MS. pp. 1–10. doi:10.23919/OCEANS.2009.5422460.

Stark, N., Radosavljević, B., Quinn, B.M., and Lantuit, H. 2017. Application of a portable free-fall penetrometer for the geotechnical investigation of the Arctic nearshore zone. Canadian Geotechnical Journal, 54(1): 31–46. doi:10.1139/cgj-2016-0087.

Stark, N., Wilkens, R., Ernstsen, V.B., Lambers-Huesmann, M., Stegmann, S., and Kopf, A. 2012. Geotechnical Properties of Sandy Seafloors and the Consequences for Dynamic Penetrometer Interpretations: Quartz Sand Versus Carbonate Sand. Geotechnical and Geological Engineering, 30(1): 1–14. doi:10.1007/s10706-011-9444-7.

Steiner, A., Kopf, A.J., L'Heureux, J.-S., Kreiter, S., Stegmann, S., Haflidason, H., and Moerz, T. 2014. In situ dynamic piezocone penetrometer tests in natural clayey soils—a reappraisal of strain-rate corrections. Canadian Geotechnical Journal, 51(3): 272–288. doi:10.1139/cgj-2013-0048.

Stephan, S. 2015. A rugged marine impact penetrometer for sea floor assessment. Ph.D. Dissertation, University of Bremen, Bremen, Germany.

Stephan, S., Kaul, N., and Villinger, H. 2015. Validation of impact penetrometer data by cone penetration testing and shallow seismic data within the regional geology of the Southern North Sea. Geo-Marine Letters, 35(3): 203–219. doi:10.1007/s00367-015-0401-y.

Stoll, R.D., Sun, Y.F., and Bitte, I. 2007. Seafloor properties from penetrometer tests. IEEE Journal of Oceanic Engineering, 32(1): 57–63. doi:10.1109/JOE.2007.890943.

Terzaghi, K., Peck, R.B., and Mesri, G. 1996. Soil mechanics in engineering practice. John Wiley & Sons.

True, D.G. 1976. Undrained vertical penetration into ocean bottom soils. Ph.D. Dissertation, Department of Civil Engineering, University of California-Berkeley, Berkeley, CA.

Villet, W.C.B., and Mitchell, J.K. 1981. Cone resistance, relative density and friction angle. In American Society of Civil Engineers. Cone penetration testing and experience: proceedings of a session at the ASCE National Convention. St. Louis, MO. pp. 178–208.

Yamamuro, J.A., Abrantes, A.E., and Lade, P. V. 2011. Effect of Strain Rate on the Stress-Strain Behavior of Sand. Journal of Geotechnical and Geoenvironmental Engineering, 137(12): 1169–1178. American Society of Civil Engineers. doi:10.1061/(ASCE)GT.1943-5606.0000542.

Yamamuro, J., and Lade, P. 1993. Effects of Strain Rate on Instability of Granular Soils BT - Effects of Strain Rate on Instability of Granular Soils. Geotech. Test. J. 16: 304–313.

Yu, H.-S. 2013. Cavity expansion methods in geomechanics. In Springer Science & Business Media. Springer Science & Business Media. doi:10.1007/978-94-015-9596-4.

Yu, H.S., and Mitchell, J.K. 1998. Analysis of Cone Resistance: Review of Methods. Journal of Geotechnical and Geoenvironmental Engineering, 124(2): 140–149. doi:10.1061/(ASCE)1090-0241(1998)124:2(140).

Chapter 5: In-situ geotechnical investigation of nearshore sediments with regard to cross-shore morphodynamics

The contributions of authors to the composition of this manuscript are delineated as follows:

Ali Albatal:

- Conducted the literature review; performed all analyses; prepared figures and tables; wrote the draft manuscript.
- Addresses the comments and suggestions of the coauthors in developing a draft manuscript.
- Addressed the reviewers' comments and prepared the final version of the manuscript.

Jesse E. McNinch

- Participated in the field survey.
- Reviewed and edited the draft manuscript.
- Reviewed and edited final version of the manuscript.

Heidi Wadman

- Participated in the field survey.
- Reviewed and edited the draft manuscript.
- Reviewed and edited final version of the manuscript.

Nina Stark:

- Planned, supervised and participated in the field survey.
- Supervised the study.
- Reviewed and edited the draft manuscript.
- Reviewed and edited the response to reviewers' comments and final version of the manuscript.

In-situ geotechnical investigation of nearshore sediments with regard to cross-shore morphodynamics

Ali Albatal[1], Jesse E. McNinch[2], Heidi Wadman[2], Nina Stark[1]

[1]Virginia Tech, Department of Civil and Environmental Engineering, 200 Patton Hall, Blacksburg, VA 24061. Phone: 540-231-7152; e-mail: ali2@vt.edu, ninas@vt.edu

[2]US Army Engineers Waterways Experiment Station, Field Research Facility, 1261 Duck Road, Kitty Hawk, NC 27949; e-mail: jesse.mcninch@us.army.mil, heidi.m.wadman@usace.army.mil

Published by the American Society of Civil Engineers (ASCE) as part of the Proceedings of Geotechnical Frontiers 2017: Geotechnical Materials, Modeling, and Testing, March 12–15, 2017, Orlando, FL

Reference:

Albatal, A., Mcninch, J. E., Wadman, H., and Stark, N. (2017). "In-situ geotechnical investigation of nearshore sediments with regard to cross-shore morphodynamics." Geotechnical Frontiers, ASCE, 398–408. DOI: 10.1061/9780784480472.

Relevant Appendices:

Appendix C: Comparison between nearshore zones of Cannon Beach, AK and the USACE's Field Research Facility Beach, NC

5.1 Abstract

Sediment dynamics cause continuous changes in nearshore morphology and play a major role in coastline evolution as well as for engineering activities in the coastal zone. A portable, free-fall penetrometer was used to investigate the geotechnical characteristics of surficial seabed sediments in the energetic nearshore zone of the U.S. Army Corps of Engineers Field Research Facility at Duck, NC. Penetrometer deployments were carried out along four cross-shore transects in water depths of 0.8-14.3 m. Duplicate deployments demonstrated the reproducibility of the results. The derived maximum quasi-static bearing capacities ranged from 8.7-251 kPa, with a decrease in the *qsbc* and in the scatter in the seaward direction. Significant differences in sediment strength were observed in the vicinity of the actively migrating, shore parallel sandbar. The study shows a strong relationship between geotechnical characteristics and active morphodynamics of the nearshore seabed. The depth of closure was reflected in the penetrometer results.

5.2 Introduction

The stability of nearshore structures depends on the sediment's capacity to accommodate the system's loads without failing and its susceptibility to scour. Understanding the effect of sediment dynamics on the foundations is a key factor when designing a nearshore structure (Brown and Rashid 1974). However, the morphologic features and hydrodynamic conditions in the nearshore zone are complex and dynamic (e.g., Lippmann and Holman 1990; Schwartz and Birkemeier 2004). In particular, bar migration is a main component of beach profile variability, and affects short and long-term beach stability (Lippmann and Holman 1990; Holman and Sallenger 1993; Plant et al. 1999). While offshore sand bar migration during storms is well understood, onshore migration is still a controversial topic (Elgar et al. 2001a; Masselink et al. 2006; Fernández-Mora et al. 2015).

The interactions between sediment remobilization and deposition processes, and geotechnical characteristics of the seabed surface, are still not fully understood. Due to the energetic hydrodynamics and the limited navigable depth of the nearshore region, conventional and offshore site investigation tools can at best only be deployed in this region during calm conditions, limiting their applicability (Danson 2005). Portable free fall penetrometers (PFFPs) provide an opportunity to investigate the seabed's topmost layers in such energetic coastal environments (Stoll et al., 2007;

Stark and Kopf 2011; Stark et al. 2014). For example, Stark and Kopf (2011) deployed the portable free fall penetrometer *Nimrod* over an active sandbar near Whaingaroa Harbor, New Zealand, and documented strong variations in sediment strength and uppermost seafloor layering with regard to the local morphodynamics.

A common sediment type at U.S. beaches is sand of a mean grain size in the range from 0.15-2 mm (Birkemeier et al. 1981; Dean and Dalrymple 2004). For sandy soils, the shear strength, and thus the bearing capacity, are affected by the sediment density, size, shape, gradation, composition, and sediment depth or confining pressure (Duncan et al. 2014). Free fall penetrometer measurements reflect variations of most of these characteristics for the uppermost sediment layer, including particle size (Mulukutla et al. 2011; Stark et al. 2012a), density (Akal and Stoll 1995), and composition (Stark et al. 2012b). However, without corresponding sediment samples from which to calibrate the penetrometer measurements, it is difficult to isolate these sediment characteristics in the penetrometer records.

This preliminary study is investigating the effect of nearshore morphodynamics on the geotechnical behavior of seabed surface sediments. The U.S. Army Corps of Engineers' Engineering and Research Development Center, Coastal and Hydraulics Laboratory, Field Research Facility (USACE-FRF) at Duck, NC, represents an ideal test location due to its energetic wave forcing and active sandbar (Birkemeier et al. 1981). Furthermore, the region has been intensively studied by the coastal sciences and engineering community (e.g. Birkemeier 1985; Howd and Birkemeier 1987; Lippmann and Holman 1990; Larson and Kraus 1994; Thornton et al. 1996; Gallagher et al. 1998; Plant et al. 1999; McNinch 2004; Gallagher et al. 2016). The portable free fall penetrometer *BlueDrop* was deployed along four cross-shore transects in May 2015 in order to answer the following research questions: (i) What is the effect of the nearshore sediment processes on the geotechnical sediment characteristics? And (ii), how do beach profile characteristics such as slope, presence of bedforms, and depth of closure affect the sediment response to the free fall penetrometer?

5.3 Regional Context

The USACE-FRF is located in Duck, North Carolina, at 36º10'54.6" N and 75º45'5.2" W, on the northern edge of the barrier island complex known as the Outer Banks, and bounded on the east

by the Atlantic Ocean and the west by Currituck Sound (Figure 5.1). The beach and nearshore sediments at the FRF are composed mainly of quartz sand (Howd and Birkemeier 1987), with up to 20% of carbonate shell debris (Birkemeier et al. 1981; Howd and Birkemeier 1987). A persistent lag of well-sorted, very coarse sediment has regularly been observed within the swash zone (e.g. Gallagher et al. 2016), and the remainder of the beach and nearshore region is characterized by a mean particle size of up to about 1 mm on the foreshore, decreasing offshore to a mean particle size of about 0.1 mm (Howd and Birkemeier 1987; Lippmann and Holman 1990). However, the near-surface grain size along a typical cross-shore profile in this region has been shown to be incredibly dynamic (e.g. McNinch, 2004; Gallagher et al., 2016).

The bathymetry is overall characterized by shore-parallel contours with a mild slope, except for in the direct vicinity of the FRF pier (Leffler et al. 1993). The nearshore profile in the cross-shore direction varies with hydrodynamic forcing from almost no bar to triple barred, with a single bar and double bars being the most common (Howd and Birkemeier 1987; Leffler et al. 1993). The bar migrates seaward during storms and landward during fair weather (Elgar et al. 2001a).

The monthly mean significant wave height ranged between 0.56-1.97 m (hindcasted at a water depth of 25 m) with a mean peak spectral wave period of 6.2-12.0 s, in 1980-2012 (WIS 2016). The wave forcing changes seasonally, with the winter nor'easter season being usually the most energetic (Larson and Kraus 1994). Tides are semi-diurnal with an average tidal range of about 1 m (Birkemeier et al. 1981). Wave forcing was calm during the *BlueDrop* survey with a significant wave height between 0.55-0.73 m (measured at a water depth of 17.4 m; NDBC 2016).

5.4 Method

The portable free fall penetrometer *BlueDrop* was deployed 80 times along four shore-normal transects in May 2015 (Figure 5.1). The transects were located at a distance of more than 400 m from the FRF pier in order to avoid the well documented "pier effect" on the hydrodynamics and related sediment processes immediately adjacent to the pier (e.g. Miller et al. 1983; Elgar et al., 2001b). Duplicate deployments were carried out at each location to increase the reliability of the results. The distance between the duplicated deployments depends on the movement of the Lighter Amphibious Resupply Cargo (LARC), expected to be less than 5 m.

The *BlueDrop* penetrometer measures accelerations/decelerations of up to ± 250 *g* (where *g* is the gravitational acceleration) during the free fall through the water column, the impact and penetration into the sediment, with a sampling rate of 2 kHz, and an accuracy of ± 7.39×10^{-5} *g*. *BlueDrop* is also equipped with a pressure transducer with a capacity of 2 MPa and resolution of ± 4.67×10^{-4} kPa, located behind the top of the probe. The first and second integration of the deceleration over the penetration time are used to determine the penetration velocity and depth, respectively (Dayal and Allen 1973). The impact velocity for the *BlueDrop* is sensitive to the change in the dropping height (i.e. the distance between the water surface and the penetrometer tip when deploying the device) at shallow water depths (< 2-3 m) when terminal velocity has not been reached yet, and at large water depths due to the rope drag (Stark and Kopf 2011).

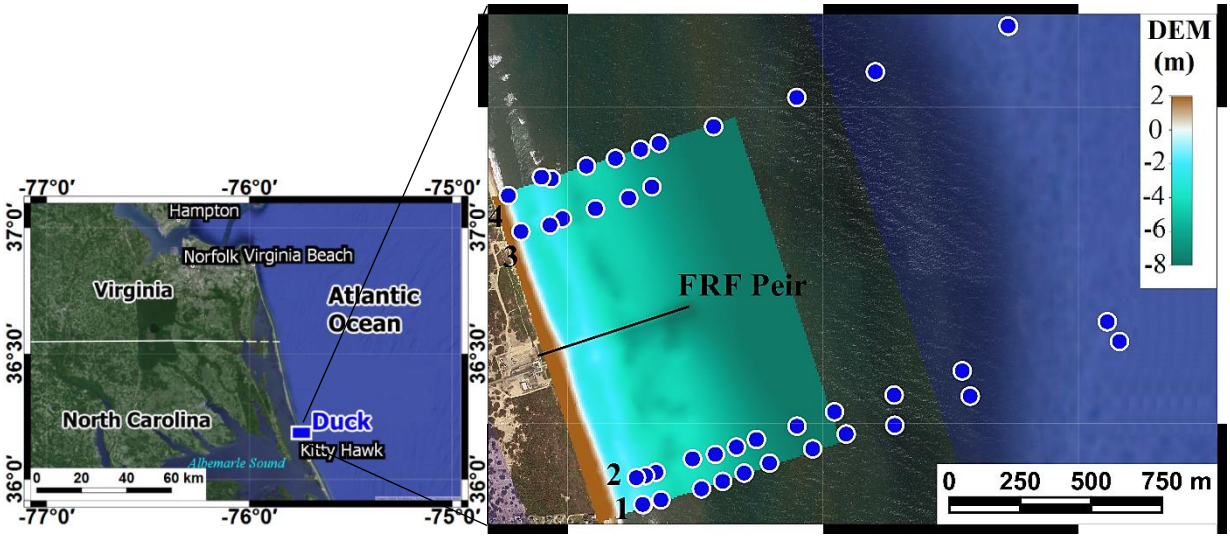

Figure 5.1. Google™ Satellite images showing the location of Duck, NC (36º10'32" N and 75º45'20" W). The blue dots represent the penetrometer deployment locations along transects 1-4. The right-hand side image shows the bathymetry near FRF from the digital elevation model (DEM) survey on April 29th obtained from http://www.frf.usace.army.mil.

Figure 5.2. The FFP *BlueDrop* (modified from www.bluecdesigns.com).

Using Newton's second law, considering the penetrometer's buoyant weight and penetration area, the soil dynamic bearing capacity is determined from the deceleration values (Stark et al. 2012a). Dayal and Allen (1973) suggested the use of a strain rate factor to convert the dynamic sediment strength (high and changing penetration velocities and strain rates) to a quasi-static value as obtained from a Cone Penetration Test at constant rate. This is important for free fall penetrometers because soil exhibits higher resistance at higher penetration velocity (i.e. higher strain rate), and because the penetration velocity changes with the advancement of the penetrometer. A reference penetration rate of 2 cm/s (standard penetration rate for the Cone Penetration Test), and the approach by Stark et al. (2012b), were used here to estimate an equivalent of the quasi-static bearing capacity (*qsbc*).

5.5 Results

The impact velocity as measured at the FRF varied between 2.63-5.57 m/s. Impact velocities increased from a water depth of 0.7 m to a maximum at a water depth of about 5 m, and decreased in deeper water depths, in accordance with the influences of terminal velocity and rope drag. The maximum deceleration of a single deployment varied between 7.3-88.1 *g*, and was primarily affected by the impact velocity and changes in sediment resistance. The derived maximum *qsbc* of the single deployments ranged from 8.7-251.4 kPa, with an average of 101.7 kPa. Significant scatter regarding the *qsbc* was observed at water depths of less than ~6.5 m. This scatter becomes less significant seaward, and is insignificant (i.e. less than the uncertainty due to the strain rate

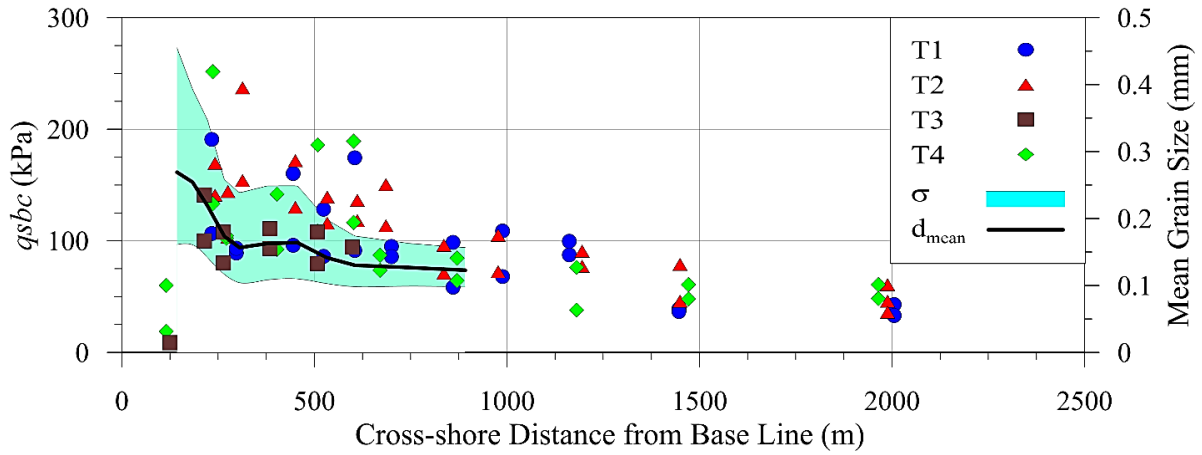

Figure 5.3. The maximum *qsbc* of each deployment along transects T1-T4 with the distance from the base line that is part of the FRF coordinate system. The base line is corresponding to an average distance of 114 m from the mean sea level shoreline (Thornton et al. 1996). The solid black line shows the average mean grain size d_{mean} while the shaded area shows standard deviation σ based on Stauble (1992).

factor) for most of the deployments at a water depths of 8.0 m and greater (Figure 5.3). Duplicate deployments showed also less agreement at shallow water depths. Examples of these differences with respect to water depth for Transect 2 are provided in Figure 5.3. An exception are the deployments near the shoreline (~20-25 m from shoreline) and water depths of less than 1.0 m (i.e. in the inner trough) that had the smallest *qsbc* values measured (Figure 5.5). For these deployments, the *qsbc* values were generally small, ranging between 8.7-60 kPa. Conversely, the largest *qsbc* value was found near the inner bar crest, with high scatter in the *qsbc* for the deployments on the bars side slopes. It should be noted that the bathymetric profile survey data were collected on May 19th, while the *BlueDrop* deployments were collected on May 28th.

Overall, penetration depths were small and ranged between 3.9-12.1 cm, with an average of 7.2 cm. An exception was noted in the inner trough, and that deployment had a penetration depth of 29.6 cm. As expected, the penetration depths follow the trend of sediment strength, being expressed through *qsbc* here. A loose sediment top layer (LSTL) was detected ranging in thickness from approximately 1-4 cm with only one deployment with thickness of 6.8 cm (Figure 5.6). This layer was characterized by a very low deceleration and small *qsbc* value (shaded area in Figure 5.4), and indicates ongoing sediment remobilization processes.

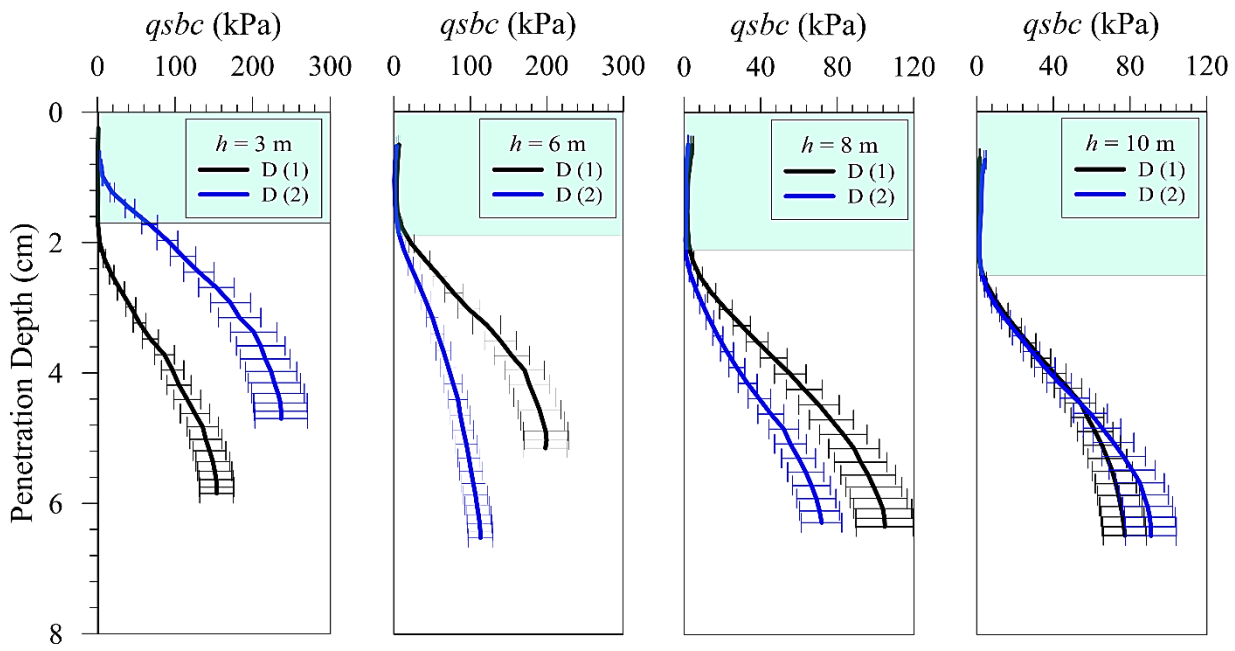

Figure 5.4. The *qsbc*-depth profiles for four duplicated deployments (D1-black lines; D2-blue lines) at different water depths *h* along transect 2. The error bars show the uncertainty due to the strain rate factor (1-1.5). The shaded areas show the loose top layer thickness at the different locations. The values at penetration depth of < 0.5 cm were impacted by deviations following the calculation approach and were neglected here.

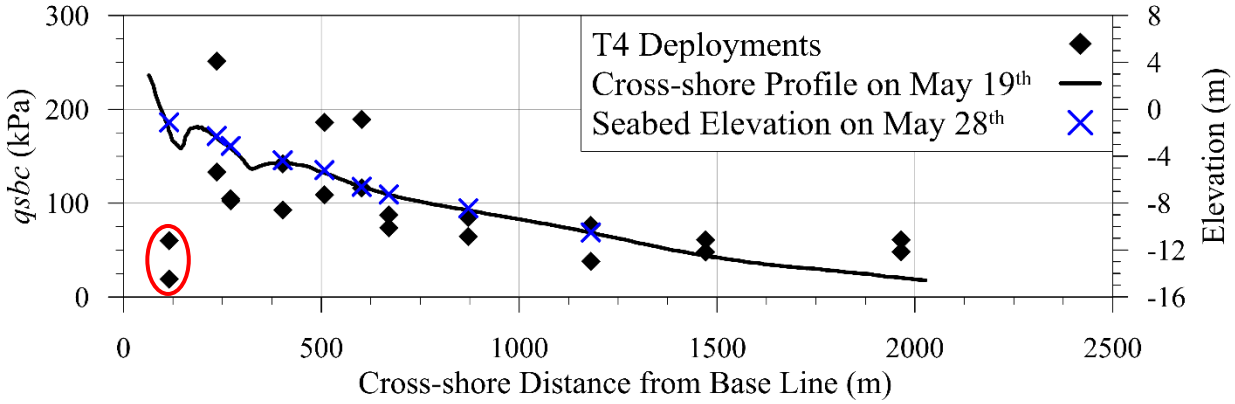

Figure 5.5. The *qsbc* variation along the survey line showing the bar location. The red ellipse indicates the deployments in the inner trough. The average foreshore slope is about 13:1 (H:V), while the average slope further offshore is about 160:1. The crosses show the estimated seabed elevation based on the pressure measurements at the deployment locations. The solid line shows the profile obtained from http://www.frf.usace.army.mil.

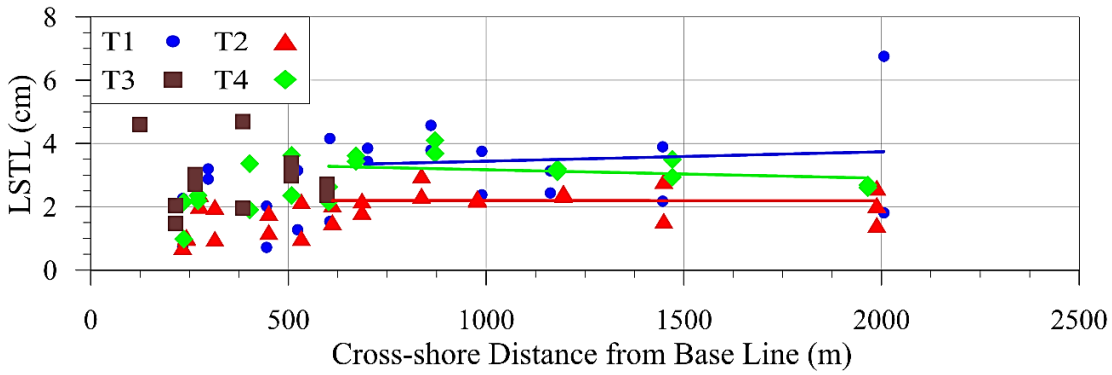

Figure 5.6. Cross-shore variation of the loose sediment top layer LSTL thickness. The lines represent the trend of the LSTL thickness for the regions where the scatter becomes relatively small.

5.6 Discussion

Results showed that sediment strength, as reflected in the *qsbc* data, of the surficial sediment layers varied based on the location along the cross-shore profile (Figure 5.5). It should be noted that ~8 days elapsed between the morphology survey and the subsequent geotechnical testing. However, the period between the two surveys was characterized by calm wave conditions. Specifically, the largest wave event in the intervening period was a short (~1 day) period of waves characterized by a significant wave height (SWH) of up to 1.87 m (measured at water depth of 17.4 m; NDBC 2016) (Figure 5.7). The migration of the bar can occur in less than one day during large storms, and the prediction of the bar migration in such moderate conditions is difficult due to the complex behavior which includes two and three dimensional morphologies (Lippmann and Holman 1990). Using Larson and Kraus' (1992) migration direction criteria, any bar migration during this mild storm would be expected to be onshore. Following these criteria, any bar migration during the following five days of calm conditions would be expected to be onshore as well (Lippmann and Holman 1990; Larson and Kraus 1992; Thornton et al. 1996; Gallagher et al. 1998; Hoefel and Elgar 2003). The potential migration direction matched the observed variations in *qsbc*. The area of expected erosion, the bar crest, exhibited the largest *qsbc* values, with high variation in the sediment strength for similar cross-shore locations. This can be explained with the removal of the looser top surface sediments when sediment freshly erodes, leaving behind an exposed denser and harder substratum. The areas where sediment deposition was expected, such as the troughs, showed low *qsbc* values. Specifically, the lowest *qsbc* values were observed in the inner trough (marked deployments in

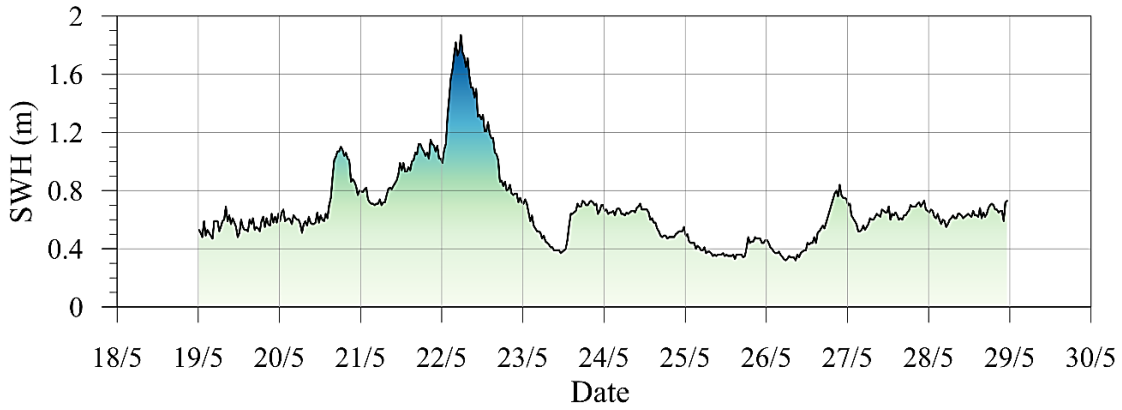

Figure 5.7. Significant Wave Height (SWH) from NOAA Buoy Station 44056 (36°12'0" N 75°42'50" W) for the period between the morphology survey and geotechnical testing.

Figure 5.5), which might have resulted from recently deposited, loose sand. Accordingly, the bar migration direction, or the movement of other morphological features, can potentially be inferred from the *qsbc* values where low *qsbc* values (loose sand) indicate sediment deposition, and thus, the migration direction of the bar. This result is in line with the observation by Stark and Kopf (2011) who also suggested that the sandbar migration in Whaingaroa Harbour, New Zealand, was reflected in the geotechnical signature of the seabed surface, and that the migration direction can be interpreted from the geotechnical data. However, periodic surveys are needed in order to understand the detailed relation between the bar migration direction and the soil characteristics.

Significant scatter in the *qsbc* values was measured between the shallow areas in the vicinity of the bar along different cross-shore transects (Figures 5.3 and 5.5). Possible explanations are variations in sediment particle size, and the presence of small morphological features, such as those previously observed in the nearshore at Duck by Hanes et al. (2001). The shear strength, and the associated bearing capacity, of cohesionless soil is expected to be higher for graded soil than for uniformly sized particles, because small grains fill the voids between the large grains, resulting in a denser matrix (Duncan et al. 2014). Whether this effect is applicable in areas of ongoing sediment remobilization and reorganization processes in the nearshore is still unclear. In general, the sediment particle size at the FRF is characterized by larger variations in the mean particle size at shallow water depths, and finer particle sizes with smaller variation (i.e. small gradation and more uniformity or sorted sediments) with increasing distance offshore (Birkemeier et al. 1981; Howd and Birkemeier 1987; Stauble 1992; Gallagher et al., 2016). Stauble (1992) collected surficial

sediments on approximately a monthly basis from March 1984 to September 1985, and found that the sediment particle size varied with water depth and cross-shore distance. The bar-trough area was characterized by relatively coarse sand with poor sorting, transitioning to finer and more sorted sand with increasing distance offshore (Figures 5.3), particularly at a distance of > 600-650 m from the baseline. This explains the general trend of decreasing *qsbc* and less scatter moving offshore (Figures 5.3 and 5.5).

The measured soil bearing capacity can also be affected by seabed slope. Compared to a horizontal plane, the bearing capacity for a footing is expected to be less in a sloped surface (Meyerhof 1957). The bar represents the most distinct morphological feature with variations in seabed slope, but the presence of smaller ripples is also likely (Birkemeier et al. 1981; Hanes et al. 2001). The presence of ripples is often associated with sorting processes, with coarse grain sizes on the crests and fine grain sizes in the troughs (e.g. Foti and Blondeaux 1995). In addition, the impact of sorted bedforms on sediment strength has been previously documented by Stark et al. (2012a). Similarly, the likely presence of sorted bedforms in Duck may help explain the observed variations in the *qsbc* at similar cross-shore locations.

The lack of variation in sediment strength at water depths of > 6.5 m could reflect the depth of closure (DoC), which is the minimum water depth at which no significant change in the seabed morphology is measured, and where sediment transport processes during quiescent conditions potentially become negligible (Birkemeier 1985). The depth of closure depends on the wave forcing, and can vary significantly in the short and long-term (Birkemeier 1985; Nicholls et al. 1998). However, a DoC depth of ~6.5 m, as indicated by the geotechnical testing, is potentially within the long-term (1-2 years) depth of closure range as postulated by Nicholls et al. (1998).

Although this was associated with scatter, trend of the LSTL show an effect for the wave action as well as the grain size variation. It seems that at shallow water depth (< 8m), the thickness of this layer was increasing with the water depth which might be related to the decrease of particle size offshore that makes it easier to mobilize the sediments (Van Rijn 2007). At larger water depths, the thickness of the LSTL is smaller with the increase of the water depth. This would be expected due to the reduction of the effect of waves on the seabed, versus a thicker LSTL that would be expected with larger wave effects (Bertin et al. 2008).

5.7 Conclusion

The portable free fall penetrometer results indicate a correlation between nearshore morphodynamics and sediment strength of the upper layers of the seafloor surface. The *qsbc*, representing sediment strength, reflected changes in particle size as well morphology. The geotechnical characteristics for deployments at water depths ≤ 6.5 m were the most affected by these factors, and showed high variations in the *qsbc*. This is in good agreement with the expected quiescent depth of closure at Duck. Furthermore, higher strength was measured on the crest of the sandbar, where the most recent erosion would be expected, while lower strength was measured in the region of the inner bar trough, where the most recent sediment deposition would be expected, in the context to likely sandbar migration. However, since the morphologic cross-shore profile is changing continuously with wave forcing, event-related studies and time series data are needed to draw more comprehensive conclusions about the relationships between the ongoing morphodynamics and the geotechnical characteristics of the sediments. In addition, collecting geotechnical samples while simultaneously conducting a hydrographic survey would reduce the error associated with correlating geotechnical data with potentially outdated morphology data.

5.8 Acknowledgments

This study was funded by the Institute for Critical Technology and Applied Science at Virginia Tech, and the US Army Corps of Engineers Coastal Field Data Collections Program, Coastal Morphology Unit. The authors would like to thank the staff of the USACE Field Research Facility for on-site technical assistance.

5.9 References

Akal, T., and Stoll, R. D. (1995). “An expendable penetrometer for rapid assessment of seafloor parameters.” *Proc., OCEANS'95. MTS/IEEE. Challenges of Our Changing Global Environment. Conference*, 1822-1826. IEEE.

Bertin, X., Castelle, B., Anfuso, G., and Ferreira, Ó. (2008). “Improvement of sand activation depth prediction under conditions of oblique wave breaking.” *Geo-Mar. Lett.*, 28(2), 65-75.

Birkemeier, W. A., Miller, H. C., Wilhelm, S. D., DeWall, A. E., and Gorbics, C. S., (1981). *A user's guide to the Coastal Engineering Research Center's Field Research Facility*. Instruction Rep. CERC-85-1 Coastal Eng. Research Center, U.S. Army Engineer Waterways Experiment Station, Vicksburg, MS.

Birkemeier, W. A., (1985). "Field data on seaward limit of profile change." *J. Waterw. Port C,* 111 (3), 598 – 602, ASCE.

Brown, J. D., and Rashid M. A., (1975). "Geotechnical properties of nearshore sediments of Canso Strait, Nova Scotia." *Canadian Geotechnical J.* 12(1), 44-57.

Danson, E. (2005). "Geotechnical and geophysical investigations for the offshore and nearshore developments." *International Society for Soil Mechanics and Geotechnical Eng., ISSMGE*.

Dayal, U., and Allen, J. H. (1973). "Instrumented impact cone penetrometer." *Can. Geotech. J.*, 10(3), 397-409.

Dean, R. G., and Dalrymple, R. A. (2004). *Coastal processes with engineering applications*. Cambridge University Press.

Duncan, J. M., Wright, S. G., and Brandon, T. L. (2014). *Soil strength and slope stability*. John Wiley and Sons.

Elgar, S., Gallagher, E. L., and Guza, R. T. (2001a). "Nearshore sandbar migration." *J. Geophys. Res.*, 106(C6), 11623-11627.

Elgar, S., Guza, R. T., O'Reilly, W. C., Raubenheimer, B., and Herbers, T. H. C. (2001b). "Wave energy and direction observed near a pier." *J. Waterw. Port C*, *127*(1), 2-6, ASCE.

Fernández-Mora, A., Calvete, D., Falqués, A., and Swart, H. E. (2015). "Onshore sandbar migration in the surf zone: New insights into the wave-induced sediment transport mechanisms." *Geophys. Res. Lett.*, *42*(8), 2869-2877.

Foti, E., and Blondeaux, P. (1995). "Sea ripple formation: the heterogeneous sediment case." *Coast. Eng*., 25(3), 237-253.

Gallagher, E. L., Elgar, S., and Guza, R. T. (1998). "Observations of sand bar evolution on a natural beach." *J. Geophys. Res.*, *103*(C2), 3203-3215.

Gallagher, E., Wadman, H., McNinch, J., Reniers, A., and Koktas, M. (2016). "A Conceptual Model for Spatial Grain Size Variability on the Surface of and within Beaches." *J. Mar. Sci. Eng.*, *4*(2), 38.

Hanes, D. M., Alymov, V., Chang, Y. S., and Jette, C. (2001). “Wave-formed sand ripples at Duck, North Carolina.” *J. Geophys. Res*, *106*(10), 22575-22592.

Hoefel, F., and Elgar, S. (2003). “Wave-induced sediment transport and sandbar migration.” *Science*, 299(5614), 1885-1887.

Holman, R. A., and Sallenger A. H. Jr. (1993). “Sand bar generation: a discussion of the Duck experiment series.” *J. Coastal Res.*, 76-92.

Howd, P. A., and Birkemeier, W. A., (1987). *Beach and nearshore survey data: 1981 – 1984 CERC field research facility*. Tech. Rep. CERC-87-9. U.S. Army Eng. Waterways Experiment Station, Vicksburg, MS

Larson, M., and Kraus, N. C., (1992). *Analysis of cross-shore movement of natural longshore bars and material placed to create longshore bars*. Tech. Rep. DRP-92-5. U.S. Army Engineer Waterways Experiment Station, Vicksburg, MS

Larson, M., and Kraus, N. C. (1994). “Temporal and spatial scales of beach profile change, Duck, North Carolina.” *Mar. Geol.*, 117(1), 75-94.

Leffler, M. W., Baron, C. F., Scarborough, B. L., Hathaway, K. K., and Hayes, R. T., (1993). *Annual Data Summary for 1991, CERC Field Research Facility*. Tech. Rep. CERC-93-3, U.S. Army Eng. Waterways Experiment Station, Vicksburg, MS.

Lippmann, T. C., and Holman, R. A., (1990). “The spatial and temporal variability of sand bar morphology.*” J. Geophys. Res.* 95, 11575-11590.

McNinch, J. E. (2004). “Geologic control in the nearshore: shore-oblique sandbars and shoreline erosional hotspots, Mid-Atlantic Bight, USA.’” *Mar. Geol.*, 211(1), 121-141.

Masselink, G., Kroon, A., and Davidson-Arnott, R. G. D. (2006). “Morphodynamics of intertidal bars in wave-dominated coastal settings—a review.” *Geomorphology*, *73*(1), 33-49.

Meyerhof, G. G. (1957). The ultimate bearing capacity of foundations on slopes. *Proc., 4th International Conference on Soil Mechanics and Foundation Eng,* 384-386.

Miller, H. C., Birkemeier, W. A., and DeWall, A. E. (1983). “Effects of CERC research pier on nearshore processes.” In *Coastal Structures’ 83*, 769-784, ASCE.

Mulukutla, G.K., Huff, L.C., Melton, J.S., Baldwin, K.C., and Mayer, L.A. (2011). "Sediment identification using free fall penetrometer acceleration-time histories." *Mar. Geophys. Res.*, 32(3), 397-411.

NDBC (National Data Buoy Center) (2016). “Station 44056, 36°12'0" N 75°42'50" W" <http://www.ndbc.noaa.gov/station_page.php?station=44056> (February 17, 2016).

Nicholls, R. J., and Birkemeier, W. A., Lee, G., (1998). “Evaluation of depth of closure using data from Duck, NC.” *Mar. Geol.* 148, 179–201.

Plant, N. G., Holman, R. A., Freilich, M. H., and Birkemeier, W. A. (1999). “A simple model for interannual sandbar behavior.” *J. Geophys. Res., Oceans, 104*(C7), 15755-15776.

Schwartz, R. K., and Birkemeier W. A. (2004). “Sedimentology and morphodynamics of a barrier island shoreface related to engineering concerns, Outer Banks, NC, USA.” *Mar. Geol.* 211(3), 215-255.

Stark, N. and Kopf, A. (2011). “Detection and quantification of sediment remobilization processes using a dynamic penetrometer.” *Proc. IEEE/MTS Oceans 2011 Conference*, Waikoloa, HI.

Stark, N., Coco, G., Bryan, K. R., and Kopf, A. (2012a). “In-situ geotechnical characterization of mixed-grain-size bedforms using a dynamic penetrometer.” *J. Sediment. Res.*, 82(7), 540-544.

Stark, N., Wilkens, R., Ernstsen, V.B., Lambers-Huesmann, M., Stegmann, S., and Kopf, A. (2012b). “Geotechnical properties of sandy seafloors and the consequences for dynamic penetrometer interpretations: quartz sand versus carbonate sand.” *J. Geotech. and Geol. Eng.*, 30(1), 1-14.

Stark N., Staelens P., Hay, A.E., Hatcher, B., and Kopf, A. (2014). "Geotechnical investigation of areas of difficult access using portable free-fall penetrometers," *Proc., CPT’14*, Las Vegas.

Stauble, D.K., 1992. *Long term profile and sediment morphodynamics: the FRF case history*. Tech. Rep. CERC-92-7. U.S. Army Eng. Waterways Experiment Station, Vicksburg, MS.

Stoll, R. D., Sun, Y. F., and Bitte, I. (2007). “Seafloor properties from penetrometer tests.” *Oceanic Eng. J.*, 32(1), 57-63, IEEE.

Thornton, E. B., Humiston, R. T., and Birkemeier, W., (1996). “Bar/trough generation on a natural beach.” *J. Geophys. Res.*, 101 (C5), 12097–12110.

Van Rijn, L. C. (2007). “Unified view of sediment transport by currents and waves. I: Initiation of motion, bed roughness, and bed-load transport.” *J. Hydraul. Eng*., 133(6), 649-667.

WIS (Wave Information Studies) (2016). “Station 63218, 36°15'0" N, 75°34'48" W.” <http://wis.usace.army.mil/> (May 16, 2016).

Chapter 6: Investigation of spatial and short-term temporal nearshore sandy sediment strength using a portable free fall penetrometer

The contributions of authors to the composition of this manuscript are delineated as follows:

Ali Albatal:

- Conducted the literature review; performed analyses; prepared figures and tables; wrote the draft manuscript,
- Participated in the field surveys.
- Addressed the comments and suggestions of the coauthors in developing the draft manuscript.

Heidi Wadman

- Participated in the field survey in the first four days of survey.
- Conducted all the deployments during the storm.
- Reviewed and edited the draft manuscript.

Nina Stark:

- Planned, supervised and participated in the field surveys.
- Initiated the idea of *CWS*.
- Supervised the study.
- Reviewed and edited the draft manuscript.

Cagdas Bilici

- Participated in performing the analyses.
- Participated in developing the idea of *CWS*.
- Reviewed and edited the draft manuscript.

Jesse E. McNinch

- Participated in the field surveys.
- Participated in finalizing *CWS*, and suggested using the bottom orbital velocity.
- Reviewed and edited the draft manuscript.

Investigation of spatial and short-term temporal nearshore sandy sediment strength using a portable free fall penetrometer

Ali Albatal[1], Heidi Wadman[2], Nina Stark[1], Cagdas Bilici[1], Jesse McNinch[2]

[1]Virginia Tech, The Charles Edward Via, Jr. Department of Civil and Environmental Engineering,

200 Patton Hall, Blacksburg, VA 24061. Phone: 540-231-7152. Email: ali2@vt.edu

[2]Field Research Facility, Coastal Hydraulics Laboratory, USACE, Duck, NC 27949

The authors of the following manuscript intend to submit it to Elsevier's Coastal Engineering Journal.

6.1 Abstract

In order to investigate the effect of the wave processes on the topmost sediment geotechnical characteristics, a Portable Free Fall Penetrometer (PFFP) was deployed in the energetic nearshore zone of the U.S. Army Corps of Engineers' Field Research Facility in Duck, NC. A total of 335 deployments were conducted from the FRF's 560 m long pier over six non-consecutive days in September and October 2016. During the surveying period, the significant wave heights varied between H_s=0.8-2.4 m measured at a water depth of 17.4 m. The results showed that the sediment strength is affected by the wave climate. The derived average maximum quasi-static bearing capacities (*qsbc*), which reflects sediment strength, during low energy wave periods (September 22-24 and 26; H_s = 0.8-1.3 m) ranged between 67-73 kPa with maximum *qsbc* values of 120-136 kPa, while the average values were 47-59 kPa with a maximum *qsbc* of 82-98 kPa during the high energy wave periods (October 5-6; H_s = 2.4 m). The results also showed that the sediment strength decreased in the shallow water depth regions in spite of the increase in the particle size distribution, due to the increasing wave impact on the seabed within the shallow water region. The area affected by the wave action became wider in the cross-shore direction as the wave height increased. These results suggest that the grain size governs the trends of surficial sediment strength outside of the shallow water depth region, while the wave energy dominates the variations of surficial sediment strength within the shallow water region.

6.2 Introduction

The morphology of energetic nearshore zones undergoes spatial and temporal variations in response to the variable hydrodynamics. The interaction between the hydrodynamics and seabed sediments results in complex morphodynamics (Lippmann and Holman 1990; Plant et al. 1999; Schwartz and Birkemeier 2004; Fernández-Mora et al. 2015). This can represent a concern for the stability and durability of nearshore structures. The spatial and temporal beach profile variability and associated migration of sandbars in different wave conditions have been heavily investigated (e.g., Lippmann and Holman 1990; Larson and Kraus 1992, 1994; Thornton et al. 1996; Nicholls et al. 1998; Elgar et al. 2001a; Hoefel and Elgar 2003; Hsu et al. 2006; Horrillo-Caraballo and Reeve 2008). However, the variation of the geotechnical seabed characteristics in response to the

morphodynamics and hydrodynamics has rarely been investigated, particularly for the case of energetic sandy nearshore zones and sandbar migration.

The topmost sediment layers are usually characterized by a low density and strength. These layers can vary in particle size, thickness, density and strength (Harris and Wiberg 2001, 2002; Stark and Kopf 2011). Accordingly, a detailed characterization of the sediment in areas where such layers are subjected to variable driving forces is crucial to fully understand the sediment behavior, stability, and mobility. However, using conventional geotechnical site investigation tools is expensive, and can be challenging due to the energetic hydrodynamics and limited navigable depth in the nearshore region (Danson 2005). Therefore, cost-effective and portable tools are needed to investigate the sediments in such regions.

Portable free fall penetrometers (PFFPs) have been used as cost and time-effective tools to characterize the surficial sediments in the nearshore areas (Stark et al. 2014b; Albatal and Stark 2016, 2017). PFFPs are specifically developed to determine the geotechnical properties (e.g., shear strength and bearing capacity) of the topmost seabed sediments and to investigate the sediment remobilization processes (Stark and Kopf 2011; Stark et al. 2012b; Steiner et al. 2014; Chow et al. 2017). PFFPs are of lightweight (often < 15 kg), enabling easy handling and deployment even from a rocking boat in wavy conditions. The soil bearing resistance and shear strength parameters can be estimated from the decelerations of the probe during impact and penetration measured by the PFFPs using semi-empirical equations (e.g., Dayal and Allen 1973; Aubeny and Shi 2006; Stark et al. 2011; Chow and Airey 2013). Different sediment classification schemes have been introduced based on PFFPs measurements (e.g., Stoll et al. 2007; Mulukutla et al. 2011; Albatal and Stark 2017). However, these classification schemes were mostly developed for specific locations based on laboratory tests or field tests under non-energetic conditions, which made them unsuitable to be used in energetic nearshore environments.

Bilici et al. (2018) have recently introduced a coefficient of wave impact on sediment surface strength (*CWS*) to characterize the sediments in energetic nearshore areas considering both the sediment geotechnical properties measured by PFFP and the effect of the waves represented by the ratio of the water depth to deep water wavelength. They found that *CWS* is affected by the depth of closure and wave breaking. However, Bilici et al. (2018) used the water depth to deep water wavelength ratio to represent the wave energy. This may not reflect the extent of the

variability in the wave impact on the seabed, especially in shallow waters where the depth-induced wave breaking becomes important. The interaction between the surface waves and seabed is resulting in a partial dissipation of the wave energy through wave-induced bed shear stress which is proportional to the bottom orbital velocity (e.g., Hallermeier 1980; Sallenger and Holman 1985; Wiberg and Sherwood 2008). It follows that another possible representative for the wave-seabed interaction could be wave celerity that was found compatible with common hydrodynamic models (Orlandini and Rosso 1996; Bilici et al. 2018). As one goal of this study, the *CWS* will be further investigated using PFFP deployments in different wave conditions, and using different wave parameters to represent the wave-seabed interaction.

Despite the tools ruggedness, boat deployments in energetic wave conditions can be difficult in shallow nearshore zone areas. As a safe alternative, deployments were carried out from the 560 m long pier located in the U.S. Army Corps of Engineers Field Research Facility (FRF) at Duck, NC for the purpose of surveying under wave conditions that exceed safe conditions for boat operation. The second goal of this study is to investigate the spatial and short-term temporal variations in sediment strength of sediment in nearshore areas in response to the wave climate, specifically storm conditions, and associated sediment transport. Twenty-seven locations along the pier were chosen to deploy the PFFP *BlueDrop*. A total of 335 deployments were conducted in 6 days of surveying on September 22-24 and 26, and October 5-6, 2016. The wave climate varied between calm to stormy with significant wave heights between 0.8-2.4 m, and dominant wave periods between 6.5-11.5 s during the surveys. The results showed a relationship between the wave climate and sediment strength, which can be correlated to the sediment transport and bar migration direction. The following sections provide a brief overview of the regional context, a detailed description of the methods, results, discussion and conclusions drawn.

6.3 Regional Context

The U.S. Amy Corps of Engineers' Field Research Facility is located in Duck, North Carolina, located on the Outer Banks barrier islands (Figure 6.1). The facility coordinates are 36º10'54.5"N and 75º45'4.5"W. The beach foreshore slope is steep (average slope angle of ~4.57º), and composed of quartz sand particles with gravel, with a median grain size of 1-2 mm, and up to 20% carbonate shell debris. Further offshore, the slope is more flat (slope angle of ~0.35º), and the

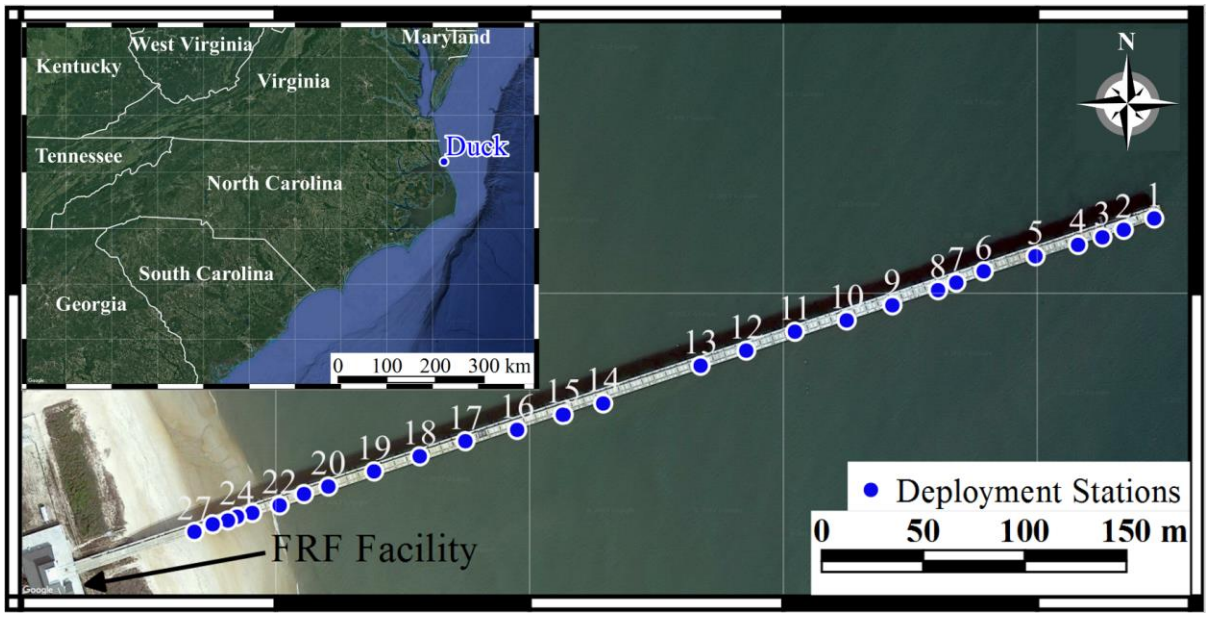

Figure 6.1. Google™ Satellite images showing the location of Duck, NC, USA (36º10'32" N and 75º45'20" W). The blue dots show the 27 PFFP deployment stations along the pier.

particle sizes are less variable and smaller with a median grain size of about 0.1-0.2 mm (Sallenger and Holman 1985; Howd and Birkemeier 1987; Lippmann and Holman 1990; Stauble 1992).

The cross-shore morphology is highly dynamic, affected by the wave environment. It varies from no sand bars to a triple-barred profile, with single and double-barred profiles being the most common (Birkemeier et al. 1981). The inner bar is located approximately at a distance of 30-120 m offshore, while the outer bar is unstable and appears during storms at distance of 300-400 m offshore (Lippmann and Holman 1990).

The facility features a 560-meter long pier that allows conducting experiments safely in stormy wave conditions. The scour processes around the pier supporting piles affect the morphology and wave characteristics of the area immediately adjacent to the pier (Miller et al. 1983; Elgar et al. 2001b) (Figure 6.2). However, it is not expected that scour has a significant impact on the results presented here, because the behavior of the nearshore bar and wave characteristics during storms near the pier is considered representative for areas away from the pier (Miller et al. 1983). Moreover, the PFFP deployments were conducted as far from the pier piles as possible to minimize such impacts. The deployments were mostly conducted at approximately the middle point between the neighboring piles (the distance between the piles is 12.2 m along the pier axis).

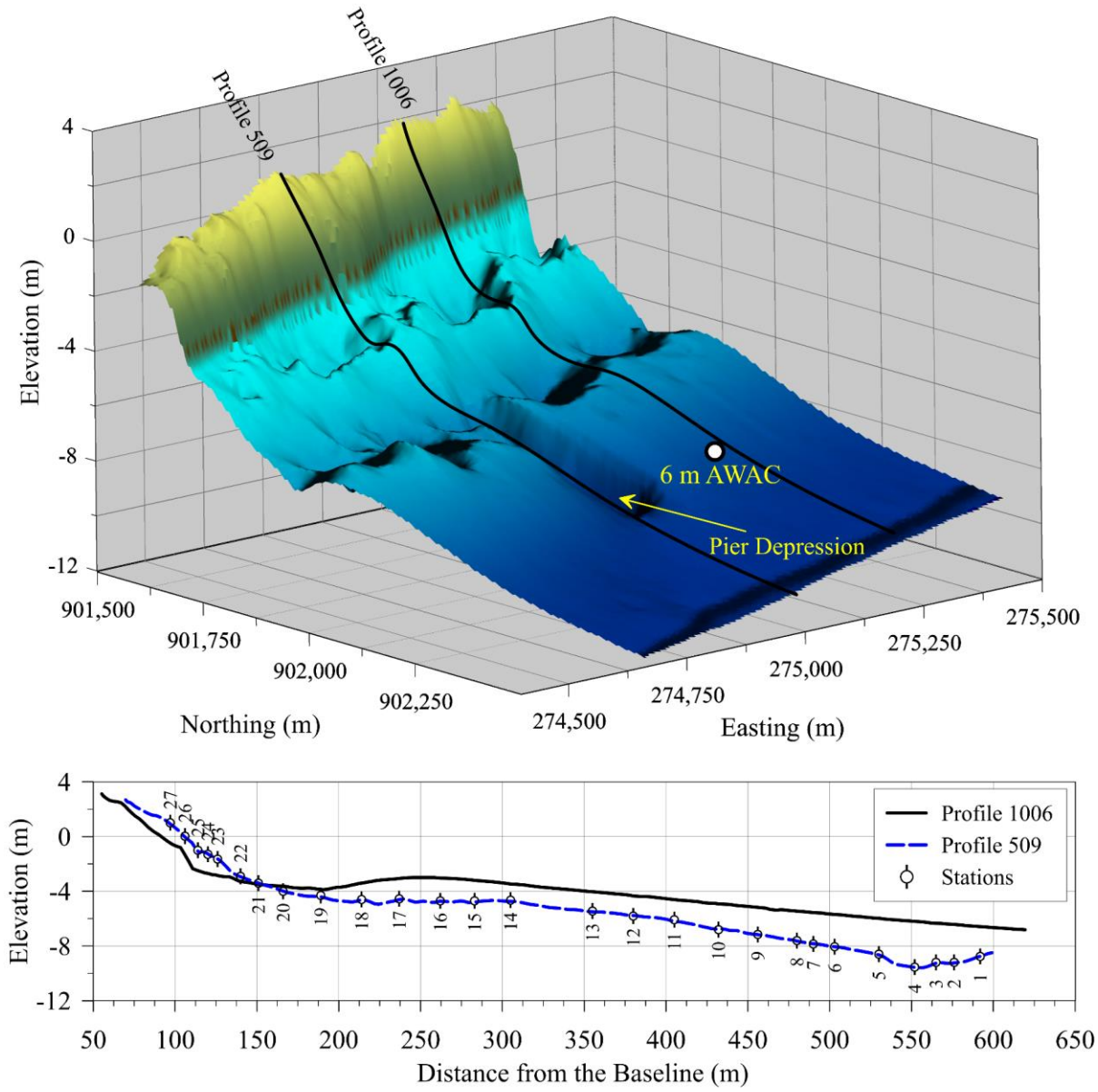

Figure 6.2. The top panel shows the bathymetry of the FRF nearshore area from a digital elevation model (DEM) obtained from *http://www.frf.usace.army.mil*. The highlighted profiles indicate profile #1006 that was used to validate the SWAN model, and profile #509 was used to calculate the significant wave heights at each deployment location. The bottom panel shows profiles #1006 and #509 surveyed on September 08, 2016 in addition to the location of each deploying station.

The wave forcing in the area varies throughout the year with the nor'easter season between the fall and early spring being the most energetic period (Lippmann and Holman 1990). The monthly mean significant wave heights ranged between 0.56-1.97 m with wave period between 6.2-12.0 s at a water depth of 25 m for the period between 1980-2012 (Albatal et al. 2017). The wave climate varied significantly during the field surveys with significant wave heights ranging between 0.84-2.36 m and a dominant wave period ranging between 6.46-11.48 s (Figure 6.3). These values were calculated as the average value for the time period of each survey, which was between 2-4 hours, from the NOAA National Data Buoy Center, Station 44056 (36°12'0"N 75°42'50"W; *http://www.ndbc.noaa.gov*) at a water depth of 17.4 m.

Tides are semi-diurnal with an average tidal range of about 1 m (Birkemeier et al. 1981). The PFFP deployments were conducted at different tide phases. On September 22-23 and October 5-6, the deployments were conducted at high tides with water levels varied between +0.77 and +1.15 m from the mean sea level (MSL). On September 24, the deployments were conducted at lower, flood tide that was between +0.08 and +0.33 from the MSL. On September 26, the deployments were conducted during low tide with water levels between -0.17 and -0.21 from the MSL. These values were determined from NOAA tides and currents website (*https://tidesandcurrents.noaa.gov*, Station 8651370).

6.4 Methods

6.4.1 Free fall penetrometer measurements and data analysis

The PFFP *BlueDrop* was used in this study. The device samples continuously at a rate of 2 kHz, and is equipped with vertical and horizontal accelerometers in addition to a pore pressures transducer. The device's five vertical accelerometers feature capacities between ±1.7 and ±250 *g* (with *g* being the gravitational acceleration) while the pressure transducer has a capacity of 2 MPa. The device has a replaceable tip, and weighs ~7.7 kg with a length of ~63 cm using the 60º conical tip that was used for this study (Stark et al. 2014b).

The PFFP is usually released just beneath the water surface, falling undisturbed through the water column. It impacts the seabed at an initial impact velocity usually between ~3-6 m/s. Typical impact velocities may vary for other probes. The penetration velocity and depth are determined

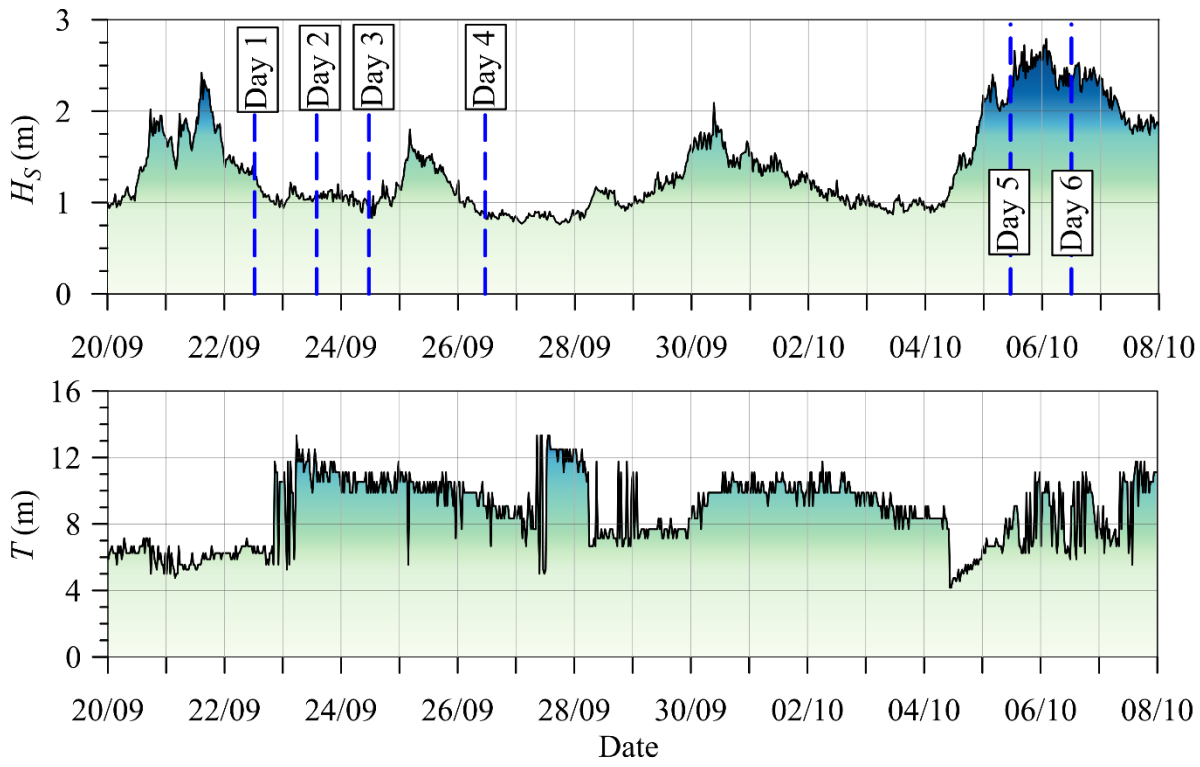

Figure 6.3. Significant wave height (H_s) and dominant wave period T during the survey periods. The data is obtained from the NOAA National Data Buoy Center, Buoy Station 44056 (36°12'0" N 75°42'50" W) at water depth of 17.4 m.

from the first and second integration of the deceleration-time records, respectively. The sediment resistance against the probe penetration governs the probe's deceleration signature (Wang 1971). By solving the equation of motion and knowing the probe's deceleration during penetration, buoyant mass, and probe area, the dynamic force opposing the penetration into the sediment can be calculated, and a bearing capacity or even shear strength may be estimated. However, the sediment's resistance against the penetration of the probe is dependent on the penetration rate (i.e., shear rate). This dynamic resistance is expected to be greater than the sediment resistance under conventional loads (i.e. static loads) due to the increase in shear strength, and the developed negative pore water pressures under high strain rates (Seed and Lundgren 1954; Dayal and Allen 1973). Thus, strain rate corrections are needed to convert the dynamic resistance to an equivalent quasi-static resistance, which is normalized for a reference constant penetration velocity (usually the standard penetration velocity of the Cone Penetration Test, 2 cm/s) (Dayal and Allen 1973; Stark et al. 2011, 2012b) (Figure 6.4). Different strain rate correction equations have been used in

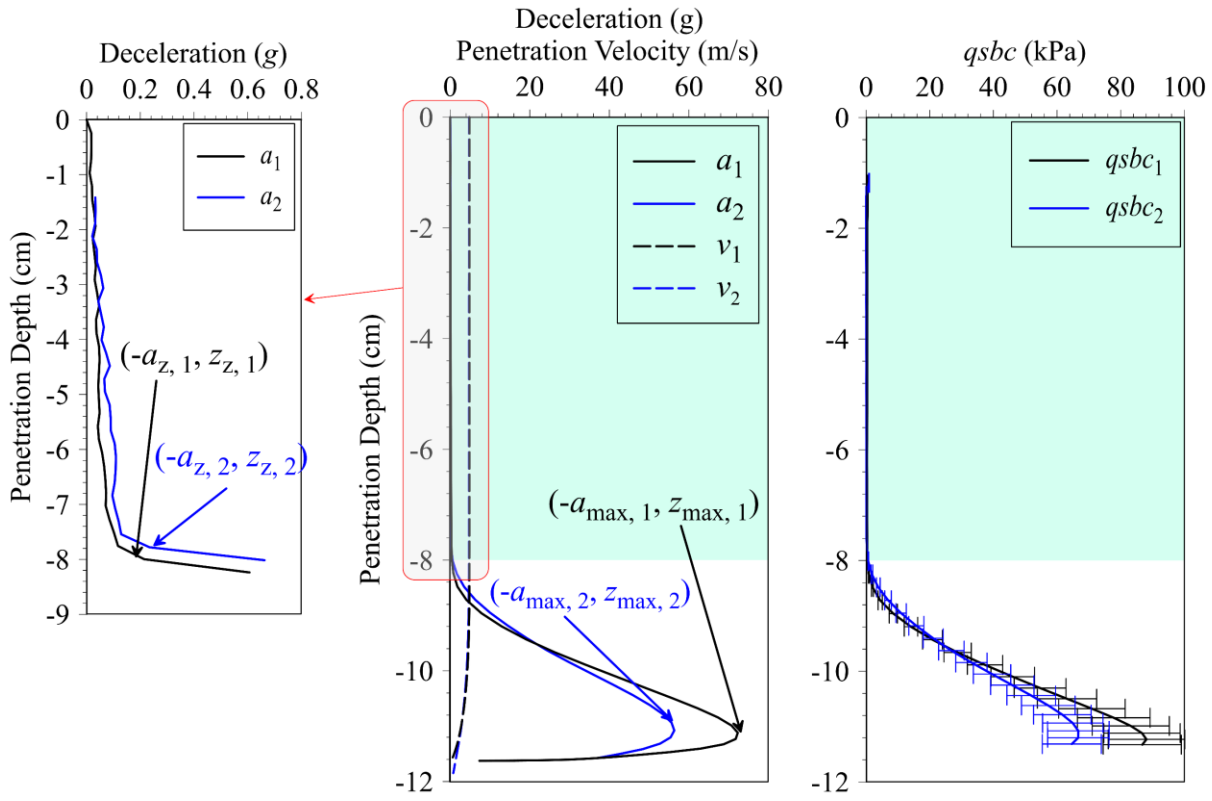

Figure 6.4. The measured deceleration *a*, and derived velocity *v* and quasi-static bearing capacity *qsbc* profiles for two deployments at the same location on September 23 at a distance of 260 m from the baseline (Station 16). The error bars show the uncertainty due to the used strain rate factor (1-1.5) following Stark et al. (2012) approach. The shaded areas show the loose top layer thickness. The figure shows how the values of the deceleration and depth *z* are selected to determine the coefficient of wave impact on sediment surface strength, *CWS*.

the literature, such as the logarithmic, inverse hyperbolic-sine and, power equations (e.g. Dayal and Allen 1973; Steiner et al. 2014). The logarithmic equation is the most commonly used approach in sandy sediments, with a strain rate factor empirical coefficient of K=1-1.5 (e.g., Stoll et al. 2007, Stark et al. 2012, Stephan et al. 2015). Accordingly, the analysis method proposed by Stark et al. (2011, 2012) was followed here using the logarithmic strain rate correction equation and an average strain rate factor empirical coefficient of K=1.25 (Figure 6.4).

Albatal et al. (n.d.) estimated the friction angle of Cannon Beach's sand in Yakutat, AK from PFFP measurements using Durgunoglu and Mitchell (1973) and Meyerhof (1961) bearing capacity methods. They found that that the logarithmic equation provides better results than the inverse

hyperbolic-sine. However, Albatal et al. (n.d.) suggested using a strain rate factor empirical coefficient of K=0.2-0.4. They also found that the Firmness Factors, FF, proposed by Mulukutla et al. (2011) (which is a function of the maximum deceleration, impact velocity and the penetration time) is correlated to the sand friction angle determined using Durgunoglu and Mitchell (1973) theory by $\phi'=39.7\ FF^{0.08}$. This correlation was also tested here using the suggested strain rate coefficient (i.e. K=0.4). The deployments conducted on September 24 were chosen to tests the validity of this correlation for FRF beach's sand because the wave climate on this day was similar to the wave climate during which Cannon Beach survey was conducted ($H_s \approx 0.9$ m).

6.4.2 Coefficient of wave impact on sediment surface strength CWS

Bilici et al. (2018) proposed a coefficient to quantify the wave impact on sediment surface strength (*CWS*) considering both the PFFP measurements and hydrodynamics. The *CWS* was initially formulated as follows:

$$CWS = \frac{a_t z_t / a_{max} z_{max}}{2h/\lambda_0} \tag{6.15}$$

where a_t is the deceleration achieved within the top layer, a_{max} is the maximum measured deceleration, z_t is the loose top layer thickness, z_{max} is the penetration depth at the maximum measured deceleration, h is the water depth, and λ_0 is the deep water wave length (Figure 6.4). The numerator part of the equation denotes the characteristics of the top layer with respect to the underlying, more stable layer while the denominator part reflects the effect of wave action on the seabed. However, using the water depth to deep water wave length ratio in the denominator part of the equation might represent a disadvantage here, because the shear stress on the seabed does not increase linearly with the water depth decrease especially in shallow water depths and in the breaking zone (e.g. Jonsson 1966). With the goal to investigate the *CWS* further, and particularly for storm conditions, in addition to using Equation 1, the denominator will be changed to a factor of the bottom orbital velocity or wave celerity.

The thickness of the mobile sediment layers is conventionally assumed to be a factor of the shear stress applied on the seabed (Harris and Wiberg 2001). Moreover, the numerator of the *CWS* equation ($a_t\ z_t/a_{max}\ z_{max}$) reflects the sediment characteristics measured by the PFFP. It can also be assumed that this part of the equation reflects the critical shear stress of the seabed against erosion

because they are governed by same sediment characteristics. Because the applied shear stress is a function of the squared bottom orbital velocity u_b^2 (e.g., Jonsson 1966; Wiberg and Sherwood 2008), the denominator of *CWS* equation can be expressed as a function of u_b^2. The seabed sediments are only mobilized when the applied shear stress is larger than the critical shear stress required for the initiation of motion. Accordingly, it will be assumed that *CWS* reflects the critical to the applied shear stress on the seabed, and thus, can be assumed to reflect the susceptibility of sediments for erosion (i.e. initiation of motion of the seabed sediments). The modified *CWS* equation considering the squared bottom orbital velocity is:

$$CWS_{u^2} = \frac{a_t z_t / a_{max} z_{max}}{gD/u_b^2} \tag{6.2}$$

where g is the gravitational acceleration and D is the *BlueDrop* diameter (8.75 cm). As the wave celerity was found compatible with common hydrodynamic models (Bilici et al. 2018), the wave length in the denominator of *CWS* equation will be replaced by the wave celerity in another expression of the *CWS*. The modified *CWS* equation considering the wave celerity c is:

$$CWS_C = \frac{a_t z_t / a_{max} z_{max}}{h/c} \tag{6.3}$$

The wave characteristics in shallow waters were determined using one-dimensional SWAN (Simulating WAves Nearshore, Version 41.20) analyses, which is a third-generation wave model specifically designed for modeling shallow water characteristics (Booij et al. 1999). SWAN considers processes such as wave breaking, wave-wave interactions, bottom friction, and refraction. The use of the numerical modeling tool was important here in order to consider the decrease in the wave energy due to the waves breaking. Wave breaking is causing a nonlinear behavior that cannot be addressed correctly using simplified analytical methods (Hallermeier 1980). The deep water wave characteristics were obtained from the NOAA WaveRider buoy located at a water depth of 17.4 m (Station 44056). The significant wave heights measured by the FRF facility AWAC located at a water depth of 6 m were used to validate the SWAN model. The validation was performed by transferring the deep water waves along the survey profile line number 1006 located at a distance of ~500 m to the north of the FRF pier (Figure 6.2). The survey along the profile was conducted on September 08, 2016. The SWAN results were compared to the measured values by the 6 m AWAC. The error in the modeled versus measured significant wave

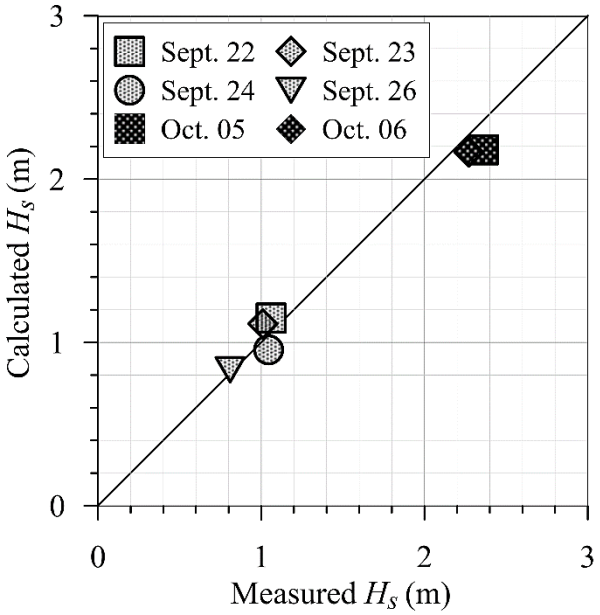

Figure 6.5. The measured significant wave heights by the 6 m AWAC versus the estimated wave height values resulted from SWAN model.

heights was between 3-10 % (Figure 6.4). Such an error margin is reasonable given that the wind effect was neglected in the model. The profile survey was conducted two weeks before the PFFP measurements. The significant wave heights obtained from NOAA WaveRider were averaged over 30 minutes, while the FRF facility AWAC wave measurements were averaged over 60 minutes. After validating the model, other SWAN runs were performed along profile 509 which is at a distance of 5 m south the pier to determine the wave characteristics and bottom orbital velocity at each deployment location.

6.4.3 Field surveys

The portable free fall penetrometer *BlueDrop* was deployed on September 22, 23, 24 and 26, and October 5 and 6, 2016, in the nearshore zone off the U.S. Army Corps of Engineers Field Research Facility (FRF) at Duck, NC. Twenty-seven locations were chosen along the southern side of the 560 m long pier starting from the end of the pier (water depth ~11 m) to the swash zone (Figure 6.1). The distance between the stations varied between 6-50 m with a smaller distance in the shallowest areas (i.e. Stations 20-25) (Figures 6.1 and 6.2). Mostly, three deployments were conducted at each location, with 335 deployments in total. The PFFP was deployed at all 27

stations on September 22 and at 14-18 stations on the other survey days. The initial results of the deployments conducted on September 22 were presented by Bilici et al. (2018).

Sediment samples were collected from nine stations on September 22 using a small-size grab sampler. The grain sizes were determined in the laboratory according to the American Society for Testing and Materials standards (ASTM D6913), and the sediments were classified according to the Unified Soil Classification System USCS (ASTM D2487).

6.5 Results

6.5.1 Grain size analysis

The sediment samples were classified according to the ASTM D2487. The soil sample collected from Stations 1-23 were classified as poorly graded sand (Figure 6.6). Station 1 (collected from the end of the pier) contained the smallest particle sizes among the collected samples with a median grain size of 0.14 mm and 1.4% fines by weight. The particle sizes of the samples collected from Stations 2-23 were approximately uniform with a median grain size between 0.20-0.22 mm. The samples collected from the upper foreshore zone (Stations 26 and 27) varied more significantly ranging from ~5-0.15 mm, and contained gravel. It should be noted that the median particle size for Station 27 was 4.89 mm, being larger than the reported range in the literature for the same location (0.1-2 mm). This may be a result of losing fines during sampling, which is expected when using grab samplers.

6.5.2 Free fall penetrometer results

The deployments covered water depths up to ~11 m. For all deployments, the measured maximum decelerations varied between 14.8-102.8 *g*. The measured maximum deceleration values for the deployments conducted on September 22-26 were generally larger than the measured values for the deployments conducted on October 5-6. The average maximum deceleration, a_{max}, for September 22-26 deployments were between 54-58 *g*, while the average values were 35 *g* and 45 *g* for deployment conducted on October 5 and 6, respectively. The derived *qsbc* for all deployments ranged between 17-149 kPa, at impact velocities ranging from 2.3 to 6.5 m/s with an average impact velocity of 4.5 m/s and standard deviation of 0.75 m/s. The average maximum *qsbc* values

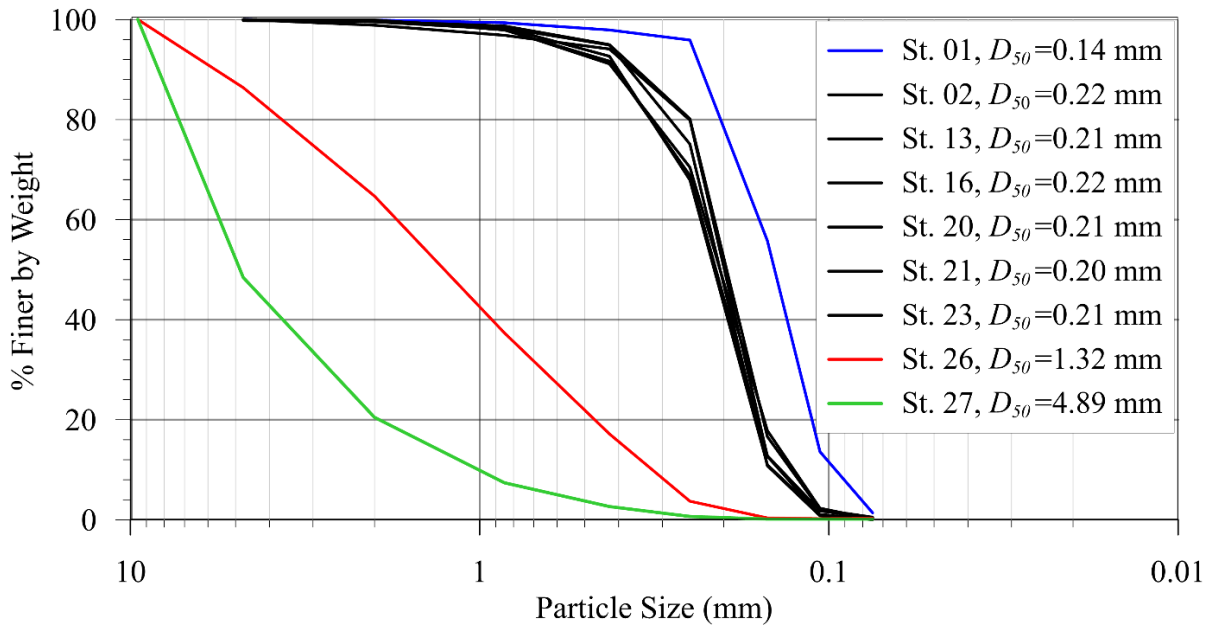

Figure 6.6. Grain size distributions for the samples collected on September 22. The legend shows the corresponding station to each line and the median grain size D_{50} for this sample.

for September 22-26 deployments equaled 67-73 kPa, while the average values were 47 kPa and 59 kPa for October 5 and 6, respectively.

Generally, the *qsbc* values were lower in shallow water depths, yielded a maximum value in a few meters water depth (1-5.8m), and decreased again in deeper water depths (Figure 6.7). Allowing the assumption that the seabed softening at shallow water depths resulted from wave action, the water depth at which the *qsbc* achieved the maximum value will be referred to as the Depth of Disturbance *DoD*. This should not be confused with the thickness of the active sediment layers. The *DoD* correlated to the significant wave height. During relatively low energy waves (i.e. September 22-26, H_s of 0.8-1.3 m), the *DoD* was shallower than 2.5 m with a maximum observed *qsbc* value between 120-136 kPa. It decreased from ~2.5 m to ~1 with the decrease in the significant wave height from 1.30 to 0.84 m (Figure 6.7). During higher energy waves (October 5 and 6, $H_s \approx 2.4$ m), the *DoD* was deeper than 3.8 m with a maximum *qsbc* value of 82 and 98 kPa on October 5 and 6, respectively (Figure 6.4). For water depths deeper than the *DoD*, the *qsbc* was lower during the high energy waves compared to the low energy waves deployments. Considering only water depths deeper than the *DoD*, the average *qsbc* ranged between 71-76 kPa for the deployments conducted on September 22-26 and was 47 and 61 for the deployments conducted on

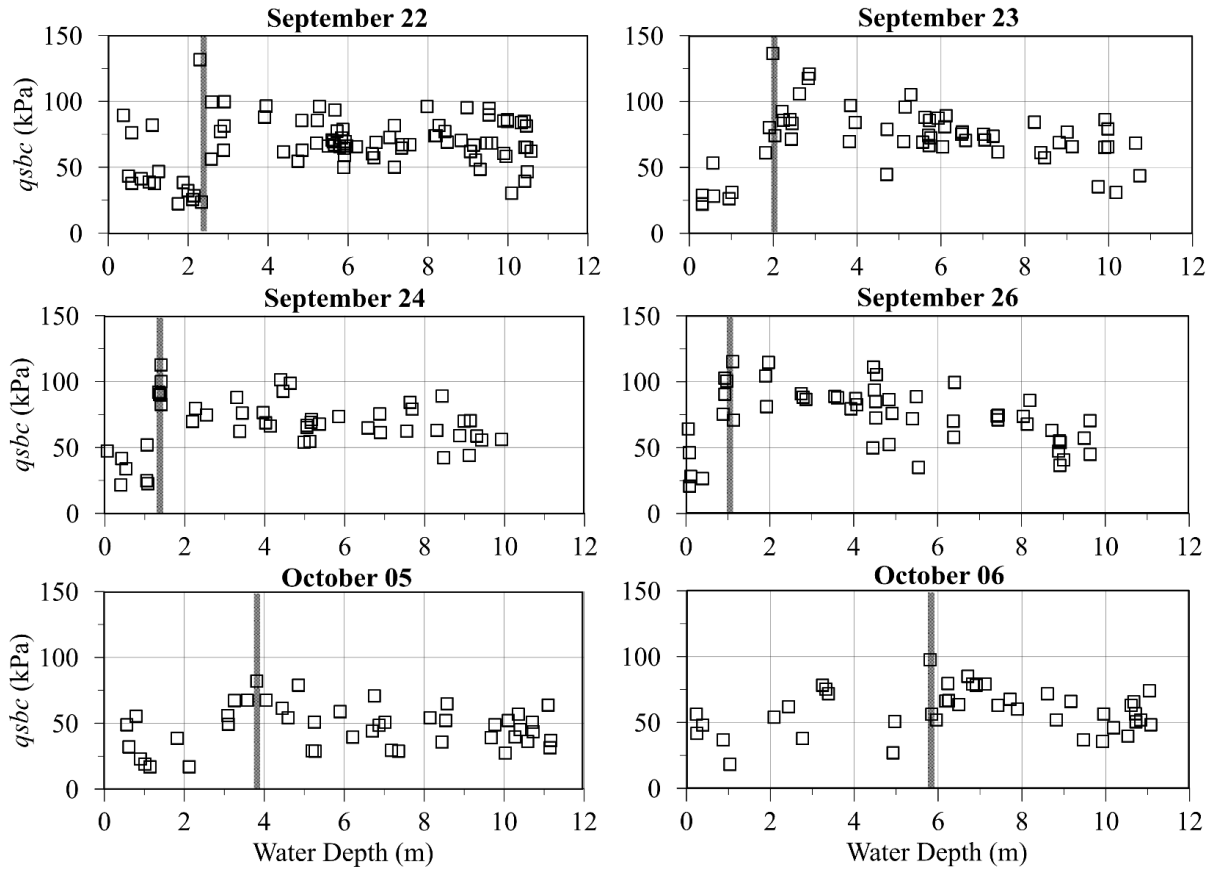

Figure 6.7. The estimated quasi-static bearing capacity *qsbc* values versus water depth for each survey day. The vertical line shows the water depth at which the *qsbc* was maximum along the profile.

October 5 and 6, respectively. Here, a decreasing trend was observed with the water depth increase (Figure 6.7). A summary of the measured decelerations and derived *qsbc* is shown in Table (1).

The average value of the *qsbc* for the deployments conducted at each station was considered to represent the sediment strength at each station. On September 22-26, the *qsbc* reaches a maximum value in a short distance from the shore (~40 m from the shoreline, which is located at a distance of 114 m from the FRF baseline (Thornton et al. 1996)) while the distance is longer on October 5-6 (Figure 6.8). Moreover, for October 5-6 deployments, the maximum *qsbc* values were smaller with higher scatter compared to the deployments at the same locations on September 22-26. The maximum scatters for water depths larger than the *DoD* was observed on October 5-6 at a distance between 240-410 m from the baseline, which is an expected location for the outer bar (Larson and Kraus 1994).

The pore water pressures PWP were mostly negative during penetration, which is an expected behavior while penetrating sandy sediments due to the dilative behavior. Following Albatal and Stark (2017), the PWP at the maximum *qsbc* was investigated. Here, to ensure full penetration of the pressure sensor to the sediments, only deployments with penetration depth larger than 10 cm

Table 6.1. Summary of the PFFP results for all the deployments

Date	H_s (m)	T (s)	N	Statistics	a_{max} (g)	v_i (m/s)	$qsbc_{\max}$ (kPa)	LTL (cm)
22 Sept.	1.30	6.46	86	Max.	102.9	6.5	131.8	27.1
				Min.	17.3	3.2	22.3	3.3
				Average	54.1	4.7	67.3	9.3
				St. Dev.	15.7	0.5	20.1	5.2
23 Sept.	1.08	11..48	58	Max.	97.5	6.3	136.6	12.4
				Min.	17.9	3.5	22.0	2.4
				Average	57.5	4.8	71.6	8.1
				St. Dev.	18.2	0.6	24.1	1.7
24 Sept.	0.96	10.19	51	Max.	92.1	6.5	115.9	10.1
				Min.	18.5	3.8	21.7	2.6
				Average	55.8	4.8	69.4	6.8
				St. Dev.	16.3	0.6	21.4	1.5
26 Sept.	0.84	9.09	52	Max.	91.8	6.4	115.3	11.1
				Min.	16.7	3.1	20.9	2.8
				Average	58.4	4.8	73.3	7.2
				St. Dev.	18.5	0.7	23.3	1.7
05 Oct.	2.35	8.05	45	Max.	64.1	5.2	82.1	20.0
				Min.	14.8	2.4	16.9	3.0
				Average	34.7	3.9	46.6	6.8
				St. Dev.	13.8	0.8	16.1	3.1
06 Oct.	2.36	9.09	43	Max.	76.3	5.9	97.7	11.0
				Min.	15.7	2.3	18.2	3.1
				Average	45.3	4.1	59.0	6.0
				St. Dev.	13.5	0.8	16.5	1.6
All deployments			335	Max.	102.9	6.5	136.6	27.1
				Min.	14.8	2.3	16.9	2.4
				Average	51.9	4.5	65.4	7.6
				St. Dev.	17.9	0.7	22.2	3.3

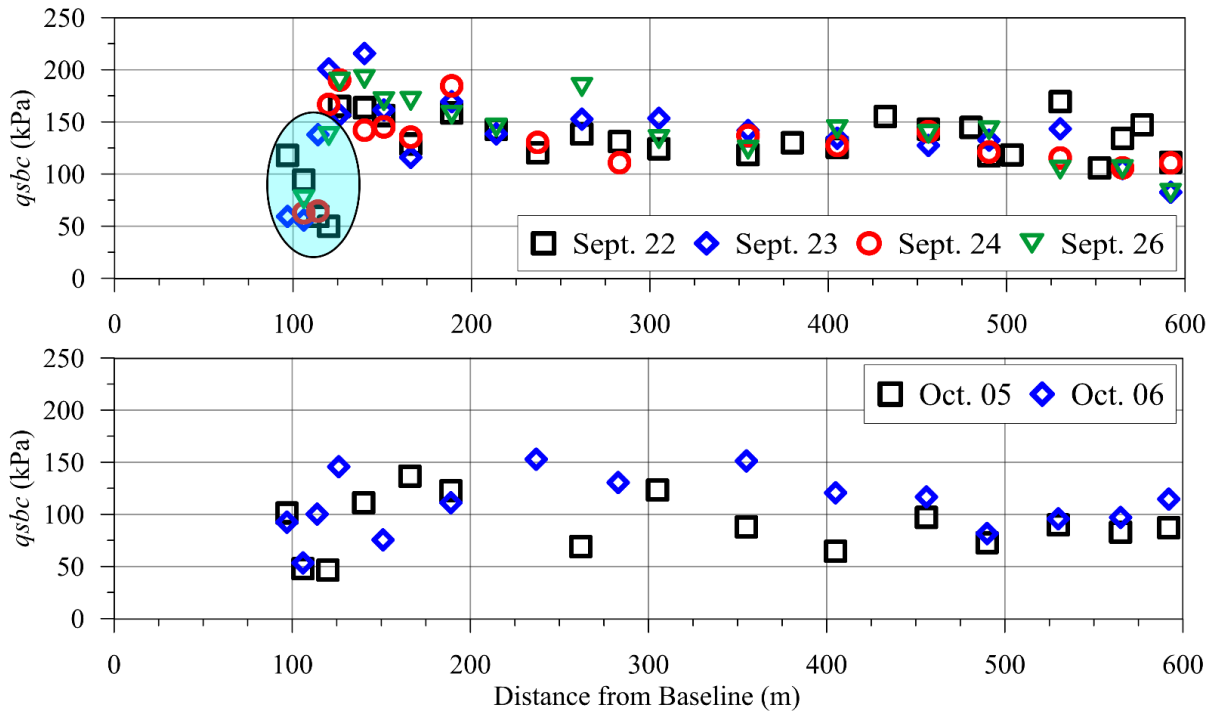

Figure 6.8. The *qsbc* as an average value for deployments conducted at the same station plotted versus the distance from the baseline. The shaded area highlights the deployments in the breaking zone

were considered. For those deployments, PWP values varied from -0.4 to -14.4 kPa. An increasing trend in the negative *PWP* and scatter was observed with the water depth increase (Figure 6.9). At shallow water depths, where the mean particle size is relatively large, the generated negative PWP is the lowest, and approaches a value of zero. With the increase in the water depth, the sand becomes finer and the particle size becomes approximately uniform.

A loosely deposited top layer (LTL) was detected with thicknesses ranged between 1-27 cm. This layer is distinguished by low measured decelerations and associated *qsbc* (Figure 6.4). The maximum thickness of this layer (27 cm) was found on September 22 and at stations 22 and 23 at a distance of 126-140 m from the baseline. On the following days, this layer was thinner at the same location with a thickness less than 10 cm (Table 1).

The in-situ friction angles of sand determined using Durgunoglu and Mitchell (1973) theory for September 24 varied between 32º-55º. Following the *qsbc* trend, the friction angles were low in water depths shallower than the *DoD*, became maximum at the *DoD*, and decreased again as the water depth increased (Figure 6.10). The estimated friction angles using ϕ'-*FF* correlation were

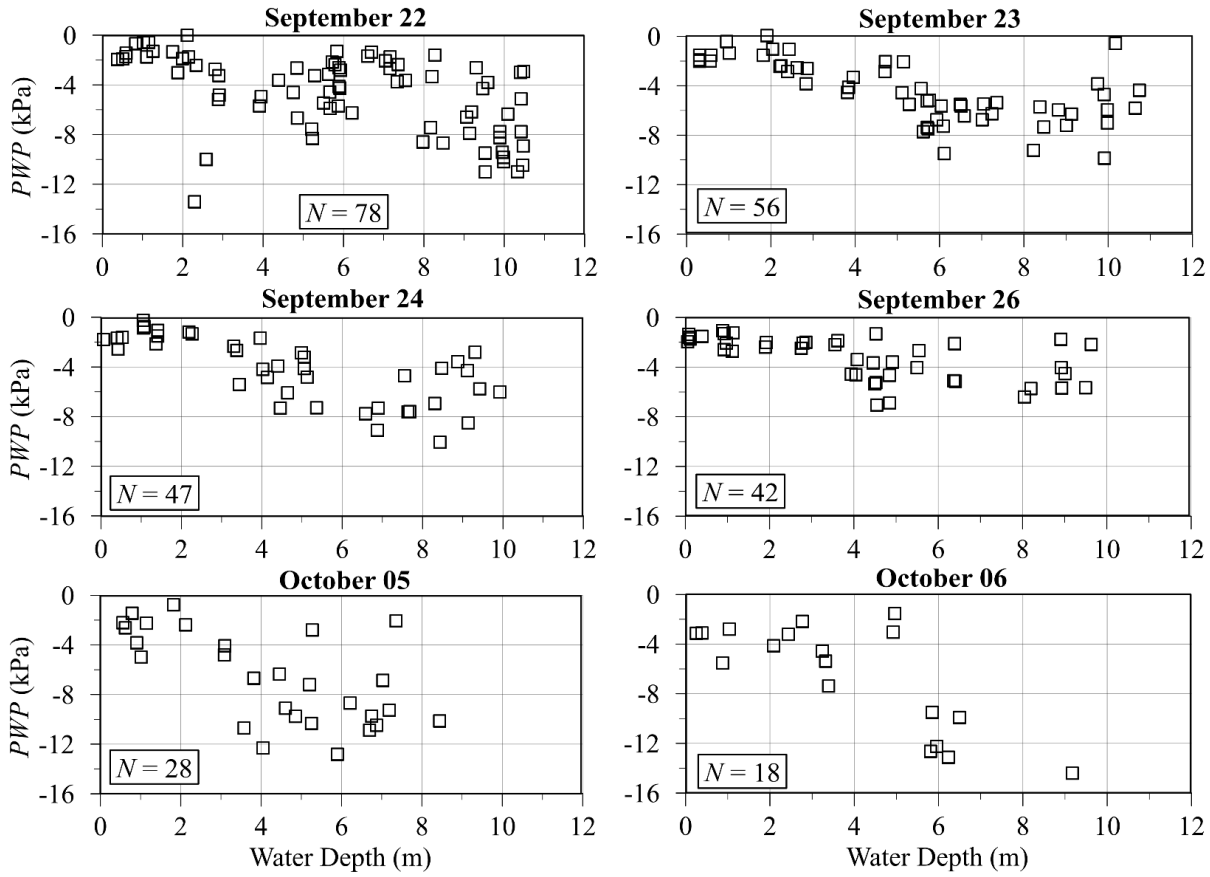

Figure 6.9. The measure pore water pressure *PWP* at maximum *qsbc* versus water depth for the deployments with penetration depths > 10 cm, with *N* being the number of deployments that achieved a penetration depth >10 cm.

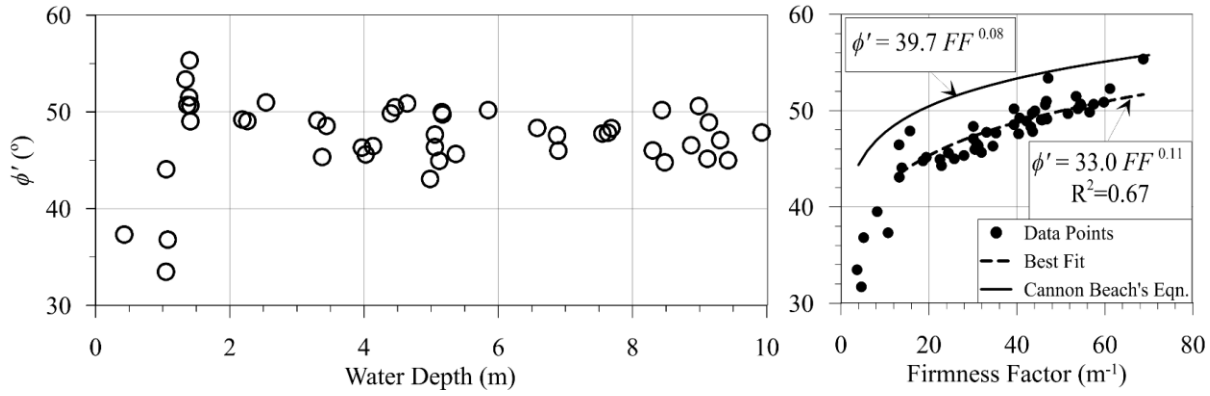

Figure 6.10. The left panel shows the estimated friction angle, ϕ', from the PFFP measurements for September 24 deployments. The right panel shows the relation between the Firmness Factor *FF* and ϕ' for Cannon Beach's sand, and for FRF beach sand considering only water depths >*DoD*.

larger than the values determined using Durgunoglu and Mitchell (1973) theory by values ranged between 0º-11º (Figure 6.10). The difference was more significant in water depths shallower than the *DoD* (Figure 6.10). Because Albatal et al. (n.d.) correlation was derived based on PFFP deployments in water depths larger than the 3 m and for uniform sand, it is more reasonable to compare only the deployments in close conditions. Accordingly, a new correlation was developed based on water depths larger than the *DoD* for FRF beach's sand. Here, the Firmness Factor was correlated to the sand friction angle determined using $\phi'=33.0\ FF^{0.11}$ (Figure 6.10). Using this equation, the friction angle determined using Albatal et al. (n.d.) correlation was greater by 2.3º-3.4º with an average of 2.8º and standard deviation of 0.3º.

6.5.3 Coefficient of wave impact on sediment surface strength CWS

The *CWS* was determined after Bilici et al. (2018) and using the two modified expressions (i.e. Equations 6.2 and 6.3). Using Bilici et al. (2018) formula, the *CWS* was small (0.01-0.375) in deep water depths, increased slightly with shallower water depths, and then peaked in the shallow water regions (Figure 6.11). The highest scatter was found in the shallowest water depths. Accordingly, three segments were considered to describe the *CWS* behavior: shallow zone, intermediate zone, and deep zone. These zones are not compatible with the known shallow, intermediate and deep waters but are introduced here to describe the *CWS* behavior. For September 22-26, the shallow zone limit was found at water depths between 2-2.5 m with average *CWS* values ranged between 1.5-2.9 and standard deviation of 1.6-5.2 while the deep zone limit was found at a water depth of ~5 m with average *CWS* values of 0.04-0.11 (Table 6.2; Figure 6.11). For October 5 and 6, the shallow zone limits were at water depths of 3.5 and 6 m while the deep water limits were at water depths of 7 and 8, respectively. The *CWS* zones limits and values are summarized in Table 2.

The significant wave heights and bottom orbital velocities were determined at each deployment locations using SWAN one-dimensional modeling (Figure 6.12). For September 22-26, the waves started to break at water depths between 1.5-2.5 m, while on October 5-6 the waves broke at a water depth of ~5.8 m. The bottom orbital velocity varied with water depth, and achieved its maximum in the breaking zone. For September 22-26, the maximum bottom orbital velocity varied between 0.9-1.1 m/s at water depths between 0.7-1.5 m, while for October 5-6 the maximum bottom orbital velocity was 1.1 m/s at a water depth of 2.2 m.

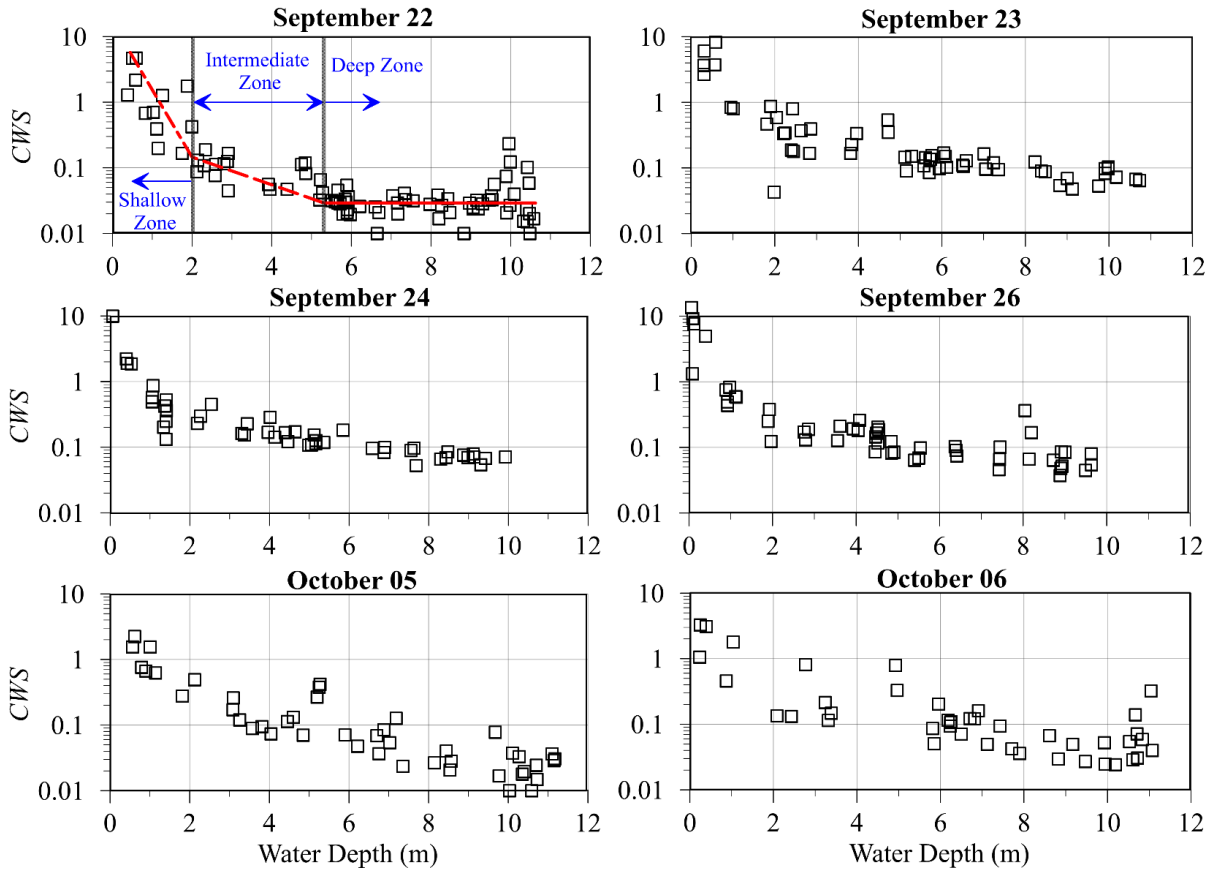

Figure 6.11. The coefficient of wave impact on sediment surface strength *CWS* versus water depth for all the deployments using Bilici et al. (2018) equation. The results on September 22 show the three suggested zones based to the *CWS* trend.

The obtained bottom orbital velocities were used to calculate CWS_{u2} using Equation 6.2. Here, CWS_{u2} exhibited a similar trend to the results using Bilici et al. (2018) equation. For September 22-26, the shallow zone limit was found at water depths larger than 2-2.5 m, while the deep zone limit was found at a water depth between 5-6 m (Table 6.2; Figure 6.13). On October 5 and 6, the shallow zone limits were at water depths of 3.5 and 6 m, while the deep water limits matched water depths of 7 and 8, respectively. The *CWS* determined considering the wave celerity (i.e. Equation 6.3) had a general trend that also agrees with the other *CWS* formulations. The shallow and deep zone limits were in agreement with observed values using the Equations 6.1 and 6.2 except for September 26 where the deep zone limit decreased from 5 to 4 m (Table 6.2; Figure 6.14). Although the determined limits using the different equations were mostly the same, the transition from the intermediate to shallow zone was less pronounced using CWS_{u2} than the other equations.

Table 6.2. Summary of the *CWS* results using the different *CWS* formulas

Date			22 Sept.	23 Sept.	24 Sept.	26 Sept.	05 Oct.	06 Oct.
CWS	SZ*	Max. Limit (m)	2	2.5	2.5	2	3.5	6
		$\overline{CWS}$	1.54	1.83	2.37	2.87	0.79	0.79
		σ	1.59	2.43	5.16	4.28	0.69	1.05
	IZ†	$\overline{CWS}$	0.10	0.22	0.18	0.16	0.16	0.09
		σ	0.04	0.15	0.05	0.05	0.13	0.04
	DZ§	Min. Limit (m)	5	5	5	5	7	8
		$\overline{CWS}$	0.04	0.11	0.09	0.09	0.04	0.07
		σ	0.03	0.03	0.03	0.07	0.03	0.08
CWS_u	SZ*	Max. Limit (m)	2	2.5	2.5	2	3.5	6
		$\overline{CWS}$ ($\times 10^{-3}$)	31.16	40.16	7.18	10.13	20.0	19.04
		σ ($\times 10^{-3}$)	27.28	13.3	4.34	9.15	12.83	17.97
	IZ†	$\overline{CWS}$ ($\times 10^{-3}$)	4.74	8.66	2.31	2.16	12.19	6.86
		σ ($\times 10^{-3}$)	2.60	3.56	0.75	0.67	10.96	2.85
	DZ§	Min. Limit (m)	5	5	6	5	7	8
		$\overline{CWS}$ ($\times 10^{-3}$)	1.04	1.5	0.93	1.00	3.08	4.25
		σ ($\times 10^{-3}$)	0.80	0.61	0.24	0.79	2.49	4.88
CWS_C	SZ*	Max. Limit (m)	2	2.5	2.5	2	3.5	6
		$\overline{CWS}$ ($\times 10^{-3}$ s^{-1})	127.42	54.33	46.36	89.10	51.87	38.84
		σ ($\times 10^{-3}$ s^{-1})	115.64	57.39	48.95	110.01	41.58	37.55
	IZ†	$\overline{CWS}$ ($\times 10^{-3}$ s^{-1})	16.18	18.22	11.92	14.28	20.61	9.96
		σ ($\times 10^{-3}$ s^{-1})	6.18	8.10	3.29	4.49	18.35	4.01
	DZ§	Min. Limit (m)	5	5	4	5	7	8
		$\overline{CWS}$ ($\times 10^{-3}$ s^{-1})	7.93	8.02	7.77	10.86	6.23	8.73
		σ ($\times 10^{-3}$ s^{-1})	7.66	2.08	1.22	8.60	4.26	9.97

*Shallow Zone, †Intermediate Zone, § Deep Zone

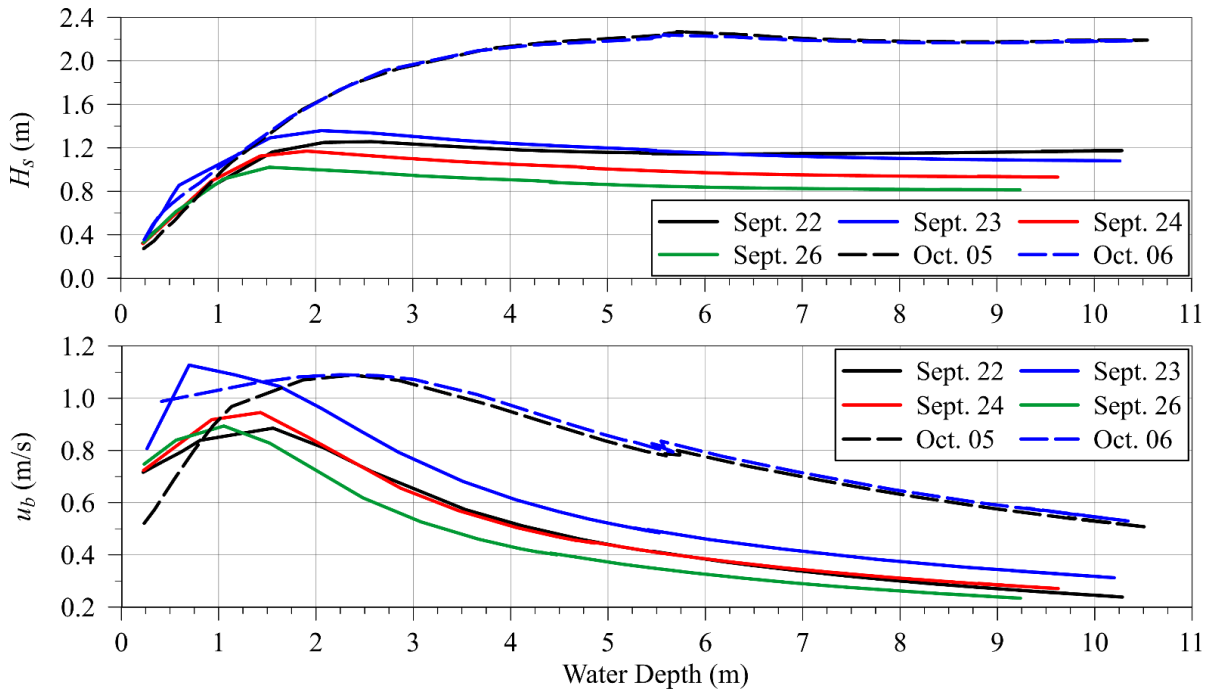

Figure 6.12. The variation of the significant wave height H_s and bottom orbital velocity u_b with water depth obtained using SWAN model.

6.6 Discussion

The results showed that there are spatial variations in surficial sediment strength, represented by the *qsbc*, along the profile. This is in line with the observations by Albatal et al. (2017) from the same location who conducted PFFPs deployments in the north and south sides of the pier (distance >400 m from the FRF pier). More specifically, Albatal et al. (2017) found that the *qsbc* decreased with an increase in water depth and the associated decrease in grain size distribution. Here, in addition to changes in sediment strength, changes in pore water pressure response correlated to changes in grain size (Figure 6.9). The pore water pressure behavior during penetration in sandy sediments can vary from partially drained to fully undrained during the PFFP penetration (Lucking et al. 2017). With smaller grain sizes and a lower permeability, the diffusion or dissipation of the generated excess pore pressures during the probe penetration slows down (e.g., Cedergren 1997). Additionally, finer sands usually pack denser, and denser sands promote a more dilative behavior that is known to result in negative pore pressure (e.g., Lambe and Whitman 1969). The results of this study reflect this clearly by exhibiting and sustaining larger negative excess pore pressures with decreasing sand size at increasing water depths (Figure 6.9).

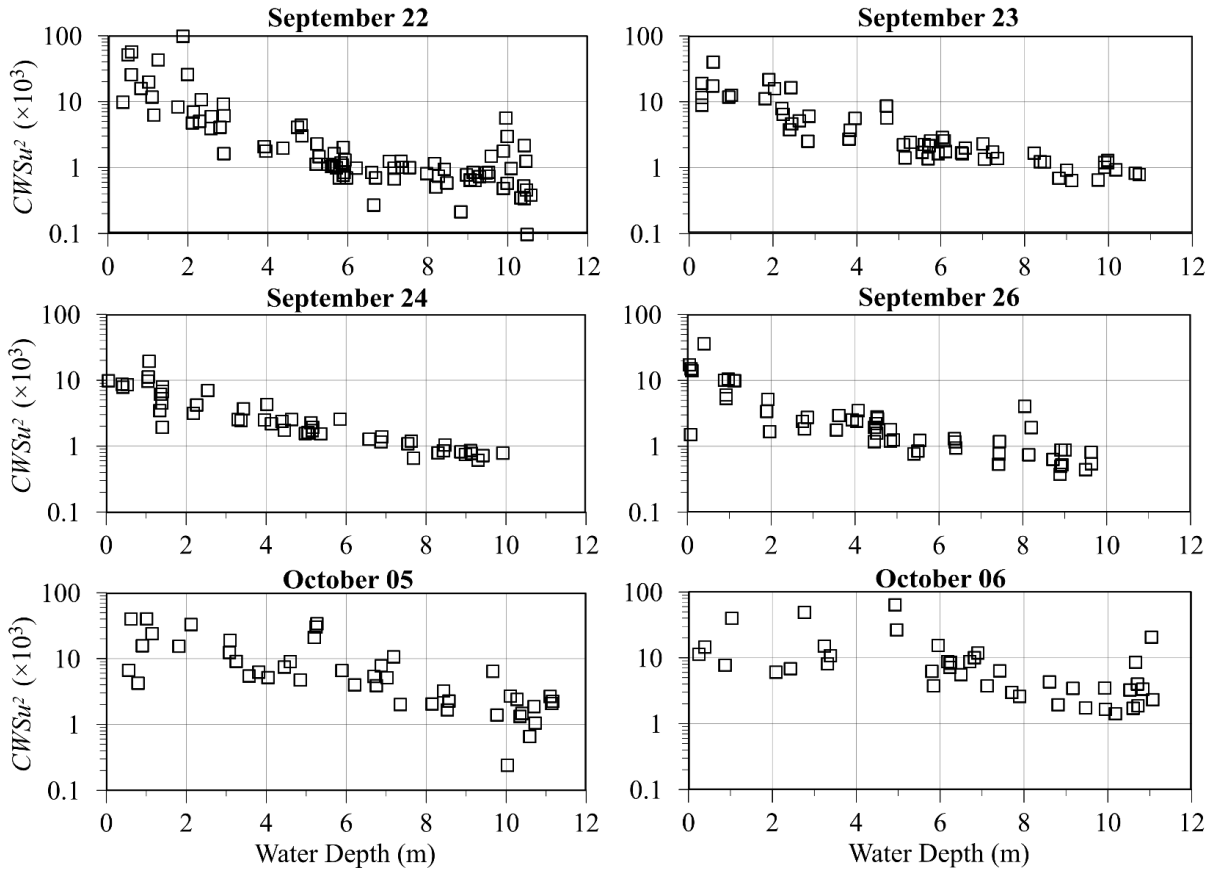

Figure 6.13. CWS_{u^2} versus water depth for all the deployments.

Albatal et al. (2017) also noticed that the presence of large-scale and small-scale morphological features in shallow water depths result in a large scatter in the *qsbc* and observed that the scatter becomes minimum at distances of 600-650 m from the baseline. This explains the observed scatter in the *qsbc* here, because the deployments here covered only a distance of up to ~600 m from the baseline limited by the pier length. Scour around the pier foundations likely caused an additional complexity in the seabed morphology. Albatal et al. (2017) found the lowest sediment strength and *qsbc* onshore of the shore parallel bar and associated that to the presence of freshly deposited sediments in this location. Here, it was found that this behavior could also be resulting from the instantaneous disturbance of the seabed sediments by wave action, and particularly breaking waves (Figure 6.7). Overall, two main factors appeared to control surficial sediment strength: sediment properties such as grain size distribution, and local wave conditions. More specifically, grain size distribution governed the trends in surficial sediment strength outside of the shallow water depth

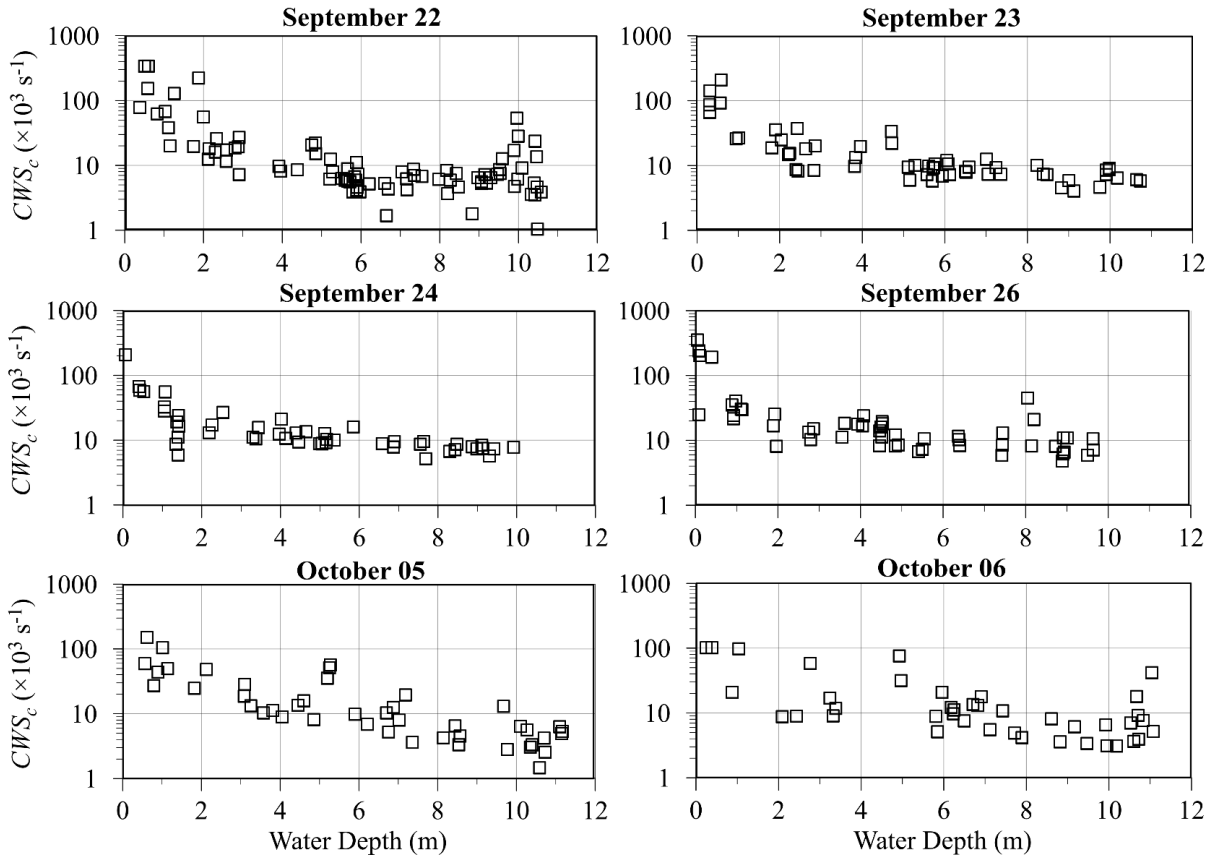

Figure 6.14. CWS_c versus water depth for all the deployments.

region, and the wave energy dominates the trends in surficial sediment strength within the shallow water region (Figures 6.7 and 6.8).

During the low energy wave period, the *qsbc* was maximum at a distance of <50 m from the shoreline with a maximum *qsbc* values reached up to 136 kPa while during the storm the *qsbc* was significantly lower (<80 kPa) at the same location (Figure 6.8). The lowest *qsbc* values along the profile were observed in the wave breaking zone. This can be explained by the associated reworking processes for the surficial sediments in this area where large bed shear stresses are generated due to the turbulence created by the wave breaking (Nielsen et al. 2012; Bilici et al. 2018). An additional possible reason is that the wave breaking washed out the fine particles leaving coarse, well-rounded, and sorted sediments (Gallagher et al. 2016), leading to a relatively low sediment strength in the wave breaking area. An exception was found at Station 27 (smallest water depth, h<0.7 m). Here, a large *qsbc* was recorded on September 22, October 5 and 6 (Figure 6.8). Nielsen (2012) explained the presence of relatively strong sediments onshore of the breaking zone

by the dissipation of the wave energy due to the wave breaking, and therefore, less bed shear stress and disturbance of sediments further onshore.

A thick loose sediment top layer (up to 27 cm) was found at 120-140 m from the baseline (i.e. Stations 22-24) on September 22 (Figure 6.2). Bilici et al. (2018) explained the presence of this top layer by recent depositions in the framework of offshore sediment transport during the storm. Accordingly, it can be assumed that the removal of this layer in the following days is due to the onshore sediment transport, and especially because of an outer bar might have formed by storms in this area. The outer bar is considered unstable and short-termed (usually less than 2 days according to Lippmann and Holman 1990). The above mentioned top layer was not observed during the storm on October 5 and 6. A possible reason is sediment transport as a suspended load during the storm, and that the ongoing high wave action was preventing sediment deposition at this time of the storm event. This is supported by the observation of large sand transport rate by suspension during storms in the pier surrounding area (Payo et al. 2009).

Generally, sediment transport appeared to be reflected in temporal variations in sediment penetration resistance. Few hours after the storm started on October 5, the *qsbc* values were the lowest along the profile (Figure 6.5). Although the storm persisted, a relatively large *qsbc* was observed on October 6. The increase in the sediment strength on October 6 might have been resulting from the erosion of the top sediments, leaving behind a more solid surface (Stark and Kopf 2011). An evidence is the difference in the seabed elevation obtained from the measured water depth on October 6 compared to October 5 (Figure 6.15). While a negligible difference in the seabed elevation was observed on September 22-26, a more significant difference was observed between October 5 and 6, which reached a maximum value of ~1.5 m at a distance of ~190 m from the baseline. The observed variations in seabed elevation, and thus, the possible erosion, was more significant at a distance of less than 200 m from the baseline, equaling water depths < 6.0 m. This matches the area where longshore bars are formed, migrate, and are erased again under storm conditions (Larson and Kraus 1992, 1994; Thornton et al. 1996; Gallagher et al. 1998; Elgar et al. 2001a). It should be noted here that the observed erosion almost stretched over the entire profile, which means that the sediments were carried out offshore and beyond the investigated region, or that there was significant longshore sediment transport. The latter is more likely since the wave approach angle was on average 53.4º (Northeast) on October 06.

The in-situ friction angles estimated for FRF's sand are in general less than the suggested values based on the correlation developed by Albatal et al. (n.d.) for Cannon Beach's uniform sand. Many factors can cause this inconsistency like differences in the sediment material properties and penetration depth, the presence of fines, differences in the particle size, water depths and seabed morphology. An important factor is the strain rate effect, which depends on the soil properties like density, permeability, mineralogy and particles shape (True 1976). Another important factor is the effect of the penetration depth where the friction angle depends on the confining pressure, which in turn increases with the penetration depth. This is taken into consideration when determining the friction angle using Durgunoglu and Mitchell's (1973) theory but not considered when using the empirical equation. The average penetration depth for September 24 deployments was larger than the average penetration depth achieved in Cannon Beach by 13%, which is another indication of a larger strength sand in Cannon Beach. Accordingly, using a strain rate factor empirical coefficient of K=0.4 might not be appropriate here and a conclusion on the most appropriate K value for FRF beach's sand cannot be drawn based on the PFFP results alone. For the deployments in shallower

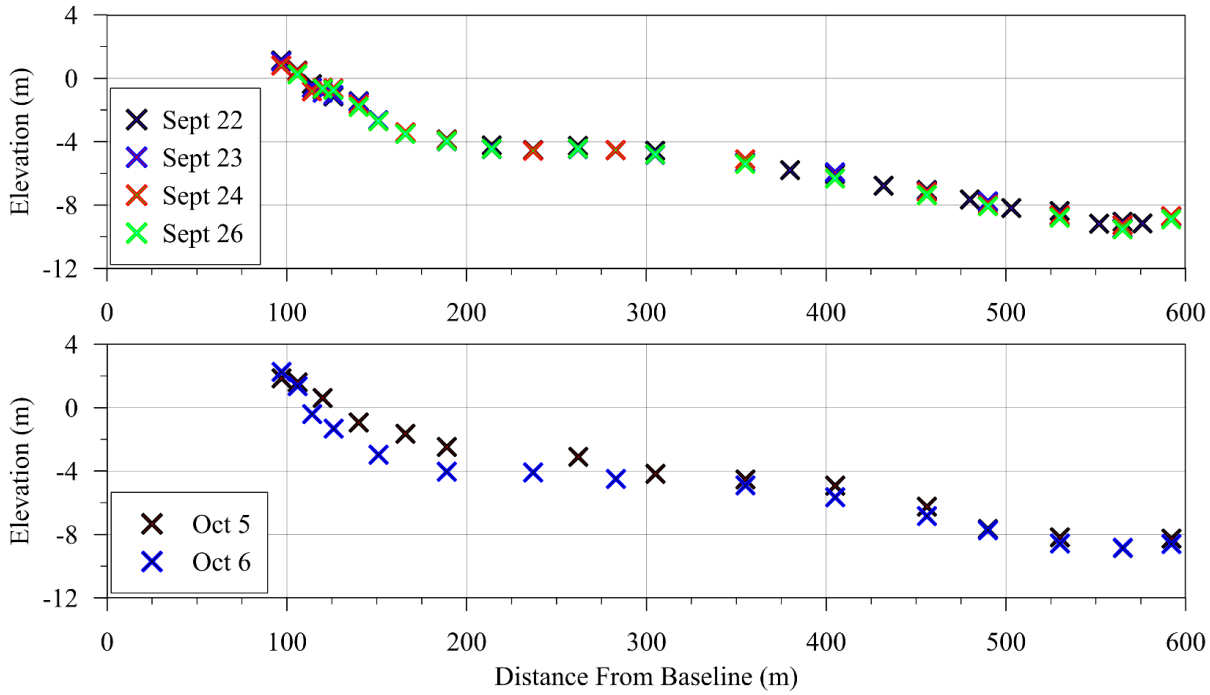

Figure 6.15. The elevation at each deployment location obtained from the measured water depth by the PFFP *BlueDrop*.

water depths than the *DoD*, the additional differences in the friction angles are due to the decrease in the shear strength affected by the wave action that discussed earlier.

A number of correlations to classify the sediment and to assess the sediment geotechnical characteristics such as shear strength utilizing PFFP results exist. However, these classification schemes only consider field tests under non-energetic conditions (Stoll et al. 2007; Mulukutla et al. 2011; Albatal and Stark 2017), questioning their reliability in energetic environments. For example, many of the deployments in the breaking zone are classified as silts or even clay using these classification schemes (maximum decelerations $<20g$ and Firmness Factor <10 m^{-1}), however, the sieve analyses for the collected samples from these locations showed that the sediments are classified as sand with 0% fines content. This illustrates the necessity of adopting a novel method to characterize the sediments based on PFFP measurements that consider the impact of nearshore wave dynamics. The *CWS* takes into consideration the sediment disturbance by the wave action, and may assist the characterization of sediments under energetic wave forcing.

For the same water depth and the same wave conditions, an increase in *CWS* can result from one of two reasons: First, there is a thick loose top layer on top of a larger resistance stable layer. Second, the strength of the top layer is approaching the strength of the stable substratum. The latter is more often associated to a weaker substratum than by a stronger top layer what would reflect a deeper sediment loosening. In both cases, this is an indication of a presence of low resistance sediment layers that might be susceptible to erosion or might offer a low sediment strength for different engineering applications. As shown in Figures 6.11, 6.13 and 6.14, *CWS* for September 22-26 starts to increase at a water depth of ~5 m. During the storm on October 5-6, this was the most wave-affected region (Figure 6.7 and 6.8). In water depths larger than the deep zone limit, *CWS* varied little (Figures 6.11, 6.13, 6.14). An exception was observed at on September 22 and October 6 at water depths between 10-11 m, which might be resulting presence of fines as found in the sediment samples collected from this location (Figure 6.6).

Bilici et al. (2018) found that the *CWS* reflects the sediment transport history and that it becomes maximum in the breaking zone. In this study, the shallow zone limit indeed coincided with the breaker zone for all three formulations of the *CWS*. An exception represented the dataset from October 05 when the shallow zone limit equaled a water depth of 3.5 m while wave breaking was hindcasted at a water depth of ~5.8 m for this day. The mismatch here can be associated to a timing

discrepancy between the penetrometer survey and increasing storm condition during the day, i.e., the penetrometer survey was performed at the early beginning of the wave event. Bilici et al. (2018) also described that the "deep zone limit" coincided with the Depths of Closure *DoC*, which is the minimum water depth at which no significant morphological changes occur (Hallermeier 1978; Birkemeier 1985). Albatal et al. (2017) also suggested that the *DoC* affected the variability in the *qsbc*. Here, the deep water limit was within <1 m difference with the observed *DoC* in similar storms by Nicholls et al. (1998). This is given that the change in the morphology near the pier is in agreement with the change far from the pier.

The general behavior of the *CWS* remained the same regardless of the wave parameter used in the denominator. Attempts were made using the deep water wavelength, significant wave height, wave celerity, and bottom orbital velocity. While the significant wave height decreases after the waves break, CWS_{u^2} and CWS_c are still achieving a maximum at the shallowest water depths. This suggests that the *CWS* is dominated by the sediment behavior and stratification rather than by local wave conditions only. Similarly, Lippmann and Holman (1990) noticed that the different wave parameters behave similarly when studied the spatial and temporal variability of sand bar morphology for the same area (i.e. FRF beach). They used significant wave height, incident wave power, offshore wave steepness, the wave part of the Iribarren surf similarity number, or the wave part of the dimensionless fall velocity parameter. Two-dimensional numerical modeling of the hydrodynamic conditions seems beneficial for considering the pier effect on the wave characteristics, which might be significant due to wave diffraction and wave-induced circulation (Elgar et al. 2001b). It is also planned to investigate the application of *CWS* in a wider time range and in other locations.

6.7 Conclusions

A portable free fall penetrometer PFFP was used to characterize the topmost sediment layers. The PFFP was deployed 335 times in six non-consecutive in September and October 2016. The deployments covered the area from the swash zone to about 11 m water depth. The wave climate varied from calm to stormy with the significant wave heights varied between 0.8-2.4 m measured at a water depth of 17.4 m. The sediments were characterized using estimates of quasi-static

bearing capacity (*qsbc*) and the coefficient of wave impact on sediment surface strength (*CWS*). The following conclusions can be drawn:

1. Two main factors control the surficial sediment strength in the sandy nearshore zone in Duck, North Carolina: the wave impact on the seabed and the variation in the sediment grain size distribution. The wave energy governed the trend in the shallow water depths region while the grain size dominates the behavior in deeper water depths.
2. At the beginning of the storm, sediment mobilization resulted in low sediment strength.
3. As the storm continued, significant erosion led to relatively hard surface sediments.
4. Negative pore water pressures during penetrometer sediment penetration became more pronounced with increasing water depth due to a decrease in particle size and the associated more dilative and less permeable sand.
5. The friction angle of sand variation follows the *qsbc* trend, and the correlation between the friction angle and firmness factor seems to be sediment type dependent.
6. The *CWS* reflected both the wave breaking and depth of closure.
7. Different input wave characteristic including the bottom orbital velocity and wave celerity in addition to the equation suggested by Bilici (2018) led to similar trends, highlighting its sensitivity to sediment properties and stratification.

The findings of this research are promising especially the use of the coefficient of wave impact on sediment surface strength *CWS* that allows using in-situ test results to predict the susceptibility of the seabed sediment for erosion. Using the PFFP measurement here allows overcoming the limitations of determining the sediment characteristics for the prediction models. However, this study represented the first attempt to use this factor and more testing in this area and other areas is planned in the future.

6.8 Acknowledgments

The authors acknowledge funding from the Office of Naval Research through award N00014-16-1-2590, and the National Science Foundation through award OCE-1434938. The authors would like to thank the Dillon Braud and the staff of the USACE Field Research Facility for on-site assistance. The authors also appreciate the recommendations by Robert Weiss (Department of Geosciences, Virginia Tech).

6.9 References

Albatal, A., McNinch, J.E., Wadman, H., and Stark, N. 2017. In-situ geotechnical investigation of nearshore sediments with regard to cross-shore morphodynamics. In Geotechnical Frontiers. ASCE. pp. 398–408. doi:10.1061/9780784480472.042.

Albatal, A., and Stark, N. 2016. In Situ Geotechnical Early Site Assessment of a Proposed Wave Energy Converter Site in Yakutat, Alaska, Using a Portable Free-Fall Penetrometer. In Geo-Chicago 2016. Chicago, IL. pp. 429–438. doi:10.1061/9780784480137.041.

Albatal, A., and Stark, N. 2017. Rapid sediment mapping and in situ geotechnical characterization in challenging aquatic areas. Limnology and Oceanography: Methods, 15(8). doi:10.1002/lom3.10192.

Albatal, A., Stark, N., and Castellanos, B. n.d.. Estimating in-situ friction angles of nearshore sand from free fall penetrometer tests. Canadian Geotechnical Journal (In review).

Aubeny, C.P., and Shi, H. 2006. Interpretation of Impact Penetration Measurements in Soft Clays. Journal of Geotechnical and Geoenvironmental Engineering, 132(6): 770–777. doi:10.1061/(ASCE)1090-0241(2006)132:6(770).

Bilici, C., Stark, N., Albatal, A., Wadman, H., and McNinch, J.E. 2018. Quantifying the effect of wave action on the seabed surface sediment strength using a portable free fall penetrometer. In 4th International Symposium on Cone Penetration Testing, CPT'18. ISSMGE, Delft, Netherlands.

Birkemeier, W.A. 1985. Field data on seaward limit of profile change. Journal of Waterway, Port, Coastal, and Ocean Engineering, 111(3): 598–602. doi:10.1061/(ASCE)0733-950X(1985)111:3(598).

Birkemeier, W.A., DeWall, A.E., Gorbics, C.S., and Miller, H.C. 1981. A User's Guide to CERC's Research Field Research Facility. Fort Belvoir, Va.

Booij, N., Ris, R.C., and Holthuijsen, L.H. 1999. A third-generation wave model for coastal regions: 1. Model description and validation. Journal of Geophysical Research: Oceans, 104(C4): 7649–7666. doi:10.1029/98JC02622.

Cedergren, H.R. 1997. Seepage, drainage, and flow nets. John Wiley & Sons.

Chow, S. h., and Airey, D. w. 2013. Soil strength characterisation using free-falling penetrometers. Géotechnique, 63(13): 1131–1143. doi:10.1680/geot.12.P.129.

Chow, S.H., O'Loughlin, C.D., White, D.J., and Randolph, M.F. 2017. An extended interpretation of the free-fall piezocone test in clay. Géotechnique,: 1–14. doi:10.1680/jgeot.16.P.220.

Danson, E. 2005. Geotechnical and geophysical investigations for offshore and nearshore developments. In Technical Committee 1, International Society for Soil Mechanics and Geotechnical Engineering ISSMGE.

Dayal, U., and Allen, J.H. 1973. Instrumented Impact Cone Penetrometer. Canadian Geotechnical Journal, 10(3): 397–409. doi:10.1139/t73-034.

Duncan, J.M., Wright, S.G., and Brandon, T.L. 2014. Soil strength and slope stability. John Wiley & Sons, Hoboken, NJ.

Durgunoglu, H.T., and Mitchell, J.K. 1973. Static penetration resistance of soils. Research report number NASA-CR-133460, prepared for NASA Headquarters, Washington, D.C. Available from https://ntrs.nasa.gov/search.jsp?R=19730019713.

Elgar, S., Gallagher, E.L., and Guza, R.T. 2001a. Nearshore sandbar migration. Journal of Geophysical Research: Oceans, 106(C6): 11623–11627. doi:10.1029/2000JC000389.

Elgar, S., Guza, R.T., O'Reilly, W.C., Raubenheimer, B., and Herbers, T.H.C. 2001b. Wave Energy and Direction Observed near a Pier. Journal of Waterway, Port, Coastal, and Ocean Engineering, 127(1): 2–6. American Society of Civil Engineers. doi:10.1061/(ASCE)0733-950X(2001)127:1(2).

Fernández-Mora, A., Calvete, D., Falqués, A., and de Swart, H.E. 2015. Onshore sandbar migration in the surf zone: New insights into the wave-induced sediment transport mechanisms. Geophysical Research Letters, 42(8): 2869–2877. doi:10.1002/2014GL063004.

Gallagher, E., Wadman, H., McNinch, J., Reniers, A., and Koktas, M. 2016. A Conceptual Model for Spatial Grain Size Variability on the Surface of and within Beaches. Journal of Marine Science and Engineering, 4(2): 1–17. doi:10.3390/jmse4020038.

Gallagher, E.L., Elgar, S., and Guza, R.T. 1998. Observations of sand bar evolution on a natural beach. Journal of Geophysical Research: Oceans, 103(C2): 3203–3215. doi:10.1029/97JC02765.

Hallermeier, R.J. 1978. Uses for a calculated limit depth to beach erosion. In Coastal Engineering Proceedings; No 16 (1978): Proceedings of 16th Conference on Coastal Engineering. Hamburg, Germany. pp. 1493–1512. doi:10.9753/icce.v16.%25p.

Hallermeier, R.J. 1980. Sand motion initiation by water waves: two asymptotes. Journal of the Waterway, Port, Coastal and Ocean Division, 106(3): 299–318.

Harris, C.K., and Wiberg, P. 2002. Across-shelf sediment transport: Interactions between suspended sediment and bed sediment. Journal of Geophysical Research: Oceans, 107(C1): 8–12. doi:10.1029/2000JC000634.

Harris, C.K., and Wiberg, P.L. 2001. A two-dimensional, time-dependent model of suspended sediment transport and bed reworking for continental shelves. Computers & Geosciences, 27(6): 675–690. doi:10.1016/S0098-3004(00)00122-9.

Hoefel, F., and Elgar, S. 2003. Wave-Induced Sediment Transport and Sandbar Migration. Science, 299(5614): 1885–1887. doi:10.1126/science.1081448.

Horrillo-Caraballo, J.M., and Reeve, D.E. 2008. An investigation of the link between beach morphology and wave climate at Duck, NC, USA. Journal of Flood Risk Management, 1(2): 110–122. Blackwell Publishing Ltd. doi:10.1111/j.1753-318X.2008.00013.x.

Howd, P.A., and Birkemeier, W.A. 1987. Beach and Nearshore Survey Data, 1981-1984, CERC Field Research Facility. US Army Engineer Waterways Experiment Station.

Hsu, T.-J., Elgar, S., and Guza, R.T. 2006. Wave-induced sediment transport and onshore sandbar migration. Coastal Engineering, 53(10): 817–824. doi:10.1016/j.coastaleng.2006.04.003.

Jonsson, I.G. 1966. Wave boundary layers and friction factors. In Proceedings of the 10th International Conference on Coastal Engineering. American Society of Civil Engineers. 127–148. pp. 127–148.

Lambe, T.W., and Whitman, R. V. 1969. Soil mechanics. John Wiley & Sons.

Larson, M., and Kraus, N.C. 1992. Analysis of cross-shore movement of natural longshore bars and material placed to create longshore bars. Coastal Engineering Research Center, Vicksburg, MS.

Larson, M., and Kraus, N.C. 1994. Temporal and spatial scales of beach profile change, Duck, North Carolina. Marine Geology, 117(1): 75–94. doi:10.1016/0025-3227(94)90007-8.

Lippmann, T.C., and Holman, R. a. 1990. The spatial and temporal variability of sand bar morphology. Journal of Geophysical Research, 95(C7): 11575. doi:10.1029/JC095iC07p11575.

Lucking, G., Stark, N., Lippmann, T., and Smyth, S. 2017. Variability of in situ sediment strength and pore pressure behavior of tidal estuary surface sediments. Geo-Marine Letters,: 1–16. doi:10.1007/s00367-017-0494-6.

Meyerhof, G.G. 1961. The ultimate bearing capacity of wedge-shaped foundations. In Proceedings of the 5th International Conference on Soil Mechanics and Foundation Engineering ICSMFE, Paris, 105–109.

Miller, H.C., Birkemeier, W.A., and DeWall, A.E. 1983. Effects of CERC Research Pier on Nearshore Processes. In Proceedings of the Coastal Structures ’83 Conference. ASCE. pp. 769–783.

Mulukutla, G.K., Huff, L.C., Melton, J.S., Baldwin, K.C., and Mayer, L.A. 2011. Sediment identification using free fall penetrometer acceleration-time histories. Marine Geophysical Research, 32(3): 397–411. doi:10.1007/s11001-011-9116-2.

Nicholls, R.J., Birkemeier, W.A., and Lee, G. 1998. Evaluation of depth of closure using data from Duck, NC, USA. Marine Geology, 148(3): 179–201. doi:10.1016/S0025-3227(98)00011-5.

Nielsen, A.W., Sumer, B.M., Ebbe, S.S., and Fredsøe, J. 2012. Experimental Study on the Scour around a Monopile in Breaking Waves. Journal of Waterway, Port, Coastal, and Ocean Engineering, 138(6): 501–506. American Society of Civil Engineers. doi:10.1061/(ASCE)WW.1943-5460.0000148.

Orlandini, S., and Rosso, R. 1996. Diffusion Wave Modeling of Distributed Catchment Dynamics. Journal of Hydrologic Engineering, 1(3): 103–113. American Society of Civil Engineers. doi:10.1061/(ASCE)1084-0699(1996)1:3(103).

Payo, A., Kobayashi, N., and Yamada, F. 2009. Suspended Sand Transport along Pier Depression. Journal of Waterway, Port, Coastal, and Ocean Engineering, 135(5): 245–249. American Society of Civil Engineers. doi:10.1061/(ASCE)0733-950X(2009)135:5(245).

Plant, N.G., Holman, R.A., Freilich, M.H., and Birkemeier, W.A. 1999. A simple model for interannual sandbar behavior. Journal of Geophysical Research: Oceans, 104(C7): 15755–15776. doi:10.1029/1999JC900112.

Sallenger, A.H., and Holman, R.A. 1985. Wave energy saturation on a natural beach of variable slope. Journal of Geophysical Research: Oceans, 90(C6): 11939–11944. doi:10.1029/JC090iC06p11939.

Schwartz, R.K., and Birkemeier, W.A. 2004. Sedimentology and morphodynamics of a barrier island shoreface related to engineering concerns, Outer Banks, NC, USA. Marine Geology, 211(3): 215–255. doi:10.1016/j.margeo.2004.05.020.

Seed, H.B., and Lundgren, R. 1954. Investigation of the effect of transient loading on the strength and deformation characteristics of saturated sands. In ASTM International. ASTM. pp. 1288–1306.

Stark, N., Hanff, H., Svenson, C., Ernstsen, V.B., Lefebvre, A., Winter, C., and Kopf, A. 2011. Coupled penetrometer, MBES and ADCP assessments of tidal variations in surface sediment layer characteristics along active subaqueous dunes, Danish Wadden Sea. Geo-Marine Letters, 31(4): 249–258. doi:10.1007/s00367-011-0230-6.

Stark, N., Hay, A.E., and Trowse, G. 2014. Cost-effective Geotechnical and Sedimentological Early Site Assessment for Ocean Renewable Energies. 2014 Oceans - St. John’s,: 1–8.

Stark, N., and Kopf, A. 2011. Detection and quantification of sediment remobilization processes using a dynamic penetrometer. In IEEE/MTS Oceans 2011. Waikoloa, HI. pp. 1–9.

Stark, N., Wilkens, R., Ernstsen, V.B., Lambers-Huesmann, M., Stegmann, S., and Kopf, A. 2012. Geotechnical Properties of Sandy Seafloors and the Consequences for Dynamic Penetrometer Interpretations: Quartz Sand Versus Carbonate Sand. Geotechnical and Geological Engineering, 30(1): 1–14. doi:10.1007/s10706-011-9444-7.

Stauble, D.K. 1992. Long-term profile and sediment morphodynamics: Field Research Facility case history. Report No. CERC-92-7. Coastal Engineering Research Center, Vicksburg, MS.

Steiner, A., Kopf, A.J., L'Heureux, J.-S., Kreiter, S., Stegmann, S., Haflidason, H., and Moerz, T. 2014. In situ dynamic piezocone penetrometer tests in natural clayey soils—a reappraisal of strain-rate corrections. Canadian Geotechnical Journal, 51(3): 272–288. doi:10.1139/cgj-2013-0048.

Stephan, S., Kaul, N., and Villinger, H. 2015. Validation of impact penetrometer data by cone penetration testing and shallow seismic data within the regional geology of the Southern North Sea. Geo-Marine Letters, 35(3): 203–219. doi:10.1007/s00367-015-0401-y.

Stoll, R.D., Sun, Y.F., and Bitte, I. 2007. Seafloor properties from penetrometer tests. IEEE Journal of Oceanic Engineering, 32(1): 57–63. doi:10.1109/JOE.2007.890943.

Thornton, E.B., Humiston, R.T., and Birkemeier, W. 1996. Bar/trough generation on a natural beach. Journal of Geophysical Research: Oceans, 101(C5): 12097–12110. doi:10.1029/96JC00209.

True, D.G. 1976. Undrained vertical penetration into ocean bottom soils. University of California, Berkeley.

Wang, W.L. 1971. Low velocity projectile penetration. Journal of Soil Mechanics and Foundations Division, ASCE, 97(SM 12): 1635–1655.

Wiberg, P.L., and Sherwood, C.R. 2008. Calculating wave-generated bottom orbital velocities from surface-wave parameters. Computers & Geosciences, 34(10): 1243–1262.

Chapter 7: Conclusions and Outlook

7.1 Conclusions

A detailed characterization of subaqueous sediments is essential to solve various problems in the coastal zone and marine environments (e.g., coastal erosion, marine slope stability, scour, and stability of nearshore and offshore structures). However, the use of well-developed and mature offshore site investigation tools (such as Cone Penetration Testing) can be prohibitively expensive especially for small projects, remote sites, and areas of difficult access. This results in a need for more cost-effective site investigation methods to characterize the subaqueous sediments in such regions. Portable Free fall penetrometers (PFFPs) are rapid and economical tools to assess topmost sediment characteristics. The basic idea is to estimate the soil resistance by measuring the deceleration of a soil impacting and penetrating probe. However, challenges are still facing PFFPs regarding data analysis and interpretation especially in sandy sediments. Moreover, to-date's research on the use of PFFPs in sandy areas is limited, in spite of the fact that sand represents the most common soil type on the continental shelves. For these reasons, the goal of this research was to advance the data analysis methods for PFFPs in unknown and/or sandy sediments, and more specifically, in energetic nearshore environments. The following paragraphs summarize how this was achieved through the performed research tasks within this dissertation.

7.1.1 Development of a methodology of creating a simple sediment classification scheme using PFFP measurements

Different soil classification schemes have been proposed based on PFFP measurements. These classification schemes use the measured decelerations produced by PFFPs or its derivatives. However, it was recognized that the measured decelerations of two different sediment types can be the same. For example, stiff, fine-grained soils can have a similar maximum deceleration to loose, coarse-grained soils. Accordingly, a sediment classification scheme based on PFFP measurements is needed that allows to distinguish between soils that may exhibit a similar maximum deceleration against the probe. Moreover, the existing systems were developed for specific sites or devices, which makes them nontransferable to another location or another device. Therefore, to take into account that the soil response varies based on the soil type and device

features, a methodology of creating a sediment classification scheme should be considered that includes validations using more than one criteria. Such a methodology will then be applicable in different locations and using different devices. Therefore, a methodology of creating a simple sediment classification scheme using PFFP measurements was proposed. This classification scheme can be easily transferred to different sites, or devices. A demonstration and proof of concept for the novel classification scheme was provided at a remote location in Alaska where little knowledge about local sediments was available, and sediments were expected to vary spatially. The results were used to fill some gaps in an existing sediment distribution map. The methodology utilizes different aspects including visual field observations, available sediment classification schemes in the literature, literature about the region, and the penetrometer measurements. It was also found that the pore water pressure results offer complementary insights into the in-situ sediment characteristics, especially the sedimentation history and presence of organics.

7.1.2 Investigation of the effect of wave forcing and geomorphodynamics on the surficial sediment strength

The interactions between wave processes and the seabed in the nearshore zone result in a dynamic seabed profile that varies on short and long-term time scales. The sediment remobilization and redeposition processes associated with the profile change influence the stability of the coastlines and nearshore structures in energetic areas. Moreover, the effects of sediment remobilization and redeposition processes on the geotechnical characteristics of the seabed surface are not fully understood, yet. To address this gap in knowledge, PFFP deployments were conducted in different wave environments in water depths up to 40 m, in the nearshore areas of Cannon Beach, AK, and the U.S. Army Corps of Engineers' Field Research Facility's beach, Duck, NC. The outcomes were utilized to examine the effect of wave breaking and storm conditions, sediment transport and bar migration, and depth of closure on the sediment resistance during the PFFP penetration. The results show that two main factors control the surficial sediment strength in sandy nearshore zones: the wave impact on the seabed and the variation in the sediment characteristics. The wave energy governed the trend in the shallow water depth region while the sediment characteristics dominate the behavior in deeper water depths. With regard to the storm effect, it was found that at the beginning of a storm, sediment mobilizations resulted in a low sediment strength while as the storm

continued the significant erosion resulted in relatively high strength surface sediments. The results also showed that there are usually variations and scatter in the sediment strength in the nearshore areas due to the variation in grain size and presence of large and small-scale morphological features. These variations become minimum at approximately the depth of closure (which is the minimum water depth at which the variations in the seabed morphology become minimum). These results advance our understanding of geotechnical soil behavior of surficial sediments under energetic hydrodynamic in-situ conditions, and are relevant for societal issues such as coastal erosion, as well as the stability of infrastructure in coastal and nearshore areas.

7.1.3 Estimate in-situ relative density and friction angle of nearshore sand from portable free fall penetrometer tests

The few existing studies on sandy sediments using PFFPs commonly concluded by showing variations in the dynamic force or the derived equivalent cone resistance versus the penetrated depth. However, in order to use the PFFP results quantitatively in design, estimating design shear strength parameters is essential. More specifically, the friction angle is an important parameter for the analysis of many nearshore and offshore problems including: scour predictions, prediction of sediment transport and erosion, and estimating the bearing capacity and piles capacity. In order to estimate the shear strength of sand using PFFP measurements, two different approaches were used to estimate the nearshore sand friction angle and to validate the results. The first approach utilizes two different laboratory tests on samples prepared at different relative densities including: (i) deploying a PFFP to large sand samples, and (ii) vacuum triaxial tests. The second approach utilizes two bearing capacity methods by Durgunoglu and Mitchell (1973) and Meyerhof (1961), which were found to obtain good estimates of the friction angle from CPT tests. Using the two approaches allowed for testing the used strain rate factor in the analyses. It was found that implementing the commonly used strain rate factor coefficient in the literature for PFFP deployments resulted in underestimated friction angles by up to 5º. Hence, a strain rate correction factor that gives matching results between the two approaches was determined. The modified values agree with the literature on estimating the friction angle based on CPT tests. However, these findings are associated to uniform sand. More tests are needed to investigate the applicability for wider grain size distributions. Nevertheless, the results offer a first attempt and demonstration that estimates of in-situ relative density and friction angle of surficial nearshore sands can be derived

from measurements of a simple tool such as PFFPs. This may revolutionize early site investigation in areas of energetic hydrodynamic conditions, as well as in areas of challenging logistics.

7.2 Outlook

This dissertation represents initial efforts and ideas to advance the limited use of PFFP in energetic sandy nearshore sediments. The results showed how valuable PFFP surveys can be for characterizing seabed sediments to provide a first estimate of the shearing parameters that are essential for designing any engineering structures. This illustrates how potentially the PFFP can be utilized to enable cost-effective nearshore geotechnical site investigations. However, while the results are promising and agree with the expected behavior of sandy sediments, more research is needed to confirm the validity of the adopted methods for different conditions, and to examine the assumptions used in this dissertation. The following recommendation are suggested for follow-on research:

1. Previous literature highlighted the possibility of using the pore pressure response during penetration and after the probe stops to extract additional information about the sediment's properties. In this study, it was demonstrated that the pore pressure behavior complements the strength measurements, and can be used for additional characterization of the sediments. While the pore pressure measurements here were used qualitatively, the results are promising for further research targeting the use of pore pressure measurements quantitatively to determine, for example, the soil permeability based on the pore pressure dissipation curve (e.g., Figure 2.11). The at-rest pore pressure response data used in this dissertation was over a period of only a few seconds. It is recommended to allow measurements over a longer period, especially in soft sediments where the pore pressure dissipation is expected to take hours.
2. The effect of storm conditions and associated sediment transport and bar migration on the sediment strength is clearly shown in this dissertation. However, the PFFP deployments covered only two days of investigations. The variations in the *qsbc* and coefficient of wave impact on sediment strength are in agreement with the expected behavior, but more investigations using a wider range of surveying periods and conditions, as well as from other sites are needed. Moreover, the coefficient of wave impact on sediment surface strength *CWS* seems to provide promising results for the prediction of the susceptibility of seabed sediment

to erosion, and for assessing the seabed trafficability. This hypothesis needs to be investigated more using a wider range of datasets and different locations.

3. Given the variability in the strain rate correction in the literature and within this dissertation, more investigation of the strain rate effect during the PFFP penetration into sandy sediments is suggested. This can be achieved through the use of calibration chamber tests and by comparing the achieved results to laboratory tests on controlled samples. Moreover, while it is common to use the same strain rate factor for the same soil, calibration chamber tests can consider different relative densities in order to investigate the variation in the strain rate with the change in the relative density. Such an effect can be significant given that the strain rate effect varies with the relative density as found by Seed and Lundgren (1954).

Appendix A: Data repository information

This appendix contains the information of the repository that contains the raw data and results of the analyses conducted in this research. All the datasets used in this dissertation are uploaded to Virginia Tech's data repository website (VTechData). The datasets can be accessed using the following link (https://doi.org/10.7294/W4VD6WMB). The data organization and content are illustrated in the readme file below, which is also associating the datasets.

A.1 Dataset Citation:

Ali Albatal (2018): Advancement of using portable free fall penetrometers in energetic sandy nearshore areas. University Libraries, Virginia Tech. https://doi.org/10.7294/W4VD6WMB

A.2 ReadMe File

This readme file was first created on 2018-03-01

TITLE OF DATASET

Advancement of using portable free fall penetrometers in energetic sandy nearshore areas

---

KEYWORDS

Free-fall penetrometer, nearshore site investigation, sediment classification, sand friction angle

---

INVESTIGATORS INFORMATION

Principal Investigator Contact Information
Name: Dr. Nina Stark
Institution: Virginia Polytechnic Institute and State University (Virginia Tech)
Address: 216 Patton Hall, 750 Drillfield Dr, Blacksburg, VA 24061
Email: ninas@vt.edu

Co-investigator Contact Information
Name: Ali Albatal
Institution: Virginia Polytechnic Institute and State University (Virginia Tech)

Address: 19 Patton Hall, 750 Drillfield Dr, Blacksburg, VA 24061
Email: ali2@vt.edu

SHARING/ACCESS INFORMATION

There are no restrictions on the datasets use and no license needed to use this datasets; however, proper citation is required when use this dataset.

GEOGRAPHIC LOCATION OF DATA COLLECTION

The data was collected from three locations

1. The U.S. Army Corps of Engineers Field Research Facility (FRF) Beach in Duck, North Carolina. The Facility Coordinates are: Latitude 36.182, Longitude -75.750
2. Cannon Beach near Yakutat City. Yakutat City Coordinates are: Latitude 59.5470, Longitude -139.7273
3. Yakutat Bay near Yakutat City. Yakutat City Coordinates are: Latitude 59.5470, Longitude -139.7273

FILES FORMAT AND CONTENT

- The data is divided as 3 main folder. Each folder contain the data belongs to one location from the three locations listed above.
- Inside each folder, there are two main subfolder. One folder contains the raw data extracted from the Free Fall Penetrometer while the other folder contains the data analysis final results.
- In the raw data subfolders, the raw data are grouped by the date of investigation. The raw data is mainly binary (.bin) files except the data collected on 2014-07-25 from Cannon Beach. For this day, the data is available as text files (.txt)
- In the data analysis subfolders, 3 file formats will be found: 1. Excel files that give a summary for the analysis results; 2. The results in a Matlab figures format (.fig); 3. The results in Tagged Image File Format (TIFF)
- The figures naming convention is DATE-FILE_NAME. Here, the DATE is in a form of Day Month Year while the FILE_NAME is in the form of bLogXXXX. The user can return to the data date and bLog number to reach the raw data file.

VARIABLE NAMES AND DESCRIPTION.

Since each dataset is associated to a different location and that some the parameters sought were different as well, the variables are different for each dataset. The user is advised to return

to the associated publications or the dissertation to know more details about the different variables.

The commonly used variables in all the analyses are:

1. Name: [Drop name]
   Description: the name of the raw data point. The figures naming convention is in DATE-FILE_NAME format.

2. Name: [Latitude]
   Description: The latitude of the data point (WGS84 Datum)

3. Name: [Longitude]
   Description: The longitude of the data point (WGS84 Datum)

4. Name: [Water depth (m)]
   Description: The water depth at which the device was deployed in meters

5. Name: [*qsbc* (kPa)]
   Description: The quasi-static bearing capacity determined following Stark et al. (2012) approach

6. Name: [PWP (kPa)]
   Description: The pore water pressure measured by the free fall penetrometer pressure sensor

---

METHODOLOGY

- While the outputs vary from location to another based on the sediment type and the parameters under investigation, the main data analysis was coducted following Stark et al. (2012) approach.
  Reference: Stark, N., Wilkens, R., Ernstsen, V. B., Lambers-Huesmann, M., Stegmann, S., and Kopf, A. (2012). “Geotechnical Properties of Sandy Seafloors and the Consequences for Dynamic Penetrometer Interpretations: Quartz Sand Versus Carbonate Sand.” Geotechnical and Geological Engineering, 30(1), 1–14.

EQUIPMENT AND SOFTWARE

- The raw data was collected using the free fall penetrometer *BlueDrop*.
- The data analysis was performed using Matlab (versions 8.5, 9.0 and 9.3).

ASSOCIATED ABSTRACTS/MANUSCRIPTS/ARTICLES.

- Albatal, A., and Stark, N. (2017). “Rapid sediment mapping and in-situ geotechnical characterization in challenging aquatic areas.” Limnology and Oceanography: Methods.
- Albatal, A., and Stark, N. (2016). “In situ geotechnical early site assessment of a proposed wave energy converter site in Yakutat, Alaska, using a portable free-fall penetrometer.” Geo-Chicago 2016, Chicago, IL, 429–438.
- Albatal, A., Stark, N., and Castellanos, B. (n.d.). “Estimating in-situ relative densities and friction angles of nearshore sand from free fall penetrometer tests.” Canadian Geotechnical Journal. (In review)
- Albatal, A., McNinch, J. E., Wadman, H., and Stark, N. (2017). “In-situ geotechnical investigation of nearshore sediments with regard to cross-shore morphodynamics.” Geotechnical Frontiers 2017, ASCE, 398-408.
- Albatal, A., Wadman, H., Stark, N., Bilici, C., and McNinch, J. E. (n.d.). “Investigation of spatial and short-term temporal nearshore sediment strength using portable free fall penetrometers”. (In Prep.)
- Bilici, C., Stark, N., Albatal, A. (2018) “Quantifying the effect of wave action on the seabed surface sediment strength using a portable free fall penetrometer” 4th International Symposium CPT’18 - Cone Penetration Testing.

Appendix B: Laboratory tests on Cannon Beach's sand

This Appendix contains a summary of the laboratory tests conducted on the samples collected from Cannon Beach, Yakutat, Alaska. Fifty-six samples were collected in total. Sieve analysis laboratory test were performed on all the samples. Afterward, Vacuum triaxial tests were performed on the samples from the lower intertidal zone. The laboratory test results are be summarized in the following figures and tables:

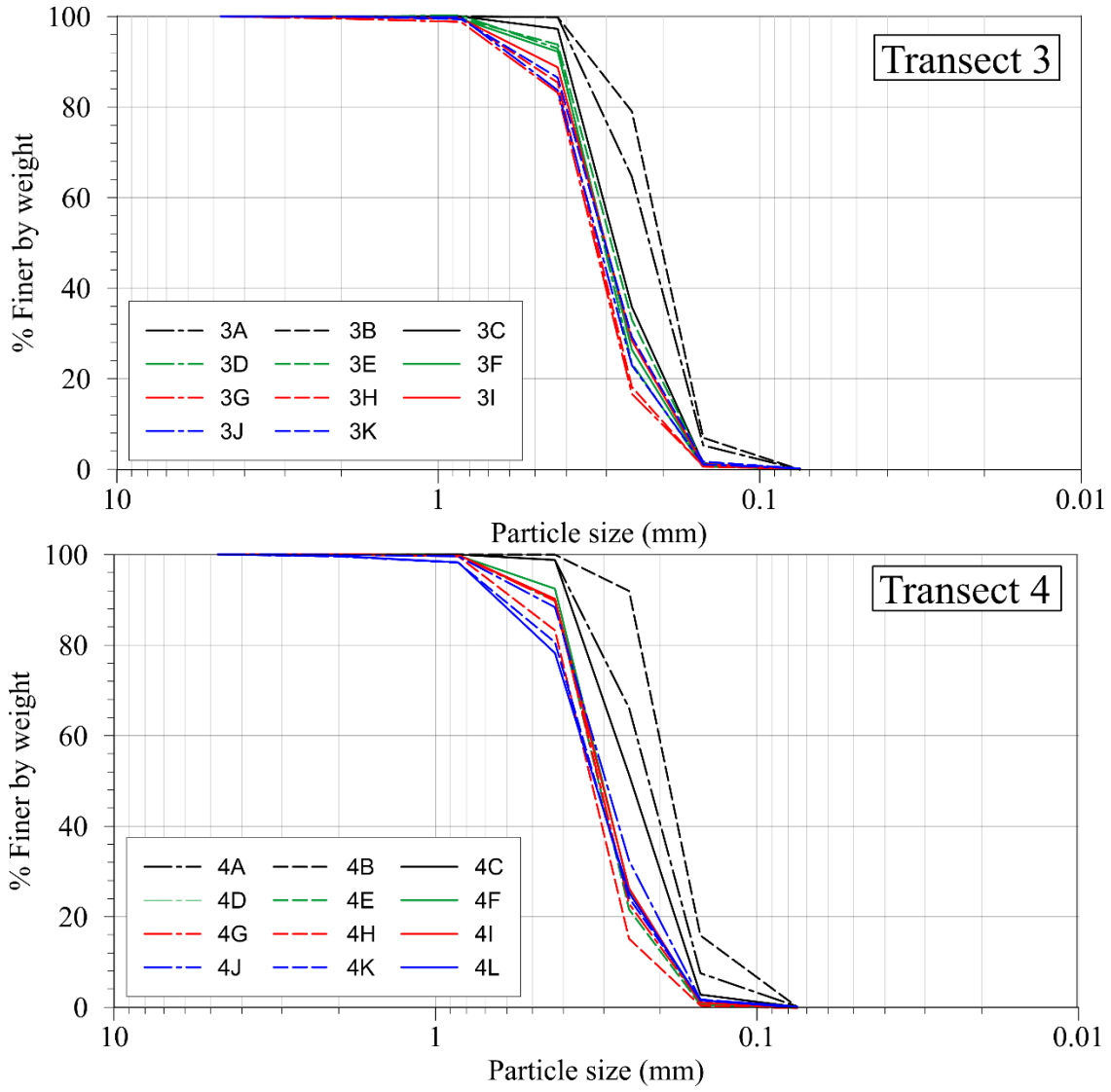

Figure B.1. The grain size distribution for the samples collected along Transects 3-4

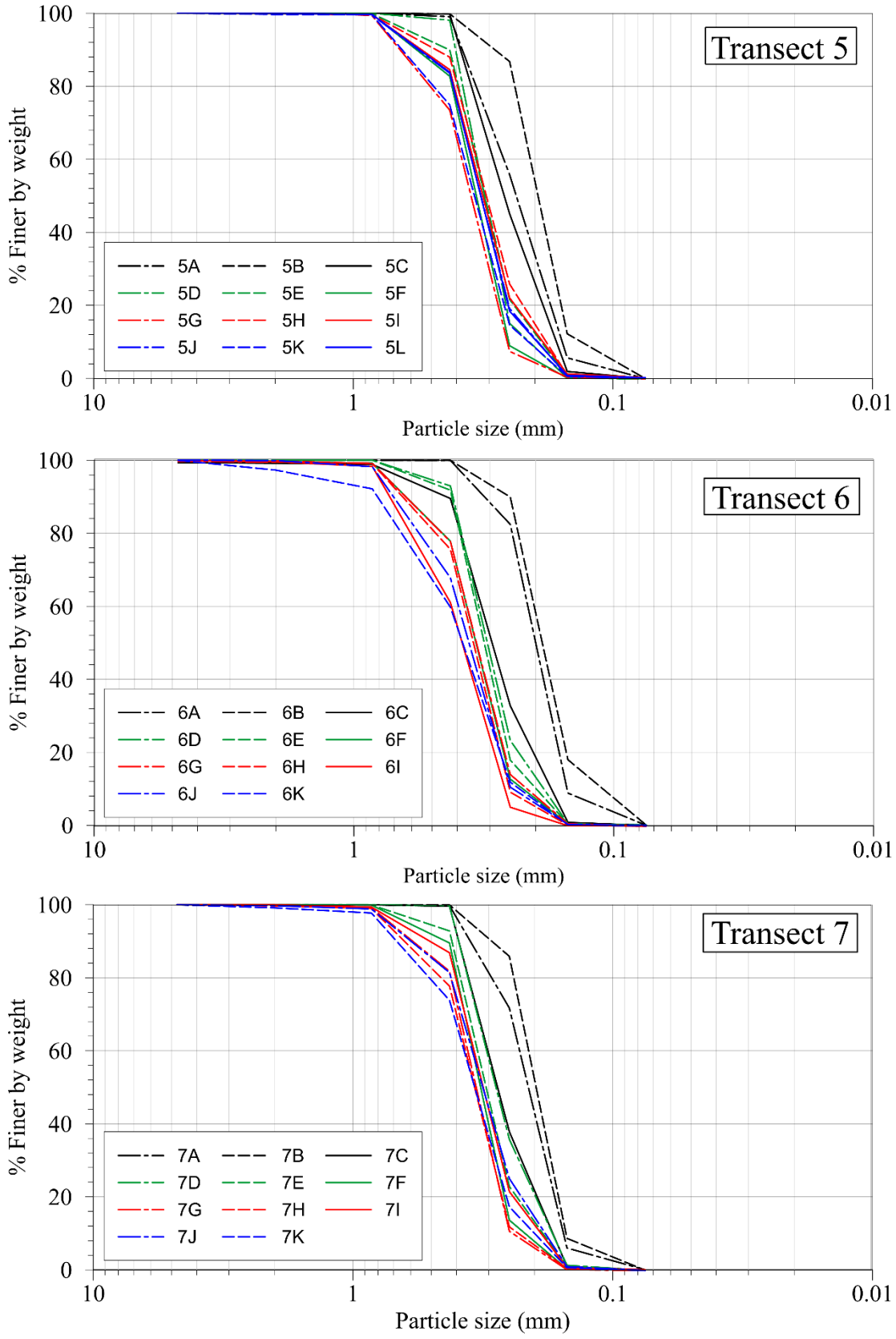

Figure B. 2. The grain size distribution for the samples collected along Transects 5-7

Table B.1 Summary of the sieve analysis tests on Cannon Beach sand.

Sample No.	Mean (mm)	D_{50} (mm)	D_{10} (mm)	D_{30} (mm)	D_{60} (mm)	C_u	C_c	USCS Classification
3A	0.23	0.23	0.16	0.19	0.24	1.53	0.96	Fine, Poorly Graded Sand
3B	0.21	0.21	0.15	0.18	0.22	1.45	0.96	
3C	0.27	0.29	0.18	0.23	0.32	1.82	0.97	
3D	0.29	0.32	0.19	0.27	0.34	1.79	1.09	
3E	0.27	0.3	0.18	0.24	0.33	1.85	0.99	
3F	0.28	0.31	0.19	0.26	0.34	1.83	1.07	
3G	0.33	0.34	0.21	0.29	0.36	1.75	1.07	
3H	0.31	0.33	0.2	0.28	0.36	1.76	1.08	
3I	0.28	0.31	0.18	0.25	0.34	1.87	1.04	
3J	0.3	0.33	0.19	0.27	0.36	1.87	1.07	
3K	0.29	0.31	0.18	0.25	0.34	1.91	1.03	
4A	0.23	0.22	0.15	0.19	0.24	1.55	0.96	Fine, Poorly Graded Sand
4B	0.19	0.19	0.12	0.17	0.21	1.7	1.12	
4C	0.25	0.25	0.16	0.21	0.28	1.71	0.91	
4E	0.3	0.32	0.19	0.27	0.35	1.79	1.09	
4F	0.29	0.31	0.2	0.26	0.34	1.7	1.00	
4G	0.29	0.32	0.2	0.27	0.35	1.74	1.04	
4H	0.33	0.34	0.22	0.29	0.37	1.7	1.06	
4I	0.29	0.31	0.19	0.26	0.34	1.84	1.06	
4J	0.28	0.31	0.18	0.24	0.34	2.04	0.92	
4K	0.32	0.33	0.2	0.27	0.36	1.82	0.99	
4L	0.33	0.33	0.2	0.27	0.36	1.84	0.98	
5A	0.24	0.24	0.16	0.2	0.27	1.68	0.93	Fine, Poorly Graded Sand
5B	0.19	0.2	0.14	0.17	0.21	1.57	1.03	
5C	0.25	0.27	0.17	0.22	0.3	1.76	0.92	
5D	0.31	0.32	0.22	0.28	0.34	1.6	1.06	
5E	0.32	0.33	0.21	0.28	0.35	1.65	1.07	
5F	0.34	0.35	0.25	0.3	0.37	1.47	0.96	
5G	0.39	0.36	0.26	0.31	0.39	1.52	0.96	
5H	0.29	0.32	0.19	0.26	0.35	1.86	1.06	
5I	0.3	0.33	0.19	0.27	0.36	1.85	1.08	
5J	0.32	0.33	0.2	0.28	0.36	1.8	1.08	
5K	0.37	0.35	0.22	0.29	0.38	1.76	1.05	
5L	0.32	0.33	0.2	0.29	0.36	1.79	1.19	

Sample No.	Mean (mm)	D_{50} (mm)	D_{10} (mm)	D_{30} (mm)	D_{60} (mm)	C_u	C_c	USCS Classification
6A	0.2	0.21	0.15	0.18	0.22	1.45	0.96	Fine, Poorly Graded Sand
6B	0.18	0.19	0.12	0.17	0.21	1.79	1.14	
6C	0.28	0.3	0.18	0.24	0.33	1.87	0.98	
6D	0.29	0.32	0.19	0.27	0.34	1.78	1.08	
6E	0.31	0.33	0.21	0.28	0.35	1.71	1.08	
6F	0.37	0.35	0.23	0.3	0.38	1.65	1.02	
6G	0.36	0.35	0.22	0.29	0.38	1.7	1.04	
6H	0.38	0.36	0.25	0.31	0.38	1.52	0.96	
6I	0.43	0.39	0.27	0.33	0.42	1.59	0.96	
6J	0.4	0.37	0.25	0.31	0.4	1.63	0.97	
6K	0.43	0.39	0.23	0.32	0.43	1.83	1.00	
7A	0.23	0.22	0.16	0.19	0.23	1.49	0.96	Fine, Poorly Graded Sand
7B	0.2	0.2	0.15	0.18	0.22	1.43	0.96	
7C	0.26	0.28	0.17	0.23	0.31	1.79	0.96	
7D	0.26	0.29	0.18	0.23	0.32	1.8	0.98	
7E	0.29	0.32	0.27	0.27	0.34	1.28	0.78	
7F	0.32	0.33	0.22	0.29	0.36	1.6	1.04	
7G	0.35	0.35	0.24	0.3	0.37	1.52	0.98	
7H	0.37	0.35	0.23	0.3	0.38	1.61	1.00	
7I	0.3	0.33	0.2	0.27	0.35	1.81	1.08	
7J	0.31	0.33	0.19	0.27	0.36	1.91	1.05	
7K	0.37	0.35	0.21	0.29	0.38	1.85	1.06	

Table B.2 Statistics of the sieve analysis tests results on Cannon Beach sand.

Statistics	Mean (mm)	D_{50} (mm)	D_{10} (mm)	D_{30} (mm)	D_{60} (mm)	C_u	C_c
Maximum	0.43	0.39	0.27	0.33	0.43	2.04	1.19
Minimum	0.18	0.19	0.12	0.17	0.21	1.28	0.78
Average	0.30	0.31	0.20	0.26	0.33	1.71	1.02
Standard Deviation	0.06	0.05	0.03	0.04	0.06	0.15	0.07

Table B.3 Summary of the vacuum triaxial test on the sand samples from the lower intertidal zone in Cannon Beach.

Test No.	Sample Weight (g)	Sample Dimensions			γ_{dry} (kN/m^3)	Void Ratio (e) (G_s=2.65)	*Dr* (%)	σ_{1f} (kPa)	σ_{13} (kPa)	ϕ' (°)
		Diameter (cm)	Height (cm)	Volume (cm^3)						
1	911.7	7.17	15.24	615	14.55	0.786	-0.5	7.24	1.72	38.1
2	909.3	7.16	15.24	613	14.56	0.785	-0.2	12.07	3.45	33.7
3	912.3	7.16	15.24	614	14.58	0.783	0.9	22.41	6.89	32.0
4	925.9	7.13	15.24	608	14.94	0.740	16.4	8.00	1.72	40.2
5	925.7	7.14	15.24	610	14.88	0.747	13.8	14.03	3.45	37.3
6	925.6	7.12	15.24	607	14.95	0.739	16.8	26.89	6.89	36.3
7	955.7	7.11	15.24	604	15.51	0.676	39.5	10.62	1.72	46.2
8	953.1	7.10	15.24	603	15.50	0.678	38.9	18.34	3.45	43.1
9	946.7	7.06	15.24	597	15.55	0.672	41.0	33.72	6.89	41.3
10	1045.1	7.21	15.24	622	16.47	0.578	74.9	14.20	1.72	51.6
11	1046.7	7.20	15.24	621	16.54	0.571	77.4	25.79	3.45	49.8
12	1039.8	7.19	15.24	619	16.47	0.578	75.0	41.85	6.89	45.8

Figure B.3 Example of a loose sample (left panel) and a dense sample (right panel) failed in vacuum triaxial tests.

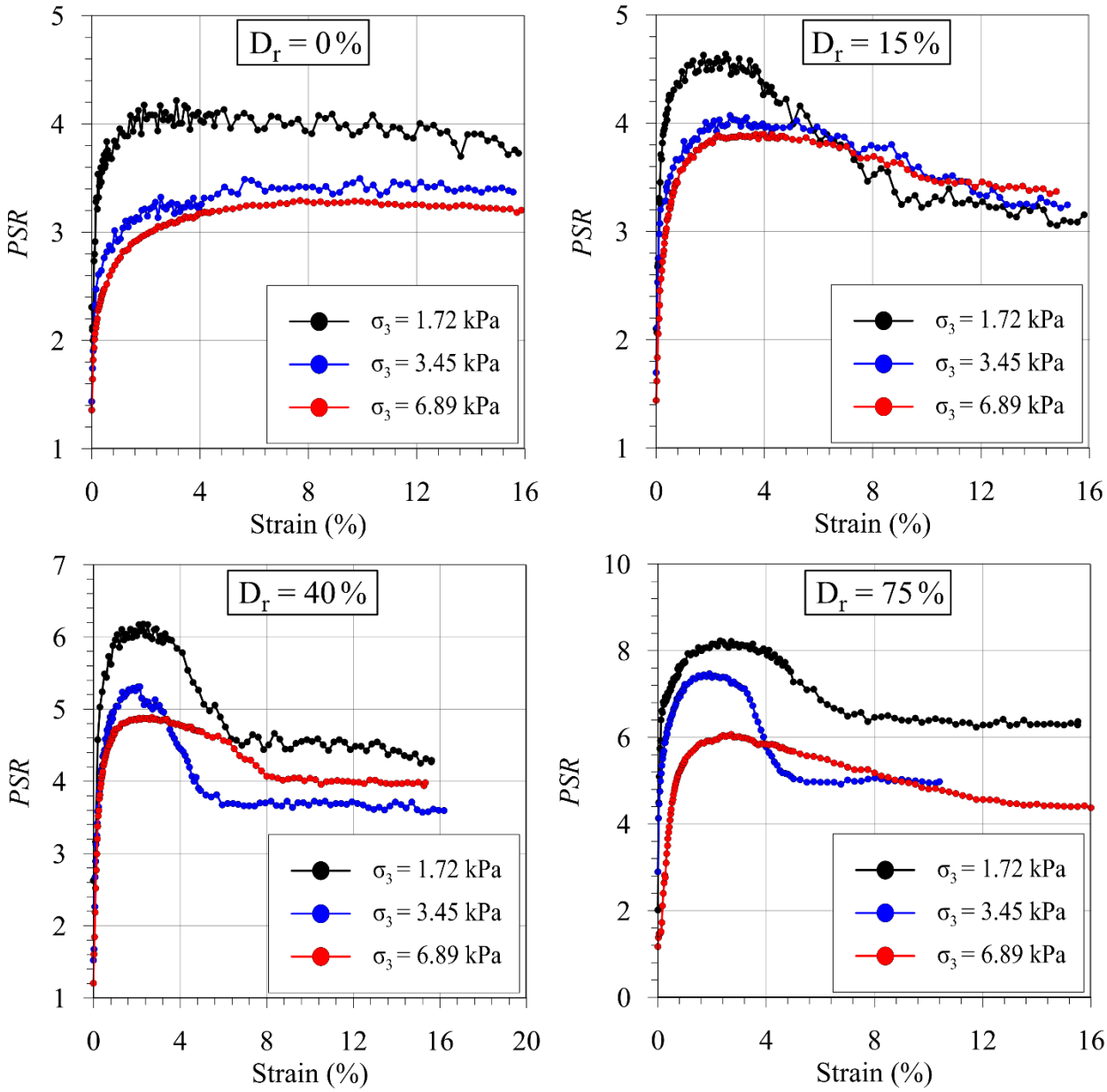

Figure B.4 Strain versus principal stress ratio ($\sigma_{1f} / \sigma_{3f}$) at different relative densities conducted using vacuum triaxial test.

Appendix C: Comparison between nearshore zones of Cannon Beach, AK and the USACE's Field Research Facility Beach, NC

Chapter 3 and Chapter 5 of this dissertation covered the investigation of the seabed sediments in the nearshore areas of Cannon Beach, AK, and the U.S. Army Corps of Engineers' Field Research Facility's (FRF) beach, Duck, NC, respectively. The two areas differ in wave conditions and sediment characteristics. More specifically, Cannon Beach is characterized by energetic waves and uniform quartz sand while the FRF beach is less energetic and characterized by variations in the grain size distribution along the cross-shore profile. The monthly mean significant wave height varies between H_s =1.0-4.3 m at Cannon Beach and H_s =0.6-2.0 m at the FRF beach. The surficial quartz sand at the FRF beach varies in particle size and gradation. The foreshore zone is characterized by a wide range of sand particle sizes and the presence of gravel. The particle size distribution decreases with the increase in water depth, resulting in approximately uniform sand at water depths in excess of ~6 m. This appendix presents a comparison of the results for the two regions to provide insight into the effect of local differences on the soil characteristics.

C.1 Duplicate deployments at approximately the same location

Duplicate deployments at approximately the same location were conducted in both areas. The distance between the duplicate deployments depends on the movement of the boat used in response to waves and currents. This distance is expected to be less than 5 m for the presented datasets. At Cannon Beach, the duplicate deployments showed mostly a matching quasi-static bearing capacity (*qsbc*), while at the FRF, the agreement between the duplicate deployments varied with the water depth. In shallow waters, noticeable scatter in the *qsbc* was observed, which became less significant moving seaward (Figure C.1). More specifically, the scatter became insignificant at water depths greater than ~6.5 m. This observation can be related to the variations in the particle size distribution. The sediment grain size and arrangement of particles can vary significantly from one location to another within a small distance in shallower waters due to the effects of the wave action and sediment mobilization processes.

C.2 Cross-shore variations in the sediment strength

Variations in the *qsbc* profiles were observed along the cross-shore direction at both locations (Figure C.2). At Cannon Beach, the *qsbc* was the lowest in shallow water depths, while it increased offshore. This trend became insignificant at a distance of about 2500 m from the shoreline (i.e. a water depth of about 15 m). The Hallermeier (1978) formula was used to determine the depth of closure based on the average significant wave heights and periods for the hourly hindcasted wave information from the Wave Information Studies (WIS 2016) website for the years 1980-2011. The resulting value for the average depth of closure was ~14.8 m. This is in agreement with the observed water depth at which *qsbc* became approximately constant. For the FRF beach, the *qsbc* was characterized by a general decrease in magnitude with the water depth increase. The relatively high *qsbc* in the nearshore area was associated with a large scatter in the values, which also decreased offshore. The scatter and *qsbc* variations became insignificant at a distance of about 750 m (water depth of about 6.5 m), which corresponds to the depth of closure range as found by Nicholls et al. (1998).

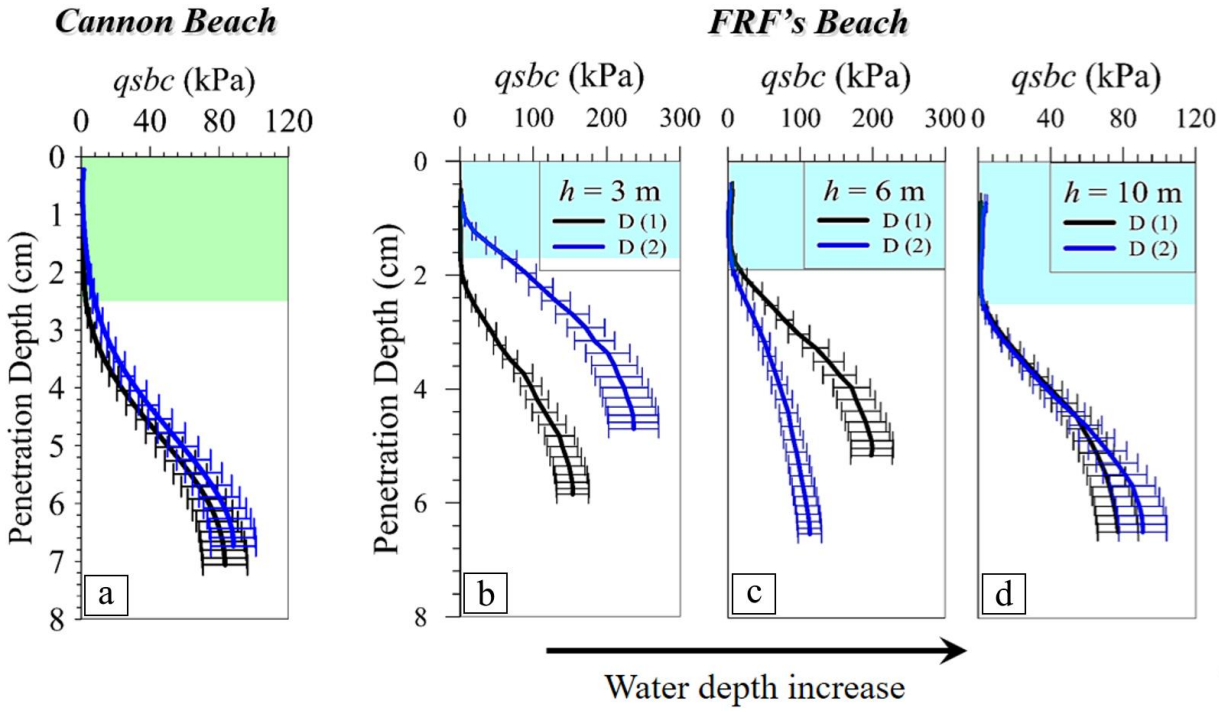

Figure C.1. Duplicate deployments at approximately the same location (a) in Cannon Beach, and (b-d) in the FRF beach. (Adapted from Figures 3.4 and 5.4)

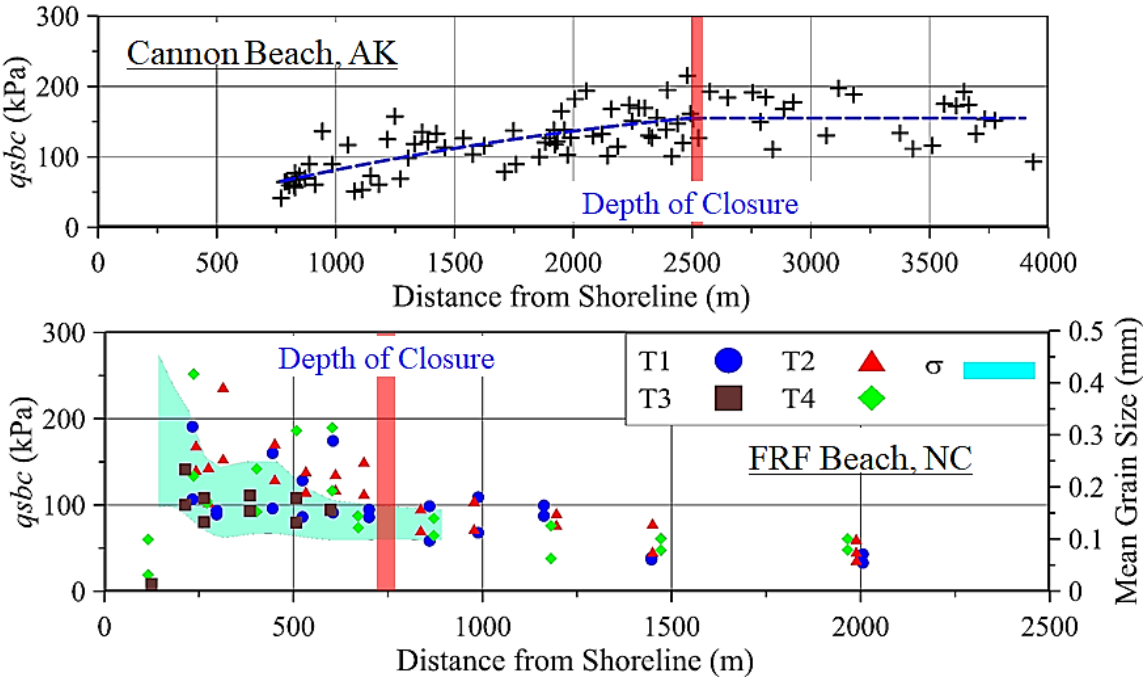

Figure C.2. The variation in the maximum *qsbc* of with the distance offshore in Cannon Beach (top panel) and the FRF beach (bottom panel). The vertical red line shows the depth of closure while cyan shaded area in the lower panel shows the variations in the grain size. (Adapted from figures 3.5 and 5.3)

C.3 Discussion

The presented results showed that the derived *qsbc* from the PFFP measurements is affected by the wave action and the grain size distribution. The uniform particle size at Cannon Beach exhibited an increase in the *qsbc* values, which corresponded with an increase in the water depth. It was hypothesized that the sediments in shallow water depths are subjected to regular disturbance by the wave action, which decreases with the water depth increase. Bagnold (1947) explained the presence of low density sediments in shallow waters is caused by the agitation of sediments due to the near-bed oscillatory movement of water. The intensity of the near-bed oscillations decreases with the water depth increase. This explains the observed increase in the *qsbc* with water depth increase. On the other hand, the presence of a wide range of particle sizes in shallow water depths at the FRF beach was reflected in the sediment behavior along the profile. The results showed a decrease in the *qsbc* values in correspondence with the water depth increase, which also associated with a decrease in the grain size distribution. This can be correlated to the effect of the sediments' gradation. As sand becomes more graded, the small particles tend to fill the gaps between the larger

particles, which results in forming a denser matrix compared to uniform sand (Duncan et al. 2014). The decrease in the *qsbc* with water depth was also observed in the data shown in Chapter 6 (Figure 6.8). These deployments were conducted at the same location in different wave conditions. This supports the hypothesis that the behavior of the *qsbc* is affected by the variation in the sediment grain size distribution.

In both locations above, the variation in the *qsbc* became minimal at the depth of closure, which is the minimum water depth at which the seabed morphology variations become insignificant. This can be explained by the disturbance of the seabed sediment by the wave action, which results in variations in the sediments' strength. Bilici et al. (2018) found that wave breaking as well as the depth of closure are reflected in the PFFP measurements. They proposed a coefficient to characterize the seabed sediments in energetic nearshore areas considering the wave action and PFFP measurements. This method was investigated in Chapter 6 of this dissertation.

C.4 Conclusions

The comparison of the sediment strengths along cross-shore profiles between Cannon Beach and the FRF beach suggested that the particle size distribution and hydrodynamics control the strength of surficial seabed sediment in nearshore environments. The uniform particle size in Cannon Beach exhibited an increase in the *qsbc* moving seaward due to the regular disturbance by the wave action in shallow waters, which also decreases moving offshore (Figure C.2). The presence of a wide range of particle sizes in shallow water depths at the FRF beach resulted in relatively larger *qsbc* values, which are associated with large scatters. The *qsbc* values and scatter decrease with increases in the water depth, which is also associated with a decrease in the grain size distribution.

C.5 References

Bagnold, R.A. 1947. Sand Movement by Waves: Some Small-Scale Experiments with Sand of Very Low Density. Journal of the Institution of Civil Engineers, 27(4): 447–469.

Duncan, J.M., Wright, S.G., and Brandon, T.L. 2014. Soil strength and slope stability. John Wiley & Sons, Hoboken, NJ.

Hallermeier, R.J. 1978. Uses for a calculated limit depth to beach erosion. In Proceedings of 16th Conference on Coastal Engineering. Hamburg, Germany. pp. 1493–1512.

Appendix D: Quantifying the effect of wave action on seabed surface sediment strength using a portable free fall penetrometer

The contributions of authors to the composition of this manuscript are delineated as follows:

Cagdas Bilici

- Conducted the literature review; performed analyses; prepared figures; wrote the draft manuscript,
- Addressed the comments and suggestions of the coauthors in developing the draft manuscript.
- Addressed the reviewers' comments and prepared the final version of the manuscript.

Nina Stark:

- Planned, supervised and participated in the field survey.
- Initiated the idea of *CWS*.
- Supervised the study.
- Reviewed and edited the draft manuscript.

Ali Albatal

- Participated in performing the analyses and preparing the figures.
- Participated in developing the idea of *CWS*.
- Reviewed and edited the draft and final manuscript.

Heidi Wadman

- Participated in the field survey.
- Reviewed and edited the draft manuscript.
- Reviewed and edited the draft and final manuscript.

Jesse E. McNinch

- Participated in the field survey.
- Reviewed and edited the draft manuscript.
- Reviewed and edited the draft and final manuscript.

Quantifying the effect of wave action on seabed surface sediment strength using a portable free fall penetrometer

Cagdas Bilici[1], Nina Stark[1], Ali Albatal[1], Heidi Wadman[2], Jesse E. McNinch[2]

[1]Virginia Polytechnic Institute and State University, Blacksburg, VA, USA

[2]Field Research Facility, Coastal Hydraulics Laboratory, USACE, Duck, NC, USA

Submitted to CPT18 - 4th International Symposium on Cone Penetration Testing

11/30/2017

Accepted for Publication 12/28/2017

Will be available online 06/21/2018

Reference:

Bilici, C., Stark, N., Albatal, A., Wadman, H., McNinch, J. (2018) 'Quantifying the effect of wave action on seabed surface sediment strength using a portable free fall penetrometer." – International Symposium on Cone Penetration Testing CPT'18.

D.1 Abstract

The surficial sediment strength of nearshore zone sands has previously been correlated to wave conditions in a qualitative manner. In this study, a coefficient of wave impact on sediment surface strength (*CWS*) is proposed to enable a quantitative assessment. The *CWS* was tested along a cross-shore transect in Duck, NC. The geotechnical input parameters for the *CWS* were measured using a portable free fall penetrometer. The offshore wavelength was extracted from a WaveRider buoy deployed in 17 m, and the water depth was derived from the penetrometer's pressure transducer. The results showed that the *CWS* coefficient reflects the change in sediment strength with wave-seabed interaction. Along the profile, the CWS ranged from 0.005 to 1.627. The CWS slightly increased at water depths shallower than the depth of closure (~4.5 m) and drastically in-creased at water depths shallower than breaker depth (~2 m), reaching a maximum value of 1.6.

Appendix E: Friction angles at sandy beaches from remote imagery

The contributions of authors to the composition of this manuscript are delineated as follows:

Nina Stark

- Initiated the idea; Planned, supervised and participated in the field survey.
- Conducted the literature review; performed analyses; prepared figures; wrote the draft manuscript.
- Addressed the comments and suggestions of the coauthors in developing the draft manuscript.
- Addressed the reviewers' comments and prepared the final version of the manuscript.

Jesse E. McNinch

- Participated in the field surveys.
- Reviewed and edited the draft manuscript.
- Reviewed and edited the final manuscript.

Heidi Wadman

- Participated in the field surveys.
- Reviewed and edited the draft manuscript.
- Reviewed and edited the final manuscript.

Hans C. Graber:

- Provided and advised regarding satellite imagery.
- Reviewed and edited the draft manuscript.
- Reviewed and edited the final manuscript.

Ali Albatal

- Conducted the laboratory tests.
- Participated in the field surveys.
- Reviewed and edited the draft manuscript.
- Reviewed and edited the final manuscript.

Paul A. Mallas

- Performed advanced satellite image analysis.
- Reviewed and edited the draft manuscript.
- Reviewed and edited the final manuscript.

Friction angles at sandy beaches from remote imagery

Nina Stark[1], Jesse E. McNinch[2], Heidi Wadman[2], Hans C. Graber[3], Ali Albatal[1], Paul A. Mallas[3]

[1]Virginia Tech, Department of Civil and Environmental Engineering, 200 Patton Hall, Blacksburg, VA 24061. Phone: 540-231-7152; e-mail: ali2@vt.edu, ninas@vt.edu

[2]US Army Engineers Waterways Experiment Station, Field Research Facility, 1261 Duck Road, Kitty Hawk, NC 27949; e-mail: jesse.mcninch@us.army.mil, heidi.m.wadman@usace.army.mil

[3]Center for Southeastern Tropical Advanced Remote Sensing (CSTARS), University of Miami, Miami, FL, USA

Submitted to Géotechnique Letters Journal 05/22/2017

Accepted for Publication 10/14/2017

Published online 11/20/2017

Reference:

Stark, N., McNinch, J., Wadman, H., Graber, H.C., Albatal, A. and Mallas, P.A. (2017) 'Friction angles at sandy beaches from remote imagery." Géotechnique Letters, 7(4), pp.292-297. DOI:10.1680/jgele.17.00053

E.1 Abstract

The rigour of extracting friction angles, and eventually lower-bound bearing strength, in sandy beach settings through slope angles determined from digital images (visual spectrum) is explored. Digital images of topographic sand features using hand-held cameras, an unmanned aerial vehicle and a panchromatic satellite sensor are analysed to determine average slope angles using three-dimensional reconstruction. Greyscale gradients and shadows are utilised in the satellite images to extract slope estimates. The slope angles matched tilt table results of samples from the same locations at the Duck, NC, and Claytor Lake, VA, field sites. Direct shear testing of sample material suggest friction angles of ~33° and ~35°, respectively. The authors test a potential pathway to derive lower-bound bearing strength using these remotely sensed slope angles. Preliminary results are encouraging, but likely sensitive to the impact of moisture content, differences between the maximum and the observed slope angle and internal friction angles.